

ADVERTIMENT. La consulta d'aquesta tesi queda condicionada a l'acceptació de les següents condicions d'ús: La difusió d'aquesta tesi per mitjà del servei TDX (www.tesisenxarxa.net) ha estat autoritzada pels titulars dels drets de propietat intel·lectual únicament per a usos privats emmarcats en activitats d'investigació i docència. No s'autoritza la seva reproducció amb finalitats de lucre ni la seva difusió i posada a disposició des d'un lloc aliè al servei TDX. No s'autoritza la presentació del seu contingut en una finestra o marc aliè a TDX (framing). Aquesta reserva de drets afecta tant al resum de presentació de la tesi com als seus continguts. En la utilització o cita de parts de la tesi és obligat indicar el nom de la persona autora.

ADVERTENCIA. La consulta de esta tesis queda condicionada a la aceptación de las siguientes condiciones de uso: La difusión de esta tesis por medio del servicio TDR (www.tesisenred.net) ha sido autorizada por los titulares de los derechos de propiedad intelectual únicamente para usos privados enmarcados en actividades de investigación y docencia. No se autoriza su reproducción con finalidades de lucro ni su difusión y puesta a disposición desde un sitio ajeno al servicio TDR. No se autoriza la presentación de su contenido en una ventana o marco ajeno a TDR (framing). Esta reserva de derechos afecta tanto al resumen de presentación de la tesis como a sus contenidos. En la utilización o cita de partes de la tesis es obligado indicar el nombre de la persona autora.

WARNING. On having consulted this thesis you're accepting the following use conditions: Spreading this thesis by the TDX (www.tesisenxarxa.net) service has been authorized by the titular of the intellectual property rights only for private uses placed in investigation and teaching activities. Reproduction with lucrative aims is not authorized neither its spreading and availability from a site foreign to the TDX service. Introducing its content in a window or frame foreign to the TDX service is not authorized (framing). This rights affect to the presentation summary of the thesis as well as to its contents. In the using or citation of parts of the thesis it's obliged to indicate the name of the author

**EFFECTS OF MELT BLENDED POSS NANOFILLERS ON POM AND ABS
THERMAL STABILITY**

Narciso Vilà Ramirez

PhD Dissertation to opt to the degree of Doctor in Materials Science
for the Universitat Politècnica de Catalunya

Advisors:

Prof. Miguel Sanchez-Soto

Thesis developed at the Universitat Politècnica de Catalunya, Terrassa (Barcelona)

Departament de Ciència dels Materials i Enginyeria Metal·lúrgica

October 2013

*A mis tesoros Lindies y Ashley,
que me iluminan cada día.*

*Al meu pare i la meva mare,
que malgrat la distància sempre els tinc amb mi.*

*To my friends and mentors,
who keep inspiring me without them knowing it.*

ACKNOWLEDGEMENTS

Despite my enduring desire to develop research skills in the polymer world, my decision to embark on a PhD program was initially doubtful and hesitant. Having a family and a full-time job makes it very challenging to allocate time on the thesis and can easily push the attention away from the dissertation challenges.

The initial encouragement and guidance I received from my first tutor, Antonio Gordillo PhD, was a key factor for me to take the first steps into the research program. On his departure, Professor Miguel Sanchez Soto took over the supervision of my research and since then I have been blessed with his continuous support, positive attitude and ability to effectively communicate regardless of the geographical distance between us, particularly on the last stages of the thesis. To both of you, I would like to express my most sincere appreciation and gratitude for being there and helping me making it through.

I would also like to acknowledge the support received from Teresa Lacorte in teaching me the FTIR procedures and Josep Palou for his assistance in the SEM analysis and in other miscellaneous areas of the Materials Science department.

CONTENTS

ACKNOWLEDGEMENTS.....	ii
CONTENTS.....	iii
NOMENCLATURE.....	vii
LIST OF FIGURES.....	xii
LIST OF TABLES.....	xvii
ABSTRACT.....	xix
RESUMEN (<i>Spanish</i>).....	xxi
RESUM (<i>Catalan</i>).....	xxiii
1. INTRODUCTION.....	2
1.1. THESIS MOTIVATION AND OBJECTIVES.....	3
1.2. THESIS STRUCTURE.....	5
1.3. STATE OF THE ART.....	7
1.3.1. NANOTECHNOLOGY: DESCRIPTION AND HINDSIGHT.....	7
1.3.2. DEFINITION OF NANOSCALE PARTICLES.....	10
1.3.3. CLASSIFICATIONS OF NANOPARTICLES.....	10
1.3.4. NANOCOMPOSITE SYSTEMS.....	20
1.3.5. THERMOPLASTIC NANOCOMPOSITES PREPARATION TECHNIQUES.....	21
1.4. THERMOPLASTIC THERMAL DEGRADATION.....	30
1.4.1. THERMAL DEGRADATION MECHANISMS.....	30
1.4.2. POLYOXYMETHYLENE THERMOXIDATION MECHANISM.....	37
1.4.3. ACRYLONITRILE-BUTADIENE-STYRENE THERMOXIDATION MECHANISM.....	42
1.4.4. THERMOPLASTIC DEGRADATION ANALYSIS.....	45
2. MATERIALS.....	48
2.1. POLYOXYMETHYLENE.....	50
2.1.1. Description.....	50
2.1.2. Production of POM.....	50
2.1.3. POM characteristics and properties.....	51
2.1.4. POM used in this study.....	55

2.2.	ACRYLONITRILE-BUTADIENE-STYRENE grafted with MALEIC-ANHYDRIDE	56
2.2.1.	Description	56
2.2.2.	Production of ABS	57
2.2.3.	ABS Characteristics and properties	58
2.2.4.	ABS grafting with maleic anhydride (ABS-g-Ma)	60
2.2.5.	ABS-g-Ma used in this study.....	63
2.3.	POLYHEDRAL OLIGOMERIC SILSESQUIOXANES (POSS)	64
2.3.1.	POSS Description	64
2.3.2.	General POSS Characteristics and properties	65
2.3.3.	Commercial use of POSS:	67
2.3.4.	POSS used in this thesis.....	68
3.	THEORETICAL FUNDAMENTALS.....	76
3.1.	POLYMER SOLUBILITY ANALYSIS	76
3.1.1.	Hoftzyer and Van Krevelen calculation method	80
3.1.2.	Hoy calculation method	81
3.1.3.	Hoy method based on group molar-attraction constant.....	83
3.1.4.	The role of the inorganic silicate cage structure in the solubility study	84
3.1.5.	Solubility calculation approach on the present study.....	84
3.2.	POLYMER DEGRADATION KINETICS	85
3.2.1.	Methods used for degradation kinetics analysis.....	85
3.2.2.	Coats and Redfern (CR) method.....	86
4.	EXPERIMENTAL METHODS	90
4.1.	SAMPLE PREPARATION	90
4.1.1.	POM/POSS's sample preparation	90
4.1.2.	ABS-g-Ma/POSS's sample preparation.....	90
4.2.	SAMPLE PRELIMINARY CHARACTERISATION	92
4.2.1.	Scanning Electron Microscopy analysis (SEM)	92
4.2.2.	Differential Scanning Calorimetry analysis (DSC).....	92
4.3.	DEGRADATION (THERMO-OXIDATION) PROCESS CONDITIONS	93
4.3.1.	POM and its nanocomposites:	93
4.3.2.	ABS-g-Ma and its nanocomposites:	93
4.4.	SAMPLE DEGRADATION CHARACTERISATION	94
4.4.1.	Fourier Transform Infra-Red Spectroscopy analysis (FTIR)	94

4.4.2. Thermogravimetric analysis (TGA)	95
4.4.3. Spectrophotometry analysis (CIELAB).....	96
5. RESULTS AND DISCUSSION	100
5.1. PRELIMINARY ANALYSIS OF POM & POM/POSS NANOCOMPOSITES.....	100
5.1.1. Solubility analysis of POM and its nanocomposites.....	100
5.1.2. SEM analysis of POM and its nanocomposites	109
5.1.3. DSC analysis of POM and its nanocomposites	115
5.2. DEGRADATION ANALYSIS OF POM & POM/POSS NANOCOMPOSITES	121
5.2.1. Fourier Transform Infra-Red analysis of POM and its nanocomposites	121
5.2.2. Thermogravimetric analysis of POM and its nanocomposites	133
5.2.3. Degradation kinetics by Coats and Redfern of POM and its nanocomposites	135
5.2.4. Spectrophotometry analysis of POM and its nanocomposites.....	138
5.2.5. Inter-relationship between FTIR and Spectrophotometry analysis	146
5.2.6. Summary of results of POM and its nanocomposites.....	152
5.3. PRELIMINARY ANALYSIS OF ABS-g-Ma & its POSS NANOCOMPOSITES.....	153
5.3.1. Solubility analysis of ABS-g-Ma/POSS and its nanocomposites.....	153
5.3.2. SEM analysis of ABS-g-Ma/POSS and its nanocomposites.....	157
5.3.3. DSC analysis of ABS-g-Ma/POSS and its nanocomposites.	159
5.4. DEGRADATION ANALYSIS OF ABS-g-Ma & its POSS NANOCOMPOSITES.....	161
5.4.1. Fourier Transform Infra-Red analysis of ABS-g-Ma and its nanocomposites.	161
5.4.2. Thermogravimetric analysis of ABS-g-Ma/POSS and its nanocomposites.....	168
5.4.3. Degradation kinetics by Coats&Redferd of ABS-g-Ma/POSS and its nanocomposites...	171
5.4.4. Spectrophotometry analysis of ABS-g-Ma and its nanocomposites	174
5.4.5. Inter-relationship between FTIR and Spectrophotometry analysis	177
5.4.6. Summary of results of ABS-g-Ma and its nanocomposites.	178
6. CONCLUSIONS.....	180
POM NANOCOMPOSITES.....	180
ABS-g-MA NANOCOMPOSITES	181
GENERAL CONCLUSIONS	183
FUTURE WORK.....	185
7. REFERENCES.....	188
8. ANNEX: PUBLISHED PAPERS	208

8.1. THERMAL DEGRADATION OF POLYOXYMEHTYLENE EVALUATED WITH FTIR AND SPECTROPHOTOMETRY	208
8.2. ENHANCEMENT OF POM THERMOOXIDATION RESISTANCE THROUGH POSS NANOPARTICLES.....	209
8.3. PLASTIC NANOCOMPOSITES FOR BETTER THERMAL RESISTANCE.....	210
8.4. EFFECTS OF POSS NANOPARTICLES ON ABS-G-MA THERMOXIDATION RESISTANCE..	211
8.5. THERMAL STABILIZATION ABILITY OF POLYHEDRAL OLIGOMERIC SILSESQUIOXANE NANOFILLERS.....	212

NOMENCLATURE

MATERIALS

POM	Polyoxymethylene also known as acetal, polyacetal and polyformaldehyde
ABS	Acrylonitrile butadiene styrene
SAN	Poly(styrene-co-acrylonitrile)
PAN	Polyacrylonitrile
PB	Polybutadiene rubber
g-Ma	Maleic anhydride (grafted)
SMA	Styrene-maleic anhydride (styrenic polymer)
PE	Polyethylene
PP	Polypropylene
PC	Polycarbonate
PA	Polyamide
PET	Polyethylene terephthalate
BMI	Bismaleimide resins
COIN	Composite organic-inorganic nanoparticles (COINs)
NSP	Nano-Scale-Particles
CNT	Carbon Nanotube
PLS	Polymer Layered Silicate
PCN	Polymer Clay Nanocomposite
QDs	Quantum Dots
POSS	Polyhedral Oligomeric Silsesquioxane
PLSN	Polymer/Layered Silicate Polymer (intercalated or exfoliated)
THF	Tetrahydrofuran

ANALYTICAL METHODS

TGA	Thermogravimetric Analysis
DTG	Derivative Thermogravimetry
DSC	Differential Scanning Calorimetry
TEM	Transmission Electron Microscopy
DMA	Dynamic Mechanical Analysis
NMR	Nuclear Magnetic Resonance spectroscopy
XRD	X-Ray Diffraction
RR	Resonance Raman spectroscopy
AFM	Atomic Force Microscope
CRTA	Control Transformation Rate Thermal Analysis
Py-GC/MS	Pyrolysis Gas Chromatography Mass Spectrometry
TVA	Thermal Volatilisation Analysis
MALDI-TOF	Matrix Assisted Laser Desorption/Ionisation Mass Spectrometry
GPC	Gel permeation chromatography
MFI	Melt Flow Index (also Melt Mass Flow Rate-MFR, Melt Volume Flow Rate-MVR)
SEM	Scanning Electron Microscopy
FTIR	Fourier Transform Infra-Red (spectroscopy)
ATR	Attenuated Total Reflectance
T_{5%}	TGA: Temperature at 5% of weight loss
T_{50%}	TGA: Temperature at 50% of weight loss
T_{MAX}	TGA: Temperature of maximum weight loss rate
λ	FTIR: Spectroscopic wavelength expressed in cm
$\bar{\nu}$	FTIR: Spectroscopic wavenumber expressed in cm ⁻¹
CIELAB	Colour space coordinates defined by the International Commission on Illumination
L*	Lightness of colour with values running from 0 (black) to 100 (white)
a*	Colour coordinate between green (-100) and red (+100)

b* Colour coordinate between blue (-100) and yellow (+100)

POLYMER (GENERAL)

CRU	Constitutional Repeat Unit
M_n	Number average Molar Mass
C_x	Crystallinity content
T_G	Glass Transition temperature in thermoplastics
T_m	Melting temperature in semi-crystalline thermoplastics
T_C	Crystallisation temperature in semi-crystalline thermoplastics
T_n	Nucleation temperature in semi-crystalline thermoplastics
T_e	End of crystallisation exotherm in semi-crystalline thermoplastics
F_V	Fractional Free-Volume content
V_f	Free Volume size

DEGRADATION KINETICS

α	Decomposed Fraction, also known as Degree of Conversion "c"
m₀	initial mass
m	actual mass at the temperature chosen
m_∞	final at the final temperature
w	Weight loss (0=initial, f or ∞ = Final)
T	Absolute Temperatures [K]
A	Frequency Factor, also known as Pre-Exponential Factor "Z"
β	Heating Rate, also known as Ramping Rate "r"
E_a	Activation Energy
R	Gas Constant
S	Shape Index
n	Order of Reaction

$f(\alpha)$	Differential expression of kinetics function
k	Rate of Reaction, also known as Degradation Rate Coefficient (Arrhenius expr.)
$kf(\alpha)$	Rate of Conversion, also known as Rate of Degradation

SOLUBILITY PREDICTION

ΔG_M	Free energy of mixing, also known as free enthalpy, Gibbs energy or Gibbs function
ΔH_M	Enthalpy of mixing, also known as heat of mixing
ΔS_M	Entropy change in the mixing process
δ_t	Solubility Parameter, also expressed as δ_{tot}
δ_p	Solubility contribution of the polar forces
δ_h	Solubility contribution of the hydrogen bonding
δ_d	Solubility contribution of the dispersion forces
F_t	Molar Attraction Function
F_p	Polar Contribution Function
G	Group Molar Attraction Constant
ρ	Density of material
M_o	Molecular Weight
E	Cohesive Energy
E_D	Dispersion cohesive Energy
E_P	Polar cohesive Energy
E_H	Hydrogen bonding Energy
V	Molar Volume
Δ_T	Lyndersen Correction for non-ideality
α	Molecular Aggregation Number
n	Number of repeating units per effective chain segment of the polymer
V_f	Free-volume size
F_v	Fractional free-volume content

HSP Hansen 3D solubility parameters

UNITS

GPa Giga Pascal: 10^9 Pascals (SI pressure unit). 1 GPa = 10^4 bar

MPa Mega Pascal: 10^6 Pascals (SI pressure unit). 1 MPa = 10 bar

bar Non-SI pressure unit. 1 bar = 10^5 Pa = Atmospheric pressure on Earth at sea level

J Joule (SI energy unit) = 1 newton of force applied through 1 meter

µm Micrometre: 10^{-6} metres ('m' being the SI length unit)

nm Nanometre: 10^{-9} metres ('m' being the SI length unit)

Å Ångström: non-SI unit of length equal to 10^{-10} m or 0.1 nm

°C Temperature unit most globally used (except for US). Also known as Centigrade.

°F Temperature unit mostly used in USA, $[°F] = [°C] \times 9/5 + 32$

K SI temperature unit, primarily used in physical sciences. $[K] = [°C] + 273.15$

ppm Pseudo-unit defining Parts Per Million

wt Pseudo-unit: Concentration of an additive expressed in weight percentage terms

ORGANISATIONS

ASTM American Society for Testing and Materials

IUPAC International Union of Pure and Applied Chemistry

ISO International Organization for Standardization

SI International System of Units

LIST OF FIGURES

Figure 1: Market distribution by nanoparticle type as of 2010.....	9
Figure 2: Dimensionality of nanoparticles	12
Figure 3: Morphology of nanoparticles	13
Figure 4: Composition of nanoparticles.....	14
Figure 5: Uniformity and agglomeration of nanoparticles	15
Figure 6: Agglomerated POSS (represented as spheres for simplicity) in a polymer matrix.	23
Figure 7: Intramolecular hydrogen transfer and β -scission process	31
Figure 8: Chain stripping process.....	33
Figure 9: Depolymerisation process	34
Figure 10: Cross-linking process	35
Figure 11: Initiation.....	36
Figure 12: Propagation.....	36
Figure 13: Continuation	36
Figure 14: Evolution of formaldehyde at the early stages of degradation starting at unstable chain-ends.....	37
Figure 15: Formation of formaldehyde gas by main chain cleavage.....	38
Figure 16: Thermoxidative degradation of POM forming hydroperoxide groups.	38
Figure 17: Formation of cyclic compounds via transacetalisation	39
Figure 18: Structure of polyacetal homopolymer and copolymer	50
Figure 19: DuPont's route for polyacetal homopolymer.....	50
Figure 20: Ticona's route for polyacetal copolymer	51
Figure 21: Distribution of end-use applications of POM	54
Figure 22: Structure of Acrylonitrile-butadiene-styrene	56

Figure 23: Monomer structure of the ABS constituencies i.e. Acrylonitrile, Butadiene and Styrene	57
Figure 24: Distribution of end-use applications of ABS	59
Figure 25: Chemical structure of maleic anhydride	60
Figure 26: Silsesquioxane cage structure	64
Figure 27: Silsesquioxane partial-cage structure	64
Figure 28: POSS structure and main characteristics	66
Figure 29: G-POSS structure	69
Figure 30: GI-POSS structure	70
Figure 31: A-POSS structure	71
Figure 32: PEG-POSS schematic	72
Figure 33: T-POSS structure	73
Figure 34: Graphical parameters to calculate the shape index 'S'	88
Figure 35: Recollection of solubility parameters of POM and the different POSS nanofillers with the resulting difference in solubility of the nanocomposite system and its comparison to the corresponding SEM images	108
Figure 36: SEM 5,000x magnification micrograph of POM and the Nanocomposites prepared at 2.5% concentration	110
Figure 37: Comparison of the SEM images of POM/A-POSS at 2.5% and at 10% add-ratio	112
Figure 38: Comparison of the SEM images of POM/PEG-POSS at 2.5% and at 10% add-ratio	113
Figure 39: POSS agglomerate interface morphologies	114
Figure 40: DSC second-heating plot for POM and the 4 different nanocomposites	115
Figure 41: DSC plot (2nd Heating) at the melting peak of POM/PEG-POSS sample	117
Figure 42: DSC plot (Cooling) at the crystallisation temperature spectrum of POM/PEG-POSS and POM samples	118
Figure 43: FTIR spectra of POM homopolymer versus POM copolymer at the characteristic absorption bands corresponding to CH ₂ wagging and bending.	121

Figure 44: FTIR spectra for an injected POM submitted at 220°C for different times in the band region corresponding to the carbonyl aldehyde group and the methylene bending.	123
Figure 45: Comparison of absorption progress of bands corresponding to end-groups carbonyl referred to the methylene absorbance.	124
Figure 46: Degradation groups based on different Iso-Carbonyl yields referred to ageing temperature and storage time.	125
Figure 47: FTIR spectra of POM submitted at 220°C for 60min versus another one submitted at 240°C for 30min.	126
Figure 48: Stacked FTIR spectras of Standard POM copolymer, POM/PEG-POSS, POM/G-POSS, POM/GI-POSS, and POM/A-POSS, respectively.	128
Figure 49: FTIR spectra for an injected POM/Glycidyl POSS submitted at 240°C for different times in the band region corresponding to the carbonyl aldehyde group and the methylene bending.	129
Figure 50: Comparison of absorption progress of bands corresponding to end groups carbonyl referred to the Methylene absorbance.	130
Figure 51: Photos taken at the different POM samples submitted at 260 °C x 75 min and categorised in different Carbonyl/Methylene ratio	132
Figure 52: Thermogravimetric curves for POM/POSS composites and neat POM, showing the evolution of weight loss (a) and the derivative weight loss (b).	134
Figure 53: Graphical method to calculate the shape index 'S' (POM/GPOSS sample).....	135
Figure 54: Kinetics of the thermal degradation for POM, POM/PEG, POM/G, POM/Gi and POM/Amino.	136
Figure 55: Progress of Lightness L*, Coordinate a* (redness-greenness) and Coordinate b* (yellowness-blueness) as degradation proceeds for each of the temperatures.....	139
Figure 56: Interpolated Lightness limits L* and Iso-chromaticities a* and b* versus temperature and time.	140
Figure 57: Colour route followed by the material along aging times up to 90 min. at different temperatures, represented on the CIELAB space for the hue chromaticity values (a* and b*).	143
Figure 58: Progress of Lightness L*, Coordinate a* (redness–greenness), and Coordinate b* (yellowness–blueness), as degradation proceeds for each of the temperatures.....	144

Figure 59: Colour route followed by the different nanocomposites along the CIELAB space with different aging times up to 90 min at 240°C representing the hue chromaticity values (a^* and b^*).	145
Figure 60: Inter-relationship between colour appearance [L^* , a^* , b^*] and Carbonyl/Methylene absorbance ratio, showing the correspondent pictures of the POM samples belonging to each of the degradation groups.	147
Figure 61: Degradation of POM/POSS nanocomposites in terms of Carbonyl Yield and Colour variation when submitted at 240°C for 45 min.	149
Figure 62: Degradation of POM/POSS nanocomposites in terms of Carbonyl Yield and Colour variation when submitted at 260°C for 30 min.	149
Figure 63: Recollection of solubility parameters of ABS-g-Ma and the different POSS nanofillers with the resulting difference in solubility of the nanocomposite system and its comparison to the corresponding SEM images.	156
Figure 64: Morphologies of ABS-g-Ma and its nanocomposites: (a) ABS-g-Ma/APOSS; (b) ABS-g-Ma/GPOSS; (c) ABS-g-Ma/TPOSS nanocomposites.	158
Figure 65: DSC heatflow plot during the second heating of ABS-g-Ma and its nanocomposites ABS-g-Ma/APOSS, ABS-g-Ma/GPOSS and ABS-g-Ma/TPOSS.	159
Figure 66: FTIR Spectra of ABS-g-Ma/APOSS blend in comparison with the pure ABS-g-Ma and the pure APOSS (a), and likewise ABS-g-Ma/ GPOSS (b) and ABS-g-Ma/TPOSS (c).	162
Figure 67: Spectra in the carbonyl area of ABS-g-Ma and the three nanocomposites in their original state (continuous line) and after thermo oxidation under 240°C@75min (dashed line).	163
Figure 68: Spectra of ABS-g-Ma undergoing thermo oxidation under 320°C in steps of 15 min until 75 min.	165
Figure 69: Overlay of the Butadiene ratio in the four original samples prior to degradation	167
Figure 70: Ratio butadiene/CH ₂ bending absorbance of each material submitted at 200, 240, 280, and 320°C up to 75 min in steps of 15 min.	167
Figure 71: TGA thermogram for ABS-g-Ma, ABS-g-Ma /APOSS, ABS-g-Ma/GPOSS, and ABS-g-Ma/TPOSS.	168
Figure 72: Derivative Weight thermogram (DTG) for ABS, ABS-APOSS, ABS-GPOSS, and ABS-TPOSS.	169
Figure 73: Method to calculate the shape index “S” and the order of reaction “n”.	171

Figure 74: Kinetics of the thermal degradation for ABS, ABS-APOSS, ABS-GPOSS, and ABS-TPOSS.	172
Figure 75: Photos of the four different materials tested under the conditions 240°C for 75 min.	174
Figure 76: Progress of Lightness L*, Coordinate a* (redness-greenness), and Coordinate b* (yellowness-blueness) as degradation proceeds at 240°C.	175
Figure 77: Colour route followed by the different nanocomposites along the CIELAB space with different aging times up to 90 min at 240°C representing the hue chromaticity values (a* and b*).	176
Figure 78: Degradation of ABS-g-MA and its POSS nanocomposites in terms of Butadiene decay and Colour variation when submitted at 280°C for 75 min.	177

LIST OF TABLES

Table 1: Differences in properties between POM homopolymer and copolymer.....	52
Table 2: TDS Hostaform C13021 (POM-C)	55
Table 3: General properties of ABS.....	58
Table 4: TDS Bopndyram 6000 (ABS-g-Ma)	63
Table 5: POSS nanoparticles used in this study	68
Table 6: Solubility calculation tables for POM	102
Table 7: Solubility calculation tables for GPOSS	103
Table 8: Solubility calculation tables for GIPOSS	104
Table 9: Solubility calculation tables for APOSS	105
Table 10: Solubility calculation tables for PEGPOSS	106
Table 11: DSC second-heating melting temperatures (T_m) and crystallinity values (X_c) for each sample.	116
Table 12: Relevant FTIR absorption bands for the characterization of POM, POSS and thermoxidative degradation.	127
Table 13: TGA-Summary of results for POM and its nanocomposites expressed in $T_5\%$, $T_{50\%}$ and T_{max}	133
Table 14: Summary of thermogravimetric and kinetic results of POM, POM/PEG, POM/G, POM/Gi and POM/Amino.	137
Table 15: Maximum temperature allowance at different aging periods for each material when carbonyl/methylene ratio is 0.5-1 and colour shift ΔE reaches 50%.....	150
Table 16: General summary of results from SEM, DSC, FTIR, TGA/DTG, Kinetics and Spectrophotometry analysis for POM and the POM/POSS nanocomposites.	152
Table 17: Solubility calculation tables for ABS-g-Ma	154
Table 18: Solubility calculation tables for TPOSS.....	155

Table 19: Summary of Tg values found on ABS and its nanocomposites.....	159
Table 20: Drop in butadiene/CH ₂ ratio between the virgin material and the degraded sample at 280°C for 75min for each material.....	168
Table 21: Summary of thermogravimetric and kinetic degradation of ABS-g-Ma, ABS-g-Ma/APOSS, ABS-g-Ma/GPOSS and ABS-g-Ma/TPOSS.....	173
Table 22: General summary of results from SEM, DSC, FTIR, TGA/DTG, Kinetics and Spectrophotometry analysis for ABS-g-Ma and the ABS-g-Ma/POSS nanocomposites.	178



ABSTRACT

The developments in nanotechnology in recent years and its application in materials is providing a range of possibilities to improve the performance in areas such as mechanical resistance, thermal stability, optical and electrical properties to name a few. On the other side, the engineering challenges involving plastics materials are pushing the boundaries of polymer properties to the limit, and there is an increasing need to being able to tailor specific polymer structures with enhanced properties in one or several of the areas aforementioned depending on the particular application required.

Despite the attention that the thermoplastic nanocomposites have been receiving in recent years, the knowledge base in this field is still fairly undeveloped and accordingly further research of what and how much can be expected from the numerous possibilities available is essential.

The objective of this thesis is to contribute to the above knowledge base by creating and assessing a new range of thermoplastic based nanocomposites. In particular, a focus is taken on the enhancement of the thermal resistance through the addition of Polyhedral Oligomeric Silsesquioxane nanofillers (POSS) on two popular engineering plastics known by their low thermal stability, one being a semi-crystalline copolymer i.e. polyoxymethylene (POM) and the other an amorphous copolymer i.e. acrylonitrile butadiene styrene grafted with maleic anhydride (ABS-g-Ma). Different nanocomposites have been produced, from which its morphology, miscibility, structure, thermal properties and appearance behaviour before and during the thermoxidative degradation is herein quantified and discussed together with the resulting benefits and drawbacks.

All the nanocomposites have been produced via melt-blending, using the nanofillers Glycidyl, Glycidyl-Isobutyl, Aminopropyl-isobutyl and Poly(ethylene-glycol) for the POM matrix, and Amino-Propyl Isobutyl, Glycidyl, and Trisilanol for the ABS-g-Ma matrix.

The incorporation adequacy of the nanofillers into the matrix has been pre-assessed with the Hoy's solubility calculation method and later on corroborated with scanning electron microscopy (SEM) and differential scanning calorimetry (DSC). The quantification of the thermal degradation behaviour of each sample at different temperatures and exposure times was carried out through Fourier transform infrared spectrography (FTIR), thermogravimetric analysis (TGA) including the degradation kinetics and, ultimately, the sample appearance progress has been assessed in terms of yellowing by means of colour spectrophotometry (Cielab).

The results showed that the presence of different POSS's used with the POM matrix improves dramatically the thermal stability of the base material and that such improvement is proportionate to the solubility compatibility between matrix and the nanofiller. The best performance was found with Aminopropyl-isobutyl, whereby the temperature of maximum rate of degradation (T_{MAX}) increased by 22°C. Said improvement is also seen in the conditions at which the nanocomposite developed only 2% of carbonyl yield and 8% of yellowing compared to the standard POM copolymer, which is taken as the base reference with 100% deterioration suffered in the above two indicators.

However, the performance of the different nanocomposites produced in this work with ABS-g-Ma has not been as encouraging as the POM-based nanocomposites described above. Although the SEM morphological analysis show adequate incorporation and miscibility of the nanofillers into the matrix, the GPOSS and the TPOSS nanocomposites provided no relevant improvements in thermal stability when compared to the base ABS-g-Ma, and the APOSS blend exhibits a very slight decay in almost all the quantitative analysis carried out in this work.

RESUMEN



Los avances producidos en años recientes en el campo de la nanotecnología y sus aplicaciones en los materiales están aportando grandes mejoras en el rendimiento de los mismos en áreas como la resistencia mecánica, estabilidad térmica, propiedades ópticas y eléctricas, entre otras. Por otro lado, el mundo de la ingeniería y el diseño de componentes plásticos está llevando los materiales cada vez más a su límite, con el fin de poder ofrecer el máximo rendimiento al mínimo coste. Esta realidad implica la necesidad creciente de customizar estructuras poliméricas con propiedades mejoradas en áreas específicas para cada aplicación.

A pesar de los desarrollos que se han estado produciendo últimamente en nanocompuestos termoplásticos, el conocimiento en este campo es aún limitado, y requiere de más iniciativas de investigación y desarrollo sobre el amplio campo de posibilidades que nos ofrecen los nanocompuestos.

El objetivo de esta tesis es contribuir en el conocimiento de los nanocompuestos a través del estudio de los efectos de varias nanocargas del tipo Polyhedral Oligomeric Silsesquioxanes (POSS) en el comportamiento de la resistencia térmica del copolímero semicristalino polióxido de metileno (POM) y del terpolímero amorfo acrilonitrilo-butadieno-estireno (ABS), los cuales son dos plásticos técnicos susceptibles a la termoxidación.

Diferentes nanocompuestos se han elaborado con el fin de estudiar su morfología, miscibilidad, estructura, propiedades térmicas y apariencia, así como los beneficios y contrapartidas que resultan de ellos.

Los nano-compuestos han sido elaborados mediante el método de mezcla en estado fundido (melt-blending), utilizando cuatro nano-cargas distintas para el POM, siendo Glicidil, Glicidil-Isobutil, Aminopropil-isobutil y Poli(etilen-glicol), y tres nano-cargas para el ABS, siendo Amino-Propil Isobutil, Glicidil y Trisilanol.

La compatibilidad teórica de las nano-cargas se ha calculado mediante el método de solubilidad de “Hoy”, y se ha corroborado con microscopía electrónica de barrido (SEM) y calorimetría diferencial de barrido (DSC). Posteriormente, cada material base y sus distintas variantes de nano-compuestos se han sometido a diferentes condiciones de termo-oxidación en términos de temperatura y tiempo de exposición. El comportamiento a la degradación de cada muestra se ha cuantificado mediante los métodos de espectroscopia de infrarrojos por transformada de Fourier (FTIR), análisis de termogravimetría (TGA) incluyendo cinética de degradación, y finalmente mediante espectrofotometría (Cielab) para definir el progreso de la apariencia de la muestra en términos de amarilleamiento.

Los resultados derivados de la inclusión de los diferentes POSS utilizados en la matriz de POM han mejorado sustancialmente la estabilidad térmica del mismo, y dicha mejora es proporcional a la compatibilidad de solubilidades entre el POM y los POSS utilizados. El mejor comportamiento se produce con la incorporación de la nanocarga aminopropil-isobutil, con una temperatura de máxima degradación (T_{MAX}) incrementada en 22 °C sobre la T_{MAX} del POM original tomado como referencia. Esta mejora se refleja también con una reducción muy notable en la formación grupos carbonilo y en el amarilleamiento sufrido en la superficie de la muestra, siendo un 2% y 8% respectivamente comparados con los resultados obtenidos con la muestra equivalente del material POM original.

En referencia a los nanocompuestos basados en ABS-g-Ma, a pesar de la adecuada solubilidad teórica entre la matriz y las diferentes nano-cargas, así como la buena miscibilidad obtenida en la elaboración de las muestras y evidenciada en el análisis morfológico SEM, no se han podido obtener mejoras en términos de estabilidad térmica. Concretamente, la adición de GPOSS y TPOSS no han aportado beneficios relevantes en las propiedades del nanocompuesto final, y la nanocarga APOSS ha incluso afectado negativamente a la matriz con una ligera caída de la resistencia térmica.

RESUM



Els avenços produïts en els últims anys tant en el camp de la nanotecnologia com en les seves aplicacions en els materials, està contribuint en la millora del rendiment dels mateixos en àreas com la resistència mecànica, l'estabilitat tèrmica, i les propietats òptiques i elèctriques entre d'altres. Per altra banda, el món de l'enginyeria i el disseny de components plàstics està portant els materials cada vegada més al seu límit amb la finalitat de poder oferir el màxim rendiment al mínim cost, i això comporta una necessitat creixent de customitzar les estructures polimèriques amb propietats específicament millorades en àreas molt concretes en funció de l'aplicació requerida.

A pesar del desenvolupament que s'ha estat produint últimament en l'àrea de nanocompostos plàstics, el coneixement en aquest camp és encara limitat, i requereix de més iniciatives d'investigació per cobrir el potencial que ofereix aquesta classe de materials, així com conèixer també les seves limitacions.

L'objectiu d'aquesta tesi es el de contribuir en l'enteniment dels nanocompostos plàstics a través de l'estudi dels efectes de varies nanocàrregues del tipus Polyhedral Oligomeric Silsesquioxanes (POSS) en el comportament de la resistència tèrmica del poli(òxid de metilè) (POM) com a material semicristalí, i l'acrilonitril-butadiè-estirè (ABS) com a material amorf. Val a dir que la selecció d'aquests dos polímers tècnics ha estat en part motivada per la seva susceptibilitat inherent a la termodegradació.

Diferents nanocompostos basats amb aquests materials s'han elaborat amb la finalitat d'estudiar la seva morfologia, miscibilitat, estructura, propietats tèrmiques i aparença, així com els beneficis i contrapartides que resulten d'ells.

La preparació dels nanocompostos ha sigut mitjançant el mètode de barreja en estat fos (melt-blending), utilitzant quatre nano-càrregues diferents per el POM, siguent glicidil, glicidil-Isobutil, aminopropil-isobutil y poli(etilenè-glicol), i tres nano-càrregues per el ABS, siguent amino-propil isobutil, glicidil i trisilanol.

La compatibilitat teòrica de les nano-càrregues s'ha calculat mitjançant el mètode de solubitat de "Hoy", i s'ha corroborat amb microscopia electrònica d'escombrat (SEM) i calorimetria diferencial d'escombrat (DSC). Posteriorment s'ha sotmès cada material base i les seves diferents variants de nanocompostos a diferents condicions de termo-oxidació en termes de temperatura i temps d'exposició.

El comportament a la degradació de cada mostra s'ha quantificat mitjançant els mètodes d'espectroscòpia d'infraroigs per transformada de Fourier (FTIR), anàlisi de termogravimetria (TGA) incloent cinemàtica de degradació, i finalment mitjançant espectrofotometria (Cielab) per a definir el progrés de l'aparença de la mostra en termes d'engroguiment.

Els resultats han mostrat, per una banda, que la inclusió dels diferents POSS utilitzats en la matriu de POM ha millorat substancialment l'estabilitat tèrmica del mateix, i aquesta millora és proporcional a la compatibilitat entre les solubitats del POM i del POSS. El millor comportament s'ha produït amb l'addició de la nano-càrrega d'aminopropilisobutil, amb una temperatura de màxima degradació (T_{MAX}) millorada en 22°C en relació a la obtinguda amb la matriu de POM.

Aquesta millora també es reflexa amb una reducció molt notable en la formació de grups carbonil i en l'engroguiment sofert en la superfície de la mostra, siguent un 2% i 8% respectivament comparats amb els resultats obtinguts amb la mostra equivalent del material POM original.

En contrast, els nanocompostos basats en ABS-g-Ma no han ofert millores en termes d'estabilitat tèrmica, a pesar d'una adequada solubitat teòrica entre la matriu i les diferents nano-càrregues utilitzades, així com la bona miscibilitat obtinguda en l'elaboració de les mostres i posteriorment evidenciada en l'anàlisi morfològic SEM. Concretament l'addició de GPOSS i de TPOSS no han aportat beneficis en les propietats del nanocompostos final, i la nano-càrrega APOSS ha afectat negativament a la matriu amb una lleugera caiguda de la resistència tèrmica.

CHAPTER 1
INTRODUCTION

1. INTRODUCTION

This section is intended to introduce the reader with the essential background of this thesis by providing an insight in the following areas:

- Thesis motivation and objectives: The framework in which the thesis was conceived and the antecedents driving the development of this work.
- Thesis structure: The architecture of the document to assist in understanding the information arrangement along the different sections of the document.
- State of the Art: The first section covers the current developments in nanotechnology applied in thermoplastic materials, nanoparticles, the preparation methods, the different types of existing nanofillers and particularly POSS nanoparticles.
- Thermoplastic thermal degradation: The fundamentals of thermoplastic thermal degradation, its different mechanisms and the different methods typically used to analyse and ascertain thermal degradation on polymers.

1.1. THESIS MOTIVATION AND OBJECTIVES

The work presented in this thesis is part of the doctorate program from the Department of Materials Science and Metallurgy (CMEM) at Universitat Politècnica de Catalunya (UPC, Barcelona), and adds on to a series of research lines focused on studying POSS nanocomposites. The experimental has been carried out in UPC, CCP (Centre Català del Plàstic) and PPT (Precision Process Technolgy S.A.), the latter being the author's employer from 2004 to 2011.

The plastics processing industry, and particularly the injection moulding processes, often experience quality issues due to material degradation inflicted during one or various stages of the manufacturing chain, be it inadequate storage, material dehumidification, incorrect equipment, inadequate process conditions , poor tool venting or excessive exposure of the finished product at a high temperature. This prevalent problem in thermoplastics became of great interest in the eyes of the author and made him consider developing analytical and research skills to better understand the degradation mechanism of polymers and to be able to explore possibilities to enhance their thermal stability without resorting to complex copolymerisation methods.

On the other side, among the different areas of polymer research promoted by UPC/CCP, the nanocomposite field has been in their spotlight with numerous research initiatives taking place over the recent years.

Studies on polymer nanocomposites are a relatively new area that has been gaining a lot of interest in both the research and advanced engineering polymer manufacturers due to the potential benefits that can be obtained from them.

With the above, the objectives set with this thesis are the following:

- To pre-assess the adequacy of certain POSS nanofillers for a given base material based on solubility analysis
- To analyse the thermo-oxidation process and the thermal stability of the base-materials and different POSS nanocomposites with various analytical methods.
- To establish a correlation between the degree of thermoxidation of a natural (uncoloured) polymer with its yellowing aspect by means of spectrophotometry.
- To ascertain the contribution of the selected nanoscale particles to the thermal stability of the nanocomposites.

1.2. THESIS STRUCTURE

This thesis has been structured in 8 chapters following the criteria below:

The first section of the document is intended assist the reader by providing the contents, the relevant nomenclature, the list of figures and tables as well as the abstract of the dissertation.

Chapter 1 (current section) is intended to put the reader into context by explaining the objectives of the thesis, the current developments of the scientific community regarding nanocomposites and the fundamentals of polymer thermodegradation. Additionally, a special focus on the specific degradation mechanisms of the materials selected is also covered.

Chapter 2 covers the description and characteristics of the base materials, the nano-fillers and the chemical intermediate used in the preparation of samples used in this thesis.

Chapter 3 runs through the theoretical fundamentals of each of the two prediction methods used to assess the adequacy of the sample integrity and expected performance in thermal stability i.e. polymer solubility and polymer degradation kinetics respectively.

Chapter 4 details the experimental methods carried out on each material, going from the sample preparation through to each of the different analytical techniques employed i.e. SEM, DSC, FTIR, TGA and Spectrophotometry.

Chapter 5 comprises the compilation and discussion of the results obtained with the experimental and associates the empirical results with the theoretical predictions defined in

chapter 2. Accordingly, each material is reviewed in two sections i.e. the preliminary examination of the sample, and the corresponding post-degradation analysis.

Chapter 6 covers the conclusions of this thesis and suggests supplementary research for future work.

Chapters 7 and 8 contain respectively the References and the Annexed articles published by the author.

1.3. STATE OF THE ART

1.3.1. NANOTECHNOLOGY: DESCRIPTION AND HINDSIGHT

The prefix *nano-*, derived from the Greek “nanos” signifying *dwarf*, is becoming increasingly common in scientific literature. This term has become a popular label for much of modern science, and many “nano-“ words have recently appeared in dictionaries, including: nanometer, nanoscale, nanoscience, nanotechnology, nanostructure, nanotube, nanowire, and nanorobot.

The nanotechnology is a science that deals with the manipulation of matter on an atomic and molecular scale, encompassing the understanding of the fundamental physics, chemistry, biology and technology of nanometre-scale objects. Generally, nanotechnology works with materials, devices, and other structures with at least one dimension sized from 1 to 100 nanometres. Nanotechnology is now recognized as one of the most prosperous fields in the 21st century for technological development.

In hindsight, the first known precursor of what nanotechnology is today goes back in 1959 at a meeting held by the American Physical Society whereby a lecture given by Richard Feynman with the name “There’s Plenty of Room at the Bottom” suggested the possibility to manipulate atoms in order go beyond the conventional chemical synthetic methods to prepare materials [1].

The first written paper embracing unambiguously the term nanotechnology was published in 1974 by Norio Taniguchi [2], who presented this term as a discipline for ultra-precision processing of materials in the nanoscale.

In the early 1980s, the advent of scanning tunnelling microscopy and scanning probe microscopy facilitated research on materials with atomic resolution [3].

The concept of nanotechnology started to be exposed outside the scientific arena with the book *Engines of Creation* written the Eric Drexler in 1986 [4], which is deemed to be the first written precursor of nanotechnology as we know it today. In that same year, the first nano-particle was produced in the form of fullerenes by Kroto et.al. [5], which subsequently led to

nanotubes. In 1993, Toyota Research Group in Japan reported successful mechanical and thermal improvements on a nylon-6 nanocomposite based on montmorillonite nanoclay [6]. Several European countries have pursued their own nanotechnology agenda since the late 1980s. Among the first was the United Kingdom in 1986, while France and Germany followed later. In addition, the European Commission funded many research projects in the early 1990s and made nanotechnology one of its research priorities under the current Research Framework Programme established in 2004 [7]. Similarly, nanotechnology became an established discipline in United States with the creation of the National Nanotechnology Initiative (NNI) in the year 2000 under the Bill Clinton administration.

The advances in the ability to characterise, produce and manipulate nanometre-scale materials have led to their increased use as fillers in new types of nanocomposites. Manufacturers now mix nanoparticles made of metals, oxides and additional materials with polymers and other matrix materials to optimize the composite properties with respect to tensile strength, modulus and heat distortion temperature, as well as colour/transparency, conductivity, flame retardancy, barrier properties, magnetic properties and anticorrosive properties. These enhanced properties usually result in much higher performance levels when compared to conventional composite and non-composite materials.

1.3.1.1. Global nanocomposite materials consumption

With the above, global usage of nanocomposites has increased rapidly, and the following facts [8] depict the current status of nanocomposite global consumption, which are also depicted in figure 1:

- The global consumption of nanocomposites in 2010 was 118,768 metric tons with a value of over \$800 million.
- Clay nanocomposites accounted for more than 50% of total nanocomposite consumption by value in 2010. Its market share is expected to increase to approximately 58% in 2016.

- Carbon nanotube composites accounted for 21% of total nanocomposite consumption in 2010 and this market share is expected to decrease to 16% in 2016.
- The current forecast indicates that by 2016, the market should amount to 333,043 metric tons and \$2.4 billion, a five year compound annual growth rate (CAGR) of 19.2% in unit terms and 20.9% in value terms.

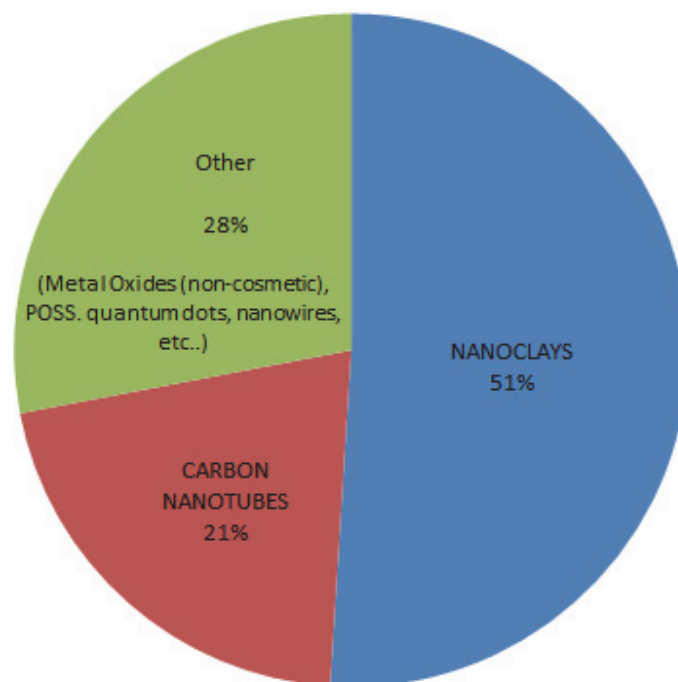


Figure 1: Market distribution by nanoparticle type as of 2010.

1.3.2. DEFINITION OF NANOSCALE PARTICLES:

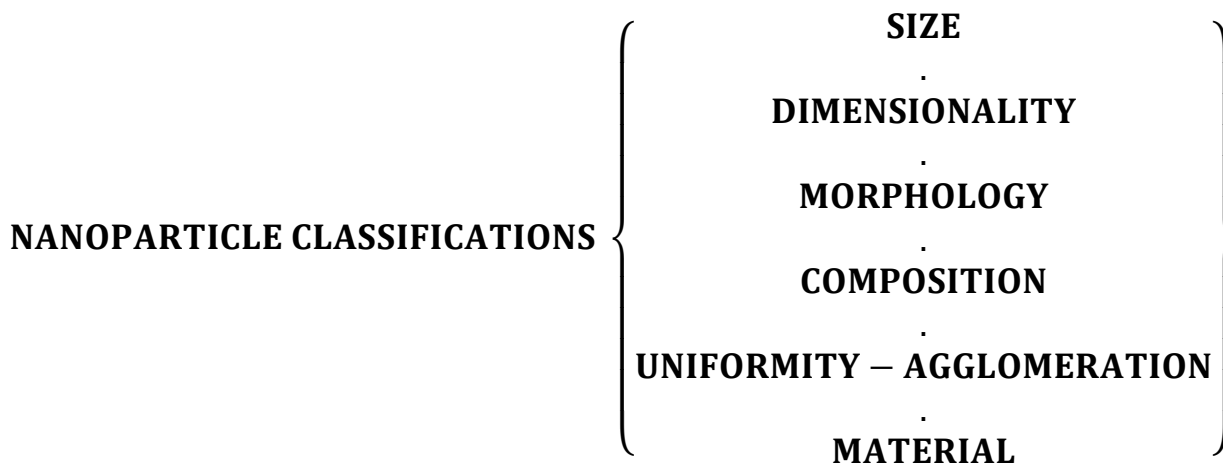
Nanoscale particles are often abbreviated in the literature as “NSP” and are defined for most of U.S. and British nanotech experts as particles smaller than 100 nanometres (nm)—that is, 0.1 micrometre or micron (μm)—in any one dimension. Nanoparticles can have amorphous or crystalline form and their surfaces can act as carriers for liquid droplets or gases. To some degree, nanoparticulate matter should be considered a distinct state of matter, in addition to the solid, liquid, gaseous, and plasma states, due to its distinct properties (large surface area and quantum size effects) [9].

International standardisation bodies including ISO, IEC, ANSI, ASTM have been discussing the standardization of terminology, metrology, characterization, and approaches to safety and health of NSPs. Unambiguous terms and conditions of the definition of the nanoparticle term was not achieved until 2006 and 2008 by ASTM and ISO respectively.

At this point in time, the relevant references from the two main standardisation bodies are the ISO/TS 27687:2008 *“Nanotechnologies - Terminology and definitions for nano-objects - Nanoparticle, nanofibre and nanoplate”* and ASTM E2456 - 06(2012) *“Standard Terminology Relating to Nanotechnology”*.

1.3.3. CLASSIFICATIONS OF NANOPARTICLES

Nanoparticles are generally classified based on their size, dimensionality, morphology, composition, uniformity, and agglomeration. These attributes play an important role in the nanoparticle interaction with the host matrix material and therefore in the selection, conception and development of nanocomposites. Several classifications are currently found in literature, and this section describes the most common:



Scheme 1: Common nanoparticle classifications

SIZE: As stated previously, there is a general agreement to assign the size range of nanoparticles from 1 to 100nm. Since most particles have more than one dimension, the ASTM standard defines two or three dimensions must be between 1 – 100 nm. This provides for nanotubes with a diameter of 10 nm, but a length > 100 nm [12-13].

In addition to the above considerations, particles smaller than 10nm are starting to be categorised as **quantum dots (QD)**. The physical justification for such term is that the energy levels of these particles become quantised and their behaviour becomes similar to that one of atoms instead of classic particles. For example, the colour of macroscopic gold is yellow; however gold quantum dots are red, due to surface plasmon excitation i.e. a quantum of plasma oscillation. Their application was originally oriented into exploratory medicine and bio-tech industries, however they are beginning to make an appearance in consumer products, for instance in laser diodes and home pregnancy tests [12].

DIMENSIONALITY: Nanoparticles can be classified on their number of dimensions which is a generalization of the aspect ratio concept. Below a description of each type followed with a graphical representation in figure 2:

- **1D nanomaterials:** Typically thin films or surface coatings, and include the circuitry of computer chips and the antireflection and hard coatings on eyeglasses. Thin films have been developed and used for decades in various fields, such as electronics, chemistry, and engineering. They can be deposited by various methods and can be grown controllably to be only one atom thick as a monolayer.
- **2D nanomaterials:** These include 2D nanostructures firmly attached to a substrate, or nanopore filters used for small particle separation and filtration. Free particles with a large aspect ratio, with dimensions in the nanoscale range, are also considered 2D nanomaterials. Asbestos fibres are an example of 2D nanoparticles.
- **3D nanomaterials:** These include thin films deposited under conditions that generate atomic-scale porosity, colloids, and free nanoparticles with various morphologies including spherical, pyramidal and polyhedral cages. Indeed, POSS (polyhedral oligomeric silsesquioxanes) would be an example of 3D nanoparticles.

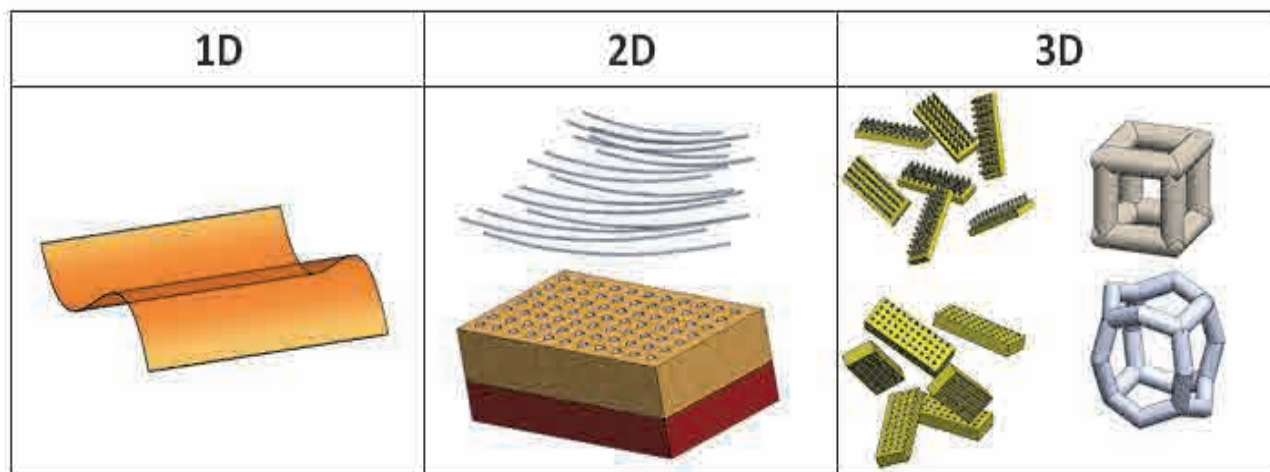


Figure 2: Dimensionality of nanoparticles

MORPHOLOGY: The morphological characteristics of a nanoparticle are usually determined by its flatness, sphericity and aspect ratio, and the primary typologies can be seen in the following figure 3.

The main implication of this classification is to do with the aspect ratio. **High aspect ratio** nanoparticles include nanotubes and nanowires, with various shapes, such as helices, zigzags, belts, or perhaps nanowires with diameter that varies with length between 0.5-2nm. **Small-aspect ratio** morphologies include, among others, spherical, oval, cubic or prism.












High Aspect Ratio	Low Aspect Ratio
Nanowires 	Nanospheres 
Nanohelices 	Nanohelices (thick) 
Nanozigzags 	Nanopyramids 
Nanopillars 	Nanocubes 
Nanotubes 	Other polyhedral shapes (example: POSS) 
Nanobelts 	

Figure 3: Morphology of nanoparticles

COMPOSITION: Nanoparticles can be composed of a single constituent material or be a composite of several materials. The nanoparticles found in nature are often agglomerations of materials with various compositions, while pure single-composition materials can be easily synthesized today by a variety of methods. Figure 4 below would be a representation of the different compositions that can be found in nanoparticles.

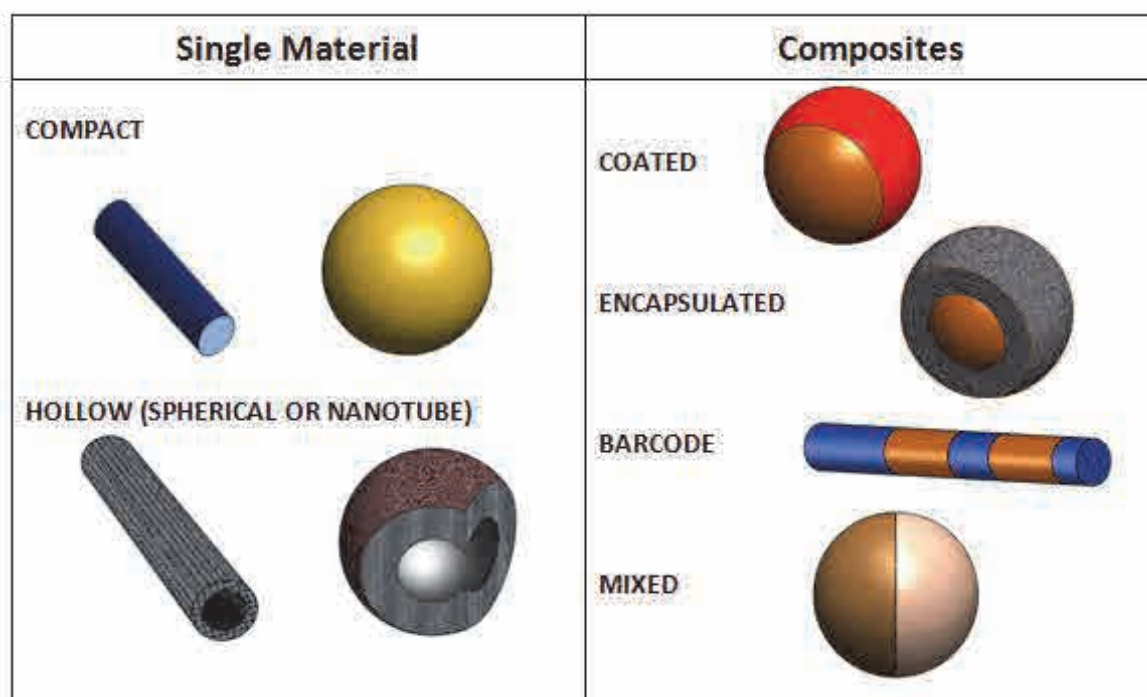


Figure 4: Composition of nanoparticles

Composite nanoparticles with well-defined material fractions are also starting to be a reality. To name a few, nanospheres of silica with ferrous crystal nucleus were developed by Taboada et al. [13], quantum dots in silica spheres were prepared by Darbandi et al. [14], Zhu et al. synthesised robust sandwich-like silica-metal-silica fluorescent nanoparticles [15].

UNIFORMITY AND AGGLOMERATION: Based on their chemistry and electro-magnetic properties, nanoparticles can exist as dispersed aerosols, as suspensions/colloids, or in an agglomerate state (see Figure 5). For example, magnetic nanoparticles tend to cluster, forming an agglomerate state, unless their surfaces are coated with a non-magnetic material. In an agglomerate state, nanoparticles may behave as larger particles, depending on the size of the agglomerate.




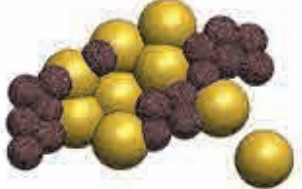
	ISOMETRIC	INHOMOGENEOUS
DISPERSED		
AGGLOMERATES		

Figure 5: Uniformity and agglomeration of nanoparticles

MATERIAL: Nanoparticles are currently made out of a wide variety of materials, although they can be grouped into the following four main sources:

Carbon: *Carbon black* is probably the most famous example of a nanoparticulate material that has been produced in mass production for decades. Nowadays the sizes used range from 10nm to 500nm [9] and produces approximately 1.5 million of tons every year mainly for the tyre industry [16]. It is worth noting, however, that according to the nanoparticle definitions explained in section 1.3.2, carbon black could not be strictly considered as a nanoparticle due to its size reaching magnitudes up to 500nm, hence, only a fraction of the carbon black usage falls within the nano-scale category.

Fullerenes is the other subgroup of carbon based nanoparticles, consisting of a carbon allotrope similar to the better known allotropes graphite and diamond. Conceptually, fullerenes are graphene sheets rolled into tubes or spheres in the nanoscopic scale. The cylindrical version of the above is generally referred to as *carbon nanotube (CNT)* and can be formed individually as a single-walled particle or stacked concentrically one into another becoming a multi-walled nanotube. The physical properties of nanotubes are rather unique with extremely high tensile strength, which could be as high as 300 GPa in theory (steel is 1-2 GPa), as well as extremely high electrical current capacity or thermal conductivity [17]. Accordingly, CNT have a great potential to improve the properties of the host polymers, more so, considering that functional groups can be added to the surface of the nanotube to establish covalent bonds to the matrix and the aspect ratio can be enhanced with increased length of the nanotube.

With the above benefits, nanotubes have been gaining popularity reaching 21% of total nanocomposite consumption back in 2010 [8]. The broad use of nanotubes, however, is limited due to certain difficulties to obtain of particle uniformity in terms of length, diameter and electrical conductivity, which involves expensive filtration processes to obtain CNT within pre-defined specifications [12]. Another challenge in using nanotubes for nanocomposites is to be able to implement their properties in composites at the macroscale, combining the choice of materials with the appropriate processing method [18].

CNT are currently used in coatings to dissipate or minimize static electricity such as fuel lines, in hard disk handling trays, or in automobile bodies to be painted electrostatically [11].

Metal Oxides: After carbon black, this is the group that currently has the largest number of commercial nanomaterials, and includes those such as titanium dioxide (TiO_2), cerium dioxide (CeO_2), zinc oxide (ZnO), aluminium dioxide (AlO_2) and iron oxide (FeO). They are available as dry powders or liquid suspensions and are widely used in ceramics, chemical polishing agents, scratch-resistant coatings, cosmetics, and sunscreens [19]. To give an idea of the consumption scale of these nanoscale materials, the quantities currently used just in the skincare market sectors, titanium dioxide being one of the most common, amount to

1,000–2,000 tonnes per annum worldwide, with the nanoscalar component materials worth approximately \$10 to \$100,000 per tonne [3]. These statistics, however, apply mainly for the cosmetic and consumer products, and not so much for nanocomposite applications.

Silicon: Silicon is the second most abundant element in the earth's crust, making up about 27% of the average rock [20], and it is also a fundamental source of an increasing number of advanced nanoparticles with multiple characteristics as described in the coming paragraphs. *Nanoclays* are the most popular silicon based nanoparticles accounting for more than 50% of total nanocomposite consumption¹ in 2010 [8]. They consist of sheet-structured hydrous silicates generally referred as phyllosilicates [21] and mainly produced from bentonite, which is a naturally occurring aluminium phyllosilicate formed by the in situ alteration of volcanic ash as well as ancient oceanic ashes. Bentonite is an impure clay producing typically different classes of subclays namely montmorillonite, hectorite, illite and kaolinite. From these, montmorillonite has become overwhelmingly the nanoclay source mostly used in a broad variety of polymeric nanocomposites. Montmorillonite belongs to the smectite group of clays, which are generally defined as hydrous aluminium silicates containing iron and magnesium as well as either sodium or calcium. More particularly, montmorillonite consists of ~ 1 nm thick aluminosilicate layers surface-substituted with metal cations and stacked in ~ 10 µm-sized multilayer arrays [22-23]. Depending on surface modification of the clay layers, montmorillonite can be dispersed in a polymer matrix to form a polymer-clay nanocomposite. The optimal incorporation of nanoclays within the polymer matrix is called exfoliation, which consists in having the individual nm-thick clay layers fully separated and forming plate-like nanoparticles fully dispersed with different orientations, hence providing a very high (nm × µm) aspect ratio [24-25].

¹ The global consumption of Carbon black and Metal Oxides are not strictly considered as nanocomposite consumption for the reasons explained earlier in this section regarding the range of particle size and the non-polymeric applications respectively.

Polymer/clay hybrids have been used commercially since Toyota introduced the first auto parts using this technology in the 1980s. Currently, organically-modified nanoclays (organoclays) are becoming very popular as an attractive class of hybrid organic-inorganic nanomaterials with potential uses in polymer nanocomposites, as rheological modifiers, gas absorbents, flame-retardant and drug delivery carriers [26-28].

Besides nanoclays, silicon is also the base material for a range of nanoparticles with different morphologies such as nanowires, nanospheres, quantum dots, mesoporous silica and polyhedral oligomeric silsesquioxanes (POSS).

Silicon *nanowires* would be the analogues to carbon nanotube materials, and are beginning to be used in applications including field-effect transistors [29], photovoltaics [30], sensors [31], lithium batteries [32] and catalysts [33]. Silicon *nanospheres* have been found to give outstanding results in terms of hardness with diameters of between 40 and 100 nanometres, whereby their properties were not just harder than silicon but among the hardest materials known, falling between sapphire and diamond [34]. Alternatively, silicon nanospheres have shown in laboratory conditions to have the capacity to generate hydrogen 1,000 times faster than similar reactions using bulk silicon, hence giving encouraging potential in clean energy applications [35].

Silicon *quantum dots* are having an increasing presence in photovoltaic cells, electronics and biomedical applications [36], and silicon *mesoporous nanofilms* have been successfully functionalised for multiple applications in medicine and chemistry [37].

Polyhedral oligomeric silsesquioxanes (POSS), the focus of this thesis, have become more popular in the recent years within the nanocomposite engineering community. POSS are nanosized silica cage structures that are generally represented by $(\text{RSiO}_{1.5})_8$, where R can be functionalised with a broad variety of organic groups. These nanostructured skeletons use silicon atoms linked to said functional groups that are able to react with covalent bonds and

link to a broad range of organic groups providing different functionality, solubility, polarity and reactivity depending on the group chosen. The bottom line is that the addition of POSS can provide notable improvements in thermal stability, oxidation resistance, viscosity and lower flammability [38-43]. Being the focus of this dissertation, chapter 2.3 will cover more extensively the description and characteristics of this unique nanoparticle type.

Cellulose: There is also an important source of nanoparticles and nanofibres in wood. Cellulose chains aggregate to form *nanofibrils*, which are long threadlike bundles of molecules stabilised laterally by hydrogen bonds between hydroxyl groups and oxygens of adjacent molecules. Depending on their origin, the nanofibril diameters range from 2 to 20nm for lengths that can reach several tens of microns. These nanofibrils consist of monocrystalline cellulose domains with the nanofibril axis parallel to the cellulose chains, and have an estimated modulus of 150 GPa and a strength of 10GPa [18].

1.3.4. NANOCOMPOSITE SYSTEMS

In materials research, the development of polymer nanocomposites (PNC) is rapidly emerging as a multidisciplinary research activity whose results could broaden the applications of polymers to the great benefit of many different industries. PNC are polymers (thermoplastics, thermosets or elastomers) that have been reinforced with small quantities (usually less than 5% by weight) of nano-sized particles having high aspect ratios ($L/h > 300$) [44]. According to IUAPC (2007), and consistent with the definition of nanoparticle covered in the previous chapter, a nanocomposite is a composite in which at least one of the phase domains has at least one dimension of the order of nanometres. In turn, a conventional composite is defined as multi-component material comprising multiple, different (non-gaseous) phase domains in which at least one type of phase domain is a continuous phase in the order of microns or above [45].

Today's scientists and engineers are finding a wide variety of ways to see and control individual atoms and molecules in the range of 1 to 100 nanometres to customise the intrinsic characteristics of thermoplastic materials to an unprecedented degree, allowing them to deliberately make materials at the nanoscale and take advantage of combining the properties of traditional organic polymer systems (i.e. processability, toughness, lighter weight, cost) with the properties of inorganic compounds² (i.e. strength and thermal/oxidative stability, among others) resulting in generally superior hybrid materials when compared to their traditional larger-scale fillers in macrocomposites [38-43].

For the above reason Nanotechnology applied in engineering materials has been gaining interest over the last years and is already being used in a broad variety of applications going from, to name a few, medical, industrial, automotive and military products. The global consumption of nanocomposites in 2010 reached an estimated 118,768 metric tons with a value of over \$800 million [8].

² Note there are exceptions to this general approach with the incorporation of organic cellulose nanoparticles into the host polymer [18].

1.3.5. THERMOPLASTIC NANOCOMPOSITES PREPARATION TECHNIQUES

Thermoplastic nanocomposites can be prepared by means of various processes aiming to incorporate the nanofiller into the base material. The most frequent methods fall into the category of **blending** as a simple and less expensive, yet not always effective, and **grafting** or **copolymerisation**, both with higher process complexity but rewarded by higher rates of success [39, 42-43, 46-49]. This section goes through the different specific incorporation methods from the above categories used in the preparation of nanocomposites.

1.3.5.1. Melt Blending

Melt blended nanocomposites are based on incorporating the nanoparticle into the polymer matrix by means of conventional processing methods used for polymer compounds and traditional microcomposites such as single screw extruders, counter-rotating twin screw extruders (preferable), and internal mixers (for lab scale purposes). This involves shearing the nanoparticles and the polymer in the melt, at a temperature equal or greater than the melting point of the polymer so that the material disperses to the desired extent. The major variables to take into account from the equipment and process point of view are: design of screw, length and position of mixing zone, screw length, melt temperature, residence time of melt and shear.

Under suitable conditions, extrusion is usually a very fast method and has blending times of the order of minutes, and therefore results in high output with relatively small and basic equipment. Generally no organic solvents are used, hence its low environmental impact [51]. The above constituencies make melt blending the most commonly used technic because of its efficiency, operability, versatility, inexpensiveness and environmental containment [50-51] and numerous matrices with a range of nanofillers have been already studied over the last decade i.e. PP [52-61], PE [62-68], PS [69-71], PMMA [71-72], PC [71,73], PET [74-76], PA6 [77-80], PA66 [81], EVA [82-83], LCP [84-85] and POM [43,49].

The major challenge of this approach is achieving a homogeneous dispersion of the nanoparticles in the polymeric matrix due to their tendency to agglomerate, and therefore successful nanocomposite melt blending requires very careful design of the processing conditions. In addition to the equipment choice and processing variables mentioned above, the choice of proper compatibilising agents and nanoparticle functionalization is of paramount importance to succeed, along with constant monitoring and strict control of the resulting material properties during trial periods to define the most adequate processing conditions [51].

Indeed the above challenges also apply to POSS nanocomposites prepared via melt blending methods, which applies to this thesis, making the achievement of chemical-physical interactions between the POSS and the matrix of paramount importance. In addition to the processing conditions mentioned earlier, this pursuit also relies greatly on the tailorable organic groups covalently attached to the Si-O cage.

More particularly, the great differences in the properties of polymer and silica materials can often cause phase separation, particularly when added with a poor dispersion during the preparation and melt-blending process. These conditions can easily allow the silanol groups residing on adjacent particles to strongly interact with each other by means of hydrogen bonding and lead to the formation of aggregates in the form of strong loosened clusters of particles, which remain intact even under the best mixing and shearing conditions [87]. Once mixed, agglomerates may cause an adverse impact on the nanocomposite properties, sometimes resulting in lower properties than the pristine polymer matrix or conventional particle/polymer systems.

A representation of a POSS agglomerate setting within a polymeric matrix is depicted in the following Figure 6.

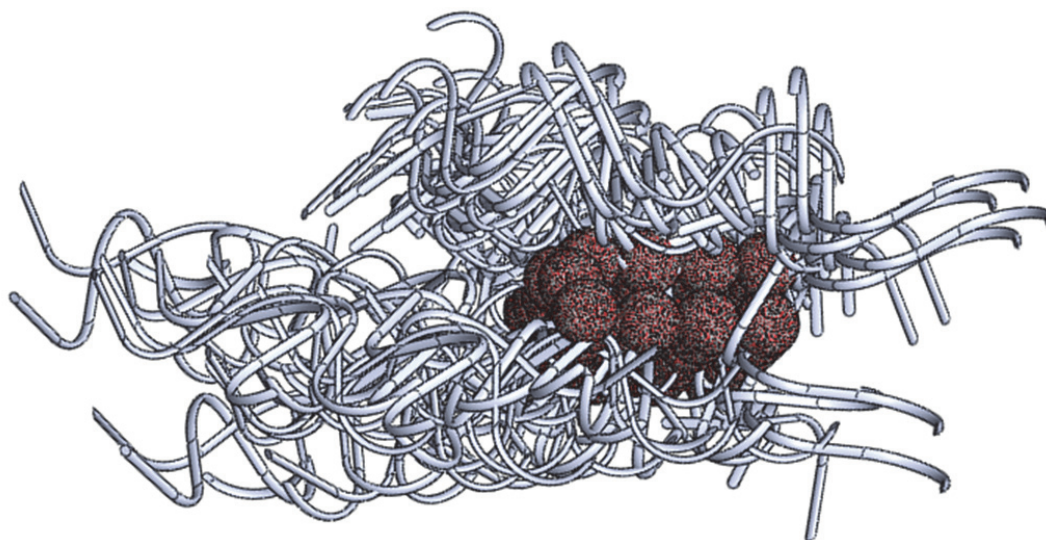


Figure 6: Agglomerated POSS (represented as spheres for simplicity) in a polymer matrix.

1.3.5.2. Solution Blending

Solution blending is a liquid state powder processing method that brings about a good molecular level of mixing and is widely used in material preparation and processing. In this method, fillers are added to a polymer solution using solvents such as toluene, chloroform and acetonitrile to integrate the polymer and filler molecules [88]. Contrary to the limitations of melt mixing method, and with the proviso the solvent is adequately formulated to be effective with all constituencies involved, solution blending can effectively dissolve and disperse high concentrations of POSS, with extreme cases of up to 75%(wt) of nanofiller successfully prepared with this method [89]. The downside of solution blending, however, is the added cost of the adequate solvent and its recovery after processing the nanocomposite [90-91] as well as the not environmentally friendly usage of solvents.

Literature of POSS nanocomposites prepared with this method can be found with polystyrene (PS) [89, 94-95], poly(methyl methacrylate) (PMMA) [89], poly(isobutyl methacrylate) (PIBMA) [89]. Other examples of silica nanoparticles incorporated via solution blending can be found with PA6 with silica filler particles [92], and PEO/Silica nanocomposites [93] to name a few. The aforementioned literature corroborates the fact

that in order to achieve optimal interaction between nanofiller and matrix, the solvent has to provide adequate compatibility with the constituencies of the nanocomposite.

1.3.5.3. Reactive blending through radical grafting

Whereas melt blending usually leads to physical interactions between polymer and POSS, it does not provide the right conditions to trigger the chemical reactions necessary to covalently bind the nanofillers into the matrix. Radical grafting is a reactive blending approach that provides such conditions and by that, it becomes a method with a higher effectiveness to produce new and improved properties to the resulting nanocomposite. This approach is widely used for the compatibilisation of immiscible polymer blends [96-97] or for the preparation of functional polymers [98-99]. Within this approach, there are different techniques to activate and/or enhance the reaction, including thermal, irradiation, photochemical and plasma treatments.

Most of the research work so far for this method is focused on polyolefins, in which free radical grafting processes have been widely studied in order to obtain functionalisation and consequently better compatibilisation by means of various organic groups including maleic anhydride, acrylic, methacrylic and vinyl species [100-103], as well as POSS [51, 104-105]. Additionally, alternative methods have also been studied for the control of the radical mechanism as well as for the reduction of side reactions, including the use of coagents [106-107], advanced radical promoters [108] and atom transfer radical polymerisation [109].

In POSS reactive blending through radical grafting, the polymer is blended in the presence of a free radical initiator and resulting to a partial POSS grafting onto the thermoplastic chain. The assessed documented experience of POSS nanocomposites prepared with reactive blending [42, 51, 104-106, 110-112] provides an insight of the characteristics obtained with this method. The mechanical properties and crystallisation behaviour of these nanocomposites are strongly affected by bound POSS, leading to a higher modulus and to a significant increase in nucleation rate [105]. The rheological properties are also affected, such that the viscosity of the reactive blending composites is found to increase with

increasing POSS content [110]. This behaviour differs greatly to that of nanocomposites prepared with physical blending, whereby it is common to see the viscosity drop at low POSS content (0.5-1%) due to a plasticisation effect, but with increasing viscosity at higher concentrations.

Zou et al. [42] compared also the thermal properties of a PP-POSS system prepared with physical blending and reactive blending, demonstrating that the latter hybrids had better thermal stability than the former. POSS grafting on PP was also explored by in situ γ -ray radiation on previously prepared PP-monofunctional methacryl POSS blends [111-112]. Radiation induced grafting of POSS was confirmed by FTIR, proving a complete and thorough reaction of all POSS particles resulting in an increase of the mechanical properties.

The main limitations of free radical reactions is the propensity of having undesired side reactions such as polymer degradation and POSS homopolymerisation, and accordingly this method requires a high degree of pre-evaluation study and constant monitoring of the process conditions. Although there is currently increasing literature on POSS radical grafting, further research on this area is necessary to fully understand and reliably tailor the reactive blending conditions with minimum side effects.

1.3.5.4. Polymerisation methods: In Situ Polymerisation and Copolymerisation.

Polymer reactions in POSS nanocomposites are based on using the POSS units acting as monomers for a subsequent polymerisation with the host polymer, with the capability to further polymerise with additional monomeric constituencies to become part of a copolymer system. The functionalization of the POSS particle plays an important role on the polymerisation capabilities, not only from a qualitative but also from a quantitative point of view. Indeed, **monofunctional** POSS can be utilised as a polymer modifier to be directly incorporated onto polymer chains [113], but it can also perform as a polymerisable substituent entity to further copolymerise with the host polymer, e.g. methacrylate-POSS

acting as a monomer in copolymerisation with other acrylate monomers [114]. Polymer/POSS hybrids have also been prepared through ring-opening metathesis polymerization (ROMP) using a norbornene-POSS compound as a monomer [115]. **Difunctional** POSS derivatives typically serve as monomers in polycondensations to prepare polymers possessing POSS pendent groups. One example is preparation of polyimide/POSS hybrids using a diamine-POSS as a comonomer [116]. A difunctional POSS-containing trifluorovinyl ether was also utilised in a thermal polymerisation to prepare POSS-perfluorocyclobutyl aryl ether copolymers [117]. On the other hand, **multifunctional** POSS derivatives are widely used in preparation of crosslinked polymer/POSS nanocomposites. Further details and examples of in-situ polymerisation and copolymerisation are explained below.

In-Situ Polymerization is an especially effective way to construct a nanocomposite material whereby the filler is added directly to the liquid monomer during the polymerization stage and stirred under specific conditions of temperature and time. The polymerisation can be initiated either by heat, radiation or by the diffusion of an initiator [118].

Usually the monomer is very fluid and allows impregnation without undue or disturbing the nanoparticle arrangement. After polymerisation, the material is finished with little necessary finishing consisting in removing the unreacted monomer in a solution and filtrated. Different synthetic routes have been developed, including **free radical polymerisation**, **polyaddition**, **polycondensation**, and **ring-opening metathesis polymerization (ROMP)** [119].

Examples of POSS nanocomposites prepared via *in situ* polymerisation can be found with PET/POSS, where the nanofiller was dispersed via sonication with ethylene glycol to become the initiator in the polymerisation reaction with dimethyl terephthalate (DMT), resulting in higher mechanical and thermal resistance properties in those nanocomposites with low POSS content i.e. 1%, and lower properties in those with higher POSS content i.e. 5% [120]. Different PS/POSS nanocomposites were prepared with an initial solution of PS monomer with various POSS resuming to a radical initiation polymerisation resulting in good dispersion

and generally noticeable improvements in thermal resistance properties [121-123]. PBT/POSS was prepared with an initial synthesis of POSS to make it act as initiator to subsequently polymerise it with the cyclic butylene terephthalate oligomer via ring opening and resulting in a more thermally stable nanocomposite [124]. PTT/POSS was prepared with the nanofiller mixed with dimethyl terephthalate (DMT) and 1,3 propanediol (PDO) via ball milling and placed in a autoclave prior to adding the catalyst and resume the polycondensation process. Successful results were obtained with both the nanofiller dispersion and the properties enhancement of the nanocomposite [125]. PA6/POSS was prepared by Ramasundaram et al. with limited improvements on the thermal resistance despite the good incorporation of the POSS nanofillers [126] and Ullah et al. prepared nanocomposites based on (Ti)POSS and two polymer matrices, i.e. PA6 and a PSMA (styrene-maleic anhydride) by three different approaches being in situ polymerization, melt blending and grafting, and investigated the dispersion level of (Ti)POSS within the organic polymer matrices [127].

Copolymerisation is based on the same methods applied for In Situ Polymerisation, whereby the POSS particles are initially synthesised as either homopolymer or copolymer with another monomer under specific conditions of reagents solution, stirring, temperature, time, precipitation, filtering and drying. Once this initial fraction is concluded, it is further copolymerised with the host polymer with similar procedures i.e. **free radical solution, condensation** and **ring opening metathesis (ROMP)**.

Examples of POSS nanocomposites prepared with copolymerisation methods can be found with PE/POSS with an initial POSS-norbornylene homopolymerisation followed with a copolymerisation with Cycloctene [128], PS/POSS nanocomposites with an initial styrene + POSS + methylaluminoxane homopolymerisation followed with a copolymerisation with CpTiCl₃ [129], PMMA/POSS with an initial POSS + MMA solution followed with a free radical copolymerisation with the corresponding reagents and initiator [114] and PI-MMA/POSS

copolymerisation with an initial cross-linking process of a multifunctional MMA-POSS followed with a copolymerisation with PI [130].

1.3.5.5. Other Blending methods

Despite the different common alternatives explained previously, some combinations of nanofillers and polymeric matrix may still exhibit difficulties to achieve proper dispersion. This is usually due to a high particle load, high polymer melt viscosity or high insolubility between components. One way to overcome these problems is to process the polymer in the solid state, which avoids the thermal and solvent problems encountered with traditional technologies while providing almost infinite design flexibility and processing simplicity. **Cryogenic mechanical alloying** or cryogenic ball milling (cryomilling) is such a solid-state method that can effectively improve blending intimacy and enhance compatibility [131]. Li et al. [132] prepared PET/SiO₂ nanocomposites by cryomilling. The process consisted of a three-stage model, whereby the first step consisted in a dramatical reduction of particle size and the transformation of PET from big blocks into flakes, meanwhile the SiO₂ conglomerations were broken up into smaller particles and submitted to a first stage of dispersion, forming primary composite particles of about 400nm in size. The second stage consisted in a further gradual dispersion of single SiO₂ nanoparticles into PET flakes, and the formation of secondary composite particles due to the conglomeration of the refined PET/SiO₂ system resulting in agglomerates of about 7.6µm in size. The third stage was characterised by the constant size of the secondary composite particles and the further homogeneous dispersion of nanometre SiO₂ in PET matrix. It was shown that upon cryomilling for 10h, SiO₂ nanoparticles were well separated into single particles (≈30nm) that get homogeneously dispersed in the PET matrix. This method has proved to provide dispersion homogeneity far beyond the capabilities of conventional methods, and consequently the improvement in mechanical and thermal properties was likewise notable. The main factors contributing to this success were the high mechanical energy of ball milling acting upon a solid state material thanks to the cryogenic processing temperatures. A similar

experience with PMMA/SiO₂ nanocomposite was reported by González-Benito et al. [133]. It is worth noting, however, that this method is still very costly and currently only workable at laboratory scale.

Another promising approach to achieve nanocomposite blends with thorough nanofiller dispersion is ***thermal spraying***. This method was originally conceived for high performance coatings, and consists of a process whereby the material is heated, accelerated and propelled by a high temperature jet through a confining nozzle toward a surface. The individual molten or softened droplets impact, spread, cool, and solidify to form continuous coatings. High-velocity oxy-fuel (HVOF) provides thermal energy for heating by combusting fuels with oxygen. Petrovicova et al. [134] produced nylon 11 coatings filled with nanosized silica using the HVOF combustion spray process following a ball milling preparation similar to the one explained in the previous paragraph. Powders were prepared for spraying by dry ball-milling nylon 11 together with the nanoparticulate phase for 48h in a ball mill using zirconia balls to create a composite powder. The composite powder aided both the distribution of the filler in the coating and the simultaneous powder feeding into the HVOF spray jet.

1.4. THERMOPLASTIC THERMAL DEGRADATION

This section covers the different mechanisms of thermal degradation in thermoplastic polymers in order to contextualise the deterioration process inflicted on the samples analysed in this work, which have been degraded under thermo-oxidative aging conditions through oven-storage. With a special focus on the polyoxymethylene (POM) and Acrylonitrile-butadiene-styrene (ABS), this section will also provide the reader with a basic understanding of the common thermal degradation routes that can occur in thermoplastic materials.

1.4.1. THERMAL DEGRADATION MECHANISMS

The heat stability of polymers is highly dependent on the bond energy of the chemical linkages present; hence the strength of the weakest bond in the polymer chain is the factor that usually limits its thermal stability. The thermal degradation can follow three major pathways depending on the polymer nature i.e. chain scission (random or end-chain), side-group elimination and depolymerisation. That said, oxidation also plays an important role in the thermal degradation process, therefore it is also covered in the following section.

1.4.1.1. Chain scission (random or end-chain):

Chain scission involves the cleavage of a carbon-carbon bond in the backbone of the polymer to generate two radicals. This may be initiated at random positions throughout the polymer and give rise to a monomer and oligomers or it may be initiated strictly at the ends of the

chain, causing the so-called end-chain scission. End-chain scission results in the exclusive formation of a monomer and is initiated at unsaturated chain ends [135].

Accordingly, random scission involves the production of free radicals along the backbone of the polymer, which causes the macromolecule to be fragmented into smaller molecules usually differing in chain length by the number of carbons. One of these radical centres typically with a methylene group, a primary radical, while the other will be likely on a carbon that results in a secondary or tertiary radical, regardless of the substituents present in the polymeric unit. The reactive primary radical ordinarily will abstract hydrogen from a neighbouring intramolecular position to give a more stable secondary or tertiary radical, or it may also abstract the hydrogen from a close intermolecular position of another polymer strand to do likewise. This new secondary or tertiary radical can then undergo further degradation, typically by the formation of a new primary radical and an unsaturated species. The thermal cracking of hydrocarbons leading to the splitting of the carbon-carbon bond and thus forming free radicals is commonly known as β -scission and its mechanism can be represented as per Figure 7 below [135-136].

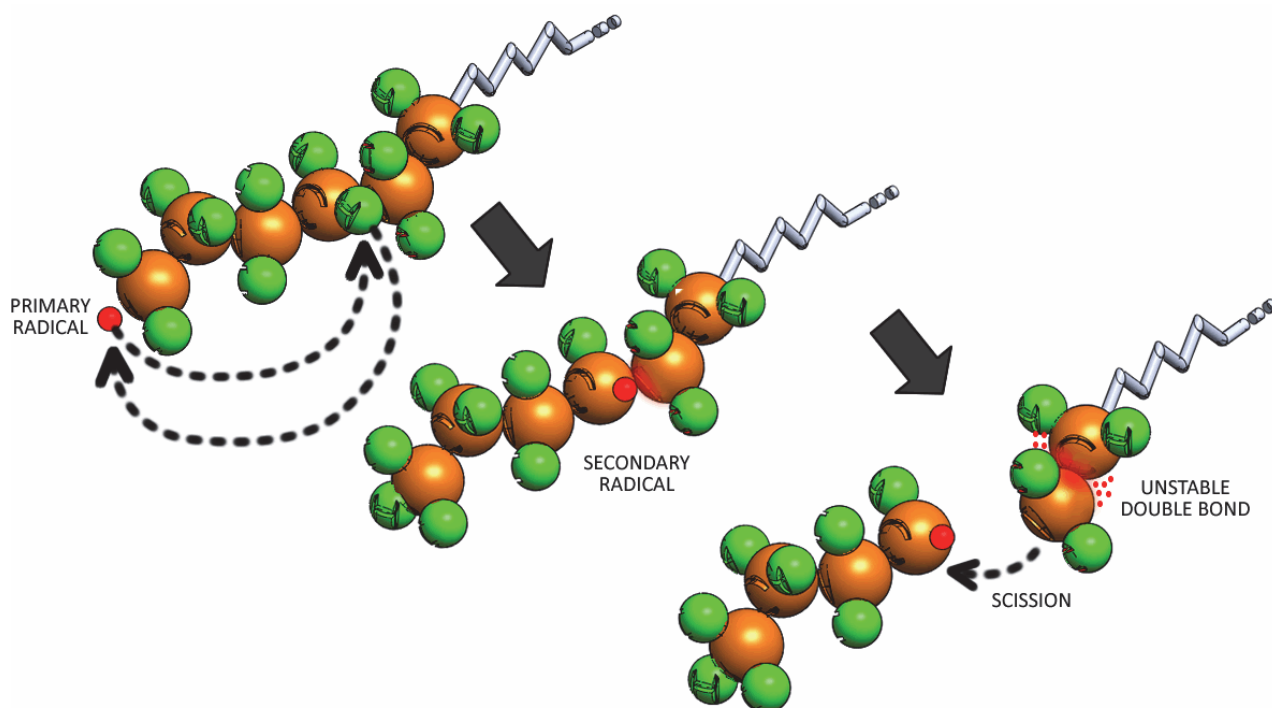


Figure 7: Intramolecular hydrogen transfer and β -scission process

End-chain scission occurs when hydrogen transfer is inhibited, for instance, if the substituents adjacent to the primary radical site are groups other than hydrogen atoms. One method to differentiate between end-chain and random scission is based on the identification of the products generated during degradation. If only monomer is produced, it is quite likely that only end-chain scission has occurred. [135]

If such chain scission events are repeated successfully in a polymer and its degradation products, the backbone splits into fragments that break again into smaller fragments and so on, resulting in a decrease in molecular weight and ultimately weight loss whereby the degraded products have a broad range of carbon number and become small enough to evaporate without further cleavage. This statistical fragmentation of the polymer backbone can be initiated not only thermally but also by chemical, radiation or mechanical activation. [135-136]

1.4.1.2. Side-group elimination (or chain stripping process)

Groups that are attached to the side of the backbone are held by bonds which are weaker than the bonds connecting the chain. Heat can trigger the side groups to be stripped off from the chain before it is broken into smaller pieces.

Side-group elimination generally takes place in two steps. Firstly, side groups attached to the backbone of the polymer are cleaved, leaving an unstable polyene macromolecule i.e. an unsaturated hydrocarbon chain containing one or several carbon-carbon double bonds (see Figure 8 below). Secondly, the unstable polyene fraction undergoes further reactions, including scission into smaller fragments, the formation of char or the formation of aromatic molecules such as benzene, toluene and naphthalene (also called aromatisation) [135-136].

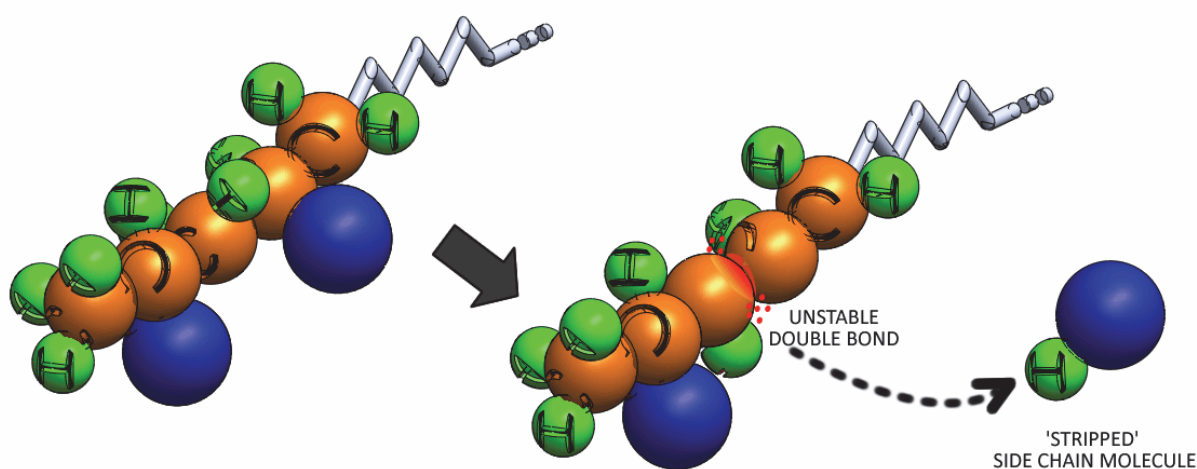


Figure 8: Chain stripping process

1.4.1.3. Depolymerisation (also known as unzipping or depropagation)

Depolymerisation is a free-radical mechanism, such that the polymer is degraded to the monomer or comonomers that the (co)polymer was initially made of, i.e. the mechanism according to which monomeric units split off from the end of the polymeric chain is the reverse mechanism to polymerisation. The formation of a free radical on the backbone of the polymer causes the polymer to undergo scission to form unsaturated small molecules and propagate to the free radical on the polymer backbone until the equilibrium between monomer and polymer at a given temperature is reached in a closed reaction system. Figure 9 below depicts this process in a very simplified fashion. The mechanism of depolymerisation can occur under the same conditions (high temperature) as the chain scission [135-136].

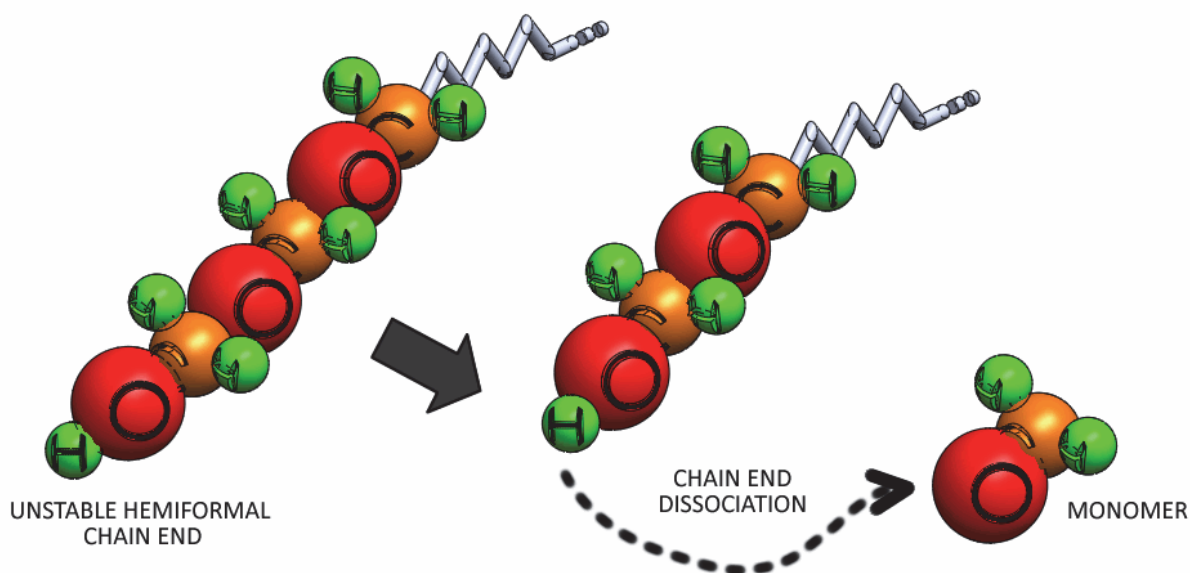


Figure 9: Depolymerisation process

1.4.1.4. Cross-linking (or chain branching, recombination)

The main degradation process of the polymer can sometimes co-exist with ongoing cross-linking of degraded molecules as depicted in Figure 10 below [137]. This phenomenon is typically caused by the macro-radicals produced during the chain scission of the degradation process, which have the potential to react with each other giving rise to cross-linking (or branching) as depicted in the schematic below [138].

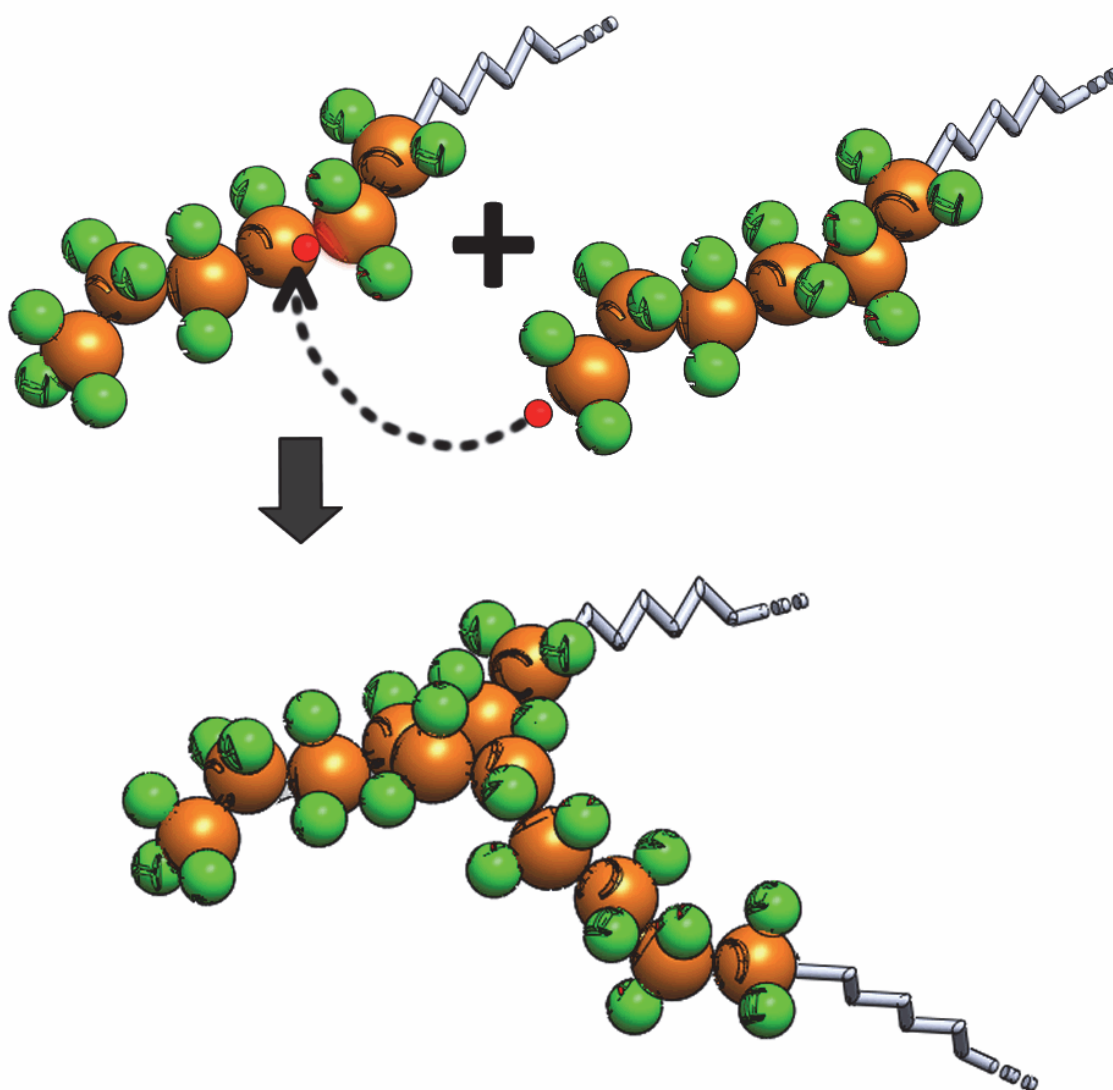


Figure 10: Cross-linking process

1.4.1.5. Thermoxidative degradation

While polymer degradation is often studied in inert atmospheres, the involvement of oxygen plays a very important role in the degradation kinetics. From the representability point of view, thermoxidation is also more realistic approach, as most of thermal degradation failures in real applications occur in oxygen environments. Oxidative degradation is characterised by random scission in the polymer backbone, beginning via an initiation step which produces the radical precursors following the following events whereby RH would represent the original polymer molecule and R* the radical precursor originated in the initiation step: [135, 139]



Figure 11: Initiation

Initiation may be induced by physical (e. g., temperature, UV radiation, mechanical treatment) and/or chemical factors (e. g., traces of initiators such as peroxides and hydroperoxides used). When oxygen is allowed to react with the newly formed chain radical (R*), a peroxy radical (the bivalent group $-\text{O}_2-$, represented as ROO* below) is produced during the propagation step.

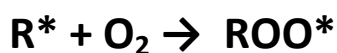


Figure 12: Propagation

This highly reactive ROO* then abstracts a labile hydrogen from another polymer molecule giving rise to the hydroperoxide species ROOH, as well as another polymer radical R*, through which the process can continue.



Figure 13: Continuation

1.4.2. POLYOXYMETHYLENE THERMOXIDATION MECHANISM

There is a general agreement that standard POM has a low thermal stability and typically undergoes depolymerisation at processing temperatures above 150°C with relatively short induction times [140-142]. Both neighbouring oxygen atoms exert a labilising effect³ on the methylenic hydrogen atoms. This explains clearly why they are highly sensitive to free radical attack and subsequent oxidation [143]. It is also understood that POM degradation initiates either by bond dissociation at chain-end for POM hydrate, or by random main-chain scission for the end-capped polymer followed by unzipping [144-145]. Usually decomposition takes place by the random law, yielding products such as formaldehyde (H₂CO) at the initial stages of degradation following the mechanism below:

- a) **Initiation step:** Unstable hemiformal chain-end dissociation producing formaldehyde by-product.

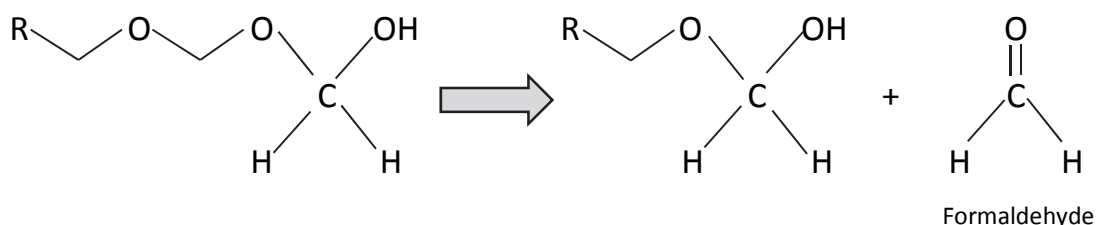


Figure 14: Evolution of formaldehyde at the early stages of degradation starting at unstable chain-ends.

- b) **Propagation step:** Random chain-scission accelerating degradation rate with rapid formation of formaldehyde gas, which increases the concentration of hemiformal end-groups. This process occurs simultaneously with certain degree of ordinary thermal degradation at chain ends.

³ Labilising effect: A reduction in the activation energy and an increase in the rate of reaction, making the polymer more prone to chemical reactions [146].

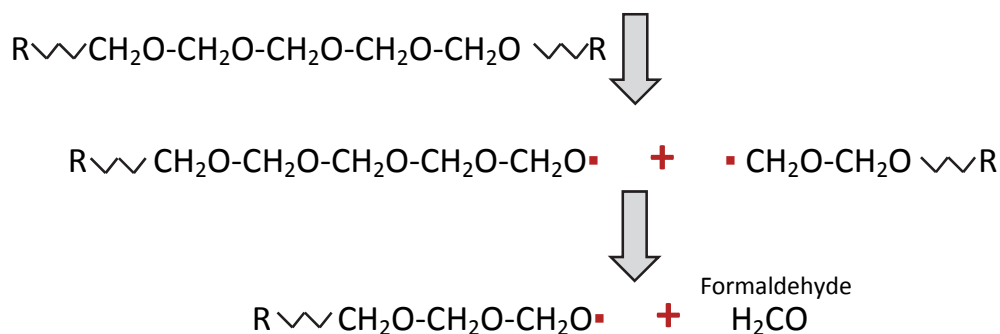


Figure 15: Formation of formaldehyde gas by main chain cleavage.

Indeed the presence of oxygen during the thermodegradation process plays a crucial role in accelerating the overall reaction. The high reactivity of the etheric methylene groups to abstract hydrogens by radicals results in a relatively easy oxidation initiation [147]. Radical chain oxidation is deemed to generate hydroperoxides (-OOH), which are responsible to autoaccelerate the degradation kinetics upon their inherent self-decomposition process reported to occur above 160°C [148] and interaction with the methylene groups, causing chain scission followed by the formation of formaldehyde [148-149].

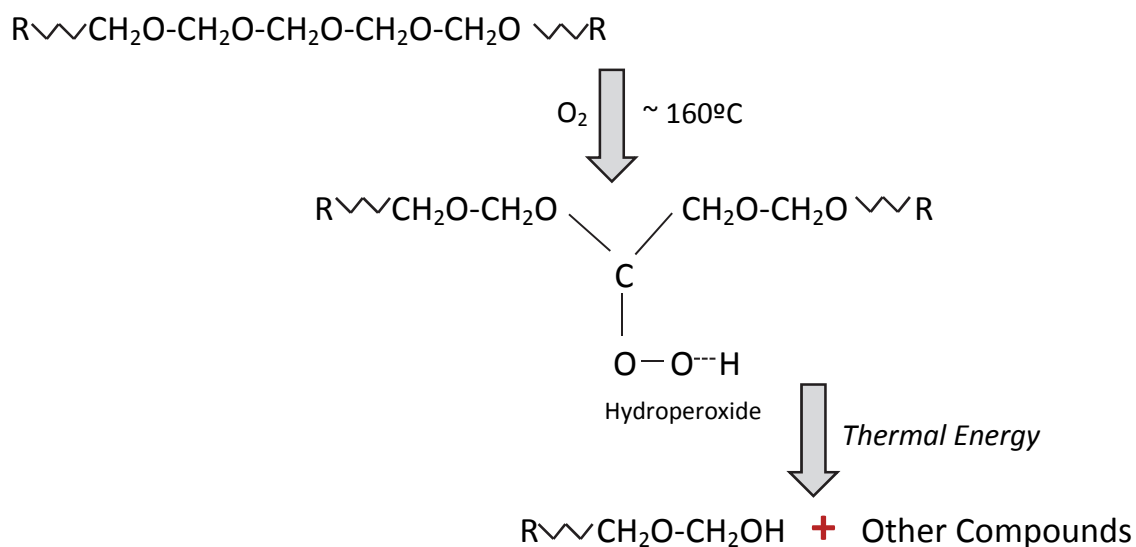


Figure 16: Thermoxidative degradation of POM forming hydroperoxide groups.

Furthermore, oxygen has the ability to transform the formaldehyde monomer into formic acid (CH_2O_2), which acts as a catalytic element for rapid depolymerisation at only moderate temperatures by a zipper mechanism yielding the monomer again through the so-called acidolysis [142-143, 150]. Additionally, another reaction with acid, the transacetalisation, can occur with the formation of cyclic compounds or new linear POM chains, and the ongoing oxidation of formic acid can evolve to water and carbon dioxide. [151].

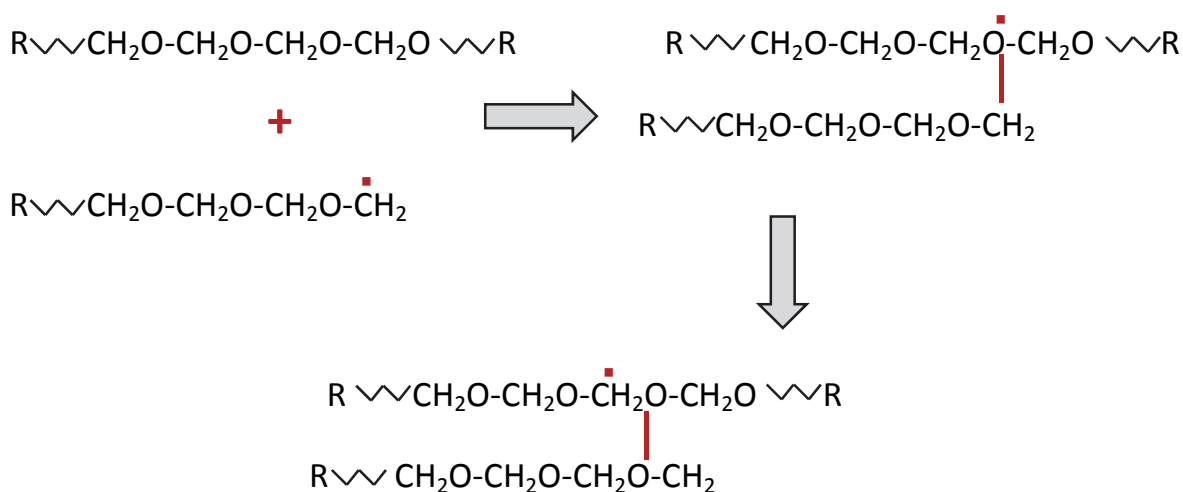


Figure 17: Formation of cyclic compounds via transacetalisation

The tendency of POM to depolymerize is reduced in commercial products by means of a variety of stabilization methods, being the following some common approaches found in the literature:

- a. End-Capping: By conversion of unstable hemi-acetal hydroxyl ($-\text{O}-\text{CH}_2-\text{OH}$) end groups to stable acetate (e.g. CH_3CO_2^-), ether ($\text{R}-\text{O}-\text{R}'$) or acetyl (COCH_3) groups [185-186]. This process is also called acetylation [143].

- b. Radical scavenging: Copolymerisation of formaldehyde with a phenyl from a hindered phenol or a cyclic ether such as trioxane ($C_3H_6O_3$), 1,3-dioxolane ($C_3H_6O_2$) or ethylene oxide (C_2H_4O), which make the degradation driving processes to be decelerated or even stopped at the first comonomer unit [143, 148, 152].

- c. Occasional incorporation of molecules containing two successive methylene groups ($-CH_2-CH_2-$), which reduces the tendency of the molecules to unzip as they act as stoppers for the depolymerisation reaction [142-145, 153].

However, even stabilised polyacetals are prone to degradation because of their native structure and thermo-oxidation with stabilized end-groups is also initiated by random main-chain scission once the stabilising compounds are consumed [154].

Thermal degradation and oxidation of polyoxymethylene up to the melting temperature has received fair amount of attention in recent years. The papers found have been concentrated on the mechanism of POM degradation with stabilised and unstabilised end groups through the course of a variety of thermodegradation processes. The analytical methods used in the literature range from with IR spectra, weight loss progress, sample viscosity, oxygen uptake, molecular weight, morphological structure and degree of crystallinity at the different stages of degradation [148, 154-157].

Notwithstanding the above background in the field, it is found that the degradation of POM at and above processing temperatures has been a subject of minor interest. These extreme and usually unintended conditions do occur in accidental events such as long remaining times in the processing barrel, hot-runner systems and temperature-related malfunctions in the equipment used during the manufacturing as well as the end-use product.

1.4.2.1. POM yellowing mechanism

As in many organic compounds, yellowing is caused by the formation of chromophores. Chromophores are molecular regions where the energy difference between two different molecular orbitals falls within the range of the visible spectrum, hence making them responsible for generating colour.

As a result of the chemical reactions involved with the degradation process of polyoxymethylene and its stabilisers, the chromophores appear in the form of carbonyl groups derived from the production of by-products such as CO, CO₂, HCOOH and CH₃OCHO [158].

The above discussion is only intended to provide a general background on the yellowing phenomena, and the chromophore behaviour as well as the effects of nanoparticles to them goes beyond the scope of this dissertation, as it implies further analysis on the chromophore yield, size and how it bonds to the POSS molecules before and during the thermo oxidation process.

1.4.3. ACRYLONITRILE-BUTADIENE-STYRENE THERMOXIDATION MECHANISM

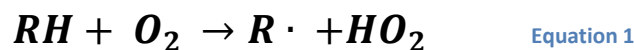
As mentioned earlier, ABS consists of a bimodal polymer system of polybutadiene particles dispersed in a styrene-acrylonitrile copolymer (SAN). Most aliphatic compounds are oxidised by the atmospheric oxygen below 200°C via a free radical chain process, and isolated non-stabilised polybutadiene containing both the unsaturated and the allylic hydrogen is reported to oxidise at even lower temperatures [159].

A more recent work has applied the TG-FTIR technique to investigate the degradation behaviour of ABS as well as its constituent polymers, namely PAN, PB, SAN and PS. The investigation demonstrated that the evolution of butadiene constituency commenced at 340°C in a limiting oxygen environment, the one corresponding to styrene at 350°C, and the one for acrylonitrile began at 400°C, being the degradation by-products ammonia and hydrogen cyanide in the gas fraction [136, 160, 161].

Other thermal degradation studies on ABS have shown that the kinetics and mechanisms of degradation highly depend on the chemical structure of each particular ABS copolymer [162-163], and successful thermal enhancements have been found in more sophisticated grades grafted with methacrylic acid [160] and binary copolymers based on polyacrylonitrile and styrene-acrylonitrile [164]. With the above, there is a general agreement that the weakest constituency of the ABS terpolymer is the butadiene fraction [159, 165-166].

Although the thermoxidation mechanism of ABS can be complex due to the multiple terpolymeric combinations available, in a perhaps over-simplified way ABS is reported to follow a chain-end and random scission mechanism [159, 167] as per following steps:

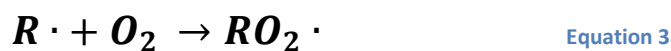
c) **Initiation step:** resulting from the attack of atmospheric oxygen on the polymer RH, as shown in equations 1 and 2 below:



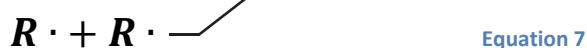
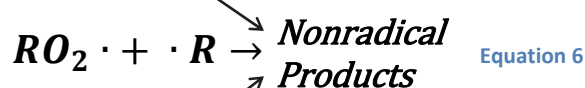
or



d) **Propagation step:** involving the attack of alkylperoxyl radicals on the polymer as shown in equations 3 and 4 below, which describe the oxidation and crosslinking of polybutadiene in ABS. Alkyl radicals are reactive short-lived species which react rapidly with oxygen (first equation below), and the propagation rate is controlled by the second equation.



e) **The termination step:** involves the combinations of free radicals to non-radical products as shown in equations 3, 4 and 5. Since $R \cdot$ is very reactive and low in concentration, the termination rate is controlled by the generation of nonradical products.



1.4.3.1. ABS Yellowing mechanism

Like polyacetals, ABS discoloration, fading and yellowing can be attributed to the formation of photoproduct chromophores during degradation, which arise in the form of conjugated double bond systems(-C=C-)_n. Chromophores absorb energy in the UV visible spectrum and cause discoloration of the resin by absorbing certain wavelengths of visible light and transmitting or reflecting others, hence providing a different colour feature [168-171]. According to the literature, both the PB and SAN phases are found to form chromophores upon oxidation, Kim and Kang [172] studied the mechanical recycling of ABS where all materials turned yellowish, and the colour of ABS specimens with the highest butadiene content were found to change faster than the others; they attributed the dominant variable in ABS colour to butadiene content. Moreover, Tiganis et al. [173] studied the thermal degradation of ABS by ageing at high temperatures. The result obtained was that as the ageing time increased, a brown coloration developed as a consequence of the thermo-oxidative degradation of the butadiene phase, but only at the surface. Accordingly, the initial darkening of ABS was attributed primarily to the degradation of the butadiene phase, which appeared to be consistent with the results found in the FTIR analysis following the butadiene absorbance.

Although the manufacturer of the ABS-g-MA used in this work confirmed the absence of heat stabilisers in the material, it is difficult to ascertain the purity of the ABS matrix in terms of having other types of additives potentially causing additional yellowing over neat ABS. Moreover, the different nanofillers used can also cause additional colour shifting during oven aging as each one of them has its own particular deterioration process and interaction with the host polymer. Nevertheless, as all samples were based on the same ABS-g-Ma, the differences in yellowing are expected to come from the specific POSS degradation process and its influence to the matrix stability.

1.4.4. THERMOPLASTIC DEGRADATION ANALYSIS

The rate and extent of degradation may be monitored by changes in the mass of the sample, its molecular weight, detection and quantification of reaction enthalpy changes, quantitative analysis of reaction by-products and/or measurement of oxygen consumption.

With the above, the methods most commonly used to quantify degradation in polymers are Thermogravimetric Analysis (TGA) [38, 47, 49, 131, 174-179], Differential Scanning calorimetry (DSC) [38, 47, 51, 131, 174-175, 177-178, 180-181], Fourier Transform Infrared Spectrometry (FTIR) [94, 115, 131, 138, 160, 182-185], Pyrolysis Gas Chromatography Mass Spectrometry (Py-GC/MS) [135, 186-188], Thermal Volatilisation Analysis (TVA) [189-192], Matrix Assisted Laser Desorption/Ionisation Mass Spectrometry (Maldi-TOF) [193-195] and Melt Flow Index (MFI) [196-197], among others.

CHAPTER 2
MATERIALS

2. MATERIALS

Since the discovery of polyhedral oligomeric silsesquioxanes in 1946 [198], the ability to prepare useful compounds of this kind has taken more than four decades to come into fruition just in terms of gaining global scientific interest. Although during this period, the papers found on POSS were scarce, it is worth mentioning the work of Voronkov and Lavrent'yev from 1982, which provides an excellent summary of what is now early work in the POSS conception and preparation process [199].

As discussed earlier, the main objective of creating POSS nanocomposites is to achieve chemical-physical interactions between the POSS and the matrix, and the tailorable organic groups covalently attached to the Si-O cage allows, in theory, to target adequate miscibility into organic polymers. The scientific literature covering the effects of POSS on thermoplastic structures has intensified over the last 15 years thanks to the proliferation of a wide range of POSS functionalisations available and the advances in the analytical instrumentation needed to facilitate this work. One of the first papers on this regard was from Schwab et al. in 1998, who studied the incorporation of POSS segments into different methacrylate resins resulting in increased glass transition and decomposition temperatures as well as increased oxygen permeability [200]. Since then, the amount of scientific papers published covering different POSS nanocomposite systems has been rapidly increasing, with particular emphasis on the biggest commodity plastics i.e. PP [52-61], PE [62-68] and PS [69-71], although also on engineering plastics such as PMMA [71-72], PC [71, 73, 86], PET [74-76], PA6 [77-80], PA66 [81], EVA [82-83], and LCP [84-85]. These references only cover POSS nanocomposites prepared via melt-blending incorporation method, hence it represents only a fraction of the current art relative to POSS nanocomposites.

A common denominator that can be drawn from the current literature is that the effects differ notably depending on the POSS reactivity, the nanoparticle dispersion and indeed the organo-functionalisation of the cage in relation to the host polymer constituencies. For

example, T_g is usually reduced with unreacted POSS, typically present in melt-blended systems, but in cases of reactive POSS T_g has been found to increase due to a rebuild in molecular weight. The thermal stability and flammability has been a popular area of interest in much of the literature listed above, with both successful and unsuccessful experiences related to key areas such as solubility, dispersion and agglomeration, generation of free volume and nucleation effects on crystallinity, to name a few.

With regards to the materials studied in this thesis, Illescas et al. studied the effects of different melt-blended POSS nanoparticles (glycidyl, glycidylisobutyl, octaisobutyl and trisilanophenyl) on the morphology and thermal stability of POM. The study concluded that the addition of octaisobutyl and trisilanol POSS reduced the overall thermal stability of the nanocomposite; the incorporation of glycidylisobutyl had negligible effects and only the glycidyl POSS provided benefits from the thermal stability standpoint [49]. In the same year, Sanchez-Soto et al. published the morphology and thermomechanical properties of POM/POSS melt-blended nanocomposites based on the incorporation of glycidylethyl, aminopropylisobutyl, and poly(ethylene glycol), concluding that notable improvements in thermal stability were found in the resulting materials [43]. Both studies highlighted the importance of POSS dispersion within the polymer matrix and the mix concentration.

The literature found on ABS nanocomposites reports successful thermal stabilisation effects of TPP (triphenyl phosphate) nanoparticles [201] as well as ABS/nanoclay systems [185, 202]. No studies have been found, however, on the effects of POSS nanoparticles on ABS systems.

The following sections cover the background, description and characteristics of the materials used in this thesis.

2.1. POLYOXYMETHYLENE

2.1.1. Description

Polyoxymethylene (POM) is a formaldehyde-based engineering thermoplastic, also known as polyacetal or polyformaldehyde. Its chemical structure is based on a linear ether structure $(\text{CH}_2\text{O})_n$ along its backbone, and represents the simplest polymer type within the family of aliphatic polyethers. Polyacetals can be found as homopolymers or copolymers, whereby the former relies on a perfect repetition of the aforementioned monomer $(\text{CH}_2\text{O})_n$, and the latter incorporates a second monomer so the general formula becomes $[(\text{CH}_2\text{O})_n - (\text{CH}_2\text{CH}_2\text{O})_m]$. The molecular mass available for both are ranging from $M_n=20.000$ to 110.000 .

The structures of POM homopolymer and copolymer can be represented as per Figure 18 below [153].

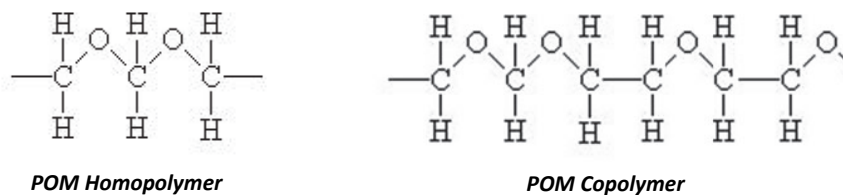


Figure 18: Structure of polyacetal homopolymer and copolymer

2.1.2. Production of POM

The first commercially available polyacetal was marketed by Du Pont in 1959 under the trade name Delrin. This producer has been leading the production of the **homopolymer** type of POM, which was originally based on a condensation reaction of polyformaldehyde and acetic acid (or acetic anhydride) [203]:



Figure 19: DuPont's route for polyacetal homopolymer

Shortly after, in 1962, came Hostaform from Ticona (a subsidiary of Celanese) with the production of the POM *copolymer*, a slightly more stable material based on the reaction of trioxane, a cyclic trimer of formaldehyde, and a cyclic ether (e.g., ethylene oxide as shown below; or 1,3-dioxalane – (CH₂)₂O₂CH₂ [203]):

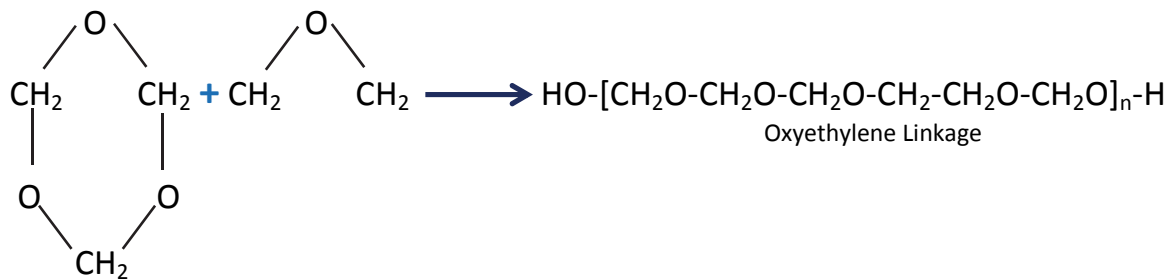


Figure 20: Ticona's route for polyacetal copolymer

2.1.3. POM characteristics and properties

Generally speaking, polyacetals are characterised with high property levels of stiffness, fatigue endurance, toughness, dimensional stability and good resistance to creep, with low coefficient of friction and easy processability.

These general characteristics are further singularised if one looks further at the specific properties corresponding to homopolymers (often referred to as POM-H) and copolymers (often referred to as POM-C). Table 1 in the next page summarises these differences based on unfilled standard references with the most common properties [153]:

	POM-H	POM-C
Specific Gravity <i>ASTM D.792</i>	Higher 1.425	Lower 1.41
Tensile strength <i>ASTM D.638</i>	Higher 70 MPa	Lower 58 MPa
Flexural modulus <i>ASTM D.790</i>	Higher 2800 MPa	Lower 2500 MPa
Deflection temperature <i>ASTM D.792 (0.48MPa)</i> <i>ASTM D.792 (1.82MPa)</i>	Higher/Lower subject to test load 170 100	Lower 158 110
Impact strength <i>ASTM D.256 (notch)</i>	Higher 0.75 - 1.23 J/cm	Lower 0.59 J/cm
Crystalline melting point	Higher 175°C	Lower 163°C
Mould Shrinkage	Higher 1.7%-2.2%	Lower 1.8%-2%
Crystallinity content	Higher	Lower
Thermal resistance	Lower	Higher
Chemical resistance	Lower	Higher

Table 1: Differences in properties between POM homopolymer and copolymer.

Many of the above divergences between POM-H and POM-C are dictated by the degree of crystallinity of each type of polyacetal, whereby the homopolymer clearly has the highest rate (typically 75% to 85%) due to the favourable nature of the (-C-O)- constituent molecule to pack more closely, making it more favourable to crystallise. The copolymer type has therefore a lower degree of structural order, and this is due to the incorporation of a cyclic ether as a second monomer, as mentioned earlier, creating a copolymeric backbone combining the native oxymethylene groups with oxyethylene groups i.e. comonomers containing two successive methylene groups. This arrangement indeed reduces the overall regularity of the backbone structure and slightly increases the tacticity of the structure. Moreover, these molecules have a longer hydrocarbon linkage that increases the spacing

between atoms in the polymer chain, which added to the less regular structure, results in lower crystallinity content.

With the above considerations, the higher crystallinity of POM homopolymers translates into better mechanical properties with higher tensile strength and modulus (in the order of 15%), additionally homopolymers also have better bearing, fatigue and creep resistance. On the flip side, the higher proportion of oxygen atoms promotes a greater susceptibility for oxidative degradation.

On the other hand, the lower crystallinity and greater intermolecular spacing of POM copolymers bring a reduction in tensile properties as well as in the upper limit on short-term use-temperature conditions. That said, while the short-term heat resistance of the homopolymer is better, the presence of the additional hydrocarbon linkages of the oxyethylene groups randomly distributed in the copolymer backbone provides improved resistance to oxidation. This translates into better property retention after long-term exposure to elevated temperatures, plus improved chemical resistance, particularly in acidic and alkaline environments. From the processability point of view, the lower crystallinity of POM copolymer makes it easier to process because it results in a melting point that is about 10°C lower than that of the homopolymer. This adds to its slightly higher thermal degradation resistance mentioned above to provide a wider processing window due its advantages at both ends of the thermal spectrum [153].

POM Applications

Typically, polyacetals are the preferred engineering thermoplastic for tribological and bearing applications thanks to their low coefficient of friction and absence of slip-stick behaviour, along with their mouldability. This area includes applications such as bearings, gears, links to conveyor belts, cams, check valves and springs. Another appealing characteristic of polyacetals is their ability to be moulded into narrowly confined shapes,

which makes them also popular in a broad variety of small and complex sized components across many segments including automotive and consumer electronics [153]. Differences in regional applications are also worth noting considering that in Asia, and particularly China, this material is essentially used in consumer goods, electrical and electronic articles. On the other hand, the automotive industry represents the biggest consumer of polyacetal in Japan, Europe and the USA [204]. With these geographical preferences in mind, the global distribution of the end-use applications of POM is depicted in the following pie graph [205]:

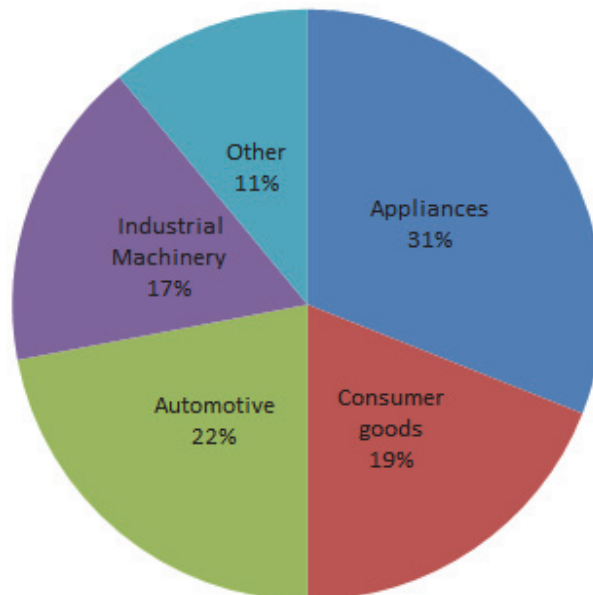


Figure 21: Distribution of end-use applications of POM

2.1.4. POM used in this study

The polyoxymethylene type used in this work was the copolymer Hostaform C 13021 supplied by TICONA. This is an easy flowing Injection moulding POM grade for precision moulded parts and thin-walled geometries with high rigidity, hardness, toughness and good chemical resistance to solvents, fuel and strong alkalis. Within the commercial polyacetals available, this is sold as a grade with good hydrolysis resistance and stabilised against thermal and oxidative degradation. From a rheological point of view, it was characterised by a volumetric melt flow rate (MVR) of $12 \text{ ml}/_{10\text{min}}$, (at $190 \text{ }^\circ\text{C}$ and 2.16 Kg). Further details of this material can be found in the manufacturer Technical Data Sheet attached below:



HOSTAFORM® C 13021 POM Unfilled			
Physical properties	Value	Unit	Test Standard
Density	1410	kg/m ³	ISO 1183
Melt volume rate (MVR)	12	cm ³ /10min	ISO 1133
MVR test temperature	190	°C	ISO 1133
MVR test load	2.16	kg	ISO 1133
Mold shrinkage - parallel	2	%	ISO 294-4
Mold shrinkage - normal	1.8	%	ISO 294-4
Water absorption (23°C-sat)	0.65	%	ISO 62
Humidity absorption (23°C/50%RH)	0.2	%	ISO 62
Mechanical properties	Value	Unit	Test Standard
Tensile modulus (1mm/min)	2900	MPa	ISO 527-2/1A
Tensile stress at yield (50mm/min)	65	MPa	ISO 527-2/1A
Tensile strain at yield (50mm/min)	8.5	%	ISO 527-2/1A
Nominal strain at break (50mm/min)	25	%	ISO 527-2/1A
Tensile creep modulus (1h)	2500	MPa	ISO 899-1
Tensile creep modulus (1000h)	1300	MPa	ISO 899-1
Charpy impact strength @ 23°C	150	kJ/m ²	ISO 179/1eU
Charpy impact strength @ -30°C	140	kJ/m ²	ISO 179/1eU
Charpy notched impact strength @ 23°C	6.5	kJ/m ²	ISO 179/1eA
Thermal properties	Value	Unit	Test Standard
Melting temperature (10°C/min)	166	°C	ISO 11357-1,-2,-3
DTUL @ 1.8 MPa	106	°C	ISO 75-1/-2
Vicat softening temperature B50 (50°C/h 50N)	151	°C	ISO 306
Coeff. of linear therm. expansion (parallel)	1.1	E-4/°C	ISO 11359-2
Flammability @ 1.6mm nom. thickn.	HB	class	UL94
thickness tested (1.6)	1.5	mm	UL94
UL recognition (1.6)	UL	-	UL94
Flammability at thickness h	HB	class	UL94
thickness tested (h)	3	mm	UL94
UL recognition (h)	UL	-	UL94

Table 2: TDS Hostaform C13021 (POM-C)

2.2. ACRYLONITRILE-BUTADIENE-STYRENE grafted with MALEIC-ANHYDRIDE

2.2.1. Description

Acrylonitrile-butadiene-styrene (ABS) became first available in the early 1950 and currently is one of the most popular engineering thermoplastics over a broad diversity of applications across different industries, only surpassed by the 'big four' commodity plastics i.e. polyethylene, polypropylene, PVC and polystyrene. This has been motivated by its excellent mechanical performance, chemical resistance, fine surface appearance, and easy processing characteristics [153].

ABS is a terpolymer covering a broad range of materials consisting of discrete, crosslinked polybutadiene (PB) rubber particles grafted on poly(styrene-co-acrylonitrile) (SAN) and embedded in a SAN matrix. The SAN copolymer, chemically bound to the PB, is referred to as grafted SAN, while the non-bound material is called free or rigid SAN [206]. The general structure of ABS is depicted in the Figure 22 below.

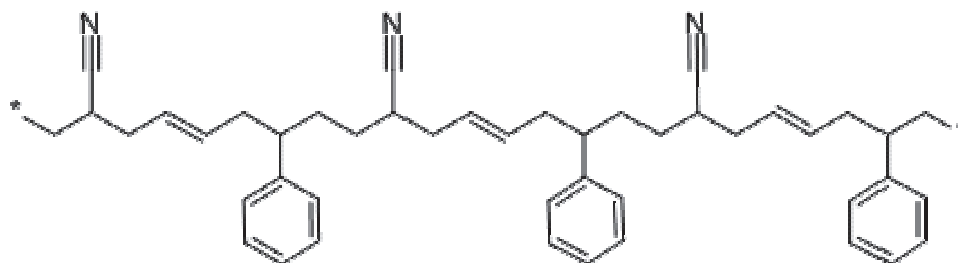


Figure 22: Structure of Acrylonitrile-butadiene-styrene

The presence of an amorphous butadiene/butadiene-acrylonitrile rubber phase into the styrene-acrylonitrile glassy phase provides a dramatic improvement in toughness and brings the properties closer to the elastomeric category.

2.2.2. Production of ABS

As mentioned earlier, ABS is made by the polymerization of Acrylonitrile, Butadiene, and Styrene monomers (see each monomer structure in Figure 23 below). Generally, the proportions of these constituencies can vary from 15 to 35% acrylonitrile, 5 to 30% butadiene and 40 to 60% styrene.

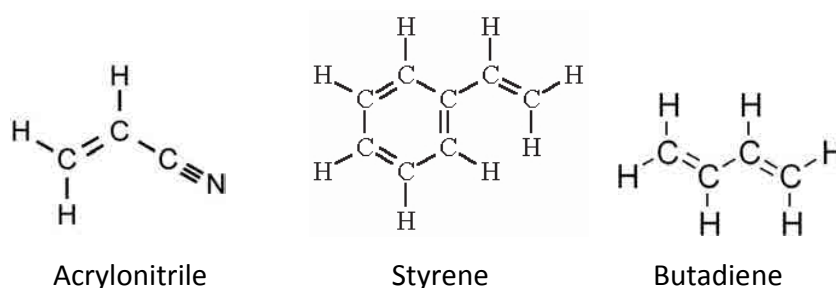


Figure 23: Monomer structure of the ABS constituencies i.e. Acrylonitrile, Butadiene and Styrene

The manufacture of ABS is carried out by a number of methods on a commercial basis. The most common polymerisation methods are those of emulsion, mass (bulk) and suspension, with variations on these processes constituting further possibilities [206].

The most general approach, however, is to add styrene and acrylonitrile to a polybutadiene latex and to warm the mixture to about 50°C to allow absorption of the monomers. A water-soluble initiator such as potassium persulphate is then added to polymerise the styrene and acrylonitrile. The resulting materials will be a mixture of polybutadiene, polybutadiene grafted with acrylonitrile and styrene, and styrene-acrylonitrile copolymer. The presence of graft polymer is essential in order to strengthen the intrinsic weak nature of the basic mixtures of polybutadiene and styrene-acrylonitrile copolymers [153].

The result is a long chain of polybutadiene criss-crossed with shorter chains of poly(styrene-co-acrylonitrile). The nitrile groups from neighbouring chains, being polar, attract each other and bind the chains together, making ABS stronger than pure polystyrene. The styrene gives the plastic a shiny, impervious surface. The butadiene, a rubbery substance, provides resilience even at low temperatures. With the above foundations, ABS polymers can be

engineered by the manufacturer to give a range of physical properties, depending on the ratio of the monomeric constituents and the molecular level of connectivity.

The major players in the ABS manufacturing industry are LG Chemicals, Chi Mei Corporation, Styrolution, Formosa Plastic Company, Asahi Kasei, KKPC, SABIC and Styron among others [207].

2.2.3. ABS Characteristics and properties

From the above discussion, it is obvious that the range of different ABS resins available in the market is overwhelming, which added to the obvious reluctance of manufacturers to divulge details regarding the chemical nature and formulation of each grade, it results difficult to provide detailed properties of these materials unless one resorts to different material data sheets of named proprietary materials. With this in mind, a general recollection of the value ranges found for the typical properties is listed below [153]:

	ABS
Specific Gravity <i>ASTM D.792</i>	0.350 - 1.26 g/cc; Average value 1.05 g/cc
Tensile strength <i>ASTM D.638</i>	20.0 - 43.0 MPa ; Average value 31.8 MPa
Flexural modulus <i>ASTM D.790</i>	Higher 1500 - 2500 GPa ; Average value: 2470 MPa
Deflection temperature <i>ASTM D.792 (0.48MPa)</i> <i>ASTM D.792 (1.82MPa)</i>	Higher/Lower subject to test load 90°C 76°C
Impact strength <i>ASTM D.256 (notch)</i>	0.5 - 3.7 J/cm
Glass transition temperature	105°C
Shrinkage	0.4% to 0.8%; Average 0.5%
Moisture absorption (Eq.)	0.200 - 0.450 %; Average value of 0.339 %

Table 3: General properties of ABS

Despite the appealing properties and characteristics of ABS, one of the main drawbacks is its inherent flammability and lower thermal stability when exposed to heat, mechanical stress, and ionizing or ultraviolet radiation. This becomes particularly critical in the presence of

oxygen because of the formation of reactive intermediates such as free radicals and hydroperoxides.

ABS Applications:

ABS is widely used in the automotive industry, telecommunications, business machines, and consumer market mainly because its property–price profile is intermediate between the lower priced commodity thermoplastics and the more expensive high-performance engineering plastics. The following pie graph depicts the distribution of the different end-use applications of ABS: [208]

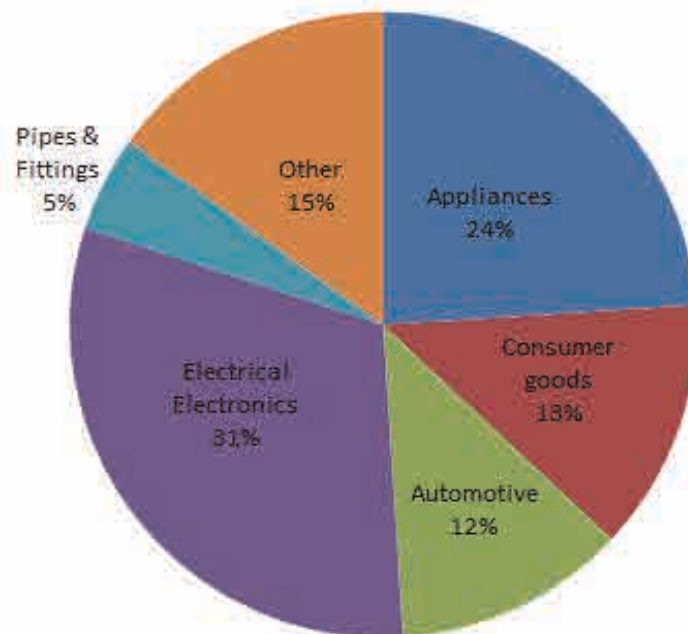


Figure 24: Distribution of end-use applications of ABS

2.2.4. ABS grafting with maleic anhydride (ABS-g-Ma):

2.2.4.1. Maleic-Anhydride: Description and properties

Maleic anhydride (Ma) is a highly reactive chemical organic compound with the formula $C_2H_2(CO)_2O$. Ma is also known as *2,5-Furandione*, *cis-butenedioic anhydride*, *toxilic anhydride* or *2,5-dioxofuran*. The chemical structure is represented in Figure 25 below:



Figure 25: Chemical structure of maleic anhydride

Maleic anhydride is solid at room temperature and becomes a clear, colourless, low viscosity liquid at 52.9 °C. This compound is soluble in water forming maleic acid.

The chemical conversions of maleic anhydride as a result of its structure are numerous. An acid anhydride group, a reactive double bond and the easy conversion of many of its derivatives into isomeric derivatives of fumaric acid make it a multifaceted resin-former and organic reactant for a variety of chemical transformations.

Applications of Maleic anhydride: Major usages of maleic anhydride include the manufacture of unsaturated polyester resins (UPR), which in turn are used in the production of lighter, stronger, fiberglass composites for boats, cars, construction, wind turbine blades and a diverse range of consumer products. It is a key ingredient in the manufacture of copolymers that enable the use of more sustainable raw materials, for example to bind wood fibres into plastic, to inhibit corrosion, create protective coatings for wire and to repel water in sunscreens. Through conversion to fumaric and malic acids, maleic anhydride is a vital component of gelling agents, flavour enhancers and food preservatives. It is also

essential to the production of elastane (Spandex) fibres, artificial sweeteners, paper-sizing, water treatments, hardeners for epoxy curing, hairsprays, pharmaceuticals, agricultural chemicals, water treatment chemicals and motor oil additives.

Relative to this thesis, maleic anhydride is also one of the most widely used vinyl monomers for the graft compatibilisation of thermoplastics, although an overwhelming proportion goes into polyolefinic materials, maleic anhydride is also used in the grafting of polymers containing butadiene. This area of application is based on the high chemical reactivity of the anhydride functionality. The performance of maleic anhydride graft-modified polymers, usually abbreviated as “-g-Ma” depends on the chemical microstructure of graft attachment (primary, secondary, tertiary sites), as well as the graft type i.e., single, oligomeric, polymeric, bridging, and/or unsaturated), which ultimately determines the adhesion and compatibilisation results [209-210]. The next section will further discuss the application of maleic anhydride as a compatibiliser when grafted onto ABS.

2.2.4.2. ABS-g-Ma: Description and properties

In many occasions, the polymers involved in compounding or blending processes are either immiscible or have some level of interfacial tension between phases resulting in a poor performance of the blend. This drawback can be overcome by either reactive blending or by compatibilising the polymers by means of an agent that assists in facilitating a favourable interaction between polymer phases. Said compatibilisation is aimed to achieve the following benefits [211]:

- Reduction of interfacial tension
- Increase adhesion between the phases in the solid state
- Balance morphological disruptions due to forming stress

One of the typical routes of reactive compatibilisation of polymers is by the graft copolymerisation of functional monomers with the existing polymers e.g. maleic anhydride.

Graft polymerisation can be initiated by various methods, such as high energy (γ -rays and electron beams) [214-215], plasma treatment [212], UV [213], chemical initiators (including graft in solution and in melt) and polymer oxidation [210].

Within styrenic polymers, styrene-maleic anhydride (SMA) copolymers have had a good market penetration in applications requiring higher levels of performance on heat resistance, rigidity, impact resistance and dimensional stability [153]. Particularly for ABS polymers, recent studies have been focusing on the resulting properties of ABS grafted with maleic anhydride, resulting in improved polybutadiene phase polarity as well as the overall matrix compatibility with the nanofillers [160, 195, 210, 216-221].

Generally speaking, the performance and compatibilisation of maleic anhydride (-g-Ma) graft-modified polymers is expected to depend on the chemical microstructure of the graft. As mentioned earlier, this microstructure is subject to the functional groups of the copolymer and the graft type [209].

The grafting of maleic anhydride onto the ABS backbone has proved in the aforementioned literature to be an effective method to enhance the polarity of the butadiene fraction, hence allowing for a successful incorporation (grafting) onto the rubber phase. Without Ma grafting, the incorporation of property-enhancing nanofillers on the ABS backbone will tend to react with those fractions with higher polarity which in the case of ABS would be the SAN phase, and it is expected to leave the weaker butadiene fraction unattended. Ma grafting does not necessarily modify the ABS Tg and flame retardancy unless further reinforcements are added such as nanoclays, POSS, etc [185].

For the reasons explained above, the ABS used in this study is purposely a maleic anhydride modified grade to ultimately increase the reactivity with the POSS functional groups. Particularly, maleic anhydride can react with amine, epoxy and hydroxyl groups, which are constituencies of the different nanoparticles used in our experimental, being glycidyl, amino and Trisilanol respectively.

2.2.5. ABS-g-Ma used in this study

The ABS-g-Ma used was Bondyram 6000 kindly supplied by Polyram (Ram-On, Israel), and it comes in the form of pellets. This ABS has the maleic anhydride grafted at a percentage weight rate of 0.6-1% with no heat stabilisers added and is ready for use in injection moulding processes. Its main application is as a compatibiliser and coupling agent for styrene compounds. Further details of this material can be found in the manufacturer Technical Data Sheet attached below:



Bondyram 6000 Maleic Anhydride-Modified ABS

Typical Property Data

Property	ISO Test Method	Unit	Bondyram 6000
MFI	1133 220° C/2.16 kg	g/10min	8
Density	1138	g/cm ³	1.05
MA content	FTIR	%	0.6-1
VICAT softening point	D-1525	°C	97°

Table 4: TDS Bopndyram 6000 (ABS-g-Ma)

2.3. POLYHEDRAL OLIGOMERIC SILSESQUIOXANES (POSS)

2.3.1. POSS Description

Polyhedral oligomeric silsesquioxanes is a family of molecules with structures based on several Si-O linkages forming a molecular skeleton having a silicon atom at each vertex with a general formula $(\text{RSiO}_{1.5})_{2n}$, where 'Si' is the element silicon, 'O' is oxygen and 'R' is a substituent group. The architecture of these compounds varies mainly with cage structures and partial-cage structures as represented in Figures Figure 26 and Figure 27 below [200, 222-223].

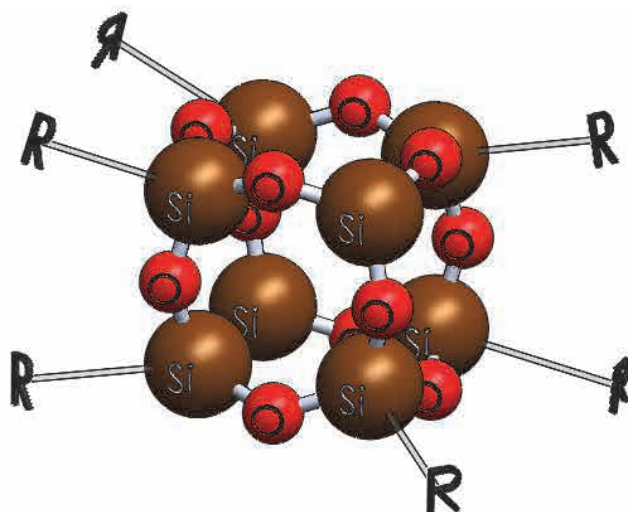


Figure 26: Silsesquioxane cage structure

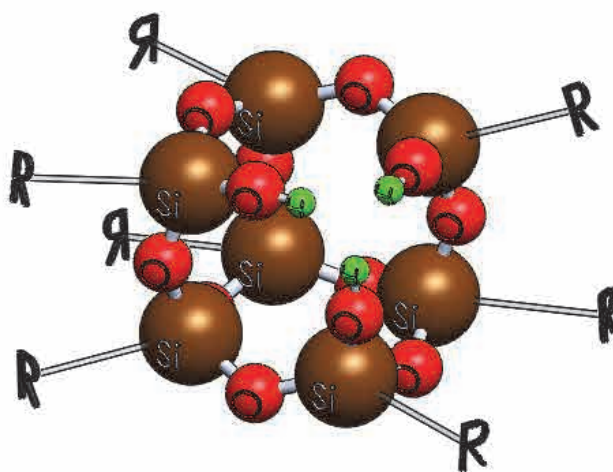


Figure 27: Silsesquioxane partial-cage structure

Some prefixes are commonly used to show the number of repeat silicon units such as hexa- (6) , octa- (8) and deca- (10) with octahedral silsesquioxane being the most commonly used with 8 links e.g. $(\text{XSiO}_{1.5})_8$. Prefixes can likewise refer to the type of 'R' substituent, with the most common ones being hydridosilsesquioxane, alkylsilsesquioxane, arylsilsesquioxane and halosilsesquioxane when the 'R' substituent is hydrogen, alkyl, aryl or halogen respectively.

Despite the increasing use of POSS particles into the so-called nanocomposites and its popularity in nanotechnology research forums, the categorisation of POSS as a nanoparticle is controversial. Strictly speaking, POSS are molecules with distinct molecular weight, specific melting points, boiling points and, unlike particles, immediate solubility in solvents. In some instances, and on the grounds that POSS are molecules that just look reminiscent of particles, they have also been referred to as "molecules" to reflect their dual nature [224].

2.3.2. General POSS Characteristics and properties

As mentioned in the previous section, POSS molecules contain organic substituents in an exo-cage arrangement around the silicon vertices. The nature of these side-groups spans the whole range of chemistry such as alkyls, phenyls, alcohols, amines, vinyls, carboxylic acids, acrylates , epoxides and silanes to name a few. These substituents can be designed to be reactive or non-reactive with the polymer matrix, hence play an important role in determining many of the physical properties of the resulting three-dimensional hybrid molecule. The variety of substituents and cage structures currently constitute more than 200 types of POSS molecules commercially available, with the prospects to further tailor more configurations in the near future [223].

The size of POSS molecules are based on a silica core with a distance of 0.5 nm between Si-Si, and an overall molecule size ranging 1 to 5 nm depending on the R-R size or the organic substituents. In the next page, Figure 28 depicts the molecular structure and main characteristics of POSS nano-entities.

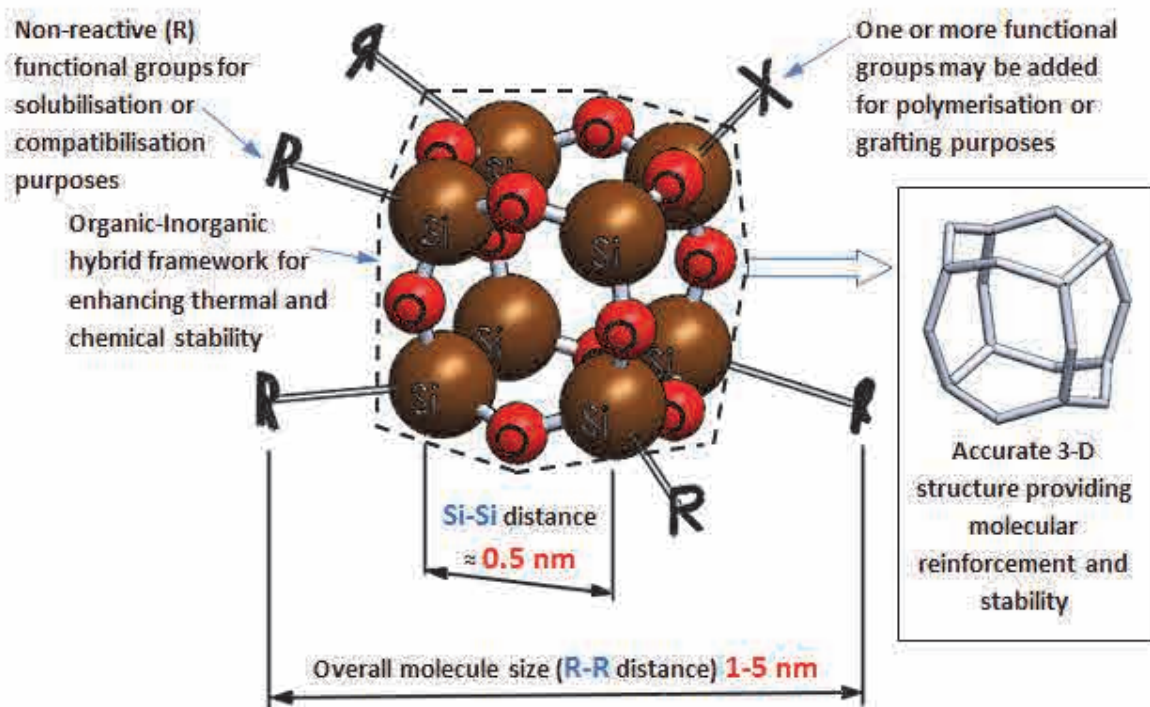


Figure 28: POSS structure and main characteristics

The main properties of POSS compounds are the following:

- Common density range between $0.9\text{-}1.3 \text{ g/cm}^3$, in some cases up to 1.82 g/cm^3 .
- Rigid cage structure, due to its strong silicon-oxygen framework.
- High thermal stability ranging $250\text{-}350^\circ\text{C}$, with $> 400^\circ\text{C}$ in some cases.
- High surface area.
- Relatively high molecular weight.
- Fully tuneable solubility, based on the capacity to functionalise the substituent groups.
- Fully tuneable reactivity, for the same reasons as above.

Unlike nanoscopic fillers, POSS molecules can have different physical forms such as crystalline solids, waxes and liquids. In general, POSS molecules can be easily dispersed at the molecular level if the organic substituents on the cage are similar in chemical structure to the polymer matrix (i.e. if they are compatible). In some cases a good dispersion of POSS molecules can be achieved by simple stirring, although this does not apply for all situations and special care must be taken in order to avoid agglomeration, as this would lead to the formation of POSS fractions exceeding the nanoscale order with a resulting decay in properties of the nanocomposite.

2.3.3. Commercial use of POSS:

An increasing number of commercial POSS applications can be found globally despite its relatively new introduction at a mass production scale just over a decade ago. Currently there are over 800 patents and more than 2000 published papers on POSS [224]. It is worth noting, however, that at the time of this thesis, the only supplier of POSS for commercial use is the U.S. based company Hybrid Plastics. This supply monopoly, along with the relatively high costs across the range of POSS types available i.e. 50-100€/kg [223], could discourage potential users, however the usually low add rate combined with its capacity to compete in high added value applications can certainly have its place in the market. The applications that have been in place so far cover a diversity of areas such as packaging, dental, aerospace, electronics and adhesives [224].

2.3.4. POSS used in this thesis

Five different POSS based on a T8 structure were supplied by Hybrid Plastics (Hattiesburg, USA). These have been tabulated below with their corresponding commercial name and identification prefix used in this work.

POSS NAME	POSS Commercial Ref.	ID prefix used
Poly(ethylene glycol)	PG1190	PEG-
Glycidyl	EP0409	G-
Glycidylisobutyl	EP0418	GI-
Aminopropylisobutyl	AM0265	A-
Trisilanolphenyl	SO1458	T-

Table 5: POSS nanoparticles used in this study

Most POSS are solid white powders and some are colourless liquids, and it is important to note that these powders are micron sized agglomerates typically in the 1-100 micron range and the nanoscopic dimension is only achieved once it is dispersed in the polymer [223].

The characteristics of each POSS are summarised in the following paragraphs:

2.3.4.1. Glycidyl cage mixture (G-POSS):

Glycidyl cage mixture belongs to the category of epoxide functionalised POSS and its most common structure is octahedral, which is the one used for this thesis. This POSS is therefore octafunctionalised with 8 identical silicon cage corners linked to glycidyl epoxy groups following Figure 29 below:

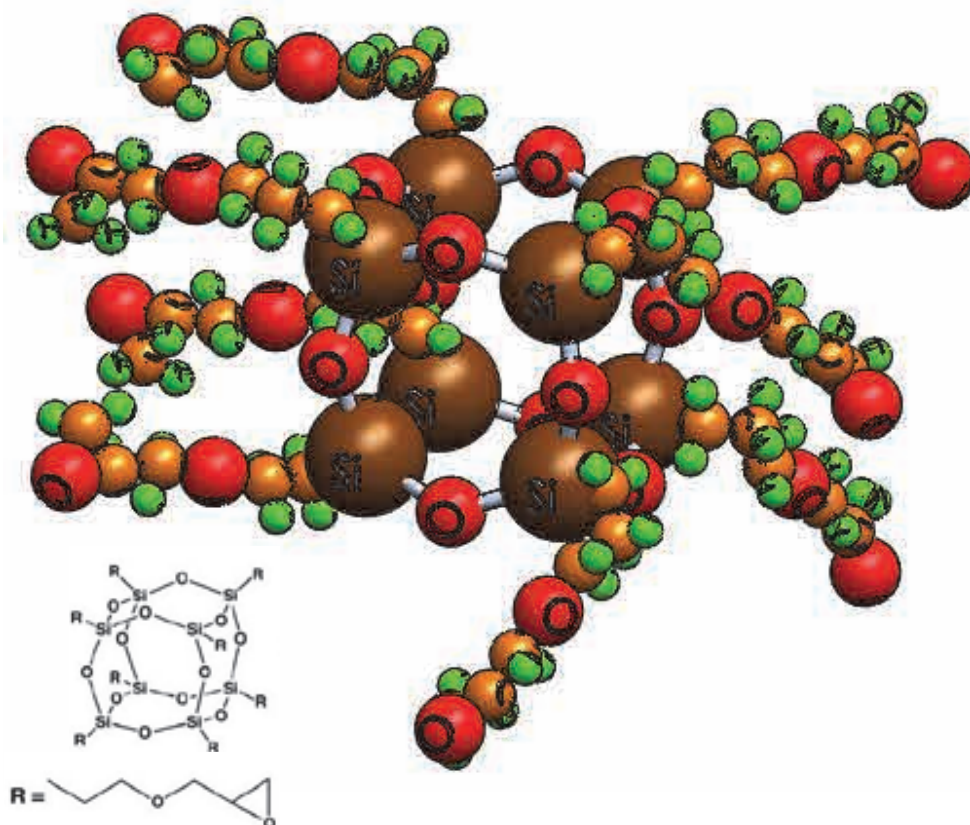


Figure 29: G-POSS structure

This product is currently in bulk production status, and it is also known with the name (trimethoxy [3 (oxiranylmethoxy) propyl]-, hydrolysed-Silane). G-POSS is a liquid at room temperature with a relatively low viscosity of 48 poise. It has a molecular weight of 1338, a density of 1.25 g/cm^3 and a refractive index 1.51. Being an epoxide molecule, it can retain almost full modulus up to 300°C [224]. It is soluble with the solvents THF, chloroform and toluene, and the aliphatic and aromatic epoxy resins

2.3.4.2. Glycidyl Isobutyl (GI-POSS):

Glycidyl i-butyl also belongs to the category of epoxide functionalised POSS and it has a octahedral structure with identical isobutyl groups on 7 corners with one glycidyl-epoxy group in the remaining corner of the cage. This POSS is represented in Figure 30 below:

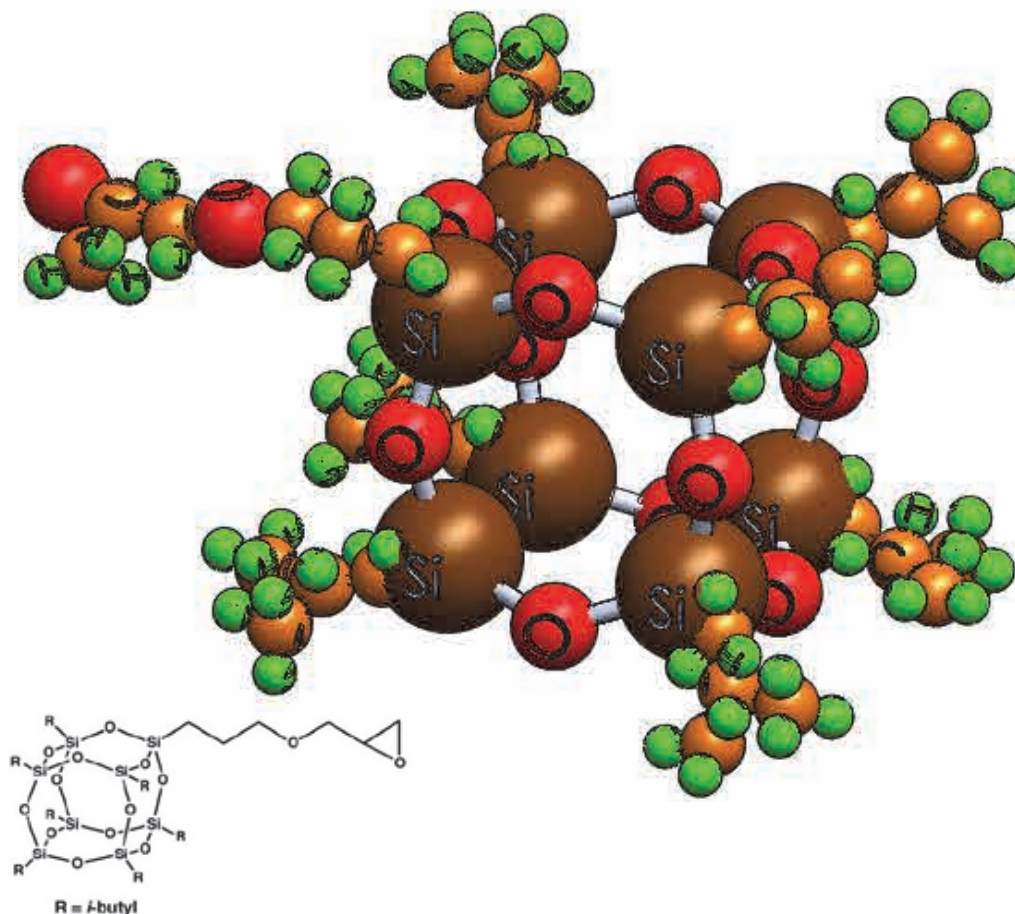
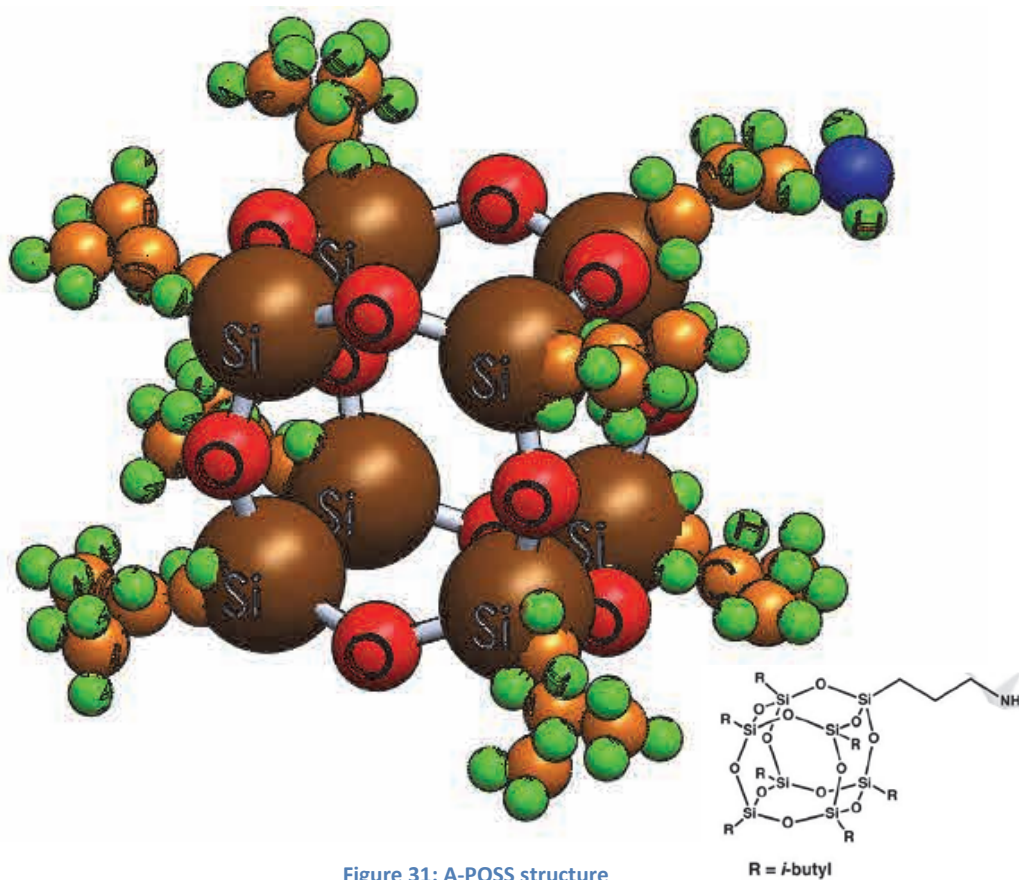


Figure 30: GI-POSS structure

Gi-POSS is also known with the name PSS-(3-Glycidyl)propoxy-Heptaisobutyl substituted. It is a white powder with a melting temperature of 129°C. It has a molecular weight of 932, a density of 1.14 g/cm⁻³ and a refractive index 1.47. As per Glycidyl POSS, it retains almost full modulus up to 300°C for being an epoxide molecule [224]. It is soluble with the solvents THF, chloroform and hexane, and the aliphatic and aromatic resins.

2.3.4.3. Aminopropyl Isobutyl (A-POSS)

Aminopropyl *i*-butyl belongs to the category of amide functionalised POSSs and it has an octahedral structure, with identical *i*-butyl groups on 7 corners with one aminopropyl group in the remaining corner of the cage. Note this molecule has architectural similarities with glycidyl-POSS described earlier, with only one corner having the aminopropyl instead of the glycidyl group. The formula and the schematic for this POSS is shown Figure 31 below:



A-POSS is currently in bulk production status. It is a white powder at room temperature with a melting temperature around 50°C. It has a molecular weight of 875, a density of 1.16 g/cm³ and a refractive index 1.49. It is soluble with the solvents THF, chloroform and hexane, and the aliphatic and aromatic amine resins.

2.3.4.4. Polyethylene glycol cage mixture (PEG POSS)

Polyethylene glycol cage mixture (PEG POSS) has an octahedral structure with 8 identical silicon cage corners linked to polyethylene glycol groups as per representation in Figure 32 below:

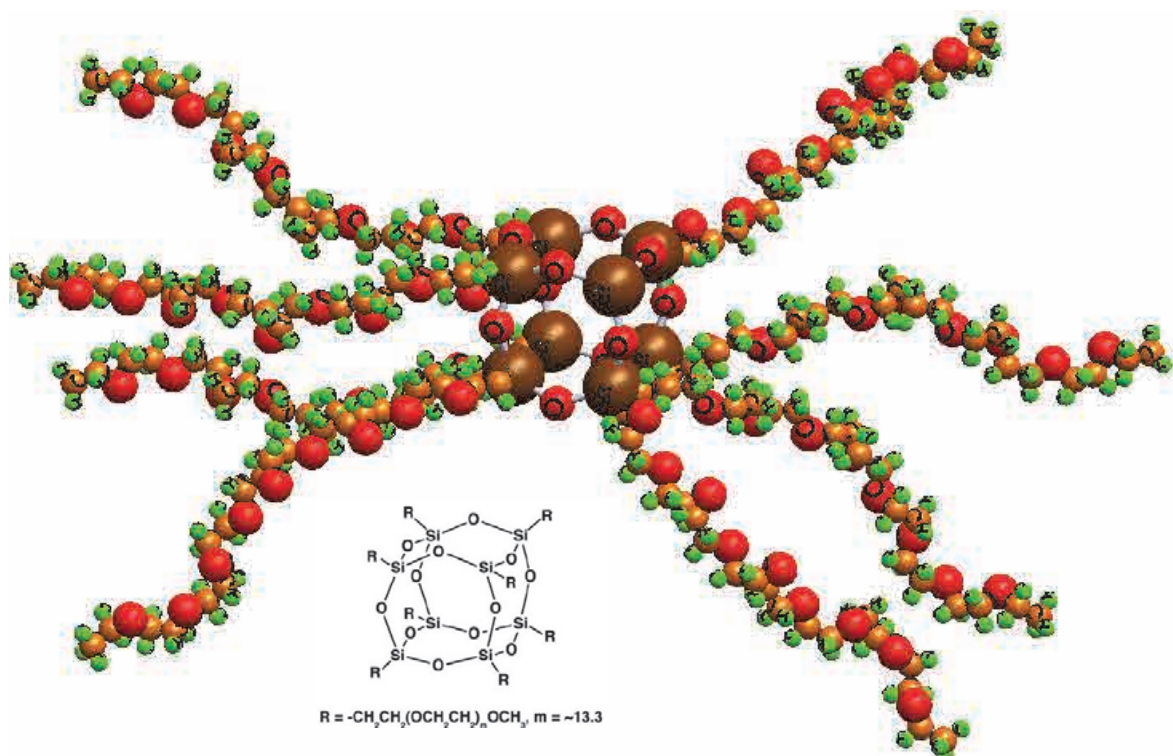


Figure 32: PEG-POSS schematic

PEG-POSS is a viscous liquid at room temperature with a melting temperature of approximately 22°C. It has a molecular weight of 5600, a density of 1.09 g/cm³. It is soluble with the solvents water and alcohols and the polyether and polyester resins

2.3.4.5. Trisilanolphenyl (T-POSS)

Trisilanolphenyl belongs to the category of silanol functionalised POSSs and it has a octahedral structure, with identical phenyl units linked to 7 seven corners of the cage with one corner open exposing three active silanol groups as represented in Figure 33 below:

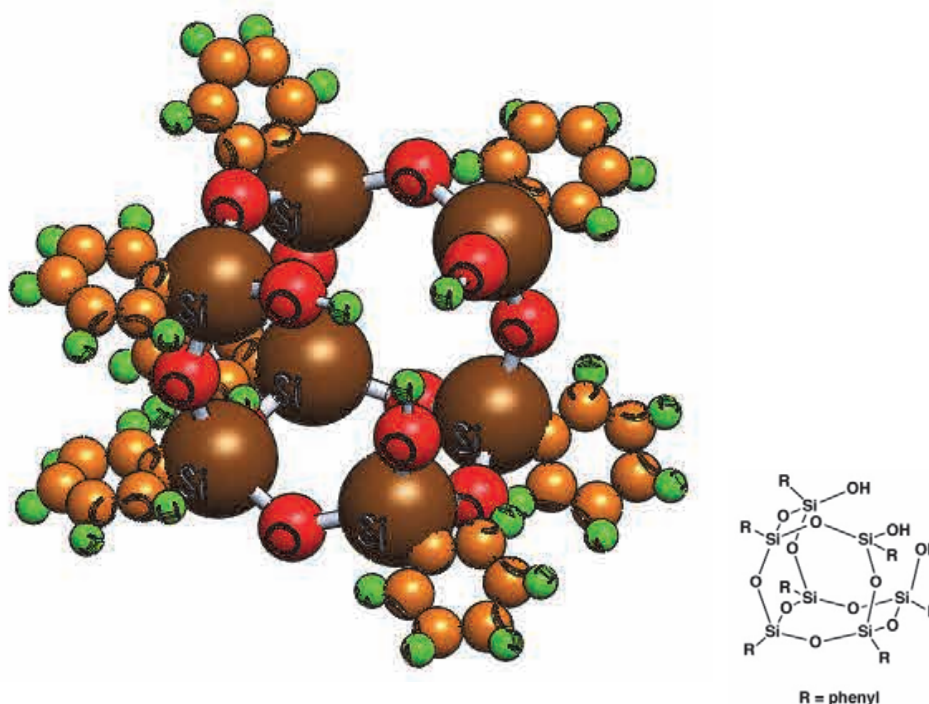


Figure 33: T-POSS structure

This product is currently in bulk production status, and it also known with the name “Tricyclo [7.3.3.15,11]heptasiloxane-3,7,14-triol, 1,3,5,7,9,11,14-heptaphenyl”. T-POSS is a white powder at room temperature with a melting temperature of 200.5°C. It has a molecular weight of 930, a density of 1.42 g/cm⁻³ and a refractive index 1.65. It is soluble with the solvents THF, chloroform and ethanol, and with most of the aliphatic and aromatic monomers, oligomers and polymers PP, PE, PA, PET and PC.

CHAPTER 3
THEORETICAL FUNDAMENTALS

3. THEORETICAL FUNDAMENTALS

3.1. POLYMER SOLUBILITY ANALYSIS

Since the early developments in the materials nanotechnology, the compatibility of the inorganic particles with the polymeric host material proved to be of paramount importance to achieve strong interactions and, by that, an effective reinforcement on the resulting nanocomposite [225-226].

In the macrocomposite field, the compatibility between filler and host material is generally achieved by modifying the particle/filler surface with an organic moiety in order match as much as possible the chemical structure of the polymer. Composites in the nano-scale are no exception to this rule, and particularly for the POSS-based nanocomposites, the compatibilisation challenge comes down to adequately choose the organic functionalities of the inorganic cage structure.

In the case copolymerisation or grafting of a POSS material to a polymer, the selection of the modifier will be led by the specific chemistry required for a given reaction scheme. In the case of melt-blending, which is the one applicable to this study, the POSS particles behave as large molecules once incorporated into a polymer and can exist in a number of states. In many instances, the POSS will simply phase separate due to a lack of compatibility with the polymer. On the contrary, if a high degree of interaction occurs, the POSS particles can be thoroughly dispersed in the nanometre scale, or even in a completely dissolved state [227]. For instance, if the interactions occur by means of hydrogen bonding, the system performs similarly to that of a copolymer or grafted nanocomposite [228]. From a molecular dispersion perspective, it has been widely accepted that POSS can also act as a plasticiser [38, 177, 229-234].

Unfortunately, a prediction of the potential interactions between POSS and the host material cannot be made solely on the analysis of the chemical structure of the materials involved, due to the difficulties found to ascertain the effects of the silicate core and the

molecular geometry will have on the interaction capacity of the POSS molecule with respect to the polymer matrix. This area of paramount importance has already encouraged various researchers to study the compatibility of different polymer-POSS systems in terms of solubility parameters to successfully assist in the prediction of the degree of compatibility and dispersion of the POSS nanocomposites [80, 235-238].

In thermodynamic terms, the solubility of a given solvent-solute system is based on the free energy of mixing ΔG_M , whereby substances would be mutually soluble if, at least, ΔG_M is negative. The free energy of mixing is expressed with the following equation [236, 238-239]:

$$\Delta G_m = \Delta H_M - T\Delta S_M \quad \text{Equation 8}$$

Where:

- ΔG_M is the Gibbs free energy of mixing
- ΔH_M is the enthalpy (or heat) of mixing
- T is the absolute temperature
- ΔS_M is the entropy change in the mixing process

The above equation shows that entropy change is beneficial to mixing. When multiplied by the temperature, this will work in the direction of promoting a more negative free energy of mixing, hence enhancing the solubility.

The entropy changes associated with polymer solutions will be smaller than those associated with liquid-liquid miscibility. Since “monomers” are already bound into the configuration dictated by the polymer they belong to. They are no longer free in the sense of a liquid solvent and cannot mix freely to contribute to a larger entropy change. This is one reason why polymer-polymer miscibility is many times difficult to achieve and due to the fact that polymer molecules are progressively larger, the contribution from entropy becomes smaller or negligible and consequently the only property left to contribute on achieving mutual compatibility is the solubility parameter [239].

The studies of solubility as such, however, did not start until 1936 with the introduction of the ‘Solubility Parameter’ (δ) by Hildebrand, correlating solubility with the cohesive properties of the solvents [240]. This solubility parameter is expressed with the equation below and can be defined as the square root of the cohesive energy density, which is the heat of vaporization divided by the molar volume. Under these criteria, this term can also be called cohesion energy parameter, since they derive from the energy required to convert a liquid to a gas [239].

$$\delta = (E/V)^{1/2} \quad \text{Equation 9}$$

Where:

- V is the molar volume of the pure solvent
- E is its (measureable) energy of vaporisation

Despite the relevance of Hildebrand’s theory including later contributions from Scott et al. [241-242], it was limited to regular solutions and does not account for association between molecules as it only took into consideration dispersion forces between structural units, hence missing important interactions such as those from polar groups and hydrogen bonding. Later on, Flory & Huggins introduced in 1953 the lattice theory for polymer solutions and provided comprehensive tables with the so-called Flory Huggins interaction parameter and the influence of temperature on the solubility [243]. In 1967 Hansen proposed an extension of the Hildebrand parameter method to estimate the relative miscibility of polar and hydrogen bonding systems by splitting it into three components: *Polar, Dispersion, and Hydrogen Bonding*; thus, the name Hansen 3D solubility parameters, also known as **HSP** [239, 244].

Although HSP method in full will not be used in this thesis, the solubility calculation methods used herein are partially based on Hansen as well as Hildebrand’s theories. Therefore it is worthwhile running through the HSP fundamentals in order to correctly interpret the methods applied on the solubility calculations of the materials analysed in section 5.

According to Hansen, there are three major types of interaction in common organic materials, which are those described below:

- **Non-polar interactions:** These are also called dispersion interactions in the literature, and derive from atomic forces. As all molecules are built up from atoms, all molecules will have this type of attraction force, and therefore this is the most predominant type of interaction. For saturated aliphatic hydrocarbons, for example, these are essentially the only cohesive interactions, and the energy of vaporisation is assumed to be the same as the *dispersion cohesive energy, E_D* .
- **Dipole-Dipole interactions:** These cause a second type of cohesion energy, called the *polar cohesive energy, E_p* . This interaction type is inherently molecular and hence is found in most molecules to one extent or another. The polar solubility parameters require experimental verification during the solubility analysis, although can be estimated from molecular parameters if they are available, which will be the case in the analysis performed in this study.
- **Hydrogen bonding interactions:** These are the third major source of cohesive energy and are called *hydrogen bonding energy, E_H* , although in some literature can also be referred to as electron exchange parameter. They also result from molecular interactions, thus in this respect they do resemble the polar interaction described above. The basis of this type of cohesive energy is attraction among molecules because of the hydrogen bonds. In this perhaps oversimplified approach, the hydrogen bonding parameter attempts to more or less gather the energies from interactions not included in the other two parameters. Alcohols, glycols, carboxylic acids, and other hydrophilic materials have high hydrogen bonding parameters.

Hansen calculation methods have direct application not only on polymers-polymer solubility predictions, but also in other scientific disciplines such as surface science, where they have been used to characterise the wettability of various surfaces, the adsorption properties of

pigments, as well as systematic surface treatment of inorganic fibres so they could be readily incorporated into polymers of low solubility parameters such as polypropylene.

The disadvantage of Hansen's method is that the three components need to be empirically adjusted to define the miscibility characteristics of the solvent in order to generate a three-dimensional structure as a graphical representation of the interaction between polymers and solvents. In a simplified way, this experimental requires a selection of good solvents and poor solvents following a specific criterion, which are then prepared in multiple solutions of good/poor solvents in different percentage ratios and subsequently tested with each particular polymer for a specific period of time. Each test results in either a clear solution or in different degrees of phase separation, which is the data used to create the 3D solubility models.

The intricacies of the above Hansen 3D solubility method encouraged Hoftyzer & Van Krevelen (1976) and Hoy (1985) to elaborate two additional methods that provided a degree of simplicity into the analysis and which will be followed for the present study.

3.1.1. Hoftyzer and Van Krevelen calculation method

The method of *Hoftyzer and Van Krevelen* predicted the solubility parameters based on group contributions through the following equations [245]:

$$\delta_d = \frac{\sum F_{di}}{V}, \quad \delta_p = \frac{\sqrt{\sum F_{pi}^2}}{V}, \quad \delta_h = \sqrt{\frac{\sum E_{hi}}{V}} \quad \text{Equation 10}$$

$$\delta_t^2 = \delta_d^2 + \delta_p^2 + \delta_h^2 \quad \text{Equation 11}$$

Where:

- δ_d is the dispersion component.
- δ_p is the polar component.

- δ_h is the hydrogen bonding component.
- F_{di} is the dispersion component.
- F_{pi} is the polar component.
- E_{hi} is the hydrogen bonding energy
- V is the molar volume of the solvent molecule or the structural unit of the polymer.

Those substances with similar solubility values are expected to exhibit greater compatibility and better dispersion characteristics. As per Hansen theory, the hydrogen bonding energy, E_{hi} , is considered to be constant per each structural group [80, 236, 238].

3.1.2. Hoy calculation method

Alternatively, the **Hoy** method suggests another simple approach to predict the solubility parameters and is based on the following equations [246]:

Expressions for δ and δ -components:

$$\delta_{tot} = \frac{F_i + \frac{B}{n}}{V} \quad \text{Equation 12}$$

$$\delta_p = \delta_{tot} \left[\frac{1}{\alpha^{(P)}} \times \frac{F_p}{F_t + \frac{B}{n}} \right] \quad \text{Equation 13}$$

$$\delta_h = \delta_{tot} \left[\frac{\alpha^{(P)} - 1}{\alpha^{(P)}} \right]^{1/2} \quad \text{Equation 14}$$

$$\delta_d = (\delta_{tot}^2 + \delta_p^2 + \delta_h^2)^{1/2} \quad \text{Equation 15}$$

Expressions for additive molar functions:

$$F_t = \sum N_i F_{t,i} \quad \text{Equation 16}$$

$$F_p = \sum N_i F_{p,i} \quad \text{Equation 17}$$

$$V = \sum N_i V_i \quad \text{Equation 18}$$

$$\Delta_{T(P)} = \sum N_i \Delta_{T,i(P)} \quad \text{Equation 19}$$

Auxiliary equations:

$$\alpha^{(P)} = \frac{777 \Delta_{T(P)}}{V} \quad \text{Equation 20}$$

$$n = \frac{0.5}{\Delta_{T(P)}} \quad \text{Equation 21}$$

Where:

- δ_{tot} is the Solubility Parameter
- δ_p is the contribution of polar forces.
- δ_h is the contribution of hydrogen bonding.
- δ_d is the contribution of dispersion forces.
- F_t is the molar attraction function.
- F_p is the polar contribution function.
- Δ_T is the Lyndersen correction for non-ideality
- α is the molecular aggregation number

- n is the number of repeating units per effective chain segment of the polymer.
- V is the molar volume of the solvent molecule or the structural unit of the polymer.

In general, the Hoy method is used to calculate the solubility parameter due to its simplicity. However, it assumes that no specific interactions such as the dispersion force, polar force and hydrogen bonding are active between the structural units of the substances involved and accordingly it can result inaccurate for crystalline polymers.

3.1.3. Hoy method based on group molar-attraction constant

Another rather simplified interpretation of Hoy method has been used by Liu et al [247] and Misra et al [80] reporting good agreement between the theoretical solubility parameters and the observed microscopic dispersion of POSS particles. In these studies, solubility parameters were based on the group molar-attraction constant (G) and the calculations following the structural formula and density (ρ) of the material using the following equation:

$$\delta = \rho \sum G_i / M_0 \quad \text{Equation 22}$$

Here $\sum G_i$ is the sum of molar attraction constants for the groups in the molecule and M_0 is the molecular weight of the material. G_i values can be obtained from Hoy's table of group molar-attraction constants [247]. The importance of this method is that we have the G value for the Si-O group, which is $278 \text{ (cal.cm}^3/\text{mol)}^{1/2}$ [248], hence providing the possibility to ascertain the effects of the inorganic cage within the overall solubility system, even though some authors have considered the effects as negligible [235].

The results of the two algorithmic methods for estimation for the solubility parameter and its components (Hoftyzer + Van Krevelen and Hoy) have the same order of error (10%). Thus the safest for estimation is to apply both methods, taking the average results [238].

3.1.4. The role of the inorganic silicate cage structure in the solubility study

In some solubility studies carried out on POSS materials, the inorganic part –Si-O-Si- is deemed not to play a relevant role in the solubility behaviour of the blend [235]. This hypothesis is based on the fact that the distance between Si and O of the –Si-O-Si- is 1.64 Å, and it is shorter than the sum of the covalent radii of POSS, 1.76 Å, meaning that there exists a partial double bond character of –Si-O-. Nonetheless, the barrier of rotation around the –Si-O- axis, and the barrier of linearization of the –Si-O-Si- angle are approximately 2.5 kJ/mol and 1.3 kJ/mol respectively, resulting in very low values to be representative. The siloxane chain is so rigid that the –Si-O-Si- angle sits between 140 to 180°, which is much wider than the tetrahedral angle, the silicon atom has a relatively large size and the substituents appear only at every second atom in the chain. These features also account for the relatively high steric hindrance effect, which indicates the siloxane group is highly stable.

3.1.5. Solubility calculation approach on the present study

The selection of the solubility calculation method depends to a great extent on what data is available at the time of the study, the accuracy required for the application and the resources at hand to carry out additional experimental tests.

Although there is a general agreement that the Hansen calculation method (HSP) provides the most accurate results, and despite the sizable number of materials assigned to the Hansen parameters, the relatively new breed of POSS materials lacks of documented data relevant to this method and would require rolling out extensive solubility tests to be able to construct the necessary models required for the Hansen 3D solubility parameters.

For this reason, and considering the ±10% of accuracy error is acceptable for the purpose of this study, the *Hoy* and *Hoftyzer & van Krevelen* methods will be applied in our solubility calculations.

3.2. POLYMER DEGRADATION KINETICS

Kinetic analysis of polymer degradation has been commonly used in scientific and research applications to effectively assist in the characterisation of degradation mechanisms as well as in predicting the thermal stability of polymers [249] including the prognosis of the polymer lifetime at different temperatures [250].

3.2.1. Methods used for degradation kinetics analysis

Most kinetic analysis methods are based on the hypothesis that, from simple TGA data, explicit values can be obtained for parameters such as activation energy, pre-exponential factor and reaction order.

Although there are common steps involved in the calculation of the kinetic parameters, which are the measurement of the weight loss behaviour during the material decomposition and the application of the Arrhenius equation to fit this data, there are multiple routes that can be taken between these two steps. Fundamentally, the kinetic data can be fitted to different reaction models based on the type of information available and the degradation mechanism (if known). A recollection of the different calculation methods found in the literature assessed during the research for this thesis is listed below with the corresponding references:

- Coats and Redfern [251- 256]
- Flynn-Wall-Ozawa [148, 251, 254, 257-258]
- Kissinger [251, 257-260]
- Friedman [261-262]
- Avrami-Erofeev [263]
- Van Krevelen [256]
- Horowitz-Metzger [256]
- MacCallum-Tanner [256]
- Carrasco [264-265]

As it can be seen, the amount of routes available to calculate kinetic parameters is very broad, and consequently one can expect differences in the results by over an order of magnitude. Indeed the reliability of the results is subject to the proper choice of the reaction model, and the following four areas must be considered when choosing a calculation model:

- Adequacy of the model fitting choice
- Isothermal or non-isothermal TGA data
- Single or multiple TGA heating rates
- Procedural variables such as crucible geometry, heating rate, pre-history of sample, and particle size.

3.2.2. Coats and Redfern (CR) method

From the different reaction models found in literature, Coats and Redfern proofs to be one of the most popular methods used in the analysis of data from nonisothermal kinetic studies of solid-state reactions involving weight loss (or gain), including its applications in the analysis of polymer degradation.

This method was conceived in 1964 by A. W. Coats and J. P. Redfern. The main reason why it has become one of the most widely used is for being one of the most uncomplicated procedures to treat kinetic data [266].

The calculations associated with this method are of the integral type and are typically applied on TGA/DTG data assuming the order to reactions based on the shape of the thermogram plot to eventually determine of the activation energy (E_a).

The nonisothermal degradation of a solid-state material can be expressed with Eq. 23 below, from which the Coats–Redfern equations (Eqs. 24 and 25) are deduced [253-255, 267-268]:

$$\frac{d\alpha}{dt} = \frac{1}{\beta} A \exp\left(\frac{-E}{RT}\right) f(\alpha) \quad \text{Equation 23}$$

$$\ln \left[\frac{1 - (1 - \alpha)^{1-n}}{T^2(1-n)} \right] = \ln \left[\frac{AR}{\beta E} \left(1 - \frac{2RT}{E} \right) \right] - \frac{E}{RT} \quad (n \neq 1) \quad \text{- Coats-Redfern I - Equation 24}$$

$$\ln \left[\frac{-\ln(1-\alpha)}{T^2} \right] = \ln \left[\frac{AR}{\beta E} \left(1 - \frac{2RT}{E} \right) \right] - \frac{E}{RT} \quad (n = 1) \quad \text{- Coats-Redfern II - Equation 25}$$

$$\alpha = \frac{(m_0 - m)}{(m_0 - m_\infty)} \quad \text{Equation 26}$$

Where:

- α is the decomposed fraction (reaction rate, degree of conversion)
- m_0 is the initial mass
- m is the actual mass at the temperature chosen
- m_∞ is the mass at the final temperature
- T is the absolute temperature expressed in °K
- A is the frequency factor (also known pre-exponential factor)
- β is the heating rate
- E_a is the sought activation energy
- R is the gas constant
- n is the order of the reaction
- $f(\alpha)$ is the differential expression of kinetics function.

As reflected in Eqs. 24 and 25, the progression from the above formulas is subject to whether or not the thermogravimetric order of reaction 'n' equals one. The order of reaction is calculated with the Equation 28, and the procedure used to calculate this parameter implies to initially determine the value of the shape index 'S' from the thermogravimetric data. The shape index is a graphical parameter based on the DTG curve, and is defined as the

absolute value of the slope ratio of the curve tangents at the inflection points following the Equation 27 [256, 259, 269]. This definition and the related graphical parameters are depicted in Figure 35 below.

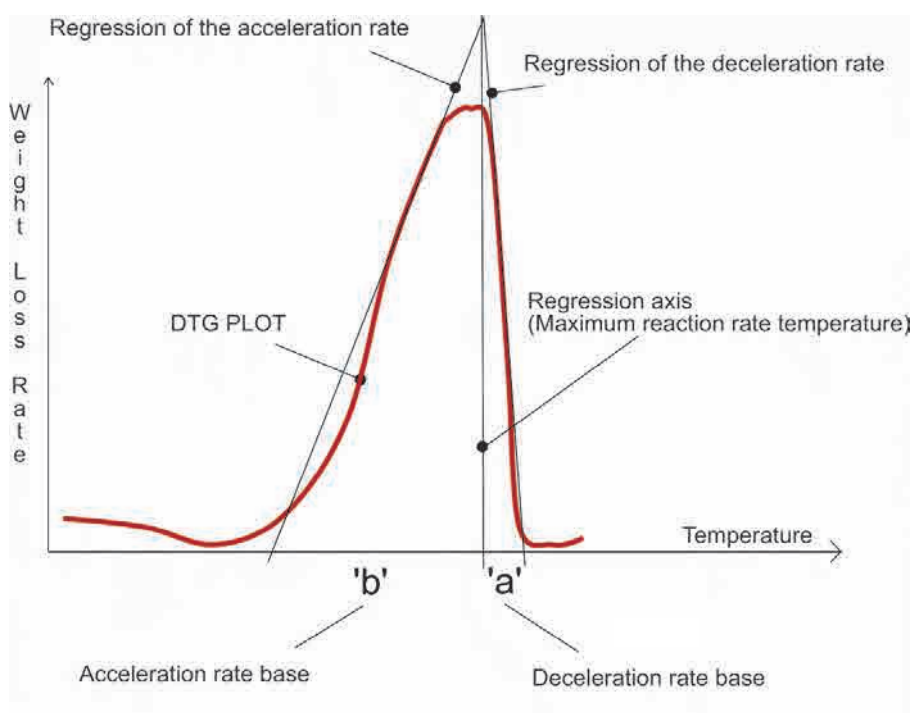


Figure 34: Graphical parameters to calculate the shape index 'S'

$$S = \frac{a}{b}$$

Equation 27: Shape Index

$$n = 1.26\sqrt{S}$$

Equation 28: Order of Reaction

CHAPTER 4
EXPERIMENTAL METHODS

4. EXPERIMENTAL METHODS

4.1. SAMPLE PREPARATION

4.1.1. POM/POSS's sample preparation

The sample preparation of the polyacetal nanocompounds was carried out by means of a twin-screw co-rotating Brabender internal mixer. The blending was performed at 190 °C with a screw rate of 60 rpm for periods of 6 min. The different POSS were added to molten POM at weight ratios of 2.5 wt%. This amount of POSS was selected and kept constant in light of the results obtained in previous works [43,49].

The samples were then moulded at 60 bar and 190 °C using an IQAP-LAP press and then cooled between two water-chilled plates. The total processing time including cooling was 11 minutes. The resulting POM/POSS specimens were squared plates 100 x 100 mm with a thickness of 0.5mm.

4.1.2. ABS-g-Ma/POSS's sample preparation

The sample preparation of the ABS nanocompounds was carried out by means of a Brabender internal mixer. The different POSS were added to molten ABS-g-Ma at weight ratios of 5 wt%. As per the POM criteria, this POSS quantity was selected and kept constant in light of the results obtained in previous works [43, 47, 49]. The temperature conditions were based on preliminary trials with the aim to optimise the mixture between the ABS-g-Ma and the nanofillers considering the different melting temperatures of the POSS's used.

Whereas APOSS and GPOSS had low T_m 's at 51.9°C and at room temperature respectively, TPOSS had the melting temperature at 200.5°C. TPOSS, however, has been previously documented to achieve adequate dispersion and blending when compounded under 190°C at 60rpm for 6min has [49]. Despite the above, these conditions revealed certain degree of degradation on the ABS-g-Ma matrix in the form of visible yellowing on the blended mixture, possibly for the shearing effect during the mixing process. Accordingly the blending temperature was progressively dropped down until reaching the 160°C, whereby no more yellowing was perceived.

The samples were then moulded at 60bar and 190 °C using an IQAP-LAP press and then cooled between two water-chilled plates. The total processing time including cooling was 11 minutes. The resulting ABS-g-Ma/POSS specimens were squared plates 100x100mm with a 0.5mm thickness.

4.2. SAMPLE PRELIMINARY CHARACTERISATION

Prior to submitting the different samples to degradation, an evaluation of the initial condition for each one of them was carried out to understand the following aspects:

- a) **Miscibility & Dispersion:** The morphological and thermal homogeneity of the blend. This analysis is also useful to assess the reliability of the theoretical solubility analysis that will be exercised in sections 5.1.1 and 5.3.1.
- b) **Effects on thermal properties:** The differences in thermal properties between the original base materials and the resulting nanocomposites.
- c) **Crystallinity:** In the case of polyacetal, the variation of crystallinity content of the nanocomposite relative to the original base material.

4.2.1. Scanning Electron Microscopy analysis (SEM)

Scanning Electron Microscopy was carried out on both the POM and the ABS-g-Ma samples to analyse the microstructure of the composites and the degree of dispersion of POSS molecules into the matrix. The instrument used was a Jeol 5610 electron microscope at an accelerating voltage of 10 kV. All sample surfaces were cryogenically fractured and sputtered with a small layer of gold to make them conductive prior to the SEM inspection.

4.2.2. Differential Scanning Calorimetry analysis (DSC)

DSC was applied to the samples also before the degradation to take place. This analysis targets the thermal transitions and the effect of the nanofillers in the overall thermal behaviour of each nanocomposite. The instrument used was a Mettler Toledo DSC822e/700 in hermetically sealed aluminium pans, under nitrogen flow ($60 \text{ mL} \times \text{min}^{-1}$). The apparatus was calibrated with a high purity indium standard. Samples of approximately 5mg were tested at a heating rate of $10^\circ\text{C} \times \text{min}^{-1}$ from 30°C to 230°C holding this temperature for 3 minutes. The complete test for each sample consisted in performing three successive runs i.e. heating-cooling-heating, whereby the first two runs were made to erase the thermal history of the polymer and establish a uniform pre-cooling.

4.3. DEGRADATION (THERMO-OXIDATION) PROCESS CONDITIONS

4.3.1. POM and its nanocomposites:

The reference POM base material and the four different POM/POSS nanocomposites were aged at different oven-storage temperatures under air atmosphere during different periods of time. The temperatures used were 200-220-240-260 °C, and each temperature condition was applied from 15 to 75 min in steps of 15 min, i.e. 5 different exposure periods. Three samples for each of the 20 resulting combinations were used.

4.3.2. ABS-g-Ma and its nanocomposites:

The reference ABS-g-Ma base material and the three different ABS-g-Ma/POSS nanocomposites were aged at different oven-storage temperatures under air atmosphere during different periods of time. The temperatures used were 200-240-280-320 °C, and each temperature condition was tested for 15 to 75 min periods in steps of 15 min, i.e. 5 different exposure periods. Three samples for each of the 20 resulting combinations were used.

4.4. SAMPLE DEGRADATION CHARACTERISATION

During the different thermoxidation conditions applied on the samples, their chemical bonding profiles were followed with FTIR analysis. On the other hand, the analysis of the thermal stability and degradation kinetics was assessed with TGA, and the surface appearance of the samples was quantified with spectrophotometry in terms of yellowing. The combination of these three methods applied on the degradation analysis of the samples allows relating the chemical modifications and polymer morphology with the physical appearance of the samples as they undergo deterioration.

4.4.1. Fourier Transform Infra-Red Spectroscopy analysis (FTIR)

The samples in pristine condition and as those resulting from each degradation condition have been examined directly in the solid state by means of an attenuated total reflectance (ATR) accessory integrated into a Nicolet 6700 Fourier Transform Infrared spectrometer. The depth of penetration of the ATR equipment is 2.03 μm at 1000 cm^{-1} and the measurements of FTIR spectra are based on 50 scanings per sample with a spectral resolution of 1 cm^{-1} and a wavenumber interval between 4000 and 400 cm^{-1} .

The presence of the POSS within the polymer matrix has been checked through the Si-O-Si stretching vibration at 1084 cm^{-1} .

For evaluation and quantification of the degradation of the POM samples, the development of the carbonyl aldehyde at 1733 cm^{-1} yielding from the thermoxidative degradation has been followed. Evidence of the reliability upon the absorption band aforementioned to quantify the material deterioration through thermoxidation is discussed thereafter.

The degradation evaluation and quantification of the ABS-g-MA and its nanocomposite samples has been based on following the absorbances of different carbonyl groups in the region between 1650 and 1800 cm^{-1} and the one of butadiene at 966 cm^{-1} in different stages of degradation. The reliability of the absorption bands aforementioned is likewise subsequently discussed.

4.4.2. Thermogravimetric analysis (TGA)

4.4.2.1. TGA and First Derivative Weight (DTG) analysis

The thermal stability of the four materials was measured by thermogravimetric analysis using a Mettler Toledo TGA/SDTA851e instrument. Samples weighing 10 ± 1 mg were loaded in aluminium pans and heated at a rate of $10 \text{ }^\circ\text{C} \times \text{min}^{-1}$. Weight loss curve was traced as each sample was heated from room temperature to $600 \text{ }^\circ\text{C}$ under air atmosphere. The use of air instead of inert nitrogen conditions is intended to bring the testing conditions as close as possible to the industrial processing conditions, hence causing auto-oxidation and reactions with secondary products. It should be noted that for the same reason the thermo-oxidation ageing in the oven has been carried out in oxygen atmosphere.

The temperature at 5% weight loss ($T_{5\%}$), temperature at 50% weight loss ($T_{50\%}$) and the temperature of the maximum weight loss rate (T_{max}) of the thermograms were collected for all samples. No particular analysis has been performed on the fraction of the solid residue at 600°C due to the low values of POSS concentration rate, although the results show proportionality in relation to the 2.5% and 5% add rate used for the POM and ABS nanocomposites respectively, whereby the Si-O constituencies of the POSS molecule evolve to Si-O₂ (silica) as the organic fraction of the sample is consumed by either decomposition, oxidation, or loss of volatiles.

4.4.2.2. Degradation kinetics by Coats and Redfern

Alternatively, the above thermogravimetric data has been further analysed by means of the Coats-Redfern kinetic analysis as per theoretical fundamentals explained in section 3.2. This method is intended to provide the activation energy E_a involved in the molecular motions and rearrangements caused by the inflicted degradation process of each sample analysed.

4.4.3. Spectrophotometry analysis (CIELAB)

Among the physical manifestations of the degradation of the polymers, yellowing is one of the most obvious. Therefore, this phenomenon can be considered as a measure of the extent of degradation [270]. This analysis was deemed to be interesting as it provides a non-destructive method to assess the extent of degradation through the surface appearance, particularly by quantifying the extent of yellowing when samples are not master-batched and are processed in their natural colour. This can therefore assist in the testing of plastic components for critical mechanical applications, by way of quantitatively finding the level of degradation in an uncomplicated and quick testing method. Furthermore, in cases of advanced degradation of the part in its application i.e. accidental burnouts in electric environments, automotive applications and so forth, to be able to estimate which range of temperatures or exposure time the part could have been submitted to.

For the spectrophotometry analysis, a Minolta CM-3600d Spectrophotometer has been used to generate the corresponding sample colour spectras upon an illuminant D65. The extracted data were reproducible to within $\pm 1\%$ and averaged of three repeated readings for each sample. The terminology used is the CIE 1976 L^*, a^*, b^* colour space with the official abbreviation CIELAB upon a rectangular coordinate system. Evaluation and quantification of the sample colour appearance has been therefore analysed upon the above $L^* a^* b^*$ parameters as an indicator of the polymer deterioration. The L^* parameter characterises the lightness of colour with values running from 0 (black) to 100 (white), a^* is the colour coordinate between green (-100) and red (+100), whereas b^* is the colour coordinate between blue (-100) and yellow (+100). Accordingly, the colour differences between samples will be expressed in terms of lightness, ΔL^* , redness-greenness, Δa^* , and yellowness-blueness, Δb^* .

In relation to yellowing, it is worth mentioning that both the POM copolymer and the ABS used in this work have undisclosed stabilisers or additives incorporated in the polymer manufacturing process. This is expected to cause additional yellowing during oven aging due to the additive deterioration, and therefore enhances the appearance degeneration on top of the inherent base-polymer yellowing process. As all samples were based on the same stabilised POM and ABS respectively, the aforementioned effect has equal impact in all cases and should not influence the comparison accuracy.

CHAPTER 5
RESULTS AND DISCUSSION

5. RESULTS AND DISCUSSION

5.1. PRELIMINARY ANALYSIS OF POM & POM/POSS NANOCOMPOSITES

5.1.1. Solubility analysis of POM and its nanocomposites

The theoretical solubility parameter of the pristine base material i.e. POM and of the different POSS nanofillers used was calculated using the following 3 different calculation methods and assumptions:

- a) **Hoy:** A widely used method due to its simplicity, although with a degree of uncertainty for not considering the effect of dispersion and polar forces and hydrogen bonding. The effect of the inorganic –Si-O- molecules of the POSS cage is also considered to be negligible [235].
- b) **Hoy G-based:** A slightly improved version of the above method as it allows to introduce the effect of the inorganic –Si-O- molecules of the POSS cage.
- c) **Hoftyzer and Van Krevelen:** This method does consider the effect of the dispersion, and polar forces by means of equations that feed from tabulated group contributions of a number of structural groups. The hydrogen bonding forces are based on the assumption that each structural group will have a constant energy. Due to the difficulties to find reliable data on the solubility parameter component for the –Si-O- cage structure group contribution, this fraction has been kept out of the equations in light of other POSS solubility studies considering the siloxane structure effects as negligible [235].

The theoretical fundamentals and formulae for each of the above methods have been explained in section 3.1, and the values of group contributions, molar attraction functions and molar volumes have been subtracted from van Krevelen et al [238].

Based on the above discussion, those methods whereby the raw data for –Si-O-Si- was difficult to achieve i.e. the standard ‘Hoy’ as well as ‘Hoftyzer & van Krevelen’, it was considered that the functional groups in the outer surface of the POSS molecules were dominating the solubility parameter, and the inorganic part with the siloxane bonding of POSS was excluded from the calculation of the solubility parameter. A more extended discussion regarding the role of the siloxane group can be found in section 3.1.4.

Overall, and based on the numerous studies published on this regard, the mean accuracy of any of the methods used falls within a 10% range [238], thus it makes sense to take the average value between the three resulting solubilities of each material to work out the final compatibility between them with an average solubility parameter.

The following pages contain the tables set up to calculate the solubility parameters for POM, POM/GPOSS, POM/GIPOSS, POM/APOSS and POM/PEGPOSS following both Hoy’s methods and the Hoftyzer&Van Krevelen approach. The chemical groups that constitute each material have been broken down in order to initially calculate the contribution of the sub-components in proportion to their presence in the molecular structure and, where applicable, the different group contributions of the polar, dispersion and hydrogen bonding forces.

POMFormula: (CH₂O)_x

POM Mo= 30.03 g/mol.

POLYOXYMETHYLENE

General formula:

CH₂O

Structural formula:



Molar mass
30,026 ± 0,0012 g·mol⁻¹
C 40 %, H 6,71 %, O 53,29 %

n	13.15789
$\alpha^{(P)}$	1.342091
δ_t	23.866
δ_p	13.21339
δ_b	12.04923
δ_d	15.80532

Sub-Total Molar Attract.Func. Values		Total groups	
Sub ΣF_t	F _p	$\Delta_t^{(P)}$	V
1	269	0	0.02
1	235	216	0.018
	504	216	0.038

Group breakdown

-CH ₂ -	1
-O-*	1

note: *O- ether

Resulting Total Function Values (Σ)

HOY's METHOD (G-based)	GROUP	(G=F _t)		Material: POM	
		Sub ΣG	ΣG	ρ	M ₀
	-CH ₃	0			
	-CH ₂ -	269	504	1.42	30.02
	-O-*	235			
	-Si-O-	0			

 δ_t 23.840

Hofzyer & Van Krevelen METHOD	GROUP	Individual Group contribution values		
		F _{di}	F _{pi}	E _{hi}
	-CH ₂ -	270	0	0
	-O-	256	400	3000

Total

Group breakdown

-CH ₂ -	1
-O-	1

note: *considered 1 plane of symmetry, x 0.6

Resulting Total Function Values (Σ)

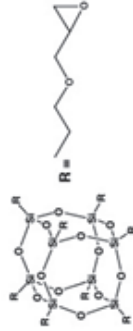
Group contribution values

δ_d	23.90909
δ_p	0 (*)
δ_b	2.489648
δ_t	24.03836

Table 6: Solubility calculation tables for POM

GPOSS : Glycidyl POSS Cage

General Formula:



FW 1337.88 D_1^{20} 1.25 D_4^{20} 1.51

n	0.419
$\alpha(P)$	1.155
δ_v	20.69
δ_p	8.787
δ_h	7.5866
δ_d	17.129

Individual Molar Attraction Function Values			
F_v	F_p	$\Delta_1(P)$	V
269	0	0.02	15.55
176	0	0.013	9.56
235	216	0.018	6.45

Sub-Total Molar Attraction Function Values			
F_v	F_p	$\Delta_1(P)$	V
40	10760	0	622
8	1408	0	76.48
16	3760	3456	103.2

Resulting Total Function Values Σ 15928 3456 1.192 801.68

GROUP	(G=F _v) Material: GPOSS		
	Sub Σ G	Σ G	M ₀
-CH ₂ -	10760	P	
>CH-	1408		
CH _{ar}	3760	20480	1337.88
-Si-O-	4552		

δ_v 19.135

GROUP	Individual Group contribution values		
	F_{di}	E_{hi}	V
-CH ₂ -	270	0	15.55
>CH-	80	0	9.56
-O-	256	400	3000

Group breakdown			
(n) Qty.	Radicals	F _{di}	E _{hi}
5	-CH ₂ -	10800	0
1	>CH-	640	0
2	-O-	2048	3200

Resulting Total Function Values Σ 13488 3200 24000 801.68

Group contribution values			
F _{di}	F _p ²	E _{hi}	V
10800	0	0	622
640	0	0	76.48
2048	3200	24000	30.4

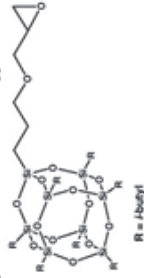
Resulting Total Function Values Σ 13488 3200 24000 801.68

Void: More than 2 planes of symmetry
 Void: More than 2 planes of symmetry

Table 7: Solubility calculation tables for GPOSS

GIPOSS : Glycidyl Isobutyl POSS Cage

General Formula:

FW 931.63 D_1^{20} 1.14 n_D^{20} 1.47

HOY's METHOD (Standard)	Individual Molar Attraction Function Values				(n) Qty. Radicals	Group breakdown	(n) Qty. Radicals	Sub-Total Molar Attraction Function Values					
	F_v	F_p	$\Delta_1(P)$	V				F_v	F_p	$\Delta_1(P)$	V		
-CH3	303.5	0	0.022	2155	0	-CH3	2	14	4249	0	0.308	302	
-CH2-	269	0	0.02	1555	5	-CH2-	1	12	3228	0	0.24	187	
>CH-	176	0	0.013	956	1	>CH-	1	8	1408	0	0.104	76	
-O-	235	216	0.018	6.45	2	-O-	0	2	470	432	0.036	3.8	
Resulting Total Function Values (Σ)													
								###	432	0.688			569

n 0.727
 $\alpha(P)$ 0.94

δ_v	17.12
δ_p	3.7192
δ_h	4.331
δ_d	16.137

GROUP	(G=F _v) Material: GIPOSS		
	Sub Σ G	Σ G	Mo
-CH3	4249		
-CH2-	3228		
>CH-	1408	13907	1.14
CH _{3r}	470		931.63
-Si-O-	4552		

 δ_v 17.017

Hoflyzer & Van Krevelen METHOD	Individual Group contribution values				Group breakdown	(n) Qty. Radicals	Group contribution values			
	F_d	F_{pi}	E_{hi}	V				F_{di}	F_{pi}^2	E_{hi}
-CH3	420	0	0	2155	-CH3	14	5880	0	0	302
-CH2-	270	0	0	1555	-CH2-	12	3240	0	0	187
>CH-	80	0	0	956	>CH-	8	640	0	0	76.5
-O-	256	400	3000	3.8	CH _{3r}	1	256	400	3000	3.8
Resulting Total Function Values (Σ)										
				10016	400	3000	569			

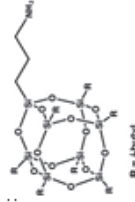
δ_v	17.62
δ_p	0.018
δ_h	0.096
δ_d	17.62

(considered 1 plane of symmetry, x 0.5)

Table 8: Solubility calculation tables for GIPOSS

APOSS : Aminopropylisobutyl POSS Cage

General Formula:
C₃₄H₇₄O₁₄Si₈



HOY's METHO (Standard d)	Individual Molar Attraction Function Values				Aminopropyl				Isobutyl						
	F _i	F _p	Δ _i (P)	V	(n)Qty.	Group breakdown	Radicals	(n)Qty.	F _i	F _p	Δ _i (P)	V	(n)Qty.	Group breakdown	Radicals
-CH3	303.5	0	0.022	2155	0	-CH3	0	14	4249	0	0.308	301.7	14	-CH3	2
-CH2-	269	0	0.02	1555	3	-CH2-	3	10	2690	0	0.2	155.5	10	-CH2-	1
>CH-	176	0	0.013	956	0	>CH-	0	7	1232	0	0.091	66.32	7	>CH-	1
-NH2	464	464	0.031	17	1	-NH2	1	1	464	464	0.031	17	1	-NH2	0
Resulting Total Function Values (Σ)															
									8635	464	0.63	541			

FW 874.58 D_i^o 1.16 ρ_s^o 1.49

n	α (P)
δ _s	0.794
δ _p	0.905
δ _a	17.97
δ _b	4.2933
δ _c	5.8343
δ _d	16.443

GROUP	(G=F _i)	Material: APOSS
SubΣG	ΣG	P
-CH3	4249	Mo
-CH2-	2690	
>CH-	1232	13187
-O-	464	1.16
-Si-O-	4552	874.58

δ_s 17.491

Hofyze & Van Krevelen METHO D	Individual Group contribution values				Group contribution values			
	F _{di}	F _{pi}	E _{hi}	V	F _{di}	F _{pi} ²	E _{hi}	V
-CH3	420	0	0	2155	5880	0	0	302
-CH2-	270	0	0	1555	2700	0	0	156
>CH-	80	0	0	956	560	0	0	67
-NH2	280	0	8400	17	280	0	8400	17
Resulting Total Function Values (Σ)								
					9420	0	8400	541

δ _s	17.41
δ _p	0
δ _a	0.169
δ _b	17.41

Table 9: Solubility calculation tables for APOSS

PEG POSS

General Formula:



Cage Mixture



PEG

General formula:
 $-CH_2CH_2(OCH_2CH_2)_mOCH_3$
 Structural formula:

Group breakdown

(n) Qty. Radicals

-CH3	1	8
-CH2-	28.6	8
-O-	14.3	

FW 5576.6 (when n = 8)

Sub-Total Molar Attraction Function Values				
F _i	F _p	Δ _T ^(P)	V	
8	2428	0	0.176	172.4
229	61547.2	0	4.576	3557.84
114	26884	24710.4	2.0592	737.88
Resulting Total Function Values (Σ)				4468.12

n 0.073409
 α^(P) 1.184458

δ _v	21.17951
δ _p	9.94433
δ _h	8.358057
δ _d	16.72797

Resulting Total Function Values (Σ)

GROUP	(G=F _i)			Material: 0
	SubΣG	ΣG	ρ	
-CH3	2428			M ₀
-CH2-	61547.2	95411.2	1.2	5576.6
CH _{3r}	26884			
-Si-O-	4552			

δ_v 20.531

GROUP	Individual Group contribution values				Total Groups	Group contribution values			
	F _{ei}	F _{pi}	E _{hi}	V		F _{oi}	F _{pi} ²	E _{hi}	V
-CH3	420	0	0	21.55	8	3360	0	172.4	
-CH2-	270	0	0	15.55	229	61776	0	3557.84	
-O-	256	400	3000	6.45	114	29286	45760	737.88	
Resulting Total Function Values (Σ)					94422	45760	343200	4468.12	

δ _v	21.13247
δ _p	0
δ _h	0
δ _d	21.13247

Void: More than 2 planes of symmetry
 Void: More than 2 planes of symmetry

Table 10: Solubility calculation tables for PEGPOSS

The results obtained in solubility terms are shown in Figure 35a, where solubility parameters have been arranged by calculation method, breaking down the dispersion, polar and hydrogen bonding contributions resulting from the standard Hoy method as well as the Hoftyzer & van Krevelen method. Generally all the results are within $\pm 10\%$ variation, hence falling within the expected error, and the introduction of the siloxane group in the formula based on Hoy molar attraction constants G_i does not differ to a relevant extent to the results obtained with the other 2 calculation methods neglecting this inorganic fraction, hence corroborating the little contribution of the $-\text{Si-O-Si}-$ structure to the overall material solubility.

Figure 35b collects the average solubility parameter for each material, calculated as the arithmetic mean value of the solubilities obtained from the 3 different calculation methods. Figure 35c shows the difference in solubility parameters between the material combination used for each nanocomposite with its corresponding SEM image.

Generally speaking, in order to have a good solubility between mixing constituents, $\Delta\delta$ should be no bigger than $\leq 5(\text{J}/\text{cm}^3)^{1/2}$ [238]. Under this criteria, POM/GPOSS would be at the limit with $5.03 (\text{J}/\text{cm}^3)^{1/2}$, and POM/GIPOSS and POM/APOSS would be just above, with a solubility difference of 6.66 and 6.29 respectively, and in fact the mixture with the highest solubility parameter difference i.e. POM/GIPOSS shows evidence of phase separation in the SEM image. Indeed, any blending process will not only depend on the solubility values of the polymers being considered, but also on other variables such as mixing temperature and time as well as characteristics of the blending equipment used.

On the contrary to the above three nanocomposites, POM/PEGPOSS yielded in a small solubility parameter difference of 2.96, suggesting a favourable enthalpy of mixing, and therefore a good miscibility between the nanocomposite fractions. Indeed, the SEM image included in section 'C' of the above figure corroborates this good compatibility with good

dispersion and the absence of agglomerates and phase separation. Further analysis of the nanocomposite morphologies is developed in the next section.

Material	HOY			①	②	HOFTYZER & van KREVELEN			③
	Solubility Components			Standard	G-based	Solubility Components			
	δ_p	δ_b	δ_d	δ_t	δ_t	δ_p	δ_b	δ_d	δ_t
	[J/cm ³] ^{1/2}	[J/cm ³] ^{1/2}	[J/cm ³] ^{1/2}	[J/cm ³] ^{1/2}	[J/cm ³] ^{1/2}	[J/cm ³] ^{1/2}	[J/cm ³] ^{1/2}	[J/cm ³] ^{1/2}	[J/cm ³] ^{1/2}
POM	13.213	12.049	15.805	23.866	23.840	0.000	2.490	23.909	24.038
GPOSS	8.787	7.587	17.129	20.692	19.135	0.000	0.000	16.825	16.825
GIPOSS	3.719	4.331	16.137	17.117	17.017	0.018	0.096	17.616	17.617
APOSS	4.293	5.834	16.443	17.968	17.491	0.000	0.169	17.408	17.409
PEGPOSS	9.944	8.358	16.728	21.180	20.531	0.000	0.000	21.132	21.132


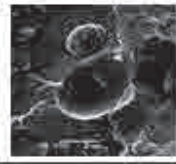


Material	Average (1+2+3) δ_t [J/cm ³] ^{1/2}	Nanocomposite	Difference in Solubility Parameter $ \Delta\delta_t $ $= \Delta\delta_{POM} - \Delta\delta_{POSS} $ [J/cm ³] ^{1/2}	Corresponding SEM images
POM	23.915			
GPOSS	18.884	POM/GPOSS	5.031	
GIPOSS	17.251	POM/GIPOSS	6.664	
APOSS	17.623	POM/APOSS	6.292	
PEGPOSS	20.948	POM/PEGPOSS	2.967	

Figure 35: Recollection of solubility parameters of POM and the different POSS nanofillers with the resulting difference in solubility of the nanocomposite system and its comparison to the corresponding SEM images.

5.1.2. SEM analysis of POM and its nanocomposites

Scanning Electron Microscopy (SEM) micrographs were obtained in order to analyse the microstructure of the composites and the degree of dispersion of POSS molecules into the matrix, taking also the POM base material as a base line to establish comparisons. The instrument used was a Jeol 5610 electron microscope at an accelerating voltage of 10 kV and the sample surfaces were cryogenically fractured.

The following Figure 36 shows 5,000x-magnification images of the reference POM and the 4 different nanocomposites prepared. The topography of the fractured surface is expected to expose the presence of aggregates or clusters within the polymer matrix in the event of poor miscibility and dispersion of the POSS nanoparticles.

Based on the above, the incorporation of G-POSS, A-POSS and PEG/POSS into the POM matrix has given good results in terms of dispersion as no aggregates or composition inhomogeneities were observed in the fractured surfaces as shown in subfigures 36b, 36d and 36e.

In the case of POM/G-POSS, the good results can be attributed to the glycidyl functionalised cage with epoxy groups, which compared to the GI-POSS, this one has the entire inorganic cage surrounded with glycidyl groups i.e. 8 instead of 1, subsequently increasing the compatibility and reactivity with the POM matrix.

On the other hand, the structure of the A-POSS cage mixture promotes intermolecular hydrogen bonding with the ether oxygen atoms of POM, as suggested in published literature regarding A-POSS [43].

With regards to the PEG/POSS, the good miscibility was already expected given the obvious similarities between the PEG pendant group and the actual POM backbone. Indeed this was also consistent with the results obtained in the previous section with the calculation of the solubility parameter difference between the POM matrix and the PEG/POSS filler.

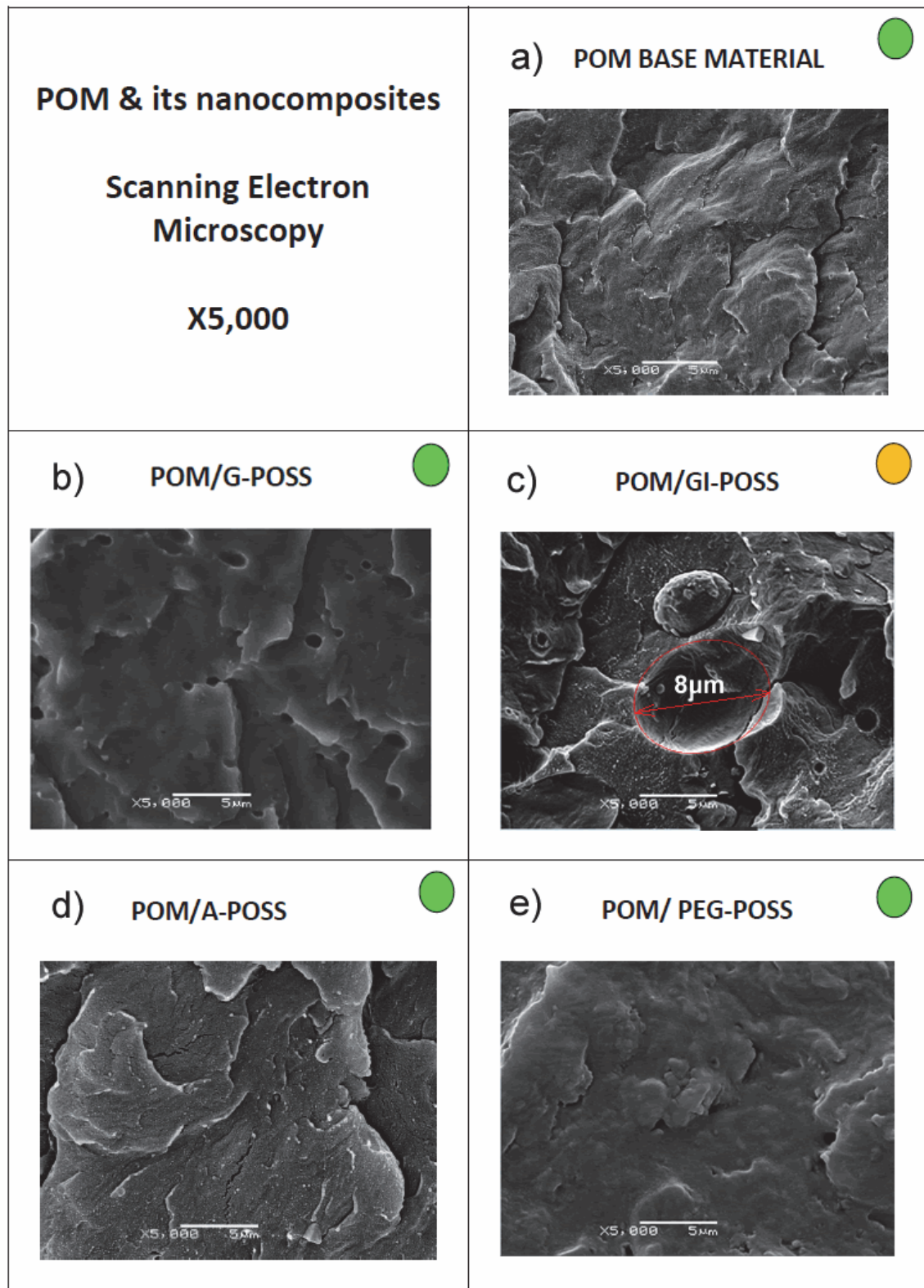


Figure 36: SEM 5,000x magnification micrograph of POM and the Nanocomposites prepared at 2.5% concentration.

Contrary to the above three cases, subfigure 36c corresponds to the fractured surface of the POM/GI-POSS nanocomposite and exhibits the presence of agglomerates with a size ranging $8\mu\text{m}$.

The spherical morphology of these micro-aggregates indicates that the phase separation took place during the melt-blend processing or during the cooling stage after it, which is more likely to induce phase separation than other nanocomposite preparation processes such as copolymerisation or dissolution, particularly if dealing with different viscosities in the melt state between the POSS and the POM. Furthermore, POSS-POSS interactions also play an important role in the agglomeration development, resulting in rich phases of POSS into the matrix forming differentiated solid fractions.

In summary, the SEM images here presented suggest adequate incorporation of the G-POSS, A-POSS and PEG-POSS into the POM matrix with no evident aggregates or modifications on the polymer fractured surface; whereas GI-POSS has produced a moderate agglomerate size indicating poor dispersion of the nanofillers.

The effect of POSS concentration on blend dispersion

It has been previously reported that certain POSS particles have the tendency to aggregate and to form crystalline structures with increasing concentration ratios within the matrix [271]. During the initial trials performed in this study to determine what would be a reasonable add ratio, we assessed the susceptibility of the different nanofillers to agglomerate keeping the same melt-blending conditions at high concentration values i.e. 10% instead of 2.5%. It should be noted that this exercise was purely for experimental purposes, as the addition of 10% of POSS is well above the standard and recommended rates used for these types of nanocomposites. High nanoparticle concentrations can have multiple effects beyond the miscibility performance, and these can be the influence on particle dispersion, viscosity of the resulting blend, coalescence and wetting with the host polymer.

This analysis showed that in addition to the GI-POSS, POM/A-POSS and POM/PEG-POSS mixed at 10% resulted in large agglomerates. Although GI-POSS already exhibited aggregates as low as 2.5% POSS concentration, as demonstrated in the previous section, at 10% these were of rather different characteristics which are worth presenting.

Figure 37 displays the comparison of the SEM images of POM/A-POSS at 2.5% and at 10% add-ratio. Note the magnification had to be set at x10,000 in order to perceive the changes in morphology as the aggregates formed at 10% POSS concentration have only a size of 3-4 μm . Although the image also indicates phase separation, which was foreseeable based on the solubility results from the previous section, this would be an example of a very low degree of agglomeration, from which more limited adverse effects on the overall nanocomposite performance are to be expected.

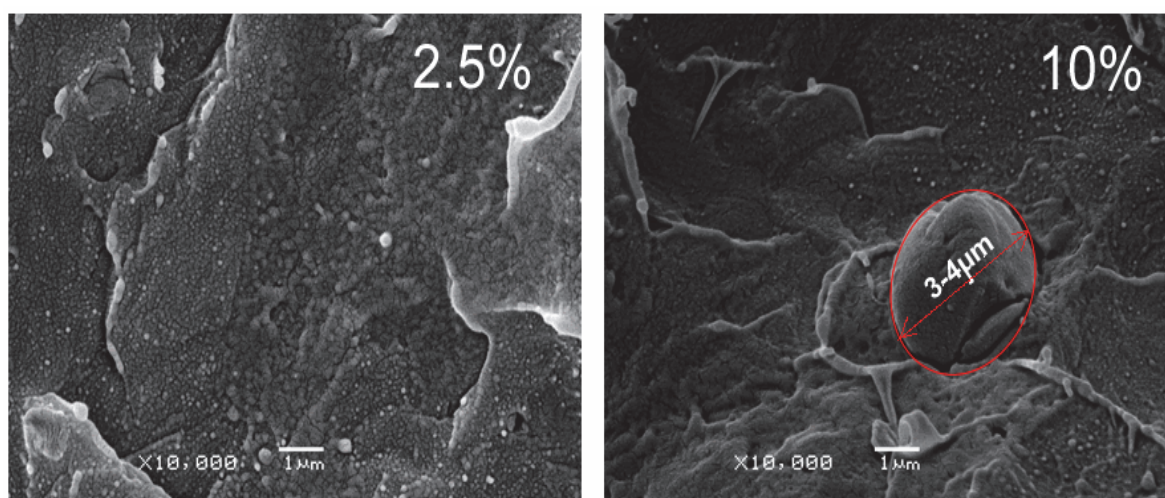


Figure 37: Comparison of the SEM images of POM/A-POSS at 2.5% and at 10% add-ratio

On the other hand, Figure 38 shows to the comparison of the SEM images with a x5,000 magnification of the nanocomposite POM/PEG-POSS at 2.5% and at 10% add-ratio. At 10% POSS concentration, well defined agglomerates of large dimensions with an exposed area of 16 μm are formed, hence with the full-sized agglomerate likely to be at least 20 μm . However,

it can also be seen good continuity throughout the interface, suggesting adequate compatibility between PEG-POSS and the POM matrix.

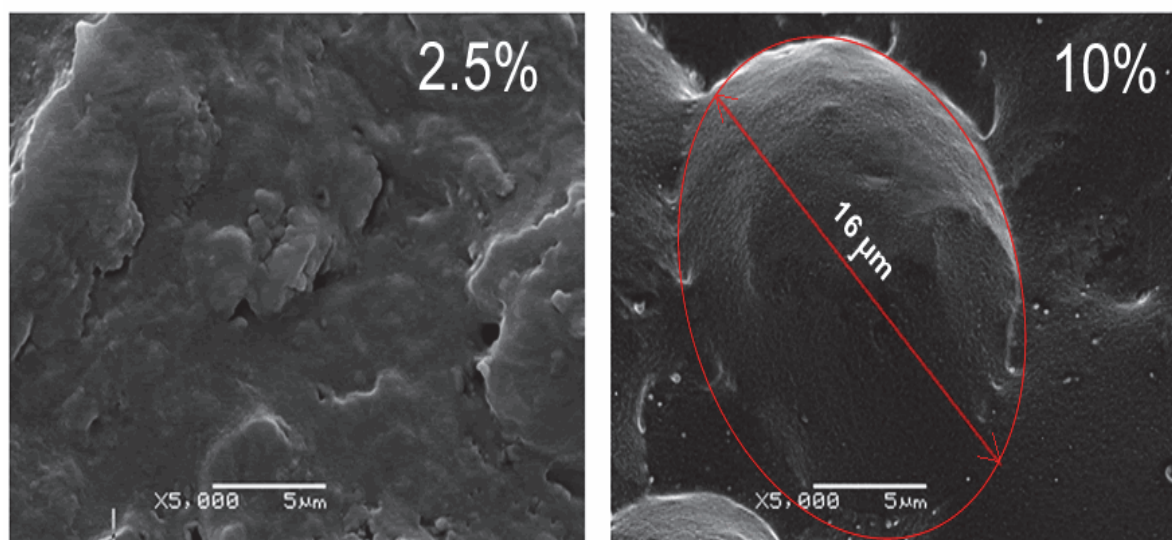


Figure 38: Comparison of the SEM images of POM/PEG-POSS at 2.5% and at 10% add-ratio

At this point we have proven the risks of bad dispersion associated with the melt-blending approach to mix nanofillers into the host polymer, as well as the adverse influence of increasing POSS concentrations in the mixture. Additionally, and just as important, the agglomeration occurring in the mixture can have two very different types of integration within the matrix i.e. with clear phase separation (split interface) or with miscible fractions (bonded interface). Both conditions have already been identified in some of the samples analysed and are displayed in Figure 40 (next page), corresponding to the samples of POM/GI-POSS at 2.5% and POM/A-POSS at 10%.

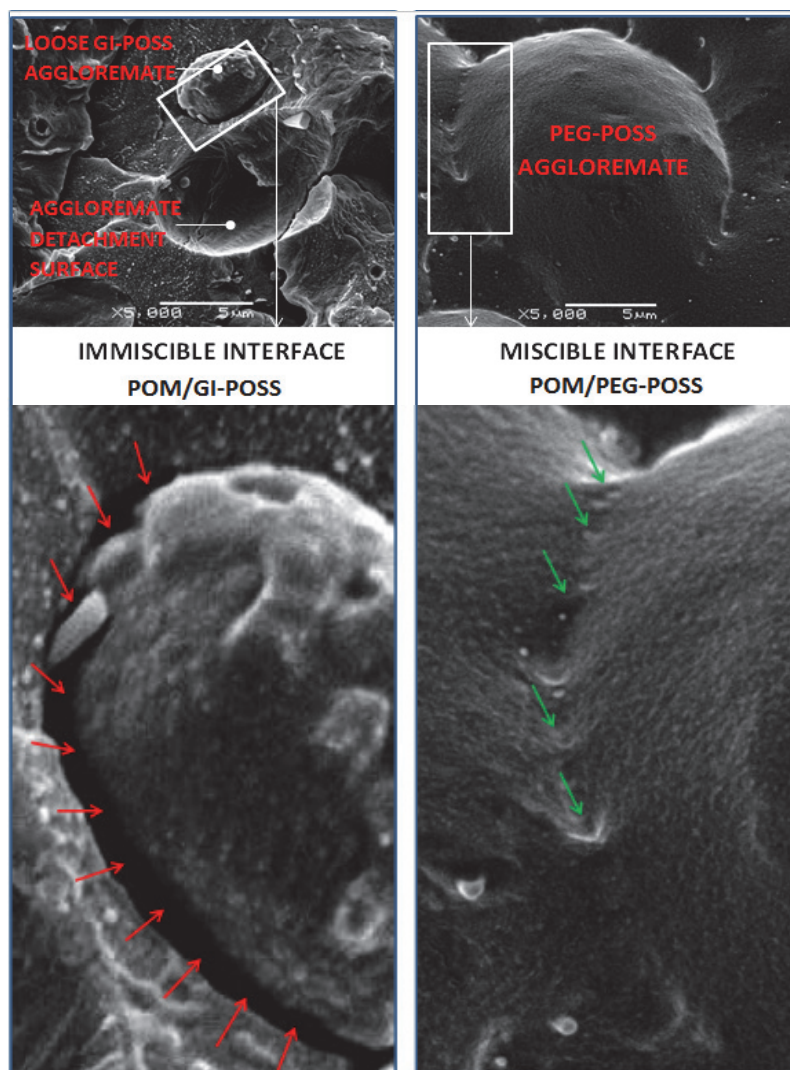


Figure 39: POSS agglomerate interface morphologies

The section on the left belongs to POM/GI-POSS at 2.5%. This nanoblend exhibits a micron-scale agglomerate which maintains a clearance (separation) with the polymer matrix. Additionally, traces of other detached aggregates are also evident on the image.

On the other side, an example of a miscible interface between the agglomerate and polymer matrix can be found on the right of Figure 39 showing the POM/PEG-POSS nanocomposite with 10% of nanofiller concentration. The SEM image shows how the agglomerate is bonded to the matrix throughout all its periphery, reflecting interaction between the cluster of nanohybrid cages and the surrounding polyacetal polymer matrix.

5.1.3. DSC analysis of POM and its nanocomposites

The thermal transitions of the samples prior to degradation and, particularly, the influence of the POSS nanofillers on the melting temperature (T_m) and crystallinity content (X_c) of the resulting nanocomposite has been evaluated by means of DSC analysis.

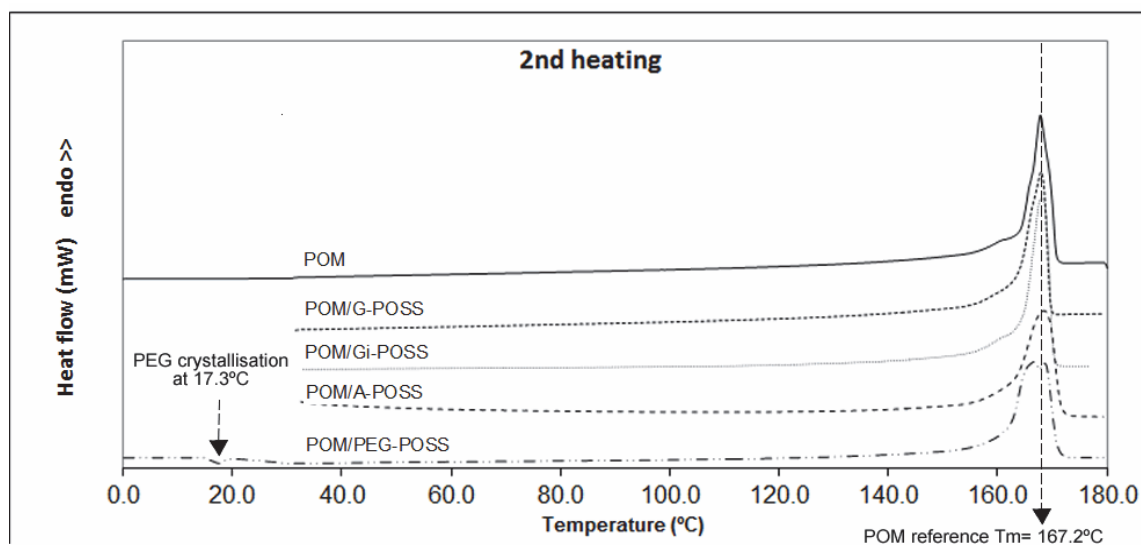


Figure 40: DSC second-heating plot for POM and the 4 different nanocomposites

Figure 40 above shows the heatflow plot for each sample during the second heating, whereby the top scan corresponds to the original and reference POM base material showing a narrow melting peak at 168.7 °C. The plots stacked underneath show the behaviour of the four different nanocomposite samples, exhibiting slight differences in T_m and endotherm peaks.

The similarity of the melting temperatures obtained from the different samples is better represented in the following Table 11, showing that these are within 1.5°C difference to the POM reference, which makes it worth noting that in some instances this temperature variation could fall within the estimated experimental variability of $\pm 1^\circ\text{C}$.

Sample	T_m , 2 nd Heating [°C]	X_c [%]
POM	167.2	61.3
POM/G-POSS	168	60.3
POM/GI-POSS	168.1	59.6
POM/A-POSS	168.5	62.9
POM/PEG-POSS	165.9 & 168.6	63.4

Table 11: DSC second-heating melting temperatures (T_m) and crystallinity values (X_c) for each sample.

Alternatively, the degree of POSS dispersion success achieved in the POM nanocomposites as the result of the melt blending process is assessed by tracking down additional isolated melting points. The known T_m 's of the pure nanofillers are 22°C, 129°C, 51.9 and 22°C for GPOSS, GIPOSS, APOSS and PEG POSS respectively. It should be noted that GPOSS and PEG POSS do have the same melting temperature, with an error of $\pm 1^\circ\text{C}$ applicable for all T_m 's. This DSC analysis is based on the fact that endothermic peaks would appear on the DSC curves at the aforementioned melting temperatures corresponding to each nanofiller if inadequate miscibility or aggregation was present.

In the case of the nanocomposites prepared with GPOSS, GIPOSS and APOSS, no peaks other than the general nanocomposite T_m were observed in any one plot. It is therefore reasonable to assume that these have been thoroughly blended and dispersed within the matrix with no crystallisation fraction of neat POSS or that the size of formed crystals is too small for being detected by DSC measurements. This was indeed expected as all the POSS used had a T_m well below that one of POM, being well and truly molten during the sample preparation process, hence facilitating the effectiveness of the mixing and blending process and minimising their domain size within the composites.

However, and unlike the favourable mixing obtained on the above three nanocomposites, the POM/PEG-POSS sample showed a subtle evidence of crystallisation of neat POSS at 17.3°C through a small exothermic peak (see bottom heatflow plot of previous Figure 40). Said T_c sits near its corresponding T_m at 22°C, and therefore indicates a small crystallised

fraction of isolated POSS. This adverse phenomenon has been previously documented, demonstrating a tendency of certain POSS particles to aggregate and form crystalline structures with increasing concentration ratios within the matrix [271], and particularly PEG-POSS nanocomposites have also been studied determining a direct relationship between the POSS percentage content and the susceptibility to aggregate [43] as seen also in the previous section of SEM analysis with a 10% POSS concentration. This finding, therefore, cannot regard the POM/PEG-POSS sample as being optimally blended and supports the results showing lower thermal stability for this particular nanocomposite.

The slight intricacy of the POM/PEG-POSS curve suggested a closer look at the broadened melting transition exhibiting two peaks during the second heating, and this detail is shown in Figure 41 below. Although the melting temperatures corresponding to the twin peaks are similar to that one of the original POM i.e. just 1.3°C below and 1.4°C above respectively, they suggest the coexistence of two main different crystalline fractions, consisting of a superposition of two endotherms and one exotherm in-between as a result of the fusion of lower stability crystals at 165.9°C and, to a limited extent, the recrystallisation of a larger crystal lamellar cluster before the second melting peak at 168.6°C.

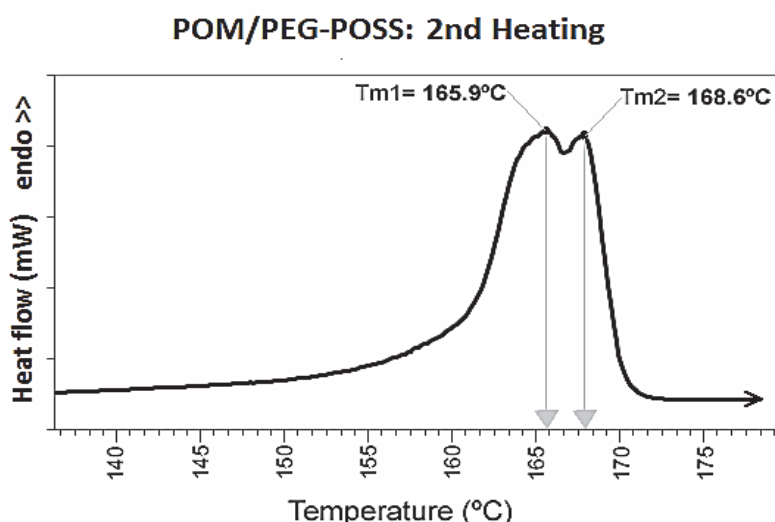


Figure 41: DSC plot (2nd Heating) at the melting peak of POM/PEG-POSS sample

Indeed, the above discussion encouraged the analysis of the crystallisation behaviour of this particular sample. For this purpose, Figure 42 shows the DSC cooling curve of the POM/PEG-POSS sample alongside that one of plain POM, whereby the former exhibits a slightly higher crystallisation temperature, i.e. $T_c=144.7\text{ }^\circ\text{C}$ instead of the $143.9\text{ }^\circ\text{C}$ corresponding to the POM sample, with a broader exothermic reaction overlapping at least 2 more secondary crystallisation points. This phenomenon is generally attributed to a nucleation effect of the POSS filler and will be discussed in more detail in the next paragraphs covering the crystallisation content analysis.

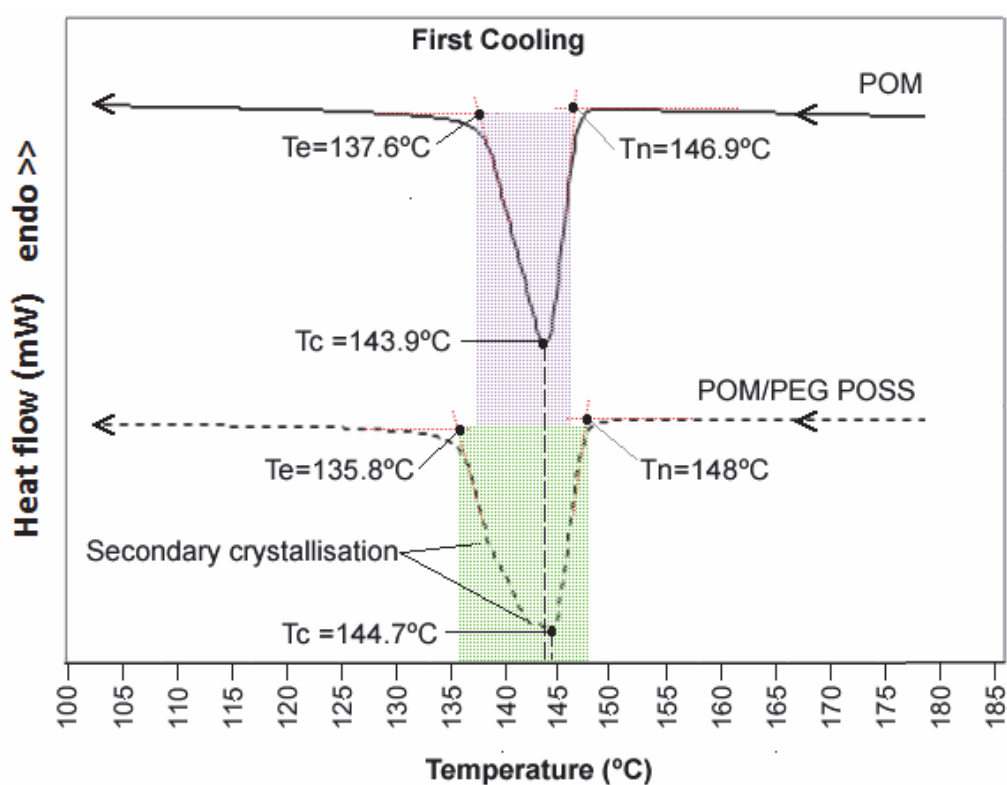


Figure 42: DSC plot (Cooling) at the crystallisation temperature spectrum of POM/PEG-POSS and POM samples.

The crystallinity content was determined by means of the ratio between the measured melting enthalpy and that one of a completely crystalline POM, considered to be 251.8 J/g

[272]. The previous Table 11 shows the crystallinity results for each sample expressed in percentage terms by the parameter X_c , where small changes are seen relative to the 61.3% of the neat POM sample i.e. POM/GPOSS with 60.3%, POM/GI-POSS with 59.6%, POM/APOSS with 62.9% and POM/PEG-POSS with 63.4%.

The composites POM/GPOSS and POM/GIPOSS showed a small X_c reduction of -1% and -1.7% respectively. This is phenomena can be a side-effect of the incorporation of POSS molecules into semi-crystalline polymers, which would be attributed to the interactions of the POSS particles with the POM backbone slightly inhibiting the tendency of the host polymer to crystallise to its original state due to the irregularity inflicted by the bulky POSS cages into the POM matrix [224]. Along these lines, it is worth noting that polyacetals have very high crystallinity content in their pristine condition (typically up to 85%) thanks to the simplicity of their linear ether structure being highly favourable to pack, thus the incorporation of new structures within the system can easily justify a reduction in the overall crystallinity. Similar findings have been reported with the addition of POSS nanofillers on structurally similar polymers such as polyethylene, whereby the formation of crystallites was disrupted by the filler-host interactions during the blending process [104]. To a certain degree, this also indicates a successful incorporation and reaction of GPOSS and GIPOSS into the base material matrix.

Unlike the previous two nanocomposites, the degree of crystallinity in POM/A-POSS and POM/PEG-POSS increased by 1.6% and 2.1% respectively, which although it cannot be considered as a remarkable increment; it could suggest a nucleating effect of the POSS molecules on the base material. This phenomenon has been reported previously with other POSS nanofillers and host materials [104, 180, 273-276].

The highest crystallisation increment corresponding to the POM/PEG-POSS sample can be better understood by revisiting the previous Figure 42 where its exotherm is compared to the one of the POM reference with the following observations:

- Although the induction periods are similar on both samples, the onset corresponding to the nucleation temperature (T_n) starts 1.1°C earlier in the cooling process of the POM/PEG-POSS sample i.e. 148°C instead of the 146.9°C corresponding the POM T_n .
- Crystallisation temperature (T_c) is 0.8°C higher, i.e. 144.7°C for POM/PEG-POSS and 143.9°C for POM.
- The end of the exotherm (T_e) is 1.8°C lower in the POM/PEG-POSS sample i.e. 135.8°C instead of 137.6°C. This means that the temperature range (T_n-T_e) during which crystallisation develops is 2.9°C broader on the PEG nanocomposite, i.e. resulting in an amplitude of 12.2°C instead of 9.3°C, which is 31% more of temperature spectrum allowing for crystallisation.
- The POM/PEG-POSS curve shows at least two secondary crystallisation peaks embedded in the main exotherm, which corroborates the different nucleating episodes occurring during the cooling process.
- The supercooling (T_m-T_n) remains almost the same in both samples, i.e. the POM/PEG-POSS is 20.6°C and POM is 20.3°C.

Notwithstanding the discussion developed in the previous paragraphs sourcing the root-cause for the changes in thermal behaviour and crystallinity, it is worth noting that any one difference in DSC temperature signals ranging $\pm 1^\circ\text{C}$ could also fall within the experimental variability. With this in mind, we can nevertheless conclude that the addition of the POSS nanofillers chosen for the POM matrix with the add rate of 2.5% has a slight to moderate repercussion to the melting temperature and crystallinity of the resulting composite, with maximum values obtained with POM/A-POSS and POM/PEG-POSS being within the range of $\pm 1.4^\circ\text{C}$ and $\pm 2.1\%$ X_c respectively when compared to those of the base material. These levels of influence are consistent with numerous studies carried out on other POSS nanocomposites [48, 248, 276-279], although there are also cases where, due to the specific POSS reactivity, solubility and compatibility with the base material, the effects on the thermal and morphological properties can be more pronounced, in some cases with a 45% increase in crystallinity [248].

5.2. DEGRADATION ANALYSIS OF POM & POM/POSS NANOCOMPOSITES

5.2.1. Fourier Transform Infra-Red analysis of POM and its nanocomposites

5.2.1.1. Examination of the original POM and its degradation behaviour

An initial comparison of IR spectra between a standard POM homopolymer with POM copolymer is carried out to have a base line and to contextualise later in this section the effects of the POSS incorporation into the POM copolymer matrix. Figure 43 depicts said comparison and shows that the absorption bands corresponding to the methylene content, i.e. CH₂ wagging and CH₂ bending at 1430 cm⁻¹ and 1465-1470 cm⁻¹ respectively have higher values on the copolymer than those for the standard homopolymer. These results were expected, as the higher absorption of methylene in the copolymer corresponds to the incorporation of successive methylene groups within the chain to obtain higher thermal stability.

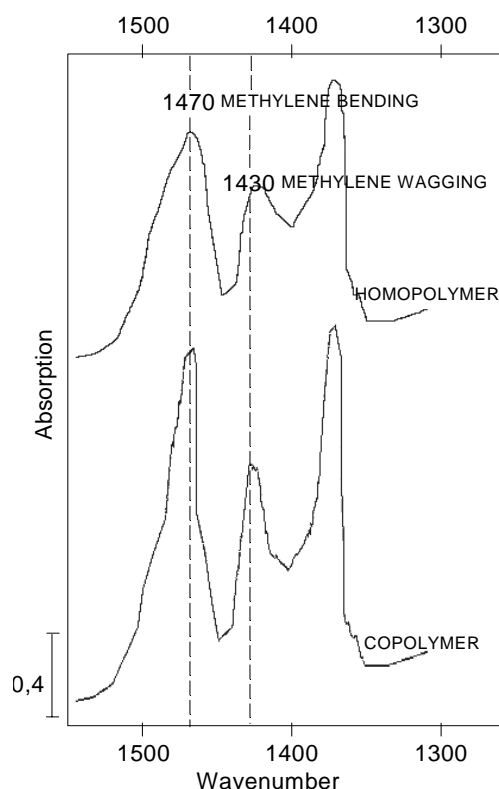


Figure 43: FTIR spectra of POM homopolymer versus POM copolymer at the characteristic absorption bands corresponding to CH₂ wagging and bending.

During the gathering process of the different spectras resulting from the degraded samples, several characteristic peaks exhibited variations as the polymer was thermoxidated through oven-storage. One of the bands considered was the one corresponding to the C-O group at 1000 cm^{-1} , which exhibited a reduction during aging. However, the absorption bands that happened to be more evident, as well as relevant for this study, were the ones corresponding to the group carbonyl from the aldehyde group (-C=O) at 1733 cm^{-1} and those from the methylene bending group (-CH_2) at around $1465\text{-}1470\text{ cm}^{-1}$.

Based on the internal pattern as a method to evaluate the results, the absorption at 1470 cm^{-1} corresponding to the methylene group is taken as the reference for working out the absorption ratios of carbonyl yield. This methylene group is considered as suitable for a reference as it appeared to be invariable during the initial stages of degradation, and can therefore reduce the differences in sample weight. Given the aging aggressiveness of the present study, it is to be expected that at some stage of degradation its applicability will cease due to severe decomposition of the polymer with the consequent and notorious decrease in the presence of the methylene group.

The following Figure 44 shows seven FTIR stacked spectras corresponding to the POM reference and the six samples thermoxidated at $220\text{ }^\circ\text{C}$ for different periods of time. From this figure, it can be clearly seen that the band exhibiting a more obvious absorption build-up as the degradation process takes place is the one corresponding to the group carbonyl – (C=O) at 1733 cm^{-1} .

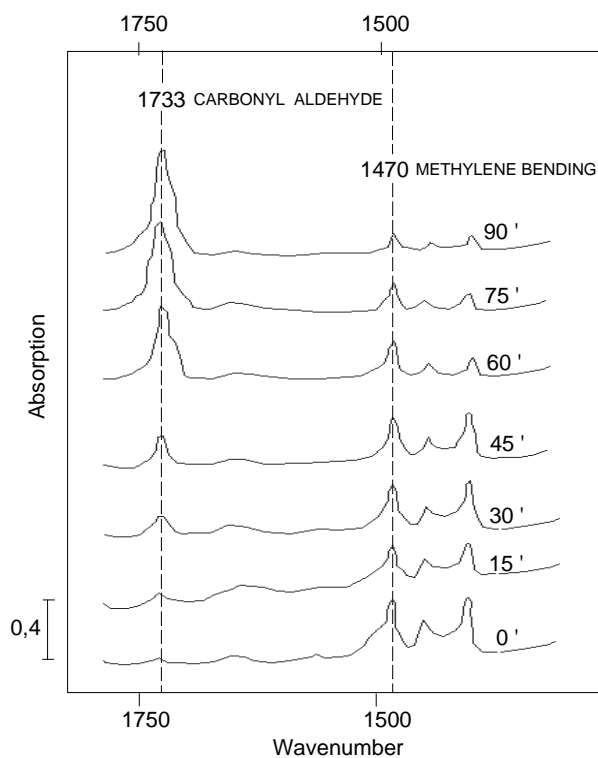


Figure 44: FTIR spectra for an injected POM submitted at 220°C for different times in the band region corresponding to the carbonyl aldehyde group and the methylene bending.

A comparison of the progress of the carbonyl absorption through the five degradation periods and five different temperatures is depicted in Figure 45, where the y axis represents the absorption ratio carbonyl/methylene. It can be seen that the carbonyl yield in proportion to the methylene absorbance has a non-linear trend as the polymer is being degraded. The steepest carbonyl yield occurs at 220°C only slightly above the processing temperatures i.e. 210°C around a timescale of 60 minutes, from which the carbonyl index increases dramatically in proportion to the methylene one.

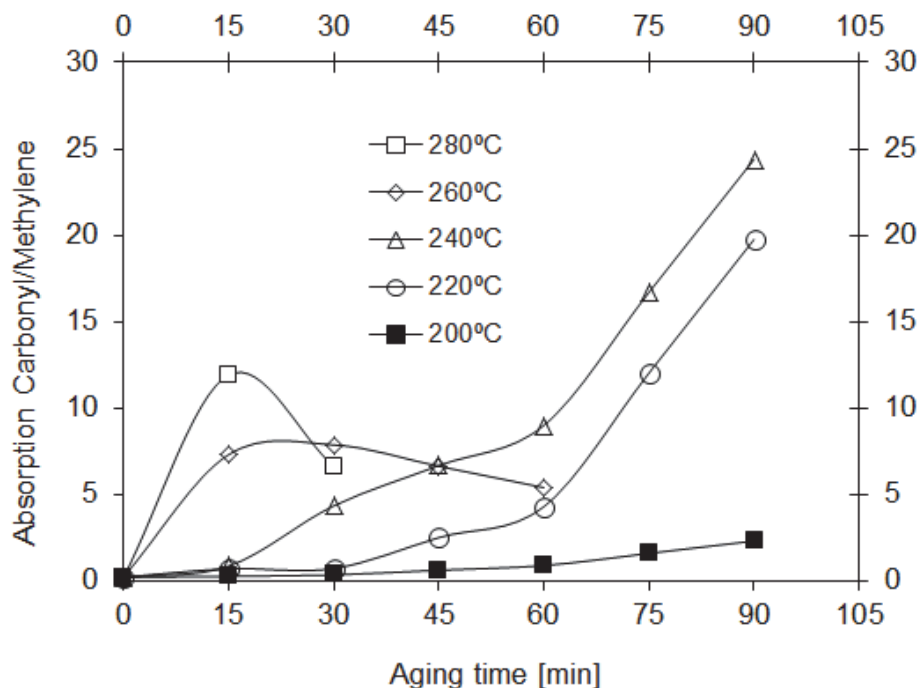


Figure 45: Comparison of absorption progress of bands corresponding to end-groups carbonyl referred to the methylene absorbance for the original POM sample.

However, upon the most aggressive temperatures such as 260 and 280 °C, the carbonyl absorption not only failed to yield to high proportions but also decreased in the ultimate experimental steps of the experiment, along with a visual decomposition of the sample. Indeed, the decomposition of the backbone no longer allows considering the methylene bending absorption as a base reference and therefore the so-called internal pattern approach loses reliability.

Previous studies on POM thermal degradation have assigned the carbonyl absorption to formoxy groups, yielding by B-scission of -O-CH- groups in the main chain as the thermoxidation process evolves [144].

It has been broadly accepted that the thermoxidative degradation of POM depends not only on temperature, oxygen concentration and chemical structure of the polymer but also on the degree of crystallinity and morphology. Bearing in mind that oxygen attacks primarily the

amorphous part of a semicrystalline polymer, it has been also attempted in this work to relate the FTIR results with the crystallinity progress as degradation took place [154, 156, 280]. However, this approach has been largely unsuccessful, as no specific trend has been found.

Considering the obvious physical manifestations that were occurring on the samples as degradation was progressing, five degradation groups based in the polymer appearance have been represented in terms of iso-carbonyl plots arisen from the combination of different temperatures and times to which the samples were submitted. This is represented on Figure 46, where each category represents a range of carbonyl yield in proportion to the methylene absorption.

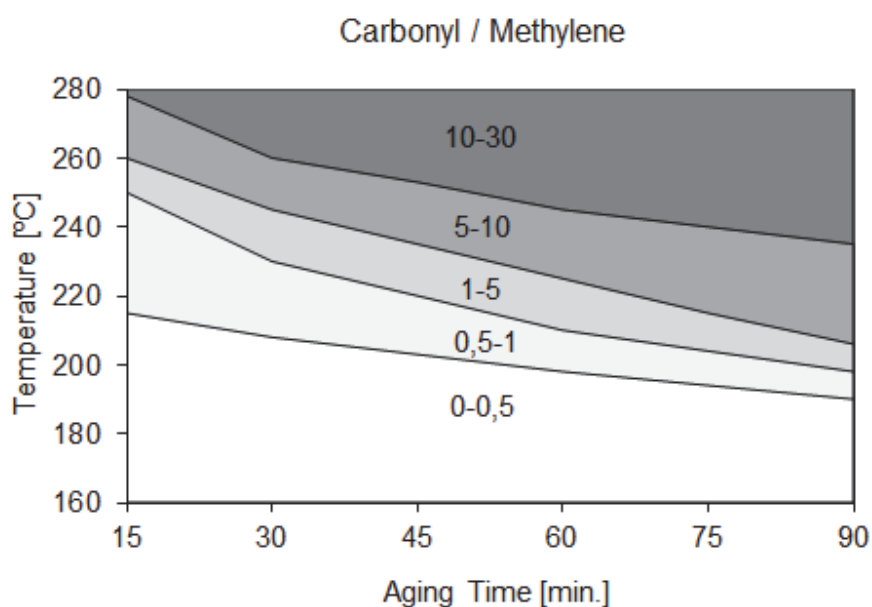


Figure 46: Degradation groups based on different Iso-Carbonyl yields referred to ageing temperature and storage time for the original POM sample.

Based on the above figure, five degradation groups are suggested:

- No apparent degradation: With a carbonyl/methylene absorption rate between 0.2-0.5, no visible degradation was perceived.
- Mid-degradation: With a carbonyl/methylene absorption rate between 0.5-1, a yellowing effect appeared at the edges of the sample.

- c. High degradation: With a carbonyl/methylene rate between 1-5, a yellowing effect was present throughout the sample along with initiation surface cracks and chalking.
- d. Complete degradation: With a carbonyl/methylene ratio between 5-10, the polymer turned into a yellow-brownish powder, with surface cracks and chalking becoming more evident.
- e. Complete carbonisation: With a carbonyl/methylene ratio higher than 10, the sample turned into a black carbonised powder.

The inter-dependence of each degradation group described above to the temperature and time variables is clearly seen, with equivalent thermoxidation states that can be achieved with lower temperatures for longer periods of time or vice versa, higher temperatures for shorter periods of time. Figure 47 proves such fact, where similar carbonyl rates are found in the sample degraded at 220°C for 60 min and that one at 240°C for 30 min. Comparable situations apply across the board of the thermoxidation conditions used.

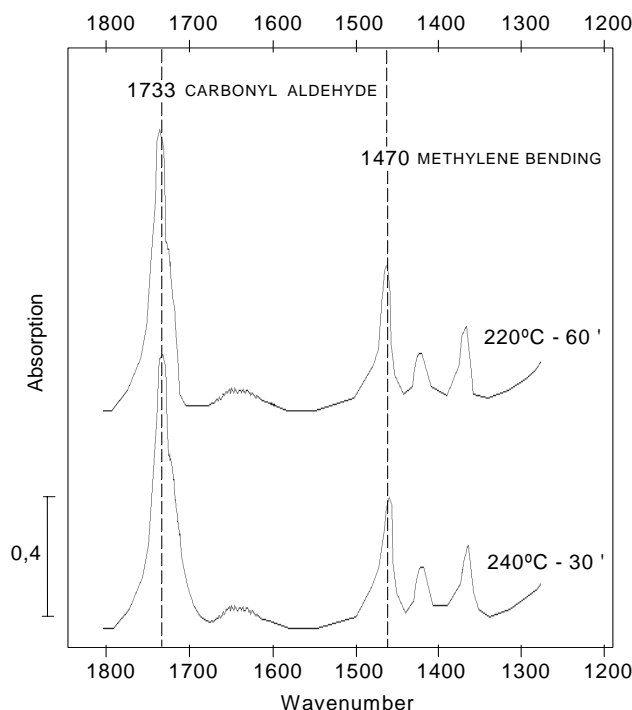


Figure 47: FTIR spectra of POM submitted at 220°C for 60min versus another one submitted at 240°C for 30min.

5.2.1.2. Examination of POM nanocomposites and their degradation behaviour

The absorption bands that were found most relevant for the POM copolymer and its nanocomposites are depicted in Table 12. On the one hand, we have the characterisation bands for the materials already analysed, which in the case of POM, the one corresponding to the symmetric stretching vibration of C-O-C ether groups at 1090 cm^{-1} can be of interest, and the one corresponding to the stretching of the Si-O-Si group at 1084 cm^{-1} is expected to be a common band for the different POSS; on the other hand, the bands chosen for monitoring of the degradation process based on the internal pattern are the methylene group as the reference at 1470 cm^{-1} and the carbonyl from the aldehyde group at 1733 cm^{-1} .

Material	Wavenumber $1/\lambda\text{ [cm}^{-1}\text{]}$		Description
POM	1090	C-O-C	Symmetric stretching vibration
POSS	1084	Si-O-Si	Symmetric stretching vibration
POM & POM/POSS	1733	$\begin{array}{c} \text{O=C-} \\ \\ \text{H} \end{array}$	Carbonyl (Aldehyde group)
POM & POM/POSS	1470	CH ₂	Methylene (Scissoring and/or Bending)

Table 12: Relevant FTIR absorption bands for the characterization of POM, POSS and thermoxidative degradation.

The different FTIR spectras obtained from each sample prior to degradation are shown in Figure 48, where no obvious differences are seen between the original POM and its nanocomposites. This is due to the proximity between the characteristic absorption of POM at 1090 cm^{-1} and the one for the POSS at 1084 cm^{-1} , whereby both characteristic absorptions are embedded into each other without showing distinguishable peaks.

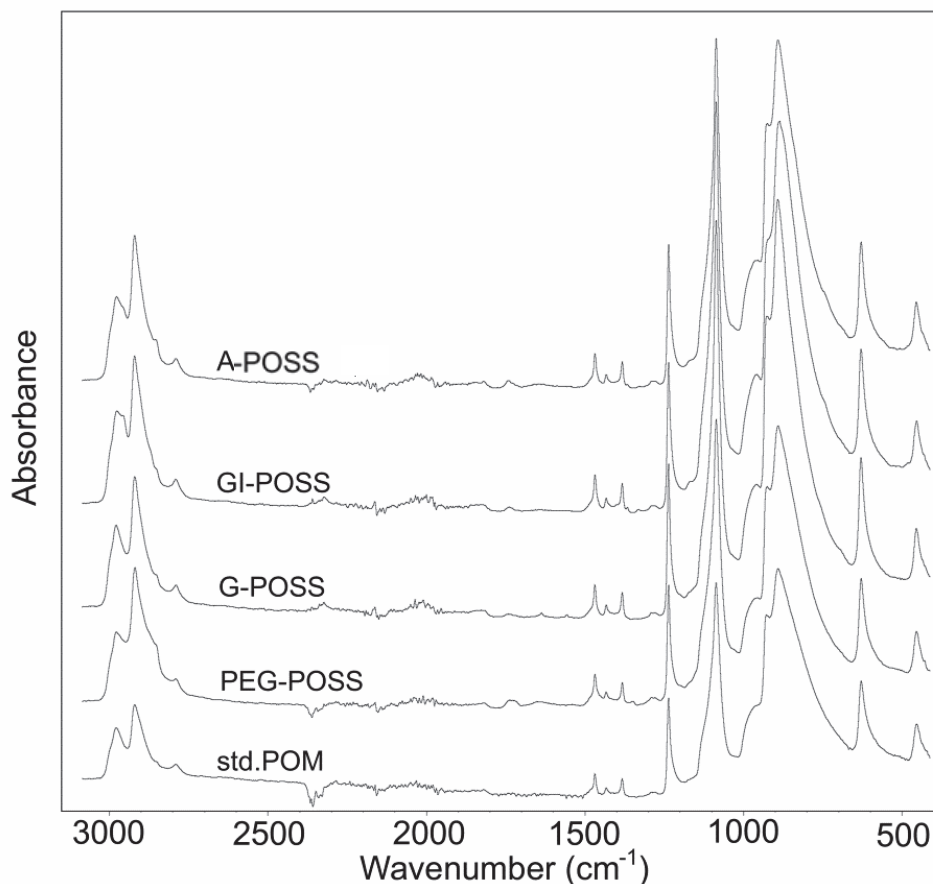


Figure 48: Stacked FTIR spectra of Standard POM copolymer, POM/PEG-POSS, POM/G-POSS, POM/GI-POSS, and POM/A-POSS, respectively.

Alternatively, the methylene group proved to be a suitable reference as it appeared to be invariable, sharp and well defined during the progressive stages of degradation, and it can also be seen in Figure 49 that the carbonyl band $-(C=O)$ exhibited an obvious absorption build-up as the degradation process takes place. Although this particular example was the POM/G-POSS submitted at 240°C, all the different POM/POSS nanocomposites analysed with different temperatures showed similar trends.

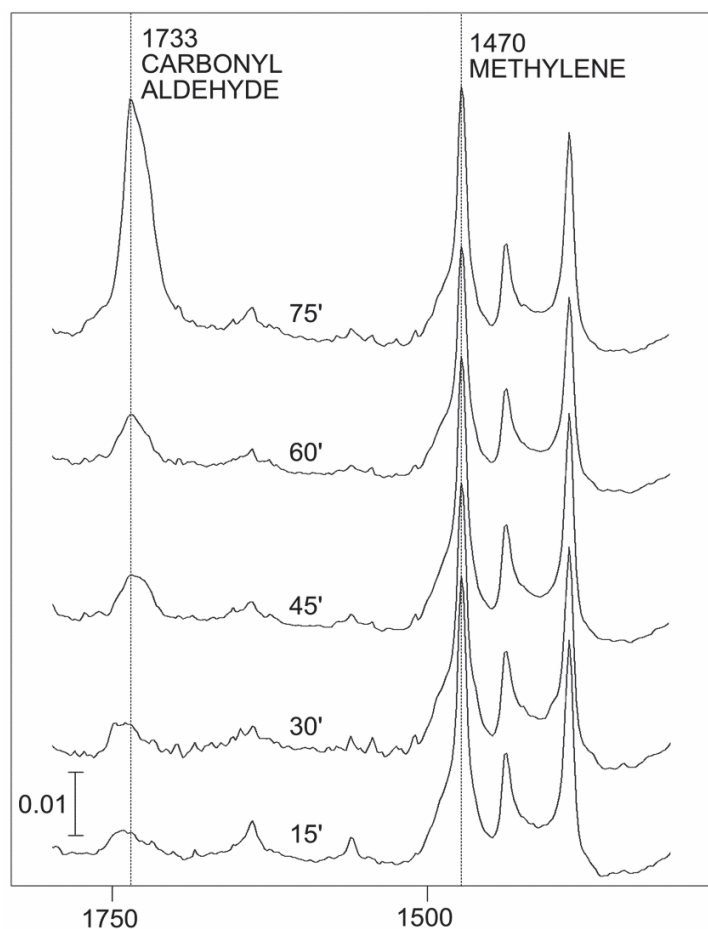


Figure 49: FTIR spectra for an injected POM/Glycidyl POSS submitted at 240°C for different times in the band region corresponding to the carbonyl aldehyde group and the methylene bending.

The aforementioned trends can also be represented by comparing the different nanocomposites in relation to the progress of carbonyl absorption at four different temperatures during five periods of time. These comparisons are illustrated in Figure 50, where the y axis represents the absorption ratio carbonyl/methylene and the x axis the exposure time. It can be seen that such ratio has a non-linear trend with the polymer degradation progress, and most importantly, that the behaviour of the different POM/POSS nanocomposites differs notably when it comes to carbonyl yield (note the scale of the carbonyl/methylene is ten times greater than the one used on the nanocomposites).

Within the overall positive results obtained with the four nanocomposites, A-POSS and GI-POSS were the best performers showing levels of the above ratio not greater than 0.5 at the

highest temperatures tested, whereas G-POSS and PEG-POSS had a higher carbonyl yield up to 1 and 2 respectively, meaning higher propensity to thermo-oxidation.

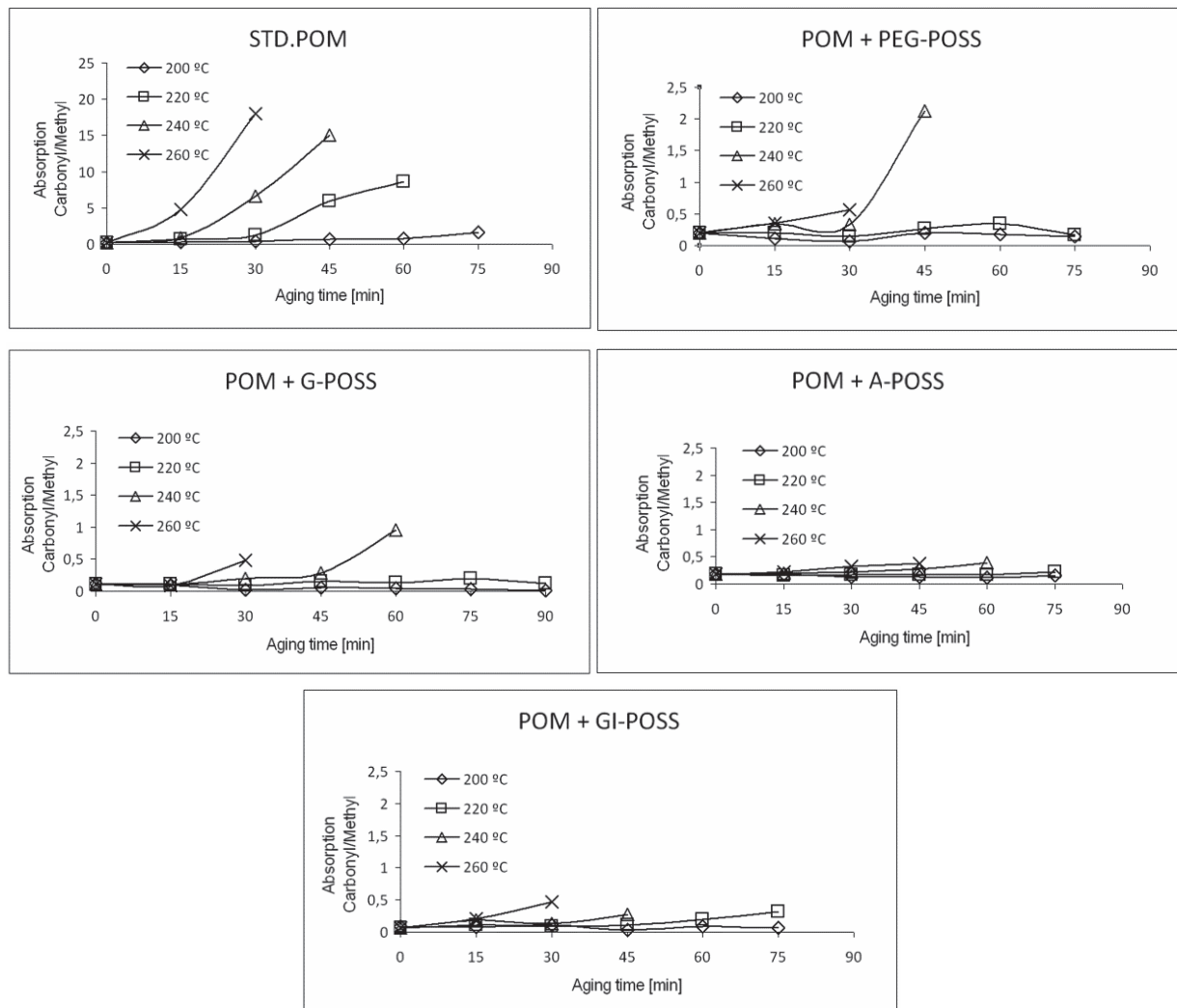


Figure 50: Comparison of absorption progress of bands corresponding to end groups carbonyl referred to the Methylene absorbance.

It is worth mentioning that upon the most aggressive temperatures such as 260°C during long periods of time, both the methylene and the carbonyl absorptions not only failed to yield to high proportions but also decreased in the ultimate experimental steps of the degradation, along with a visual decomposition of the sample. Accordingly these samples were voided.

As per our discussion in the analysis of the original POM, the carbonyl absorptions are assigned to formyloxy C=O groups as a result of the β -scission of -O-CH- groups in the main chain caused by the thermoxidation deterioration [144].

With the attempt to categorise the extent of thermoxidation of the different samples in each condition, the following degradation groups are suggested, based on the ratio between the carbonyl yield and the methylene absorption (C/M) and following the same criteria as in the previous study with POM homo and copolymers:

- a. No apparent degradation: With a carbonyl/methylene absorption rate between 0.2-0.5, no visible degradation was perceived.
- b. Mid-degradation: With a carbonyl/methylene absorption rate between 0.5-1, a yellowing effect appeared at the edges of the sample.
- c. High degradation: With a carbonyl/methylene absorption rate 1-5, a yellowing effect was present throughout the sample along with initiation surface cracks and chalking.
- d. Complete degradation: With a carbonyl/methylene ratio 5-10, the polymer turned into a yellow-brownish powder, with surface cracks and chalking becoming more evident.
- e. Complete carbonisation: With a carbonyl/methylene ratio higher than 10, the sample turned into a black carbonised powder.

With the above categorisation criteria, Figure 51 in the next page shows the comparison between a standard POM and the four different POM/POSS nanocomposites in terms of propensity to increase the carbonyl yield as temperature increases and time elapses, which alternatively depicts the same dramatic improvement shown in the previous Figure 50 in a more graphical way. Likewise, Figure 51 also presents the photos taken at the different samples submitted at 260°C during 75 min to visually comprehend the extent to which POSS provides a dramatic improvement on the thermal stability of the POM matrix. In the subsequent section we will further discuss the reasons likely to promote such stability enhancement, which are primarily based on the compatibility and the interactions between the POSS functional groups and the POM matrix.

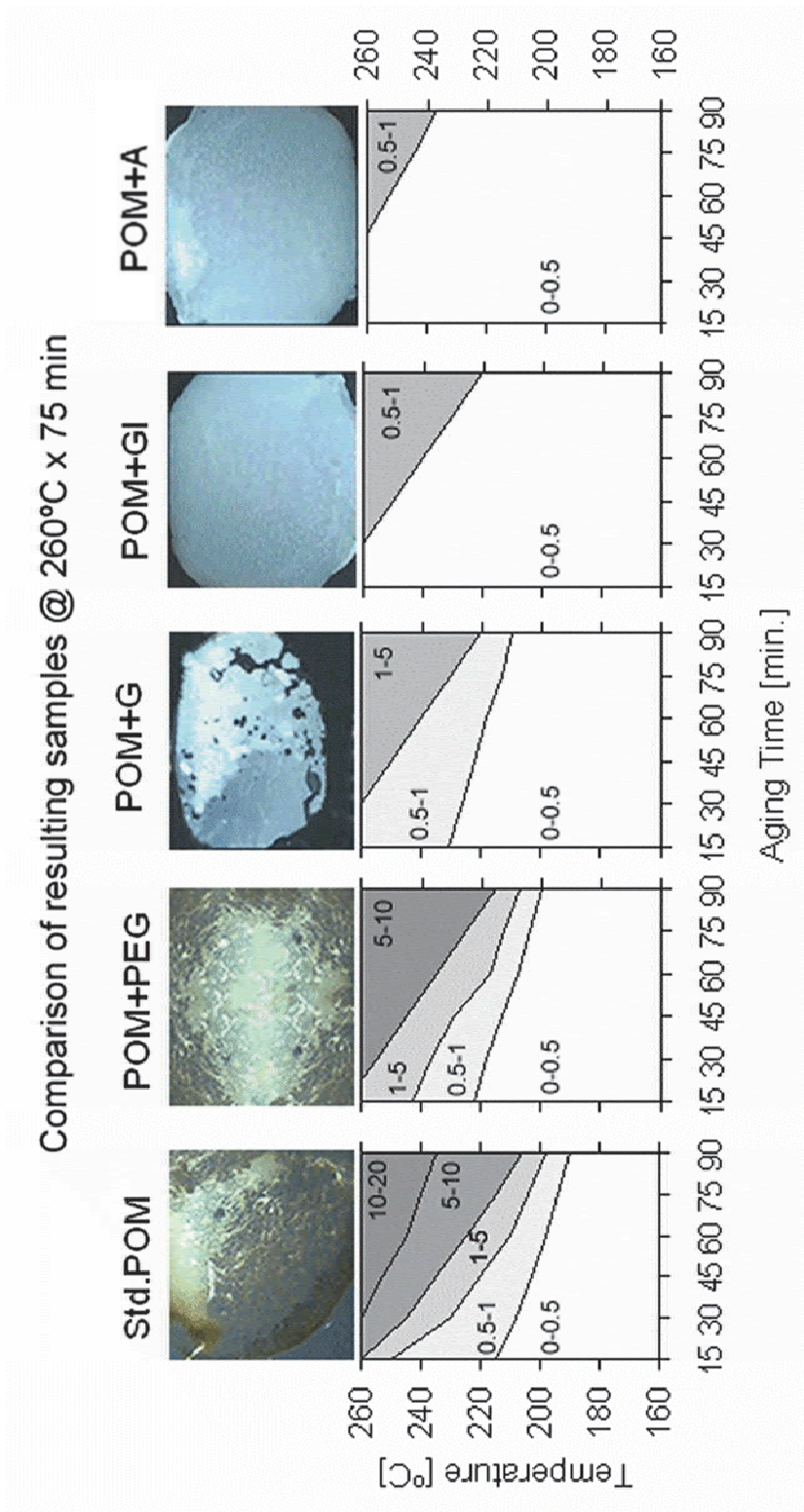


Figure 51: Photos taken at the different POM samples submitted at 260 °C x 75 min and categorised in different Carbonyl/Methylene ratio

5.2.2. Thermogravimetric analysis of POM and its nanocomposites

The temperatures at 5% weight loss ($T_{5\%}$), 50% weight loss ($T_{50\%}$) and the temperatures of the maximum weight loss rate (T_{max}) of the thermograms for all samples are shown in Table 13. The fraction of the solid residue at 600°C was not considered due to the low values of inorganic residues obtained in all blends as explained in section 4.4.2.1.

	$T_{5\%}$		$T_{50\%}$		T_{MAX}	
	°C	$\Delta^{\circ}\text{C}$	°C	$\Delta^{\circ}\text{C}$	°C	$\Delta^{\circ}\text{C}$
<i>POM</i>	253	<i>n/a</i>	281	<i>n/a</i>	288	<i>n/a</i>
<i>POM-PEG</i>	260	7	288	7	296	8
<i>POM-G</i>	263	10	296	15	298	10
<i>POM-GI</i>	261	8	295	14	302	14
<i>POM-A</i>	260	7	297	16	310	22

Table 13: TGA-Summary of results for POM and its nanocomposites expressed in $T_{5\%}$, $T_{50\%}$ and T_{max} .

The weight loss of POM took place in a single step in the temperature ranges of 250-350 °C, with an abrupt drop after 270 °C ($T_{5\%}$). As described in section 2.1.4, the thermal degradation of POM is basically due to the chain scission of the C-O-C bonds, which quickly resumes to unzipping and depolymerisation due to the hostile acidolysis caused by the formation of formic acid as a degradation by-product.

The thermal stability of POM and the POM/POSS nanocomposites is expressed in terms of weight loss (a) and the derivate weight (b) thermograms in Figure 52, and the data extracted from these thermograms have been also collected in Table 13.

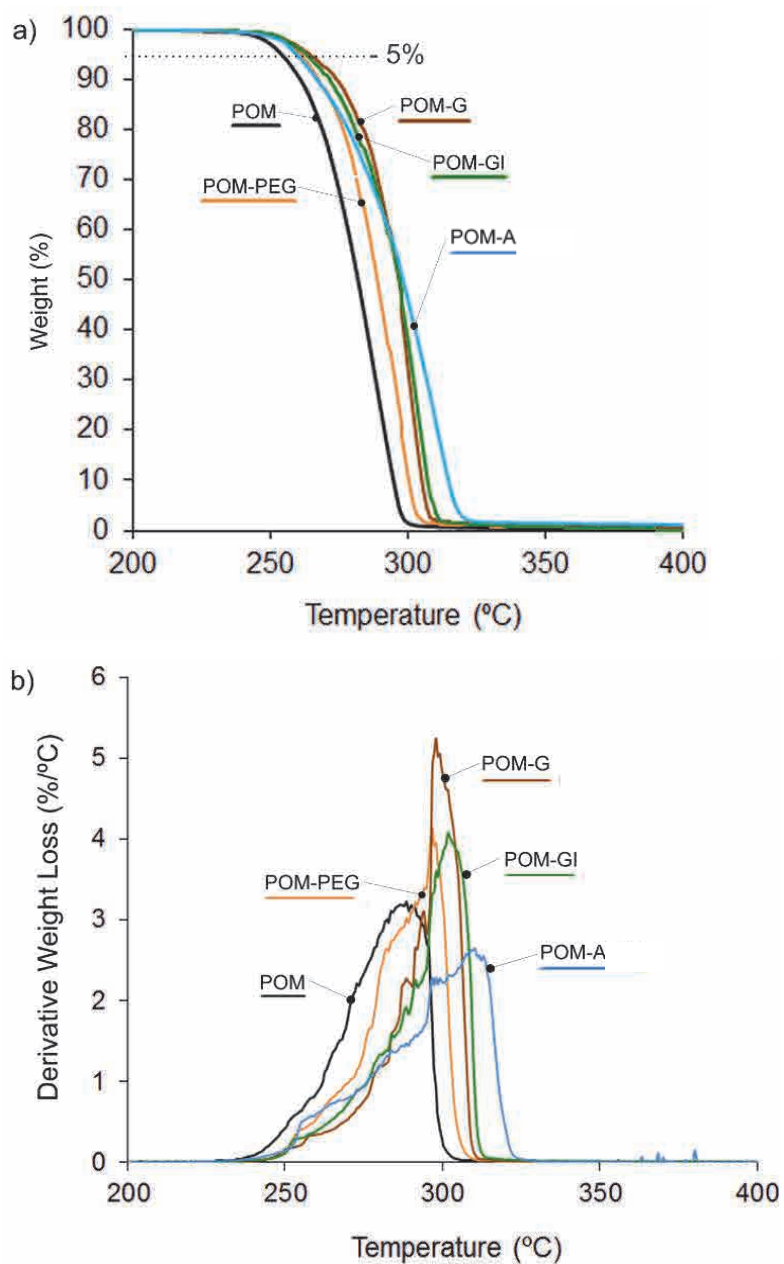


Figure 52: Thermogravimetric curves for POM/POSS composites and neat POM, showing the evolution of weight loss (a) and the derivative weight loss (b).

As it can be observed, the weight loss of the composites occurred in a single step and it was almost complete, leaving residue around 2.5 wt.% at the end of the test. These results substantiate the confirmation that the addition of the different POSS used in this work has increased the $T_{5\%}$, $T_{50\%}$ and T_{max} of the resulting nanocomposites, showing a considerable

stabilisation of the POM matrix. This thermal enhancement of the POM/POSS composites was, however, affected differently depending on the organic group of the POSS molecules. Particularly, when POM was blended with PEG-POSS, $T_{5\%}$ increased from 253°C to 260 °C, with G-POSS to 263°C, GI-POSS to 261 °C and A-POSS to 260°C.

The greatest stabilisation of POM was achieved with the addition of A-POSS, where the T_{MAX} of the composite increased by 22°C. This thermal stabilisation of POM obtained from the addition of 2.5 wt% A-POSS can be considered of great importance taking into account the small amount of POSS molecules added. This enhancement could suggest the presence of hydrogen bonding interactions between the ether oxygen atoms of POM and the POSS hydrogen atoms.

5.2.3. Degradation kinetics by Coats and Redfern of POM and its nanocomposites

Based on the theoretical fundamentals of the Coats and Redfern method for calculating the kinetic parameters explained in section 3.2, the shape index 'S' is computed from the tangent slopes of the DTG curve at the inflection points, and the graphical parameters involved are shown in Figure 53. Subsequently, the order of reaction 'n' is calculated by means of the Kissinger's eq. 28 from the aforementioned section 3.2.

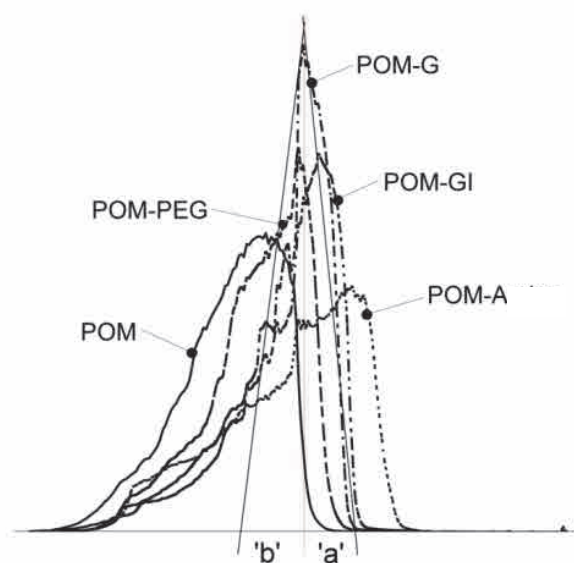


Figure 53: Graphical method to calculate the shape index 'S' (POM/GPOSS sample)

With the above method, the POM base material resulted in the highest 'n' value (order of reaction) with 0.89, and the nanoblends had notably lower figures, with POM/PEG resulting in 0.65, both POM-G and POM-Gi with n=0.69, and POM-Amino with the lowest value at 0,59. Subsequently, these 'n' values lead to the application of eq. 24 to calculate the activation energy **Ea** for the four materials analysed. Figure 54 represents the resulting graphic whereby the parameter on the **Y** axis is the value on the left hand side of said equation i.e. $\ln \left[\frac{1 - (1 - \alpha)^{1-n}}{T^2(1-n)} \right]$ and the parameter on the **X** axis is the reciprocal of the absolute temperature (1/T), becoming a linear curve for each material sample.

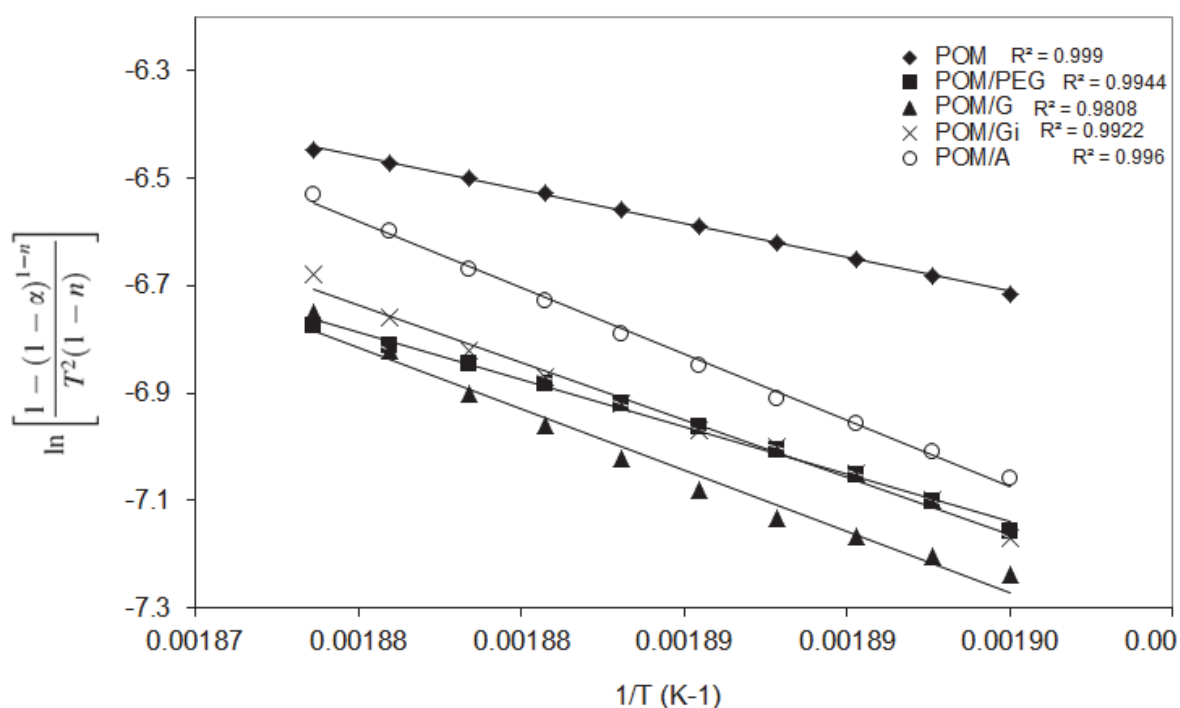


Figure 54: Kinetics of the thermal degradation for POM, POM/PEG, POM/G, POM/Gi and POM/Amino.

The activation energy (**Ea**) of each sample was calculated from the slope of the corresponding curve and its intercept value. POM-Amino has resulted being the most stable blend with $E_a=145.8$ kJ/mol, followed closely by POM-G and POM-GI with 145,5 kJ/mol and 145.2 respectively, and then going to the less stable nanocomposite being POM-PEG with

127.7 kJ/mol and finally the unmodified POM with almost the same low E_a value being 128 kJ/mol.

These values need to be contextualised in the air atmosphere environment and the $10^\circ\text{C} \times \text{min}^{-1}$ heating rate used to obtain the thermogravimetric data source. Air atmosphere favours the development of additional hostile degradation mechanisms for POM such as oxidation and acidolysis, which accelerate the degradation rate with a notable reduction of the overall activation energy required for the polyacetal degradation process to initiate and propagate. Indeed, there are other variables that can influence the value of activation energy and the published literature confirms such variations with values for POM copolymers under air atmosphere ranging from 80 to 392 kJ/mol [148, 281-283] depending on the polyacetal type (e.g. polyoxymethylene with hydroxyl, methoxy or acetate end groups, copolymer, molecular weight distribution, etc.) and the dominating depolymerisation mechanism (thermal, anionic, cationic, etc.).

To conclude the thermal stability analysis, Table 14 below summarises the most relevant results from the thermogravimetric and kinetic analysis of thermal decomposition carried out in this section, where in addition to the above paragraph, the POM-Amino shows a dramatic improvement with a T_{max} 22°C above the unmodified POM followed by POM-GI with 14°C increase, and POM-G and POM-PEG with 10°C and 8°C increase respectively.

	$T_{5\%}$		$T_{50\%}$		T_{MAX}		Kinetic Parameters			
	$^\circ\text{C}$	$\Delta^\circ\text{C}$	$^\circ\text{C}$	$\Delta^\circ\text{C}$	$^\circ\text{C}$	$\Delta^\circ\text{C}$	n	Δn	E	$\Delta\text{kJ/mol}$
<i>POM</i>	253	<i>n/a</i>	281	<i>n/a</i>	288	<i>n/a</i>	0.89	<i>n/a</i>	128.0	<i>n/a</i>
<i>POM-PEG</i>	260	7	288	7	296	8	0.65	-0.24	127.7	-0.3
<i>POM-G</i>	263	10	296	15	298	10	0.69	-0.2	145.5	17.5
<i>POM-GI</i>	261	8	295	14	302	14	0.69	-0.2	145.2	17.2
<i>POM-A</i>	260	7	297	16	310	22	0.59	-0.3	145.8	17.8

Table 14: Summary of thermogravimetric and kinetic results of POM, POM-PEG, POM-G, POM-Gi and POM-A.

5.2.4. Spectrophotometry analysis of POM and its nanocomposites

5.2.4.1. Examination of the original POM appearance during degradation

The different samples of unmodified POM have been characterised in spectrophotometry terms after being submitted to the different degradation conditions set out in section 4.3.1. The results are depicted in Figure 55, whereby the top plot shows an increase of lightness ΔL^* for low degradation temperatures along with exposure time, with a maximum increase up to 95 L*. This is caused by the chalking mechanism of polyacetal in the initial stages of thermoxidation. However, as the sample undergoes further degradation, i.e. 260-280°C, a rapid ΔL^* decrease occurs towards a 65 L* value, which becomes the bottom limit for those samples undergoing complete degradation. This reduction in ΔL^* occurs in parallel with the development of the yellowing appearance and accordingly, the increase of Δa^* and Δb^* .

The bottom plots of Figure 55 refer to the chromaticity values Δa^* and Δb^* for each sample. From these, it can be drawn that whereas at low degradation temperatures (200-220°C) no relevant changes in chromaticity are perceived, the samples submitted to further degradation conditions show the following trends:

- a) An abrupt increase in Δa^* chromaticity, from 1 up to +11, which can be translated in a much redder colour appearance as degradation takes place.
- b) An abrupt increase in Δb^* chromaticity, from -6 up to +26, which can be translated in a much yellower colour, which increases with degradation severity.

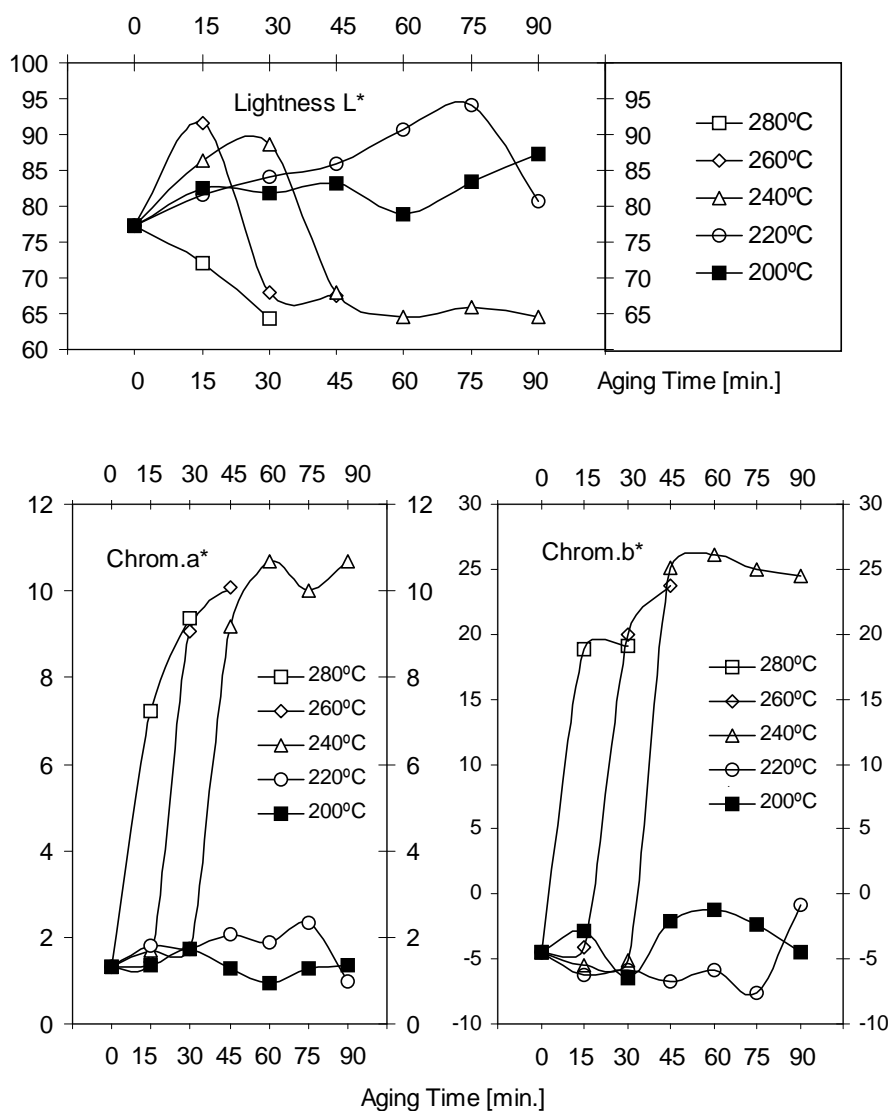


Figure 55: Progress of Lightness L*, Coordinate a* (redness-greenness) and Coordinate b* (yellowness-blueness) as degradation proceeds for each of the temperatures.

The appearances quantified by means of the three coordinates L*, a*, b* resulting from the different degradation conditions, can be comparable among different temperatures and times as they lead to similar results in terms of colour appearance. This has been depicted in Figure 56 in the form the iso-coordinate graphs for Lightness and Chromaticities a* and b* respectively. These plots show how a degraded sample with certain colour appearance in

terms L^* , a^* , b^* can be obtained equally by means of high temperatures during short times or vice versa, low temperatures during longer times.

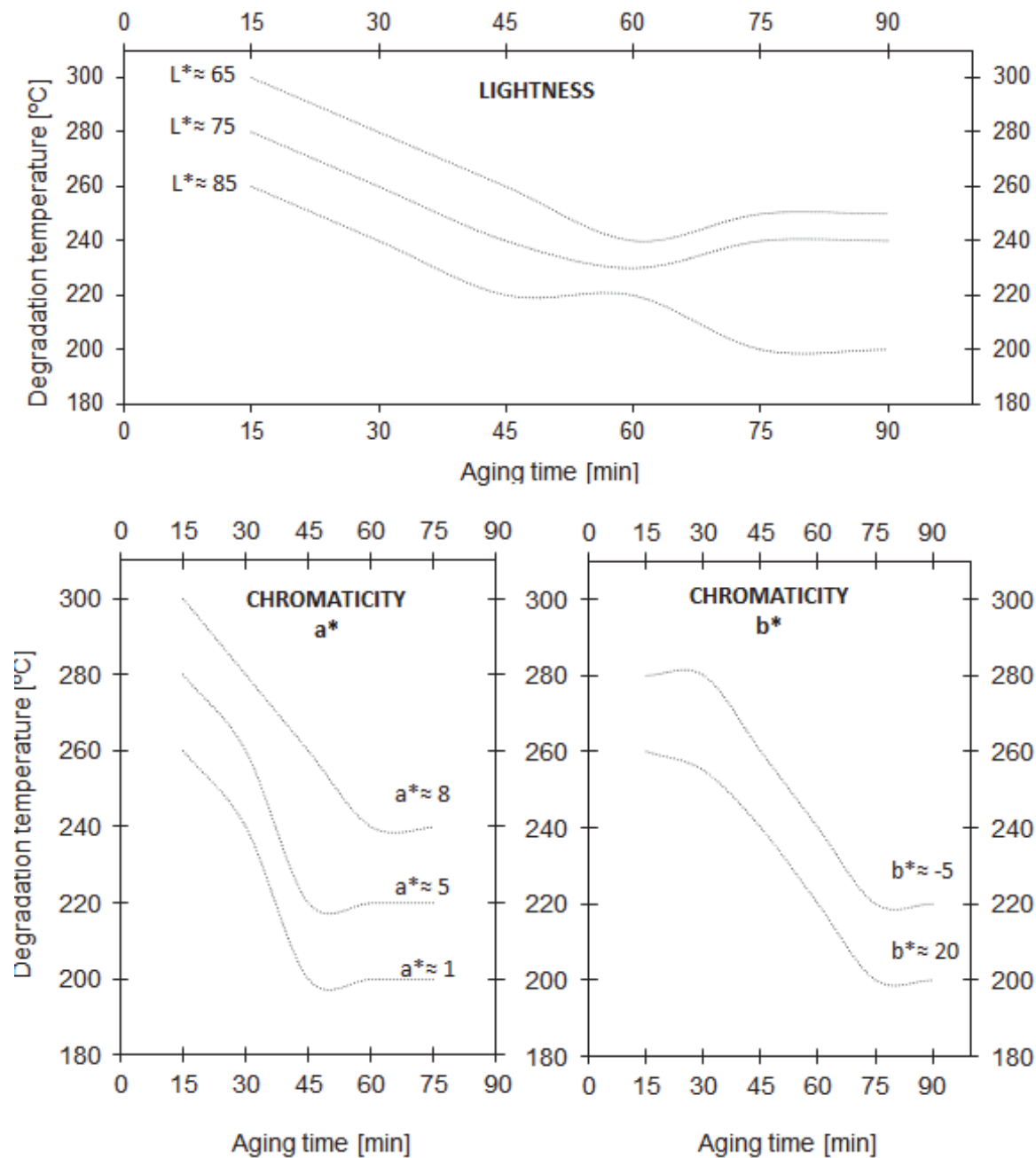
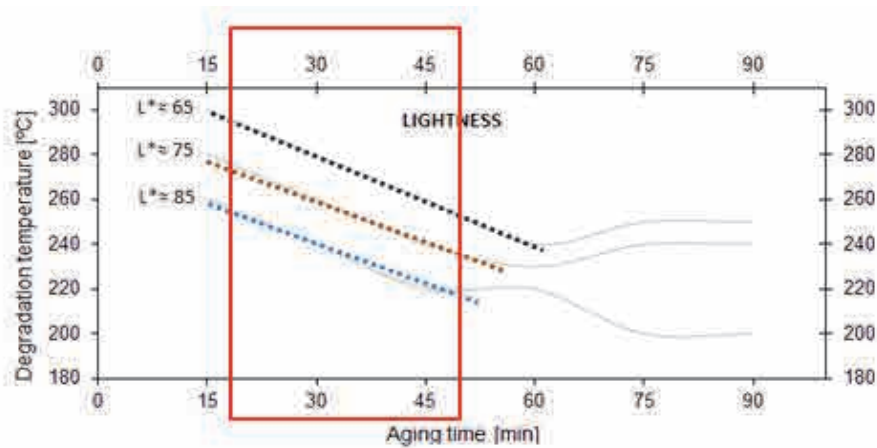


Figure 56: Interpolated Lightness limits L^* and Iso-chromaticities a^* and b^* versus temperature and time.

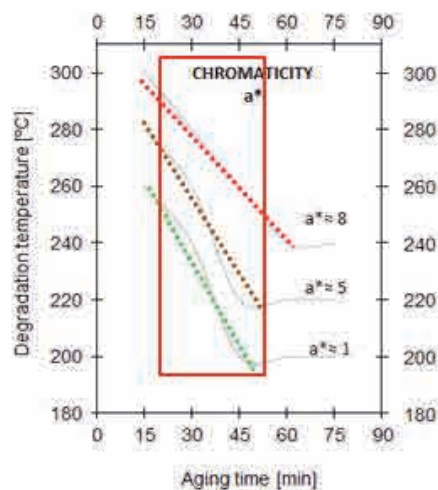
Based on the above plots, the following patterns are observed:

- a) The temperatures required for obtaining a specific Lightness L^* and chromaticity a^* have a decreasing linear trend as oven-storage times progress from 20min to 50min and likewise for the chromaticity b^* from 30min to 70min. This temperature trend could be represented with the equations 29 to 31 below:



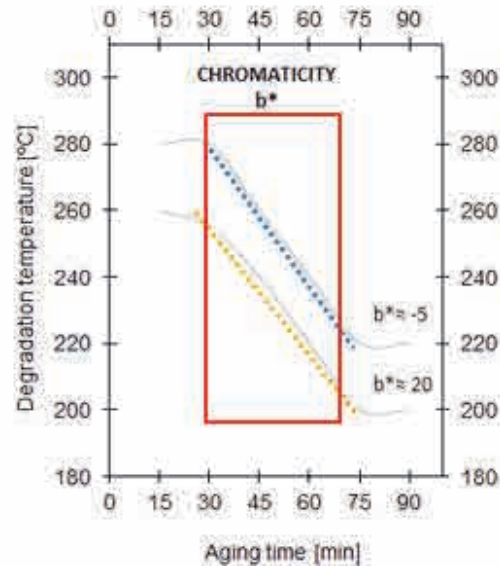
$$T_{[20 \leq t \leq 50]} = T_{L^*} - 1.6t \quad \text{Equation 29: Lightness (L*)}$$

Where t =time[min] and T_{L^*} initial temperature being assigned for the lightness values 65, 75 and 85, with T_{L^*65} =328°C, T_{L^*75} =308°C and T_{L^*85} =287°C.



$$T_{[20 \leq t \leq 50]} = T_{a^*} - 1.65t \quad \text{Equation 30: Chromaticity } a^*$$

Where t =time[min] and T_{a^*} being assigned for the chromaticity a^* values 8, 5 and 1, with T_{a^*8} =328°C, T_{a^*5} =308°C and T_{a^*1} =287°C.



$$T_{[30 \leq t \leq 70]} = T_{b^*} - 1.5t \quad \text{Equation 31: Chromaticity } b^*$$

Where t =time[min], T_{b^*} being assigned for the chromaticity b^* values -5 and 20, with T_{b^*-5} =325°C and T_{a^*20} =302°C.

- b) Lightness of L^*85 and above (up to L^*95) precedes the carbonisation of the polymer, i.e. once it is achieved, the lightness quickly goes down and beyond the initial range between L^*75 -85. This means that this latter trend does not happen with the lowest degradation temperature i.e. 200°C with the time periods tested, which ends its degradation progress at precisely L^*85 .

In addition to the colour plots depicted in this section, a CIELAB colour space in Figure 57 represents the hue appearance i.e. chromaticity values a^* and b^* of the sample when being

submitted to different temperatures up to 90 minutes. This plot represents the direction of the colour progress of all the samples and shows, as expected, that regardless of the degradation temperature kept during the degradation, the trend direction in chromaticity coordinates is the same for all samples as the degradation takes over.

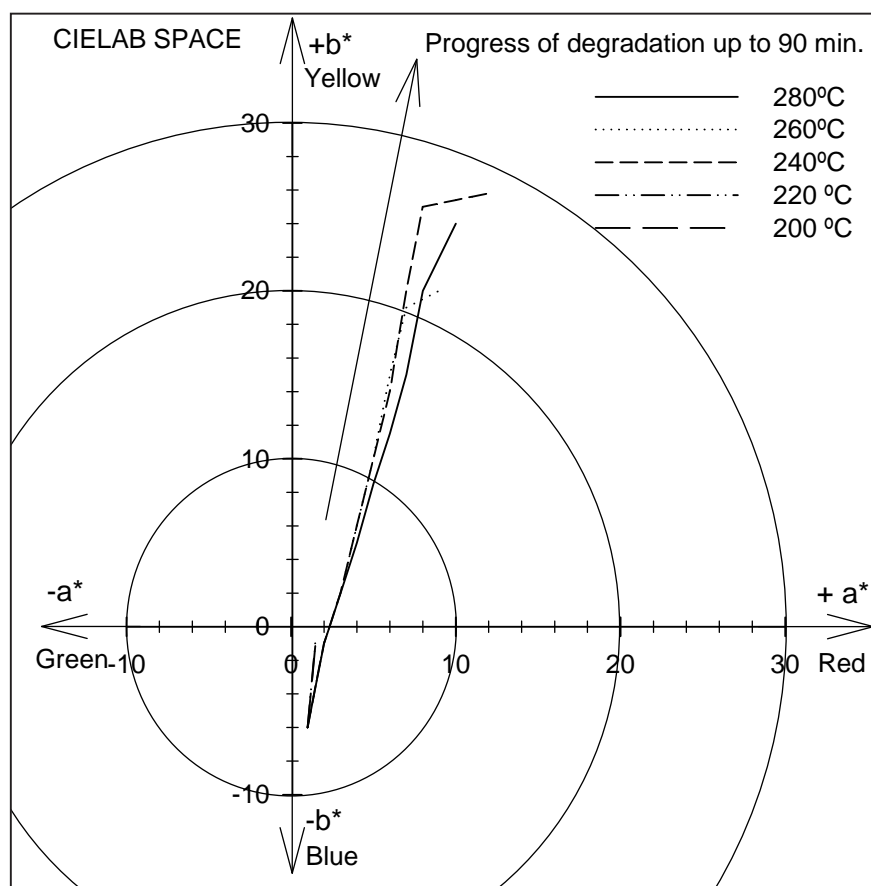


Figure 57: Colour route followed by the material along aging times up to 90 min. at different temperatures, represented on the CIELAB space for the hue chromaticity values (a^* and b^*).

5.2.4.2. Examination of POM-nanocomposites appearance during degradation

Regarding the POM nanocomposites, Figure 58a and 58b refer to the chromaticity values for each sample submitted at 240°C for different periods of time. From these, it can be evidenced that all POM/POSS nanocomposites had a much lower level of yellowing compared to the standard POM, in fact most of the nanocomposites had 50% or less the

values of chromaticity change in terms of a^* and b^* , which means that the variation of colour from the original sample was notably lower. Likewise, Figure 58c represents changes on the Lightness value L^* , which appears to be consistent with the chromaticity values where colours become darker as degradation evolves, yet being systematically lower than those obtained with the original POM material.

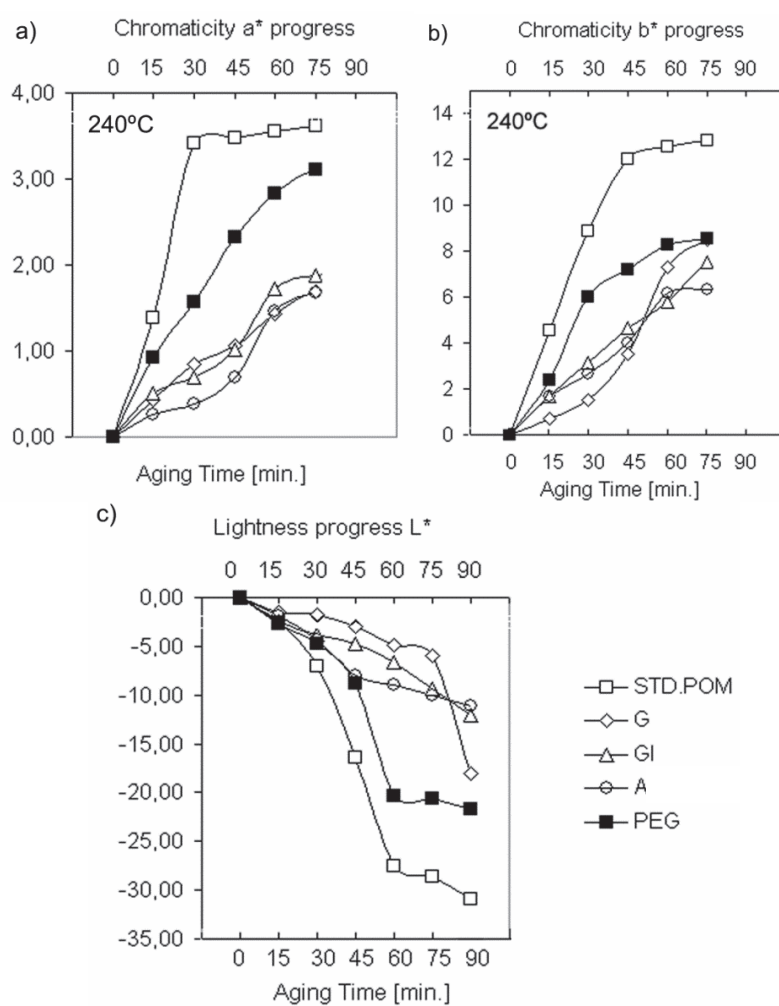


Figure 58: Progress of Lightness L^* , Coordinate a^* (redness–greenness), and Coordinate b^* (yellowness–blueness), as degradation proceeds at 240°C for different periods of time.

In addition to the colour plots depicted in this section, a CIELAB colour space in Figure 59 represents the hue appearance i.e. chromaticity values a^* and b^* of the sample as it is

submitted at 240°C up to 90 minutes. This plot represents the direction of the colour progress of all the samples and shows that regardless of the degradation conditions, the trend direction in chromaticity coordinates is the same for all samples as the degradation time evolves.

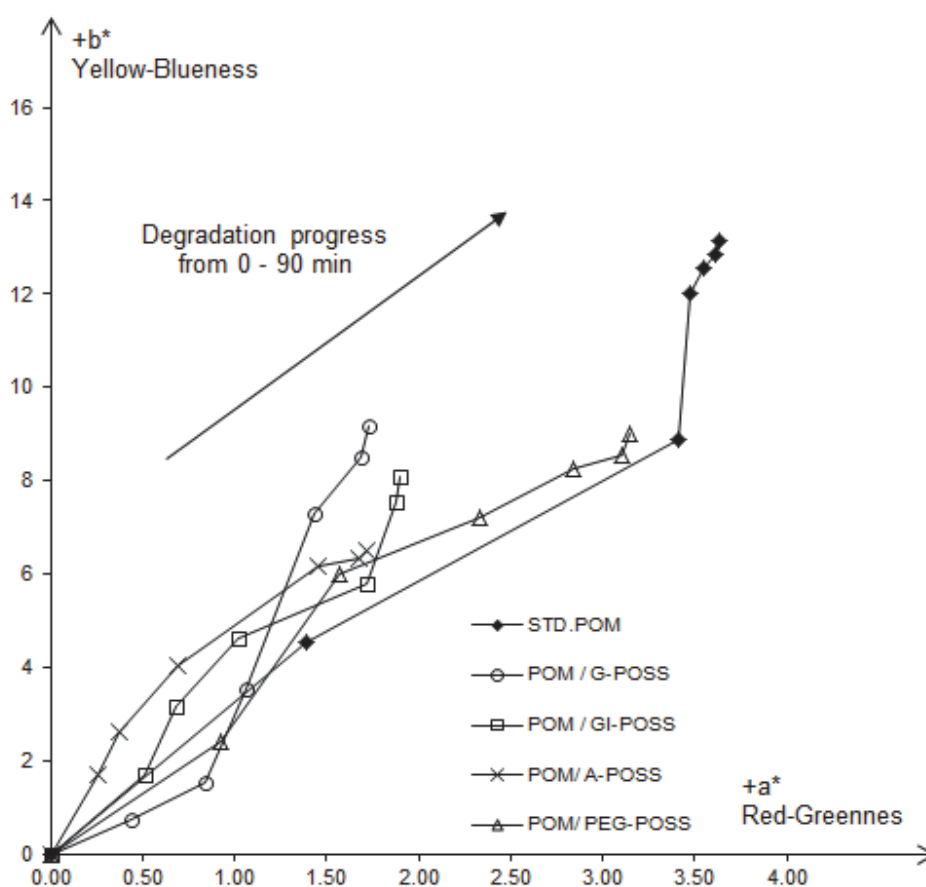


Figure 59: Colour route followed by the different nanocomposites along the CIELAB space with different aging times up to 90 min at 240°C representing the hue chromaticity values (a^* and b^*).

As discussed earlier, the above colour variation is attributed to the formation of chromophores from the carbonyl groups associated with thermoxidation process. These molecular modifications promote the absorption of certain wavelengths of visible light and transmits or reflects others, hence providing a different colour feature [168-169, 284-285].

This argument would suggest that despite the incorporation of nanoparticles into the polyacetal matrix, the yellowing process would still develop from the polymeric ether backbone of the polyacetal and not from the siloxane constituencies, and that the notable reduction in chromophore yield is due to the overall POSS thermal stabilisation effect on the polymer backbone, as reported in the previous sections.

The foregoing section relates the colour trends with the FTIR absorption results, and shows a correlation between the carbonyl build-up and the yellowing effect.

5.2.5. Inter-relationship between FTIR and Spectrophotometry analysis

5.2.5.1. Cross-examination of the original POM FTIR & Spectrophotometry results

The values obtained from the FTIR analysis of POM have been crossed with those of the Spectrophotometry, i.e. the increasing carbonyl/methylene ratio accounting for the gradual degradation of the polymer and their relationship with the colour appearance of the sample represented in terms of values L^* , a^* and b^* .

This inter-relationship is recollected in Figure 60, whereby the scale of chromaticity values are represented on the left of the Y axis, the lightness values on the right and the carbonyl/methylene ratio is represented on the X axis. Additionally, pictures of the resulting appearance of the samples are also represented and linked to the different degradation groups within the same figure.

As expected, a trend is seen in the colour appearance as the polymer undergoes the oven ageing process, particularly in the most advanced degradation conditions where the yellowing is clearly represented by redder ($+a^*$) and yellower ($+b^*$) chromaticities. Based on these trends, relationships can be drawn from Figure 60, where the polymer colour characteristics can be related to the 'carbonyl' degradation groups set out in the previously in the following categories:

- Group 'a': Carbonyl ratio 0,2-0,5: No apparent degradation with $a^* \approx 2$, $b^* \approx -2$ and $L^* \approx 78$.
- Group 'b': Carbonyl ratio 0,5-1: Mid-degradation with $a^* \approx 2$, $b^* \approx -2$ and $L^* \approx 75$.
- Group 'c': Carbonyl ratio 1-5: High degradation with $a^* \approx 2$, $b^* \approx -5$ and L^* up to 90 (Avg.83).
- Group 'd': Carbonyl ratio 5-10: Complete degradation with a^* from 2 up to 12 (redder), b^* from 0 up to 25(yellower) and L^* down to 63 (darker)
- Group 'e': Carbonyl ratio 10-20: Complete carbonisation with $a^* \approx 12$, b^* from 15 to 26 (much yellower) and L^* down to 50 (much darker).

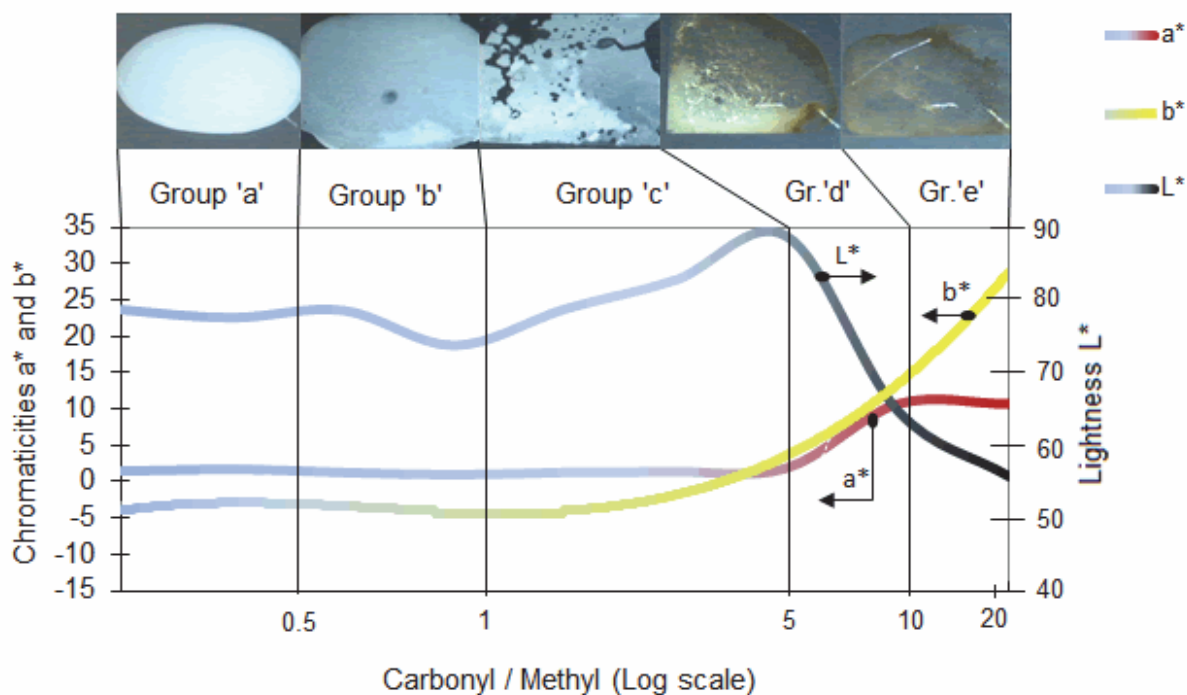


Figure 60: Inter-relationship between colour appearance [L^* , a^* , b^*] and Carbonyl/Methylene absorbance ratio, showing the correspondent pictures of the original POM samples belonging to each of the degradation groups.

The above representation suggests that in the initial stages of degradation of natural POM with carbonyl ratios under 5, the yellowing effect as such does not develop to a great extent, as both chromaticities a^* and b^* stay almost unchanged with only a slight increase in lightness. The chromaticities a^* and b^* become crucial when degradation is more aggressive from carbonyl ratios of 5 and above which is when yellowing takes place being clearly appreciable from the human eye.

Accordingly, the results show an association between the colour shift of the sample and the content in carbonyl aldehyde. Apart from the carbonyl groups, other relevant chromophores in polyacetals liable of such colour shift could be the hydroperoxides, which are located in the range of FTIR spectra $3100-3700\text{ cm}^{-1}$ as a result of the hydroxyl formation [168]. However, this region also comprehends absorptions of alcohols and peroxides, and consequently the analysis upon this band has been disregarded as perhaps not being as clear as the carbonyl absorption peak, which appears isolated with respect to the neighbouring bands.

5.2.5.2. Cross-examination of the FTIR & Spectrophotometry results of POM and its nanocomposites

The values obtained from the FTIR analysis of the original POM and the different POM nanocomposites have been compared with those corresponding to the spectrophotometry analysis, i.e. the variation in ratio of carbonyl/methylene absorbance compared to the variation on the sample colour expressed in terms of ΔE (Delta $L^*a^*b^*$), which is a single value that summarises the distance between the colour of the original sample with the corresponding degraded sample.

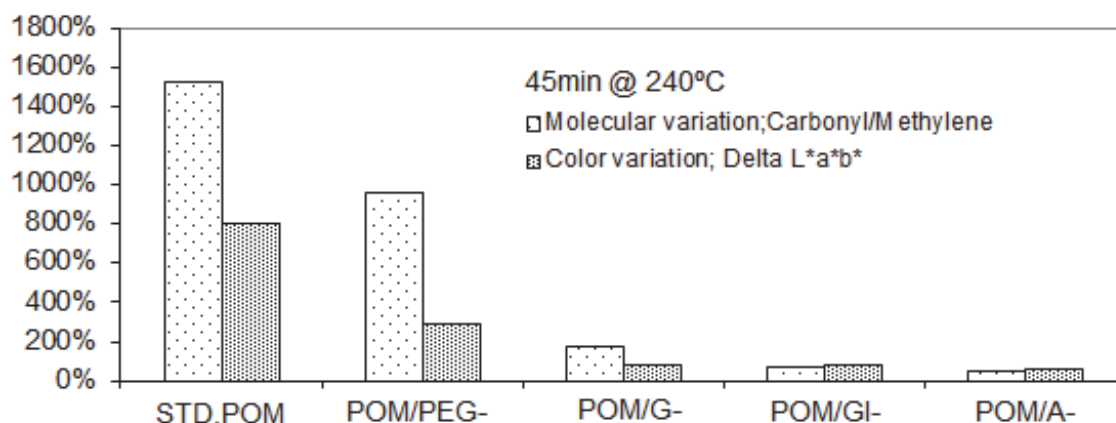


Figure 61: Degradation of POM/POSS nanocomposites in terms of Carbonyl Yield and Colour variation when submitted at 240°C for 45 min.

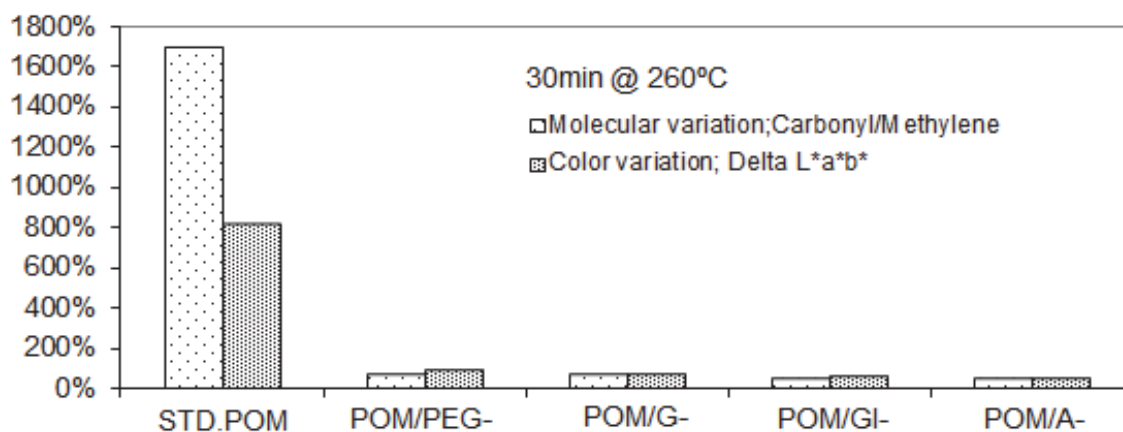


Figure 62: Degradation of POM/POSS nanocomposites in terms of Carbonyl Yield and Colour variation when submitted at 260°C for 30 min.

Figure 61 and 62 above show the comparison between the original POM (STD) with the 4 different POM nanocomposites submitted at 240°C for 45 min and at 260°C for 30 min respectively. As expected, the variation in colour shift (yellowing) and the content in carbonyl aldehyde increase proportionally as the polymer undergoes thermoxidation. Most importantly, however, is the exceptional improvement reflected in all POM/POSS nanocomposites in any of both indicators, proving the effectiveness of the incorporation of POSS in the POM matrix to enhance the degradation resistance and, by that, reducing the yellowing propensity.

This stability enhancement is further detailed in Table 15 in terms of temperature range that the material can withstand during different periods of exposure to thermoxidation until it shows an incipient degradation reaching a Carbonyl/Methylene ratio 0.5-1 and a colour variation of 50% ΔE . Although all four nanocomposites showed notable improvements in the degradation process, it is worth highlighting the performance of the A-POSS and the GI-POSS, with degradation temperatures being in the range of 25% higher than what the maximum standard POM can withstand.

	TEMPERATURE [°C] @ C/M 0,5-1 & ΔE 50%			
	TIME EXPOSURE			TEMP. RESISTANCE IMPROVEMENT
	15'	30'	45'	
STD.POM	214	208	203	-
PEG-POSS POM	223	218	217	5.3%
G-POSS POM	232	228	229	10.2%
GI-POSS POM	265	262	245	23.5%
A-POSS POM	269	265	254	26.1%

Table 15: Maximum temperature allowance at different aging periods for each material when carbonyl/methylene ratio is 0.5-1 and colour shift ΔE reaches 50%.

As suggested in the previous sections, the most stable mixture analysed i.e. A-POSS, could attribute its excellence performance to the hydrogen atoms of the amino group, which interact with the POM matrix through the ether oxygen atoms.

On the other hand, the second best performer GI-POSS had a slight better response than G-POSS. Although in previous results G-POSS has shown a better compatibility and degree of dispersion within the POM matrix than GI-POSS, the difference in stability is more likely to be attributed to the amount of glycidyl epoxy groups present in each type of nanocomposite. To this effect, G-POSS has 8 of these groups, and despite the fact that they are stable up to 300°C, the melt-blending process does not ensure effective bonding with the polyacetal molecular structure regardless of the adequate dispersion achieved. Without bonding, the 8 glycidyl epoxy groups around the silica cage of G-POSS take considerably

more space than the GI-POSS cage having 7 shorter isobutyl ramifications and only one glycidyl epoxy. In addition to these steric considerations, the 8 epoxy groups of the G-POSS also promote a higher level of reactivity, which implies more instability. According to the above discussion, the slightly better performance of GI-POSS compared to G-POSS is more likely to be attributed to the smaller free volume present in the former nanocomposite, as it results in less molecular mobility.

To conclude with the degradation performance assessment, the PEG-POSS showed less stability to thermoxidation, and in light of the lower miscibility resulting from the mixing process during the sample preparation, we could attribute the lower performance to the deficient dispersion of the POSS into the POM matrix.

5.2.6. Summary of results of POM and its nanocomposites.

The overall performance of the materials tested in the different experimental disciplines is summarised in Table 16 below by means of the most representative results of the SEM, DSC, FTIR, TGA/DTG, Kinetics and Spectrophotometry analysis for POM and the POM/POSS nanocomposites.

SUMMARY TABLE

		STD. POM	POM/PEG-POSS	POM/G-POSS	POM/GI-POSS	POM/A-POSS
SEM	Surface cryog. fractured appearance	Base material	Good miscibility No agglomerate	Good miscibility No agglomerate	Low miscibility Large agglomerates	Good miscibility No agglomerate
DSC	T _m	167.2°C	165.9°C-168.6°C	168°C	168.1°C	168,5°C
FTIR	Carbonyl incr./CH ₂ ratio [S0-S240°x45°]	1525.00%	961.00%	176.00%	66.00%	50.00%
	T _{max} Derivative weight loss	288°C	296°C	298°C	302°C	310°C
TGA	Residue after thermal decomposition	0.1%	0.4%	0.6%	0.1%	1.1%
	Coats & Redfern Activation Energy	128 kJ/mol	127.7 kJ/mol	145,5 kJ/mol	145.2 kJ/mol	145.8 kJ/mol
COLOR	Averaged Yellowing (Delta Lab %)	798.00%	294.00%	84.00%	77.00%	62.00%

Table 16: General summary of results from SEM, DSC, FTIR, TGA/DTG, Kinetics and Spectrophotometry analysis for POM and the POM/POSS nanocomposites.

5.3. PRELIMINARY ANALYSIS OF ABS-g-Ma & its POSS NANOCOMPOSITES

5.3.1. Solubility analysis of ABS-g-Ma/POSS and its nanocomposites.

The calculation methods for the solubility parameter in this section are based on the theoretical fundamentals explained in section 3.1. and will follow the same approach used with the POM material and its nanocomposites in section 5.1.1. The values of group contributions, molar attraction functions and molar volumes corresponding to the ABS and the POSS molecules have been deduced from *Van Krevelen et al.* [238].

Accordingly, the application of the *Hoy* as well as *Hoftyzer & Van Krevelen* methods considered that the functional groups in the outer surface of the POSS molecules were dominating the intermolecular interactions, and the inorganic part with the siloxane bonding of POSS was excluded from the calculation of the solubility parameter. A more extended discussion regarding the role of the siloxane group can be found in section 3.1.4.

The following pages contain the excel tables set up to calculate the solubility parameters for ABS-g-Ma and TPOSS following both *Hoy's* methods and the *Hoftyzer&Van Krevelen* approach. Note the solubility values for GPOSS and APOSS have been already calculated in section 5.1.1. The chemical groups that constitute each material have been broken down in order to initially calculate the contribution of the sub-components in proportion to their presence in the molecular structure and, where applicable, the different group contributions of the polar, dispersion and hydrogen bonding forces.

ABS : Acrylonitrile-Butadiene-Styrene
General Formula: (C₈H₈)_x(C₄H₆)_y(C₃H₃N)_z

+

Maleic Anhydride
General Formula: C₄H₂O₃

HOY's METHOD (Standard d)	Individual Molar Attract.Func.Values			Material: ABS	SubΣG	ΣG	P	Mb	
	F _k	F _p	Δ _T ^(P)						V
>CH-	176	0	0.013	9.56					
=CH2	259	67	0.019	19.17					
=CH-	249	59.5	0.0185	13.18					
>C=O	538	173	63	0.013	7.18				
-O-	235	216	0.018	17.3		4047	1.07	212.47	
-C≡N	725	725	0.054	23.1					
<i>note: -O- ether</i>									
GROUP	Individual Group contribution values			Group break			Material: ABS		
	F _g	F _p	E _h	E _n	V	F _{di}	E _{hi}	V	
>CH-	80	0	0	9.56		160	0	19.12	
=CH2	400	0	0	19.17		1600	0	76.68	
=CH-	200	0	0	13.18		1406	0	92.655	
>C=O	70	0	0	7.18		70	0	7.18	
-O-	560	770	2000	13.42		16.8	23.1	60	
-C≡N	256	400	3000	6.45		3.84	36	45	
-C≡N	758	1100	2500	24		758	1210000	2500	
Resulting Total Function Values (Σ)				4014.6	1210059	2605	219	219	

GROUP	Individual Group contribution values			Group break			Material: ABS		
	F _g	F _p	E _h	E _n	V	F _{di}	E _{hi}	V	
>CH-	80	0	0	9.56		160	0	19.12	
=CH2	400	0	0	19.17		1600	0	76.68	
=CH-	200	0	0	13.18		1406	0	92.655	
>C=O	70	0	0	7.18		70	0	7.18	
-O-	560	770	2000	13.42		16.8	23.1	60	
-C≡N	256	400	3000	6.45		3.84	36	45	
-C≡N	758	1100	2500	24		758	1210000	2500	
Resulting Total Function Values (Σ)				4014.6	1210059	2605	219	219	

Table 17: Solubility calculation tables for ABS-g-Ma

GROUP	Individual Molar Attract.Func.Values			Group break			Material: ABS		
	F _g	F _p	E _h	E _n	V	F _{di}	E _{hi}	V	
>CH-	80	0	0	9.56		160	0	19.12	
=CH2	400	0	0	19.17		1600	0	76.68	
=CH-	200	0	0	13.18		1406	0	92.655	
>C=O	70	0	0	7.18		70	0	7.18	
-O-	560	770	2000	13.42		16.8	23.1	60	
-C≡N	256	400	3000	6.45		3.84	36	45	
-C≡N	758	1100	2500	24		758	1210000	2500	
Resulting Total Function Values (Σ)				4014.6	1486.4	0.3	219	219	

n **1.668**
 a (P) **1.064**
 δ_a **19.24**
 δ_p **11.078**
 δ_h **4.7105**
 δ_d **15.005**

δ_a **18.33**
 δ_p **5.023**
 δ_h **0.233**
 δ_d **18.604**

TPOSS : TriSilanolPhenyl POSS Cage

General Formula:



FW 931.34

HOY's METHOD	Individual Molar Attraction Function Values				Sub-Total Molar Attraction Function Values
	F _t	F _p	Δ _{t^(P)}	V	
=CH-	249	59.5	0.0185	13.18	461.3
=C<	173	63	0.013	7.18	441
-OH	675	675	0.049	12.45	2025
Resulting Total Function Values (Σ)					548.91

Phenyl group		Hydroxyl radical	
General formula:	5X(=CH-) Y 1X(=C<)	General formula:	
Structural formula:		Structural formula:	
Group breakdown	=CH- 5 =C< 1 -OH 0	Group breakdown	=CH- 0 =C< 0 -OH 1
(n) Qty. Radicals	7	(n) Qty. Radicals	3
Total groups	7	Total groups	3

HOY's METHOD	Sub-Total Molar Attraction Function Values				
	F _t	F _p	Δ _{t^(P)}	V	
	8715	2082.5	0.6475	461.3	
	1211	441	0.091	50.26	
	2025	2025	0.147	37.35	
Resulting Total Function Values (Σ)					548.91

CH primary: Not Hydrogen Bonded type, as would imply bonding with another chemical group.

n 0.564653

α^(P) 1.253454δ_c 22.66595δ_p 12.24098δ_s 10.19223δ_d 16.1252

GROUP	(G=F _i) Material: TPOSS			
	Sub Σ G	Σ G	p	
=CH-	8715	16503	1.21	
=C<	1211			
-OH	2025			
-Si-O-	4552			
Resulting Total Function Values (Σ)				931.34

δ_y 21.441

Hoftyzer & Van Krevelen METHOD	Individual Group contribution values				Group contribution values			
	F _{ei}	F _{pi}	E _{hi}	V	F _{di}	F _{pi} ²	E _{hi}	
Phenyl	1430	110	0	71.4	10010	770	0	
-OH	210	500	20000	12.45	630	2250000	60000	
Resulting Total Function Values (Σ)					10640	2250770	60000	
Total groups								548

δ_c 19.416δ_p 2.7377δ_s 0.447δ_d 19.563

Table 18: Solubility calculation tables for TPOSS

The results obtained in solubility terms for ABS-g-Ma, ABS-g-Ma/GPOSS, ABS-g-Ma/APOSS, and ABS-g-Ma/TPOSS are shown in Figure 63, which gathers the information following the same structure and criteria as the one used in the POM and its nanocomposites, and showing at end of the calculation sequence the average value between the three resulting solubilities of each material to work out the final compatibility between them with an average solubility parameter.

Material	HOY					HOFTYZER & van KREVELEN			
	Solubility Components			①	②	Solubility Components			③
	δ_p	δ_h	δ_d	Standard δ_t	G-based δ_t	δ_p	δ_h	δ_d	δ_t
	[J/cm ³] ^{1/2}	[J/cm ³] ^{1/2}	[J/cm ³] ^{1/2}	[J/cm ³] ^{1/2}	[J/cm ³] ^{1/2}	[J/cm ³] ^{1/2}	[J/cm ³] ^{1/2}	[J/cm ³] ^{1/2}	[J/cm ³] ^{1/2}
ABS	11.078	4.710	15.005	19.237	20.383	5.023	0.233	18.331	18.604
GPOSS	8.787	7.587	17.129	20.692	19.135	0.000	0.000	16.825	16.825
APOSS	4.293	5.834	16.443	17.968	17.491	0.000	0.169	17.408	17.409
TPOSS	12.241	10.192	16.125	22.666	21.441	2.738	0.447	19.416	19.562

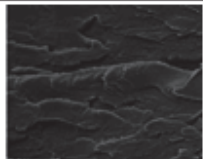
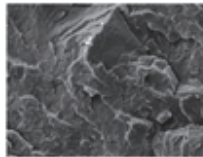
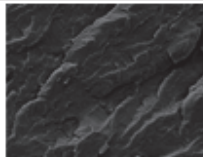
Material	Average (1 + 2 + 3) δ_t [J/cm ³] ^{1/2}	Nanocomposite	Difference in Solubility Parameter $ \Delta\delta_t $ $= \Delta\delta_{POM} - \Delta\delta_{POSS} $ [J/cm ³] ^{1/2}	Corresponding SEM images
ABS-g-Ma	19.408			
GPOSS	18.884	ABS-g-Ma/GPOSS	0.524	
APOSS	17.623	ABS-g-Ma/APOSS	1.785	
TPOSS	21.223	ABS-g-Ma/TPOSS	1.815	

Figure 63: Recollection of solubility parameters of ABS-g-Ma and the different POSS nanofillers with the resulting difference in solubility of the nanocomposite system and its comparison to the corresponding SEM images.

The results show that the three ABS-g-Ma nanocomposite mixtures have a rather small solubility parameter difference of 0.52, 1.78 and 1.81 for the ABS-g-Ma/GPOSS, ABS-g-Ma/APOSS and ABS-g-Ma/TPOSS respectively. This order of magnitude is well below the $\Delta\delta \leq 5$ $(\text{J}/\text{cm}^3)^{1/2}$ criteria [238], and therefore suggests a good miscibility between the host material and the nanofillers used in this study. The SEM images included in Figure 63 corroborate this finding by exhibiting not only good dispersion but also good miscibility, with no evidence of agglomerates or phase separation. Further analysis of the nanocomposite morphologies is developed in the next section.

5.3.2. SEM analysis of ABS-g-Ma/POSS and its nanocomposites.

The degree of dispersion of POSS molecules into the matrix prior to degradation was assessed through the micrographs shown in Figure 64 depicted in the next page. Subfigure 64a represents the image of the matrix ABS-g-Ma with a lower magnification on the left side (1,000 x) and a higher magnification on the right side (10,000 x). With the same approach, the subsequent figures 64b, 64c and 64d represent the three different POSS nanocomposites, being ABS-g-Ma/APOSS, ABS-g-Ma/GPOSS and ABS-g-Ma/TPOSS respectively.

These micrographs show no visible differences between the original ABS matrix and the ABS-based nanocomposites. Accordingly, no POSS aggregates or composition inhomogeneities were detected in any of the ABS-g-Ma/POSS hybrids, which in the case of TPOSS allows us to rule out the initial concerns over the melt blending temperature of the Brabender being too low. In summary, the SEM images not only support the conclusion that there is good dispersion and miscibility between the POSS nanofillers and the matrix, but also the fact that there are no evident modifications on the polymer surface.

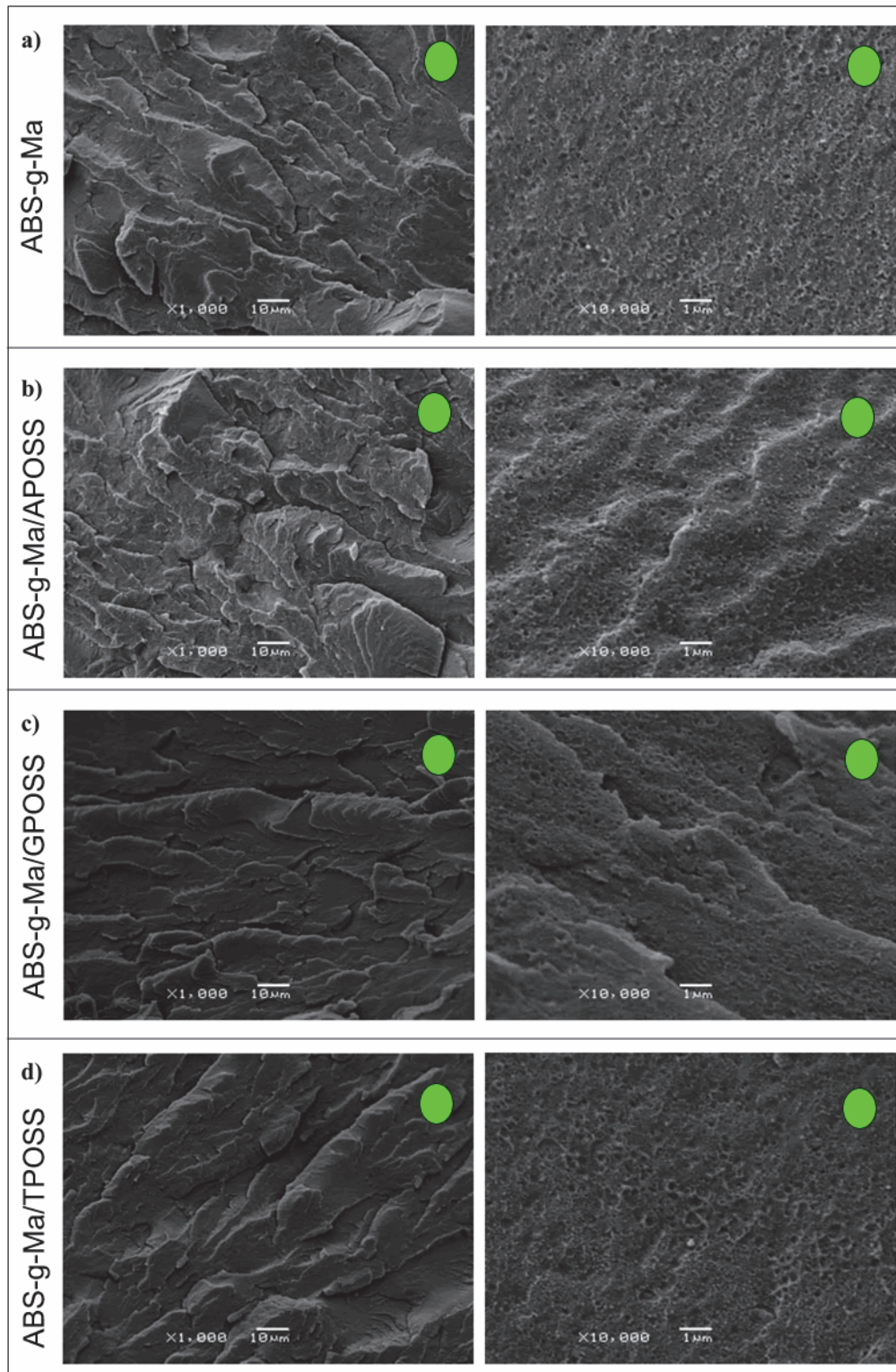


Figure 64: Morphologies of ABS-g-Ma and its nanocomposites: (a) ABS-g-Ma/APOSS; (b) ABS-g-Ma/GPOSS; (c) ABS-g-Ma/TPOSS nanocomposites.

5.3.3. DSC analysis of ABS-g-Ma/POSS and its nanocomposites.

This analysis targeted the identification of the thermal transitions of the different samples through their corresponding T_g and assessed the possible effects on the thermal properties of the nanofillers on the ABS-g-Ma matrix before submitting the samples to degradation.

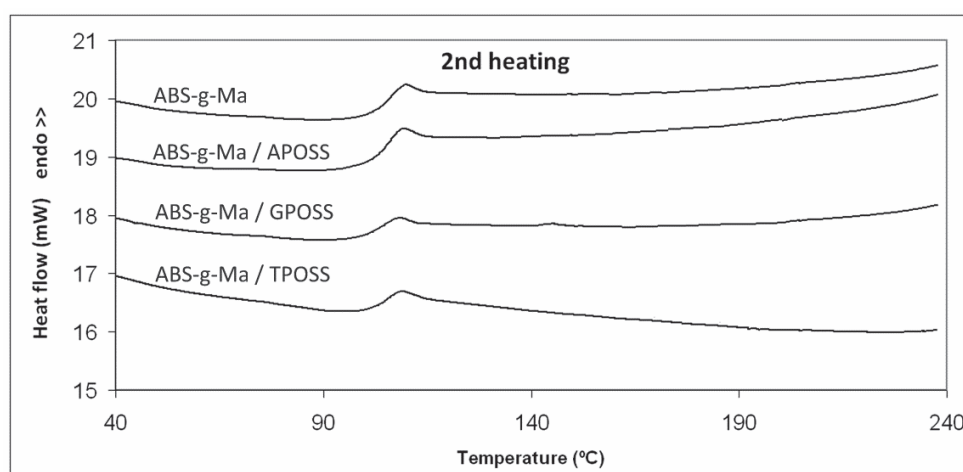


Figure 65: DSC heatflow plot during the second heating of ABS-g-Ma and its nanocomposites ABS-g-Ma/APOSS, ABS-g-Ma/GPOSS and ABS-g-Ma/TPOSS.

Figure 65 above shows the heatflow plot during the second heating where a small decay on T_g is perceived in all nanocomposites. This decrement is better represented in Table 19 below showing a drop of 1.5° to 2°C, which means that the different POSS have been acting as plasticizer despite their nanoscale rigid nature.

Sample	T _g , 2nd heating
ABS-g-Ma	104,8
ABS-g-Ma APOSS	103,7
ABS-g-Ma GPOSS	102,3
ABS-g-Ma TPOSS	103,5

Table 19: Summary of T_g values found on ABS and its nanocomposites

This behaviour can be attributed by an increase of the free-volume size (V_f) and/or fractional free-volume content (F_v) at the ABS backbone caused by the local mobility of the dispersed bulky POSS structures with their pendant R-groups, promoting higher molecular mobility. This plasticising effect of POSS nanofillers induced by an increase of free volume has been found in previous literature of POSS nanocomposites based on polyethylene (PE) [38], polypropylene grafted with maleic anhydride (PP-g-MA) [46], polystyrene (PS) [229], styrene-alt-maleic anhydride (PSMA) [230], polyimide (PI) [231], polyvinyl chloride (PVC) [232], polysulfone (PSU) [177] and polylactide (PLA) [233].

Alternatively, the degree of POSS dispersion achieved into the ABS-g-Ma matrix during the melt blending process is assessed by tracking down additional isolated melting points corresponding to the known T_m of the nanofillers at 51.9°C, 21-23°C and 220°C for APOSS, GPOSS and TPOSS respectively. This approach is based on the fact that endothermic peaks would be visible at the above temperatures in the event of having inadequate miscibility or aggregation. As no peaks other than the general nanocomposite T_g were observed in any of the plots it is reasonable to assume that each of the nanofillers have been thoroughly blended and dispersed within the matrix.

5.4. DEGRADATION ANALYSIS OF ABS-g-Ma & its POSS NANOCOMPOSITES

5.4.1. Fourier Transform Infra-Red analysis of ABS-g-Ma and its nanocomposites.

FTIR was used to check the chemical composition of the resulting ABS–POSS blends before and during degradation.

A preliminary assessment of the raw materials was carried out to understand the original condition of each sample. Figure 66a shows the spectra of ABS-g-Ma/APOSS blend in comparison with the pure ABS-g-Ma and the pure APOSS, likewise the spectra of ABS-g-Ma/GPOSS and ABS-g-Ma/TPOSS is shown in Figure 66b and 66c respectively. The three different pure POSS show a strong and symmetric Si-O-Si stretching vibration at wavelengths around the 1100 cm^{-1} , which is the characteristic absorption peak of silsesquioxane cages.

The IR spectra of the ABS–POSS nanocomposites are very similar to that of ABS-g-Ma, except that a clear Si-O-Si stretching peak has developed at around 1100 cm^{-1} , which is clearly visible in all three blends. This presence of this Si-O-Si stretching confirms that the POSS cage is truly present in the resulting nanocomposites, being consistent with the DSC analysis performed in the previous section.

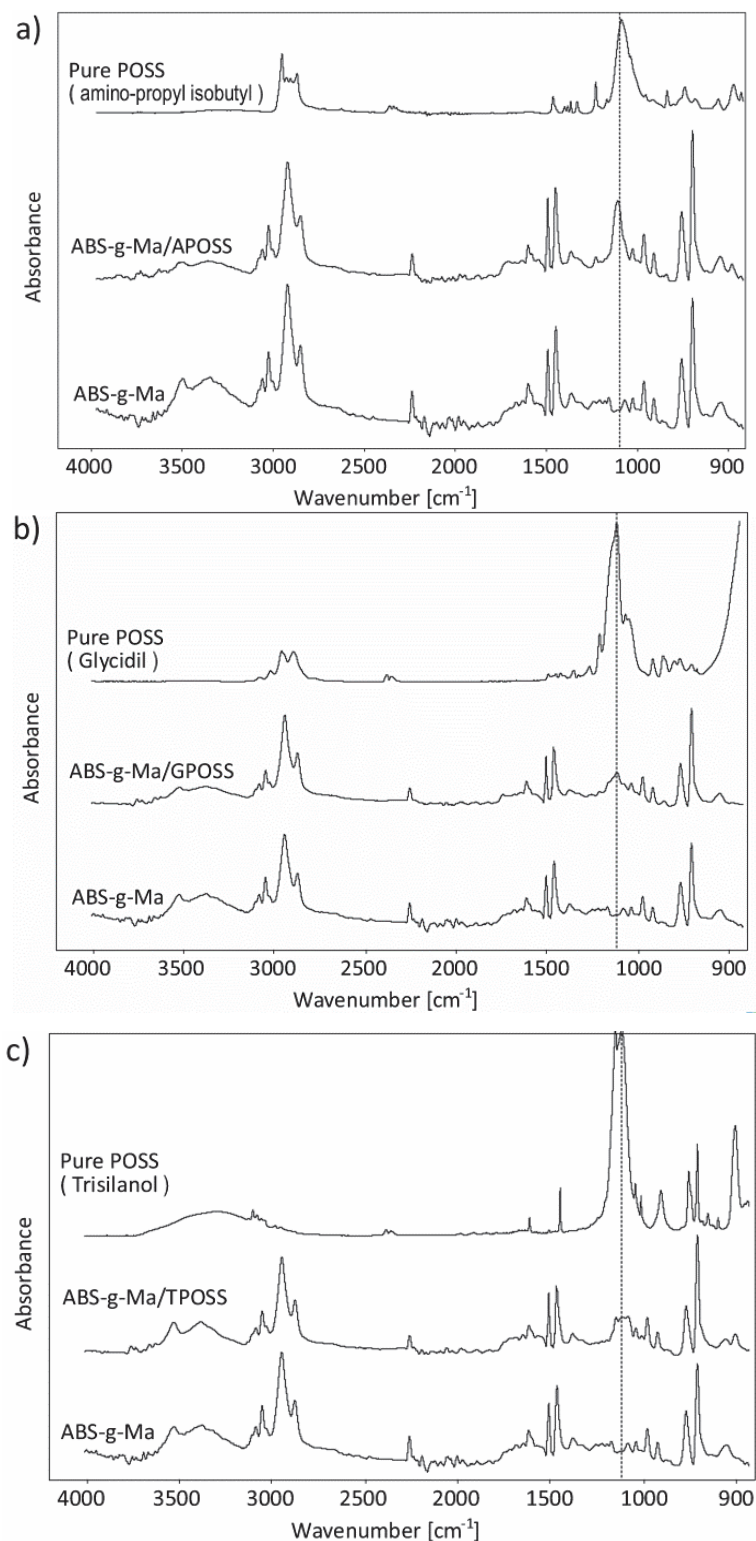


Figure 66: FTIR Spectra of ABS-g-Ma/APOSS blend in comparison with the pure ABS-g-Ma and the pure APOSS (a), and likewise ABS-g-Ma/GPOSS (b) and ABS-g-Ma/TPOSS (c).

Moving on to the degradation analysis, based on previous papers [48, 235] the carbonyl absorptions present within the wavelength range of 1650 and 1800 cm^{-1} were followed in an attempt to take a reference indicator to monitor the degradation progress. Figure 67 below shows how most of the carbonyl groups found in each sample did increase with the thermo oxidation process, however the results showed different absorption peaks for each material and the majority of these absorption peaks experienced shifts in their wavelength as degradation took place.

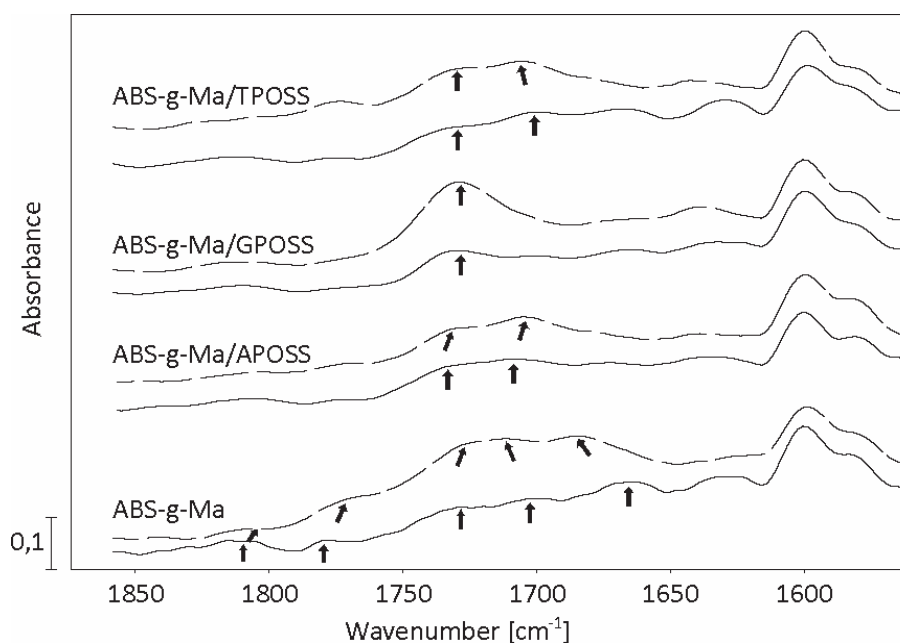


Figure 67: Spectra in the carbonyl area of ABS-g-Ma and the three nanocomposites in their original state (continuous line) and after thermo oxidation under 240°C@75min (dashed line).

In particular, the base material ABS-g-Ma showed peaks at 1775 & 1810 cm^{-1} and 1726 cm^{-1} representing the anhydride double bond and the aldehyde groups respectively. These shifted to shorter wavelengths as degradation took place. In addition to the above, two other carbonyl peaks at 1700 cm^{-1} and 1670 cm^{-1} were exhibited, assigned to the carboxylic acid and the amide groups respectively, which shifted to higher wavenumbers with degradation.

As far as the nanocomposites go, the ABS-g-Ma/APOSS showed peaks in the original sample at 1733 cm^{-1} and 1708 cm^{-1} , assigned to the aldehyde and the carboxylic acid groups respectively. These shifted to shorter wavelengths with degradation.

The ABS-g-Ma/GPOSS nanocomposite had one single aldehyde carbonyl absorbance at 1730 cm^{-1} which stayed at the same wavenumber throughout the degradation process.

Finally, the ABS-g-Ma/TPOSS nanocomposite also exhibited a stable absorbance of the aldehyde group, fixed at 1730 cm^{-1} during the thermo-oxidation process, but adding to that, another amide peak at 1700 cm^{-1} is visible in the plot and shifts to higher wavenumbers when submitted to degradation.

As it can be seen, the predominant carbonyl absorbance is the one representing the aldehyde group around the wavenumber 1730 cm^{-1} , which is the only one present in all the samples analysed. The ABS-g-Ma matrix exhibited the lowest frequency at 1726 cm^{-1} and ABS-g-Ma/APOSS the highest frequency at 1733 cm^{-1} . This phenomenon has been previously documented and the higher wavenumbers can be assigned to an enhancement of dipole-dipole interaction between the ABS matrix chains [182-183].

The frequency shiftings occurring in the other carbonyl groups can likewise be interpreted as a dipole-dipole strengthening or weakening depending on whether the frequency shifts to higher or lower wavenumbers as degradation takes place. However, the inability to interrelate different carbonyl groups between the different samples and the difficulty in finding relevant effects on the overall degradation behaviour, justifies focusing only on the aldehyde carbonyl group in further discussions.

With this in mind, the ABS-g-Ma/APOSS nanocomposite, which has the highest wavenumber for the aldehyde frequency in the undegraded sample, should have a slightly higher chain stability compared to the other blends and indeed compared to the ABS-g-Ma matrix, which has the lowest frequency. However, the effects of dipole-dipole interaction can be minor when compared with the also beneficial effects of the POSS hindrance to the overall chain

motion of the nanocomposite, in fact, Figure 67 also shows that the spectra of the carbonyl aldehyde in ABS-g-Ma and ABS-g-Ma/APOSS suffers a shifting to lower frequencies in the degraded sample, which means that said dipole-dipole interaction weakens with thermo-oxidation [184, 286]. This argument could explain to certain extent why TPOSS and GPOSS have a better thermal resistance than APOSS and is in fact consistent with the results obtained with the TGA analysis.

Unlike the FTIR analysis of POM in the previous section, the multiple absorbance behaviours explained above for the ABS and its nanocomposites would make the carbonyl group unsuitable, or at least too complex, for the purpose of a common analysis. For this reason, the FTIR degradation analysis in this section will focus on the most sensitive fraction of the ABS matrix, which is butadiene. This conjugated diene has the characteristic absorption band at 966 cm^{-1} and is expected to decrease during degradation. Accordingly, the progress of butadiene at different aging periods is represented in Figure 68.

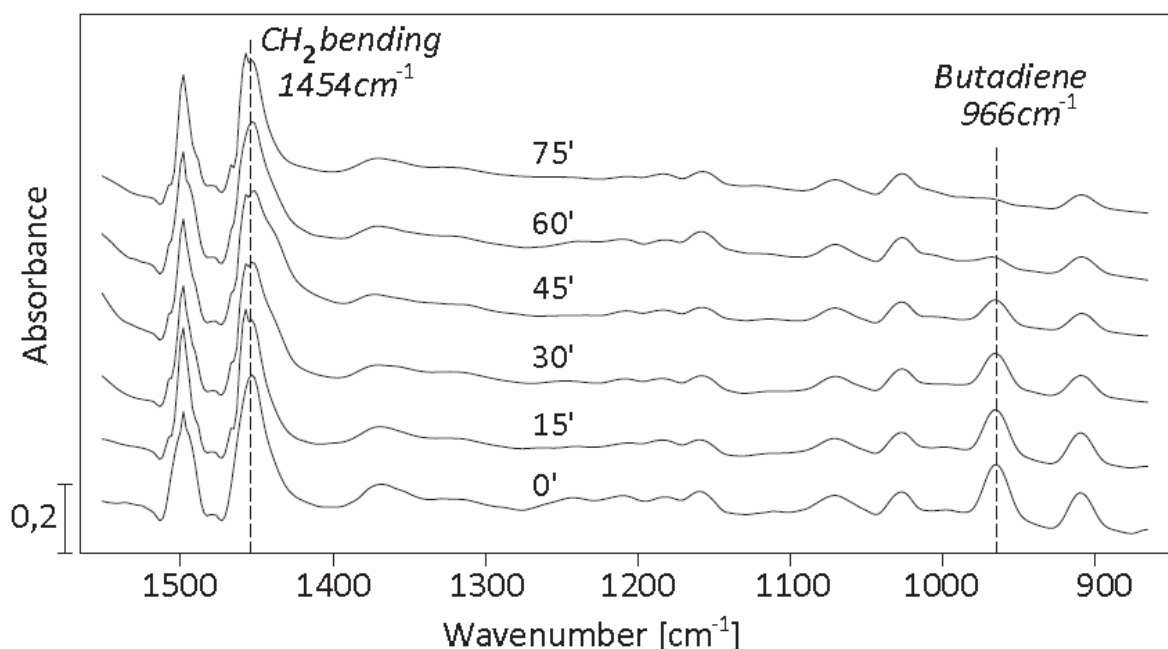


Figure 68: Spectra of ABS-g-Ma undergoing thermo oxidation under 320°C in steps of 15 min until 75 min.

In conjunction with the butadiene progress, the base reference taken when considering the degradation proportion is the strong CH₂ bending located at 1454 cm⁻¹, which has shown a very stable absorbance in all samples during a large portion of the thermo oxidation process. Figure 68 shows the progress of the ABS undergoing degradation at 320°C from 0 min to 75 min in steps of 15min, clearly showing the progressive reduction in the butadiene absorbance as thermo oxidation takes place.

Moreover, a comparison of the above ratio in the four original samples prior to degradation is represented in

Figure 69, which effectively shows no variation in the butadiene absorbance after incorporating any of the POSS nanofillers used (percentages ranging ~41%). This suggests, on the one hand, that the toughening properties of the butadiene fraction within the ABS terpolymer are expected to be kept in the new nanocomposite, but on the other hand it raises questions as to how effective is the interaction and protection of this sensitive constituency of the host polymer with the nanofillers used.

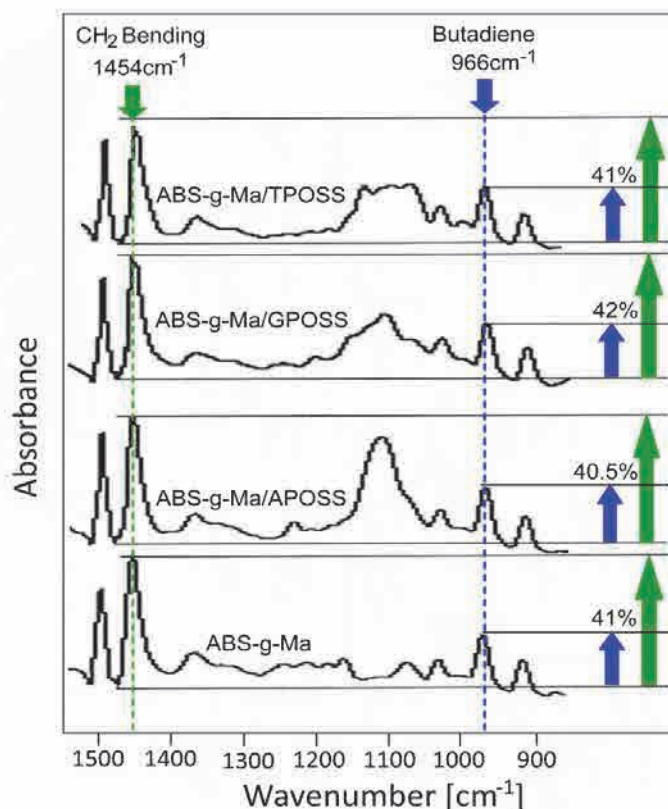


Figure 69: Overlay of the Butadiene ratio in the four original samples prior to degradation

With the above approach, Figure 70 shows the ratio butadiene/CH₂-bending absorbance of each material submitted at 200, 240, 280 and 320°C up to a period of 75min in steps of 15min, whereby the nanocomposites exhibit almost the same deterioration in terms of butadiene absorbance when compared to the original ABS-g-Ma sample, at best GPOSS and TPOSS show a little improvement under the higher testing temperatures i.e. 280 and 320°C.

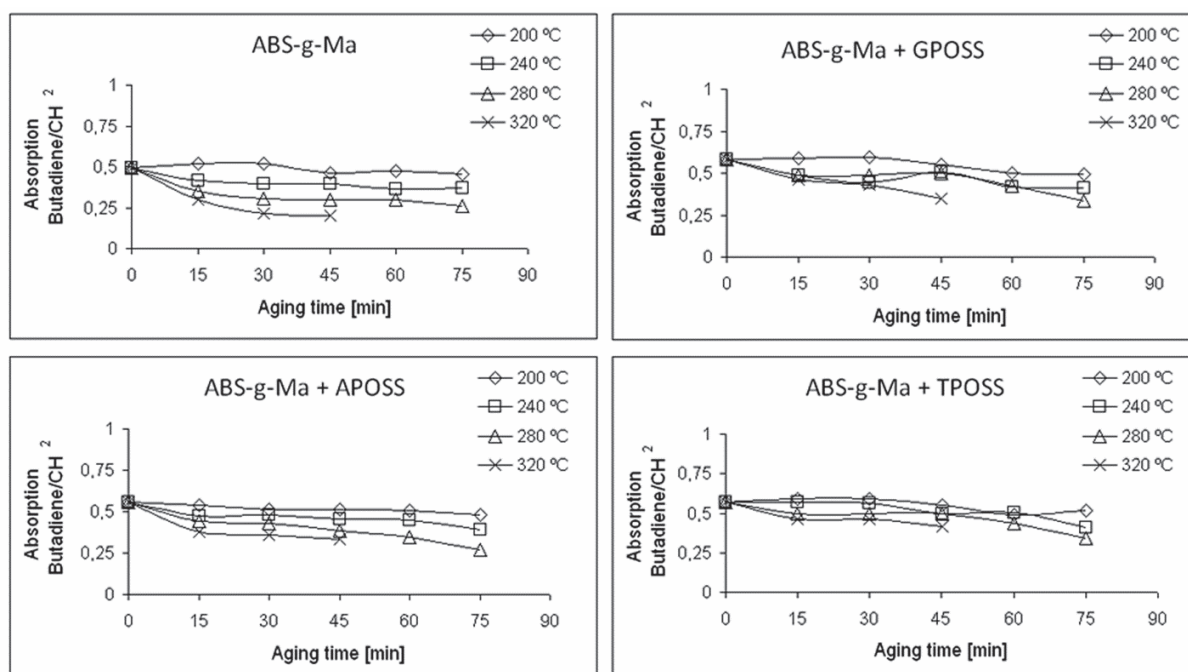


Figure 70: Ratio butadiene/CH₂ bending absorbance of each material submitted at 200, 240, 280, and 320°C up to 75 min in steps of 15 min.

In the attempt to quantify and compare between materials the effect of the melt-blended nanofillers on the thermal stability expressed in FTIR parameters, we picked the drop in butadiene/CH₂ ratio between the virgin sample and the degraded one at 280°C for 75min for each material. It is worth mentioning that 280°C was the maximum testing temperature at which samples could still be representative for FTIR analysis at 75 min of exposure, as beyond this point the CH₂ bending absorption started to decay.

Drop in butadiene/CH ² bending ratio [$S_0 - S_{280^\circ \times 75}$]	
ABS-g-MA	48,21%
ABS-g-MA/APOSS	51,24%
ABS-g-MA/GPOSS	45,02%
ABS-g-MA/TPOSS	42,87%

Table 20: Drop in butadiene/CH₂ ratio between the virgin material and the degraded sample at 280°C for 75min for each material.

Table 20 shows the small effect of the nanofillers on preventing the decay of the butadiene phase during thermo oxidation at 280°C for 75min, whereby GPOSS and TPOSS nanocomposites only improved the butadiene/CH₂ ratio by 3.2% and 5.3% respectively and the APOSS nanocomposite worsened the same ratio by 3%.

5.4.2. Thermogravimetric analysis of ABS-g-Ma/POSS and its nanocomposites.

The thermal stability of the four materials was also measured in terms of TGA weight loss, which is represented in Figure 71 below.

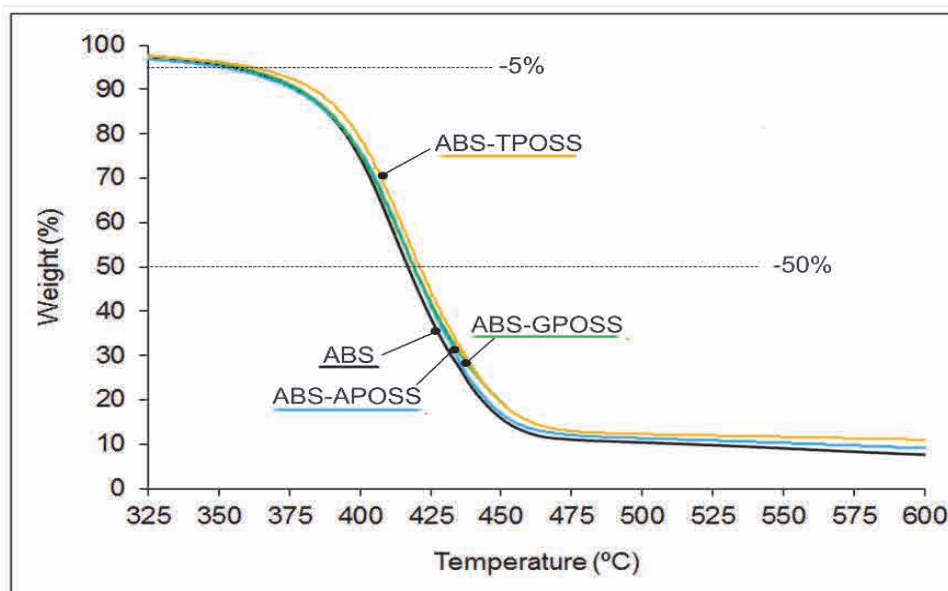


Figure 71: TGA thermogram for ABS-g-Ma, ABS-g-Ma /APOSS, ABS-g-Ma/GPOSS, and ABS-g-Ma/TPOSS.

The results of the above TGA investigations were plotted as percentage of the remaining sample mass to the initial one as a function of the temperature, whereby the corresponding curves decrease continuously to a residue level after mass loss has commenced. From this thermogram, we extracted the onset temperatures at which 5% and 50% of weight loss occurs, expressed as $T_{5\%}$ and $T_{50\%}$ respectively. These two parameters show that all nanocomposites tested have modest improvements in terms of thermal stability, as the onset temperatures are slightly higher than those of the ABS, except for ABS-APOSS at $T_{5\%}$ that lays 2°C below the ABS $T_{5\%}$. The blend that exhibited the highest onset temperatures was ABS-TPOSS with 8°C and 5°C higher for $T_{5\%}$ and $T_{50\%}$ respectively. Alternatively the derivative weight thermogram (DTG) displaying the temperatures of maximum weight loss (T_{max}) is depicted in Figure 72, whereby the three nanocomposites show a modest 2°C improvement of the T_{max} at 416°C with respect to the ABS sample at 414°C .

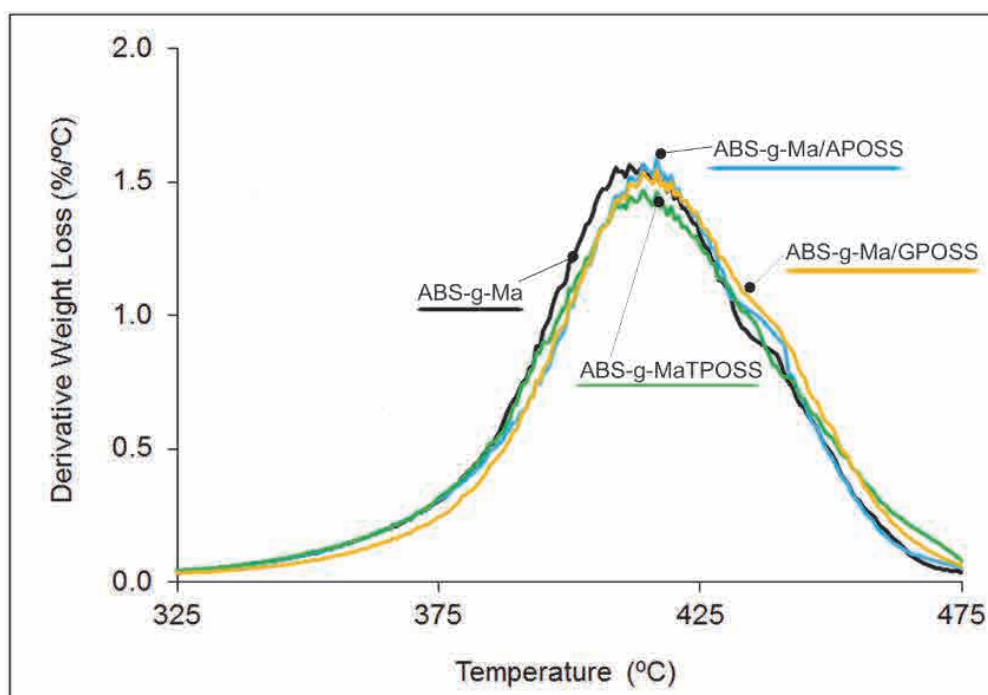


Figure 72: Derivative Weight thermogram (DTG) for ABS, ABS-APOSS, ABS-GPOSS, and ABS-TPOSS.

Although thermoplastic POSS nano-hybrids have often shown numerous cases of successful enhancement of thermal properties [38-39, 41-43], examples of limited effects have also been documented, whereby a parallelism can be established with the TGA/DTG results above in conjunction with lower T_g values obtained in the DSC section of this paper. Silva et al. experienced poor interfacial adhesion between a halide POSS melt-blended with PVC, resulting in no benefits on the thermal properties of the compound at the same time that POSS promoted a plasticizing effect, however they did not cover the root cause [232]. J.Wu et al. found a monotonically decreasing T_g with increasing POSS content on a PS/Isobutyl POSS copolymer as a consequence of competing effects between the free volume addition and the intermolecular interactions [287]. Likewise, Monticelli et al. obtained no significant effects of thermal and thermomechanical properties of Polystyrene-co-maleic anhydride (PSMA) with octaisobutyl POSS, referring also to the competing effects of the molecular constraints originated with the insertion of bulky functionalised Si-O-Si POSS cage and the free volume increase promoted by the isobutyl organic substituents of POSS [230]. Y.J.Lee et al. experienced a reduction in the T_g value of an aromatic polyimide (PI) matrix with increasing Epoxy-POSS content, also caused by the free volume increment resulting in a loose PI structure [231]. This behaviour has also certain similarities with composites over the nano range as documented by Altaweel et al., who identified an inversely proportional relationship between free volume increase and the T_g value, as well as a reciprocity between the T_g drift and the filler interaction with the matrix determining the thermal stability of the composite [181].

In addition to the above blend inefficiencies, the small onset temperature decay of ABS-APOSS at the beginning of the test can be attributed to the lower degradation temperature of the aminopropylisobutyl POSS, which in isolated state sits in the range of 90°C below the one from the ABS-g-Ma matrix and reinforces the theory of unreacted POSS fraction within the base material. Y.J.Lee et al. had a similar experience of a slight decrease in the decomposition temperature (T_d) in the PI-POSS nanocomposites relative to the pure PI due to lower degradation temperature of POSS organic segments [231].

The correlation between the literature above and the findings from the nano-hybrids examined in this section would suggest that the limited effects of the different nanofillers in hand are likely to be caused by the competing effects between the intermolecular constraints of the rigid POSS structures and the free volume increment promoted by the local mobility of the pendant R-groups of the same dispersed Si-O cages.

5.4.3. Degradation kinetics by Coats&Redferd of ABS-g-Ma/POSS and its nanocomposites.

Based on the previous TGA derivative weight plot and the fundamentals of the Coats and Redfern method for calculating the kinetic parameters explained in section 3.2, the 'S' values (Shape Index) are subtracted as shown in Figure 73, and the 'n' values have been subsequently calculated by means of the Kissinger's equation.

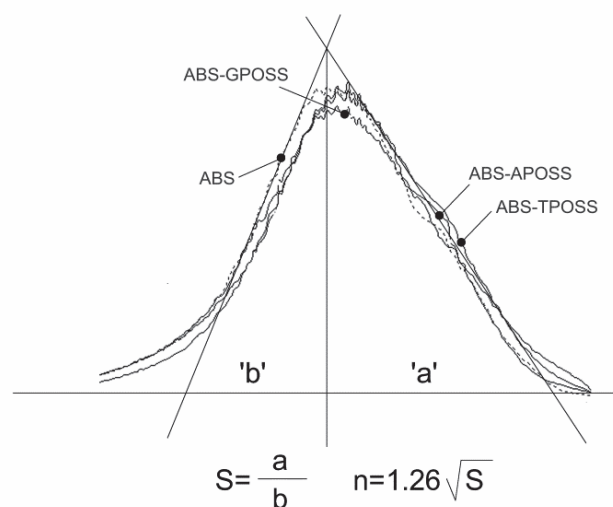


Figure 73: Method to calculate the shape index "S" and the order of reaction "n".

From the above, the 'n' values obtained went from the highest 2,54 for the ABS down to lowest 2,45 for the ABS-APOSS blend, being almost the same as for the ABS-GPOSS and ABS-TPOSS with an order of reaction of 2,46. Subsequently, these 'n' values lead to the application of Equation 24 to calculate the activation energy E_a for the four materials

analysed. Figure 74 represents the value of the left hand side of said equation i.e. $\ln\left\{\frac{1 - (1 - \alpha)^{1-n}}{T^2(1-n)}\right\}$ against the reciprocal of absolute temperature ($1/T$), where a linear curve can be obtained for each material.

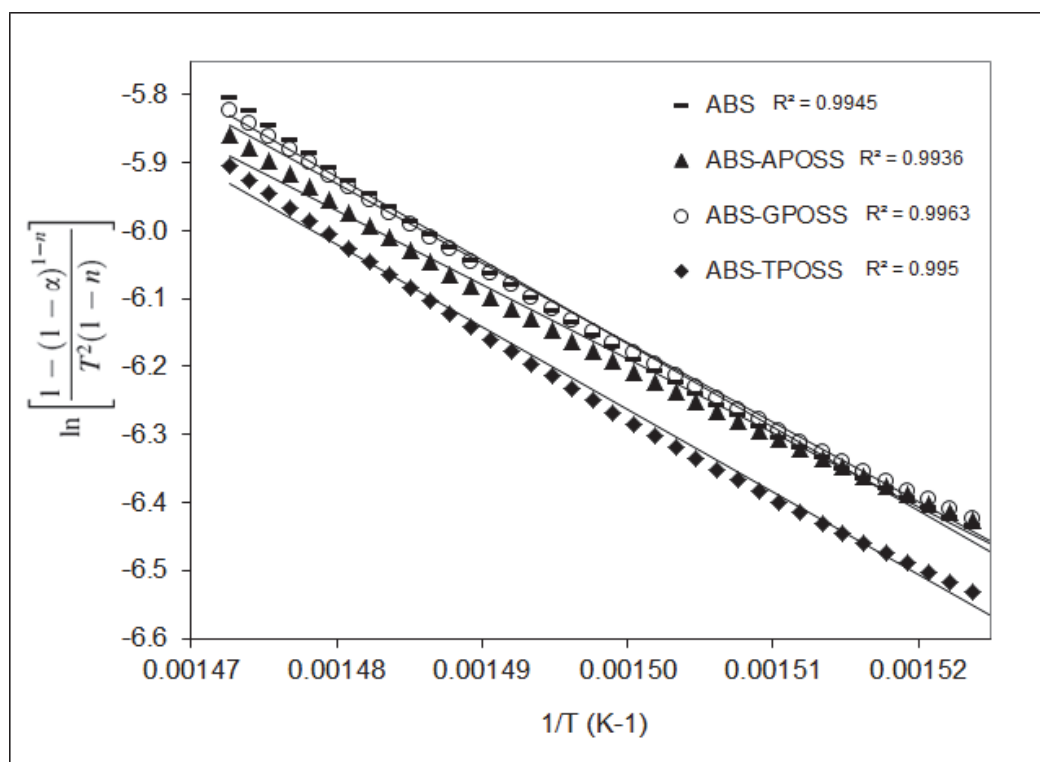


Figure 74: Kinetics of the thermal degradation for ABS, ABS-APOSS, ABS-GPOSS, and ABS-TPOSS.

The activation energy (E_a) of each sample can be calculated from the slope of the corresponding curve and its intercept value, resulting in ABS-TPOSS being the most stable blend with $E_a=106,9$ kJ/mol, followed closely by ABS-GPOSS with 106,5 kJ/mol, and then going to the less stable being the original ABS with 99 kJ/mol and ABS-APOSS with 98,8 kJ/mol. This is consistent with the results obtained in the other analytical methods carried out for the ABS and its nanocomposites assessed in this work.

D.M. Chang studied the effectiveness of stabilising ABS with different add rates of antioxidant, obtaining E_a values ranging from 75 to 103 kJ/mol [288]. This reference confirms once more the limited contribution of the different POSS's used in this work, considering

that a standard high molecular weight hindered phenol antioxidant added at concentration rate of 5% (equivalent to the POSS concentration used the nanocomposites of this work) achieves a 36% increase in E_a [288] compared to the 8% increase obtained with the best POSS performer of this section, which is TPOSS. Despite the fact that the study from Chang does not clarify if the original ABS had any stabiliser prior to the antioxidant addition, it is still fair to deem the POSS contribution as comparatively poor after confirming with the ABS-g-MA supplier that there is no heat stabiliser added in the original compound and therefore there was ample potential to improve the thermal properties of the ABS-g-Ma sample.

To conclude the thermal stability analysis in this section, Table 21 below summarizes the most relevant results from the thermogravimetric and kinetic analysis of thermal decomposition, where ABS-TPOSS shows an improvement 8°C in $T_{5\%}$ and 7.9% in activation energy compared to the original ABS, followed closely by ABS-GPOSS and having ABS-APOSS with no relevant improvements.

Materials:	$T_{5\%}$		$T_{50\%}$		T_{MAX}		Kinetic Parameters			
	°C	$\Delta^\circ\text{C}$	°C	$\Delta^\circ\text{C}$	°C	$\Delta^\circ\text{C}$	n	Δn	E [kJ/mol]	ΔE
ABS	353	<i>n/a</i>	416	<i>n/a</i>	414	<i>n/a</i>	2.54	<i>n/a</i>	99.0	<i>n/a</i>
ABS-APOSS:	351	-2	418	2	416	2	2.45	-0.09	98.8	-0.1
ABS-GPOSS:	357	4	419	3	416	2	2.46	-0.08	106.5	7.6
ABS-TPOSS:	361	8	421	5	416	2	2.46	-0.08	106.9	8.0

Table 21: Summary of thermogravimetric and kinetic degradation of ABS-g-Ma, ABS-g-Ma/APOSS, ABS-g-Ma/GPOSS and ABS-g-Ma/TPOSS.

5.4.4. Spectrophotometry analysis of ABS-g-Ma and its nanocomposites

The appearance deterioration of the different samples of ABS-g-Ma and ABS-g-Ma nanocomposites have been characterised in spectrophotometry terms after being submitted to the degradation conditions set out in section 4.3.2. An example of the deterioration effects can be seen in Figure 75 below, which shows the resulting samples after being thermoxidated at 240°C during 75 minutes, and whereby all three nanocomposites show a similar appearance when compared to the base ABS-g-MA.

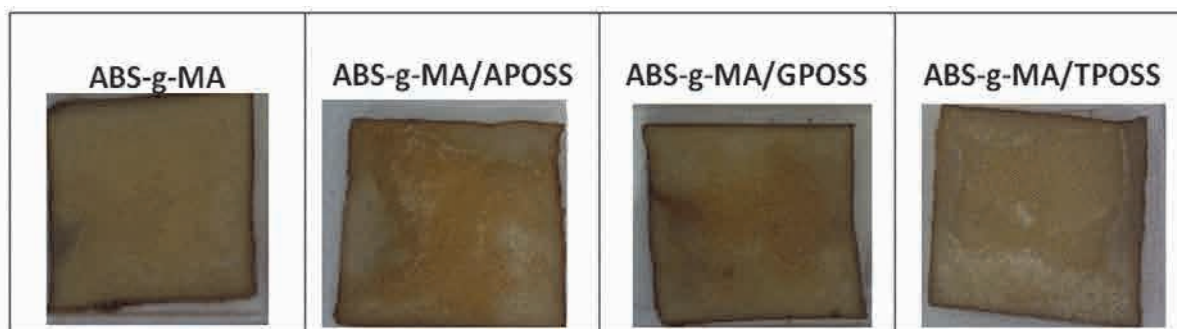


Figure 75: Photos of the four different materials tested under the conditions 240°C for 75 min.

The spectrophotometry results are based on the CIE 1976 L^*, a^*, b^* (CIELAB) method, which provides the chromaticity coordinates a^* (Redness-Greenness) and b^* (Yellowness-Blueness), along with lightness L^* . The indicator used for the yellowing assessment is the total variation of $L^*a^*b^*$ (ΔE) in relation to the initial sample prior to thermoxidation, hence the possible differences between original samples of each material are filtered.

Figure 76 refers to the chromaticity values for each sample submitted at 240°C for different periods of time. From these, it can be drawn that the three ABS/POSS nanocomposites did not improve yellowing prevention, at least to an evident extent. Likewise, the lightness trend

in the same appears to be consistent with the chromaticity values where colours darken almost at the same rate.

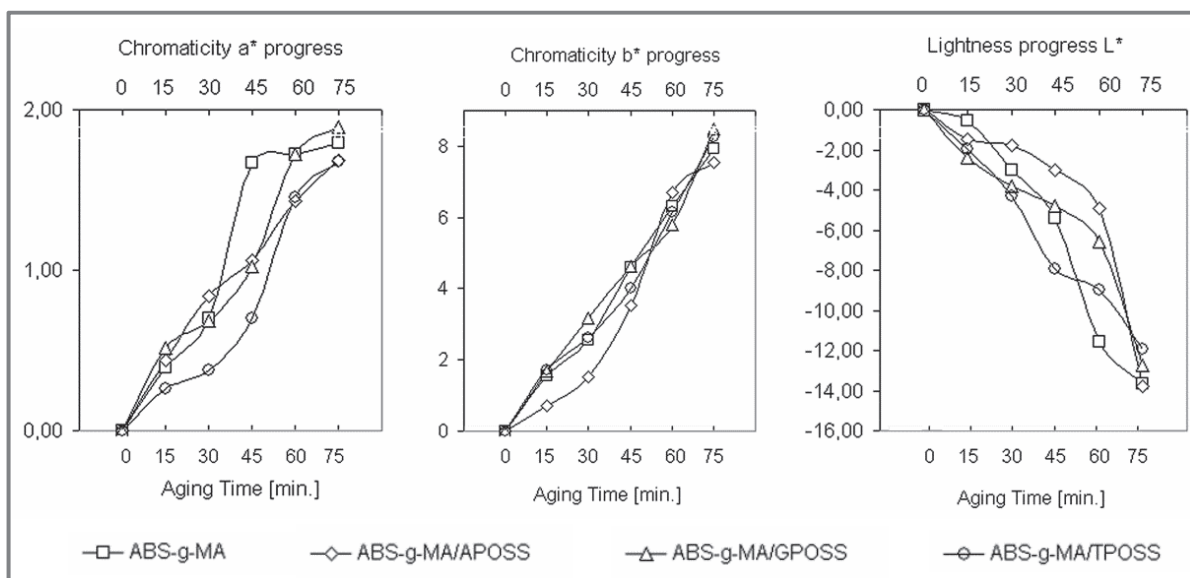


Figure 76: Progress of Lightness L^* , Coordinate a^* (redness-greenness), and Coordinate b^* (yellowness-blueness) as degradation proceeds at 240°C.

In addition to the colour plots depicted in this section, a CIELAB colour space in Figure 77 represents the progress in hue appearance i.e. chromaticity values a^* and b^* , that the sample undergoes as it is submitted from 0 min to 90 min under 240°C. This plot represents the direction of the colour progress of all the samples and shows similar trends for the four samples analysed.

This section proves that the effect of the nanofillers used i.e. APOSS, GPOSS and TPOSS is almost negligible when it comes to colour shifting stability on the nanocomposite surface when submitted to oven-storage ageing. This phenomenon was expected, as the TGA and FTIR analysis on these same nanocomposites are showing similar trends.

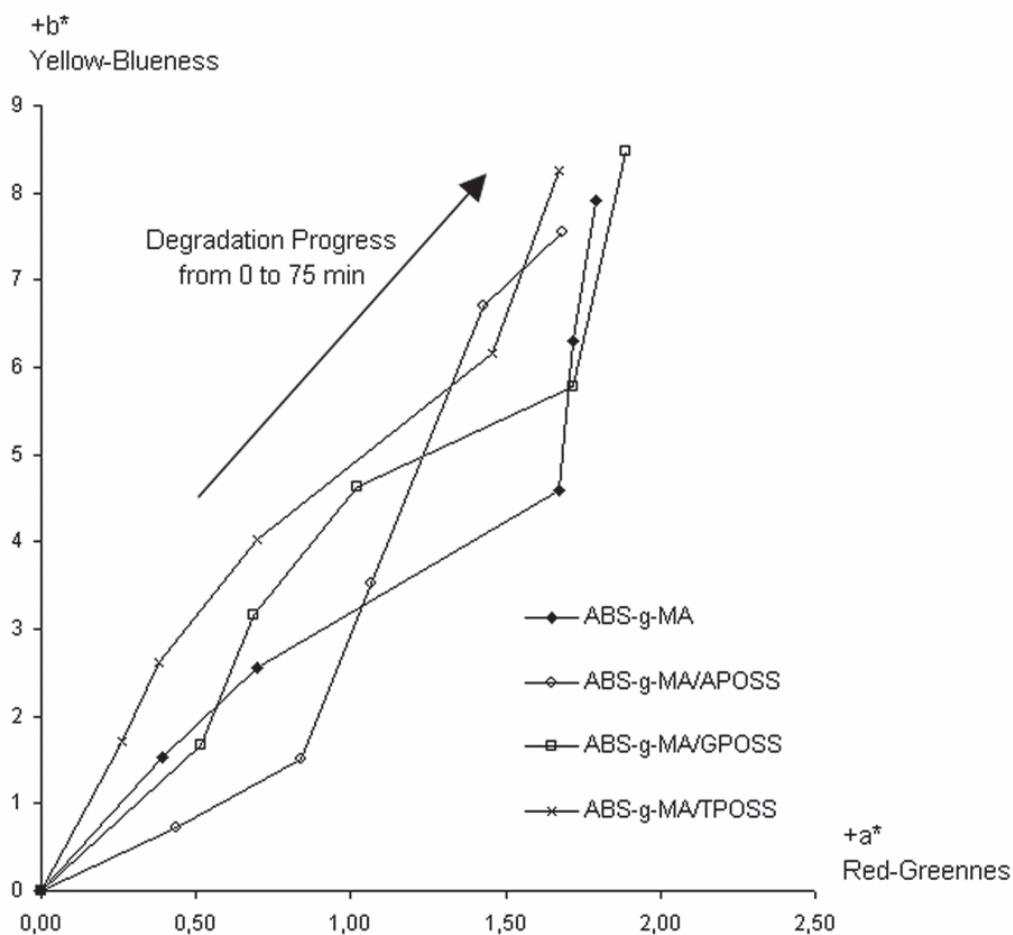


Figure 77: Colour route followed by the different nanocomposites along the CIELAB space with different aging times up to 90 min at 240°C representing the hue chromaticity values (a^* and b^*).

5.4.5. Inter-relationship between FTIR and Spectrophotometry analysis

The values obtained from the FTIR analysis of the original ABS-g-Ma and the different ABS-g-Ma nanocomposites have been compared with those corresponding to the yellowing analysis, i.e. the decay in butadiene/methylene absorbance ratio compared to the variation on the sample colour expressed in terms of ΔE (Delta L*a*b*). This comparison is depicted in Figure 78 below and is based on the conditions of 75 min of exposure at 280°C.

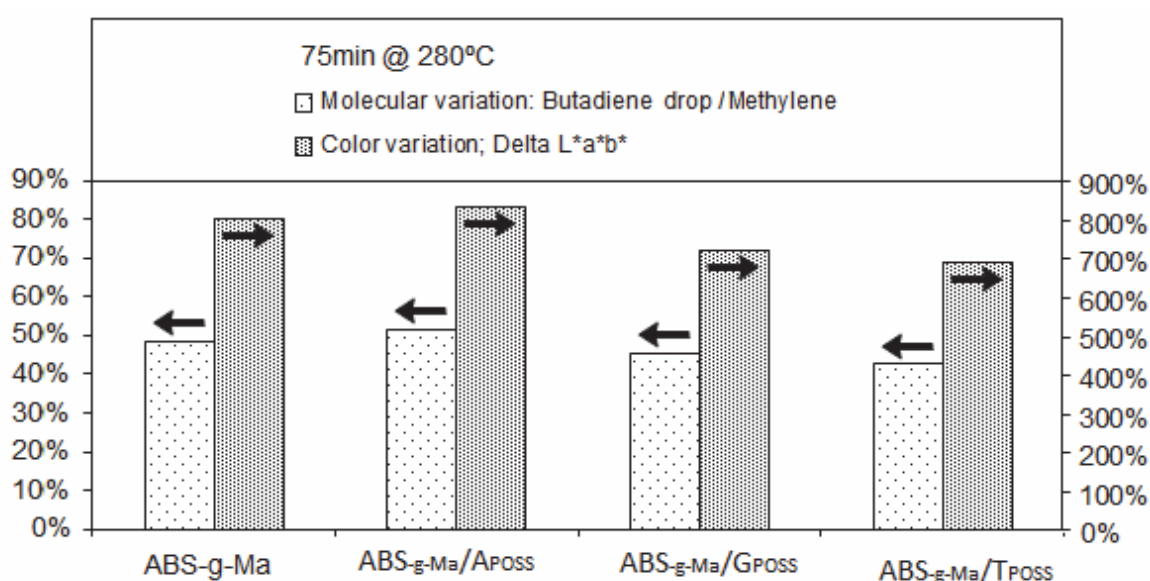


Figure 78: Degradation of ABS-g-MA and its POSS nanocomposites in terms of Butadiene decay and Colour variation when submitted at 280°C for 75 min.

As expected, the variation in colour shift (yellowing) and the decay in butadiene increase proportionally as the samples undergo thermoxidation. Although the colour shift occurs at proportions 10 times bigger than the butadiene decay, both indicators are consistently coherent in proportional terms between each other. Small improvements are seen in the GPOSS and TPOSS nanocomposites when compared to the original ABS-g-Ma, however they are relatively timid.

5.4.6. Summary of results of ABS-g-Ma and its nanocomposites.

The overall performance of the materials tested in the different experimental disciplines is summarised in Table 22 below, which shows the most representative results of the SEM, DSC, FTIR, TGA/DTG, Kinetics and Spectrophotometry analysis for ABS-g-Ma and the ABS-g-Ma /POSS nanocomposites.

SUMMARY TABLE

		ABS-g-MA	ABS-g-MA/APOSS	ABS-g-MA/GPOSS	ABS-g-MA/TPOSS
SEM	Surface cryogenically fractured appearance	Base material	Good miscibility No agglomerate	Good miscibility No agglomerate	Good miscibility No agglomerate
DSC	Tg	104,8°C	103,7°C	102,3°C	103,5°C
FTIR	Drop in butadiene/CH ₂ ratio [S0-S280°x75°]	48.21%	51.24%	45.02%	42.87%
	Tmax Derivative weight loss	414°C	416°C	416°C	416°C
TGA	Residue after thermal decomposition	7.5%	8.9%	10.6%	10.9%
	Coats & Redfern Activation Energy	99 kJ/mol	98,8 kJ/mol	106,5 kJ/mol	106,9 kJ/mol
COLOR	Averaged Yellowing (Delta Lab %)	3.52%	3.61%	3.42%	3.36%

Table 22: General summary of results from SEM, DSC, FTIR, TGA/DTG, Kinetics and Spectrophotometry analysis for ABS-g-Ma and the ABS-g-Ma/POSS nanocomposites.

CHAPTER 6
CONCLUSIONS

6. CONCLUSIONS

Different types of nanocomposites have been produced with a variety of polyhedral oligomeric silsesquioxanes (POSS) melt-blended with a semi-crystalline copolymer (POM) and an amorphous terpolymer (ABS) grafted with maleic anhydride (namely ABS-g-Ma). The POSS nanofillers used in the preparation of the four different POM nanocomposites are Polyethylene Glycol (PEG-), Glycidyl (G-), Glycidylisobutyl (GI-) and Amino-propyl Isobutyl (A-), added at a 2.5% concentration. The nanofillers used in the three different ABS-g-MA nanocomposites are Amino-propyl Isobutyl (A-), Glycidyl (G-) and Trisilanol (T-), added at 5% concentration. The resulting morphology, structure, thermal properties, degradation kinetics and extent of yellowing under thermoxidative conditions have been quantified with the corresponding discussion of the benefits or drawbacks found with each type of nanocomposite. The conclusions that can be drawn from this dissertation are the following:

POM NANOCOMPOSITES

- The solubility calculations based on *Hoy* and *Hoftyzer & Van Krevelen* methods suggest that the G-POSS and PEG-POSS would be at or within recommended criteria of $\leq 5(\text{J}/\text{cm}^3)^{1/2}$ in relation to its compatibility with the POM matrix. On turn A-POSS and GI-POSS gave values between 26-33% respectively above this threshold, meaning slightly greater difficulties to achieve a good miscibility in the melt-blending process.
- The greatest solubility difference exhibited between POM and GI-POSS was evidenced on the SEM analysis displaying agglomerates with phase separation, whereas the microscopy images of the other three POM nanocomposites showed adequate miscibility.
- The DSC analysis suggested good dispersion of POSS in the POM matrix by showing single thermogram transitions for G-POSS, GI-POSS and A-POSS with a unique and well-defined T_m within $\pm 1.5^\circ\text{C}$ of the original melting point of POM. In the case of PEG-POSS, however, a secondary crystallisation peak was exhibited near the

characteristic PEG-POSS melting point, suggesting a crystalline fraction of this particular POSS.

- During the different thermoxidation stages, all nanocomposites showed an important reduction of carbonyl aldehyde group $-(C=O)$ relative to the methylene bending absorption when compared to the standard POM. This suggests less bond dissociation and β -scission of $-O-CH-$ groups in the main chain.
- Examples of such improvement are the results obtained at 240°C for 45 min of oven-storage, with POM/PEG-POSS yielding 35% less carbonyl relative to the original POM, and most importantly the POM/A-POSS yielding 98% less carbonyl at that particular aging condition.
- The highest increment in thermal stability obtained in the thermogravimetric analysis under air atmosphere is also with POM/A-POSS, where the temperature of maximum rate of degradation (T_{MAX}) and the activation energy was 22°C and 7.8 kJ/mol above those values from the unmodified POM.
- The nanocomposites made from GI-POSS, G-POSS and PEG-POSS also showed improvements on the thermal properties, with 8 to 12°C of higher T_{MAX} .
- The higher activation energies from the nanocomposites could suggest hydrogen bonding interactions between the functionalised POSS and the POM ether oxygen atoms.
- All POM nanocomposites dramatically reduced the yellowing process expressed in CIELAB spectrophotometry parameters (ΔE), varying only a fraction between 8% and 50% of the total ΔE undergone by the standard POM.
- From the above yellowing analysis, the A-POSS was once again the best performer out of the POSS range used in this study. This is aligned with the important reduction of the carbonyl aldehyde generated during the thermoxidation process and witnessed in the FTIR analysis, which is an important contributor to the development of specific chromophores causing yellowing.

ABS-g-MA NANOCOMPOSITES

-
- The solubility values obtained with the ABS-g-Ma nanocomposites were all within the recommended criteria $\leq 5 \text{ (J/cm}^3\text{)}^{1/2}$. This was confirmed by the SEM micrographs showing good surface homogeneity with no agglomerates.
 - Likewise, the DSC analysis showed a single and well defined T_g, with no trace of melting endotherms of the corresponding POSS.
 - The DSC analysis also exhibited a small decay on T_g in all nanocomposites, which can be attributed to higher molecular mobility due to an increase of free-volume originated by the bulky POSS structures and their pendant R-groups.
 - The thermoxidation progress of ABS-g-Ma has resulted in multiple carbonyl absorptions shifting to higher and lower wavelengths, hence making this reference unsuitable for the purpose of degradation monitoring.
 - The butadiene group, being the most sensitive fraction of ABS, has resulted in a reliable degradation indicator when referred to the absorption of the methylene scissoring vibration.
 - Limited variations between unmodified ABS-g-Ma and its different nanocomposites are discernible in the FTIR analysis. Particularly, the G-POSS and T-POSS nanocomposites submitted at 280°C for 75min, showed a slight 3.2% and 5.3% improvement respectively relative to the original ABS-g-Ma, however the A-POSS blend exhibited a 3% decay when compared to the unfilled base material.
 - The above FTIR results suggest a dubious contribution of the POSS nanofillers when it comes to protect the vulnerable butadiene phase of the polymer.
 - The thermogravimetric analysis carried out on the G-POSS and T-POSS samples showed an increase of T_{5%} of 4°C and 8°C respectively, and a reduction of 2°C on the APOSS nanocomposite.
 - The same thermograms also suggested an even more timid improvement on the T_{MAX} of the three nanocomposites, only 2°C above the original ABS-g-Ma.

-
- Besides the poor contribution of the nanofillers in the overall thermal stability of the host polymer, these results also suggest that the little thermal enhancement, if any, occurs at the early stages of degradation.
 - The degradation kinetics analysis based on Coats & Redfern showed proportionate results to those found in TGA and FTIR. Particularly, G-POSS and T-POSS had 7.5% and 7.9% higher activation energy respectively when compared to the ABS-g-Ma alone, and APOSS resulted in 2% lower E_A .
 - Overall, these results can be explained by the competing effects of the molecular constraints originated with the insertion of the Si-O-Si POSS cages and the free volume increment promoted by the bulky functionalised ramifications unreacted with the host polymer.
 - The yellowing propensity analysis of the ABS-g-Ma nanocomposites indicated no relevant improvement in terms of ΔE variation. Particularly, the best result was for the TPOSS blend reducing ΔE only by a negligible 0.16% and the worst for A-POSS increasing ΔE by 0.09%, which is consistent with the poor results obtained with the other analytical methods.

GENERAL CONCLUSIONS

- This work highlights the great differences in performance that can be achieved in melt-blended POSS nanocomposites depending on the material constituencies and the blending conditions.
- On the one hand, the contribution of the POSS Glycidyl, Glycidyl Isobutyl and A-Propyl-Isobutyl on the POM matrix has provided encouraging results with major improvements in the overall thermal resistance and yellowing prevention.
- On the other hand, however, the incorporation of Glycidyl and Trisilanol in the ABS-g-MA matrix has resulted in very limited benefits, and the addition of Amino-Propyl-Isobutyl, being the best POSS performer in the POM melt blended nanocomposites, has slightly worsened the thermal properties of ABS.

- Overall, the melt blended incorporation of the three POSS used in ABS-g-MA failed in achieving an effective protection of the weak butadiene fraction of ABS against thermoxidation.
- The solubility prediction and subsequent SEM analysis on the ABS-g-MA nanocomposites prove that a good dispersion of the nanofillers does not necessarily translate into effective thermal enhancement of the nanocomposite.
- Accordingly, the compatibilisation between the host polymer and the POSS molecule not only has to address adequate dispersion and miscibility, but just as importantly, it also has to effectively target those specific constituencies of the host polymer that are known to be the weakest and most sensitive to thermoxidation.

FUTURE WORK

The simplicity and affordability of the melt blending approach for the preparation of nanocomposites has proven to be capable of yielding exceptional results when adequate nanofillers and compounding conditions are used. At the same time, however, understanding the variables dictating the level of success still requires further research, and the following areas could be of interest for future work:

- In the same way that commercial thermoplastics have plenty of literature regarding processing guidelines, having documented methods for the melt-blending conditions to incorporate each type of POSS nanoparticle would greatly assist in the preparation of this type of nanocomposites.
- To have the ability to specifically target the weaker fractions of the host polymer in order to more effectively achieve higher thermal resistance. This will require thorough understanding of the polymer labile moieties and how the nanoparticle can contribute to reduce their susceptibility to react.
- Particularly in the ABS, to being able to protect the butadiene fraction without altering its toughening role within the terpolymer system. Along these lines, for example, the solubility parameter study could be used to identify potential combinations where the miscibility between the polybutadiene and the enhancing nanoparticles is maximised.

CHAPTER 7
REFERENCES

7. REFERENCES

- [1] R. Feynman, conf.speech "There's Plenty of Room at the Bottom", Pasadena, 29 December 1959. (n.d.).
- [2] N. Taniguchi, On the Basic Concept of 'Nano-Technology', Bulletin of Japan Society of Precision Engineering, 18-23. (1974).
- [3] *Nanoscience and Nanotechnologies, The Royal Society & the Royal Academy of Engineering*, ISBN 0 85403 604 0. (2004).
- [4] K.E. Drexler, "Engines of Creation", Anchor Press/Doubleday, NewYork, ISBN 0-385-19973-2. (1986).
- [5] H. W. Kroto, J. R. Heath, S. C. O'brien, R. F. Curl, R. E. Smalley, C60: Buckminsterfullerene, Nature, 318, 162-163. (1985).
- [6] A. Usuki, M. Kawasumi, Y. Kojima, A. Okada, T. Kurauchi, O.J. Kamigaito, Mater. Res., 8, 5. 1174-1178. (1993).
- [7] *The European strategy for nanotechnology and the nanotechnology Action Plan*. (n.d.). Retrieved 6 7, 2013, from <http://cordis.europa.eu/nanotechnology/actionplan.htm>
- [8] *NANO21E, Nanocomposites, Nanoparticles, Nanoclays, and Nanotubes*, BCC Research. (2012, December 20). Retrieved from <http://www.bccresearch.com/report/nanocomposites-global-markets-nan021e.html>
- [9] C. Buzea, I.P. Blandino, K. Robbie, Biointerphases, 2, 4, p12. (2007).
- [10] Schmidt, K. (2007). Nanofrontiers: Visions for the Future of Nanotechnology. *WWICS Project on Emerging Nanotechnologies*.
- [11] (2007). *T.E. Bell, Understanding risk assessment of nanotechnology*, National Nanotechnology Coordination Office, Arlington.
- [12] M. Gleiche, H. Hoffschulz, S. Lenhert, Europ. Nanotech. Gateway, 1-30. (2006).
- [13] E. Taboada, M. Gich, A. Roig, ACS Nano, 3, 11, 3377–3382. (2009).
- [14] M. Darbandi, R. Thomann, T. Nann, Chem. Mater., 17, 23, 5720–5725. (2005).

-
- [15] Y. Zhu, Z. Li, M. Chen, H.M. Cooper, G.Q. Lu, Z.P. Xu, *Chem. Mater.*, 24, 3, 421-423. (2012).
- [16] P. Holister, J.W. Weener, C. Román-Vas, T. Harper, *Nanopart. Techn. White Pap.*, 3, 1-11. (2003).
- [17] M.F. Yu, O. Lourie, M.J. Dyer, K. Moloni, T.F. Kelly, R.S. Ruoff, *Science*, 287, 637. (2000).
- [18] W. Gacitua, A. Ballerini, J. Zhang, *Mad. Cienc. Tecn.*, 7, 3, 159-178. (2005).
- [19] L. Goldman, C. Coussens, Editors, *Implications of Nanotechnology for Environmental Health Research, Roundtable on Environmental Health Sciences, Research and Medicine*, The National Academies Press. (2005).
- [20] M.A. Korzhinsky, *Nature*, 375, p.544. (1995).
- [21] R. E. Grim, *J. Soil Mech. & Found. Div., ASCE*, 85, SM2, 1–17. (1959).
- [22] E. Manias, “Origins of the Materials Properties Enhancements in Polymer/Clay Nanocomposites”, *Nanocomposites*, 1, 1-11. (2001).
- [23] *Nano Minerals: Nanoclays* ><http://www.sigmaaldrich.com/materials-science/nanomaterials/nanoclay-building.html>> (visited 4th, March, 2013). (n.d.).
- [24] J. Harris, J. Zhao, A.B. Morgan, *Polymer*, 46, 20, 8641-8660. (2005).
- [25] M. McAlpine, J.J. Liggat, R.A. Pethrick, D. Pugh, I. Rhoney, *J. Appl. Pol. Sci.*, 99, 2614-2626. (2006).
- [26] *NAN021C, Nanocomposites, Nanoparticles, Nanoclays, and Nanotubes*, BCC Research. (2008). Retrieved 6 20, 2010, from <http://www.bccresearch.com/report/nanotechnology-market-nan031c.html>
- [27] M.D. Read, J.D. Harris, R.R. Samson, *Annual Technical Conference, SPE*, 2, 1882-1886. (2004).
- [28] A. Cadene, S. Durand-Vidal, P. Turq, J. Brendle, *J. Coll. & Interf. Sci.*, 285, 719–730 . (2005).
- [29] X. Duan, C. Niu, V. Sahi, J. Chen, J.W. Parce, S. Empedocles, J. Goldman, *Nature*, 425, 274-278. (2003).

-
- [30] J. Zhu, Y. Cui, *Nat. Mater.*, 9, 183–184. (2010).
- [31] C. Fang, A. Agarwal, . Widjaja, M.V. Garland, S.M. Wong, L. Linn, N.M. Khalid, S. M. Salim, N. Balasubramanian, *Chem. Mater.* , 21, 3542–3548. (2009).
- [32] K.Q. Peng, J.S. Jie, W.J. Zhang, S.T. Lee, *Appl. Phys. Lett.*, 93, 033105. (2008).
- [33] C.H.A. Tsang, Y. Liu, Z.H. Kang, D.D.D. Ma, N.B. Wong, S.T. Lee, *Chem. Commun.*, 39, 5829–5831. (2009).
- [34] W.W. Gerberich, W.M. Mook, C.R. Perrey C.B. Carter, M.I. Baskes, R. Mukherjee, A. Gidwani, J. Heberlein, P.H. McMurry, S.L. Girshick, *J. Mech. Phys. Sol.*, 51, 6, 979-992. (2003).
- [35] F. Erogbogbo, T. Lin. P.M. Tucciarone, K.M. Lajoie, L. Lai, G.D. Patki, P.N. Prasad. M.T. Swihart, *Nano Lett.*, 13, 2, 451–456. (2013).
- [36] *G. Pucker, E. Serra, Y. Jestin, "Quantum Dots - A Variety of New Applications", Ameenah Al-Ahmadi, ISBN 978-953-51-0483-4. (2012).*
- [37] C.C. Wu, M.J. Sailor, *ACS Nano*, DOI: 10.1021/nn305574e. (2013).
- [38] J. Wang, Z. Ye, H. Joly, *Macromol.*, 40, 6150-6163 . (2007).
- [39] M.B. Nair, F.D. Blum, *Polym. Prepr.*, 46(1), 367-368. (2005).
- [40] B. Fu, M. Gelfer, B. Hsiao, S. Phillips, B. Viersb, R. Blanski, P. Ruth, *Polymer*, 44, 1499–1506 . (2003).
- [41] S.W. Kuo, F.C. Chang, *Progr.Polym.Sci.*, 36, 1649–1696. (2011).
- [42] Z. Zhou, Y. Zhang, Z. Zeng, Y. Zhang, *Jour.Appl.Polym.Sci.*, 110, 3745-3751. (2008).
- [43] M. Sánchez-Soto, S. Illescas, H. Milliman, D. A. Schiraldi, A. Arostegui, *Macromol. Mater. Eng.*, 295, 846–858. (2010).
- [44] (2004). J. Denault, B. Labrecque, *Tech. Gr. Polym. Nanocomp.*, PNC-Tech. Ind.Matl.Inst. Québec, J4B 6Y 4.
- [45] J. Aleman, A.V. Chadwick, J. He, M. Hess, K. Horie, R.G. Jones, P. Kratochvil, I. Meisse, I. Mita, G. Moad, S. Penczek, R.F.T. Stepto, *Pure Appl. Chem.*, 79, 10, 1801-1829. (2007).
- [46] N. Vila, M. Sanchez-Soto, S. Illescas, *Polym.Comp.*, 32(10), 1584-1592. (2011).
- [47] A. Fina, D. Tabuani, T. Peijs, G. Camino, *Polymer*, 50, 218-226 . (2009).

-
- [48] F. Baldi, F. Bignotti, A. Fina, D. Tabuani, T. Ricco, *J. Appl. Polym. Sci.*, 105, 935-943. (2007).
- [49] S. Illescas, A. Aróstegui, D.A. Schiraldi, M. Sánchez-Soto, J.I. Velasco, *J. Nanosci. and Nanotechnol.*, 10, 1349-1360. (2010).
- [50] M.Q. Zhang, M.Z. Rong, K. Friedrich, *In Handbook of Organic-Inorganic Hybrid Materials and Nanocomposites; Nalwa, H. S., Ed.; American Scientific Publishers: Stevenson Ranch, CA, Vol 2, 113-150.* (2003).
- [51] A. Fina, O. Monticelli, G. Camino, *J. Mater. Chem.*, 20, 9297-9305. (2010).
- [52] C.L. Wu, M.Q. Zhang, M.Z. Rong, K. Friedrich, *Compos. Sci. Technol.*, 65, 635. (2005).
- [53] E. Moncada, R. Quijada, J. Retuert, *J. Nanotechnology*, 18, 335606. (2007).
- [54] M.Z. Rong, M.Q. Zhang, Y.X. Zheng, H.M. Zeng, R. Walter, K.J. Friedrich, *Mater. Sci. Lett.*, 19, 1159. (2000).
- [55] D.N. Bikiaris, G.Z. Papageorgiou, E. Pavlidou, N. Vouroutzis, P. Palatzoglou, G.P. Karayannidis, *J. Appl. Polym. Sci.*, 100, 2684. (2006).
- [56] M. García, G. van Vliet, S. Jain, B.A.G. Schrauwen, A. Sarkissov, W.E. van Zyl, B. Boukamp, *Rev. Adv. Mater. Sci.*, 6, 169. (2004).
- [57] K. Asuka, B.P. Liu, M. Terano, K.H. Nitta, *Macromol. Rapid Commun.*, 27, 910. (2006).
- [58] J.S. Qian, P.S. He, K.M.J. Nie, *Appl. Polym. Sci.*, 91, 1013. (2004).
- [59] L. Huang, R.B. Zhan, Y.F.J. Lu, *Reinf. Plast. Compos.*, 25, 1001. (2006).
- [60] T.H. Zhou, W.H. Ruan, J.L. Yang, M.Z. Rong, M.Q. Zhang, Z. Zhang, *Compos. Sci. Technol.*, 67, 2297. (2007).
- [61] J. Rottstegge, X. Zhang, Y. Zhou, D. Xu, C.C. Han, D.J. Wang, *Appl. Polym. Sci.*, 103, 218. (2007).
- [62] M.Q. Zhang, M.Z. Rong, H.B. Zhang, K. Friedrich, *Polym. Eng. Sci.*, 43, 490. (2003).
- [63] C.S. Reddy, C.K. Das, *Compos. Interfaces*, 11, 687. (2005).
- [64] Y.Q. Huang, S.L. Jiang, L.B. Wu, Y.Q. Hua, *Polym. Test.*, 23, 9. (2004).
- [65] Sin Vila, s. (2013).

-
- [66] E. Kontou, M. Niaounakis, *Polymer*, 47, 1267. (2006).
- [67] M. Roy, J.K. Nelson, R.K. MacCrone, L.S. Schadler, C.W. Reed, R. Keefe, W. Zenger, *IEEE Trans. Dielectr. Electr. Insul.*, 12, 629. (2005).
- [68] X.W. Gao, G.J. Hu, Z.Z. Qian, Y.F. Ding, S.M. Zhang, D.J. Wang, M.S. Yang, *Polymer*, 48, 7309. (2007).
- [69] M. Tanahashi, M. Hirose, J.C. Lee, K. Takeda, *Polym. Adv. Technol.*, 17, 981. (2006).
- [70] E. Kontou, G.J. Anthoulis, *Appl. Polym. Sci.*, 105, 1723. (2007).
- [71] F. Yang, G.L. Nelson, *Polym. Adv. Technol.*, 17, 320. (2006).
- [72] N. Katsikis, F. Zahradnik, A. Helmschrott, H. Münnstedt, A. Vital, *Polym. Degrad. Stab.*, 92, 1966. (2007).
- [73] A. Nodera, T.J. Kanai, *Appl. Polym. Sci.*, 101, 3862. (2006).
- [74] S.C. Chung, W.G. Hahm, S.S. Im, S. G. Oh, *Macromol. Res.*, 10, 221. (2002).
- [75] D. Bikiaris, V. Karavelidis, G. Karayannidis, *Macromol. Rapid Commun.*, 27, 1199. (2006).
- [76] L.V. Todorov, J.C. Viana, *Appl. Polym. Sci.*, 106, 1659. (2007).
- [77] M. García, G. van Vliet, M.G.J. ten Cate, F. Chávez, B. Norder, B. Kooi, W.E. van Zyl, H. Verweij, D.H.A. Blank, *Polym. Adv. Technol.*, 15, 164. (2004).
- [78] M.M. Hasan, Y.X. Zhou, H. Mahfuz, S. Jeelani, *Mater. Sci. Eng., A*, 429, 181. (2006).
- [79] H. Mahfuz, M.M. Hasan, V.K. Rangari, S. Jeelani, *Macromol. Mater. Eng.*, 292, 437. (2007).
- [80] R. Misra, B.X. Fu, A. Plagge, S.E. Morgan, *J. Polym. Sci., Part B: Poly. Phys.*, 47, 1088-1102. (2009).
- [81] H. Zhang, Z. Zhang, J.L. Yang, K. Friedrich, *Polymer*, 47, 679. (2006).
- [82] P. Cassagnau, *Polymer*, 44, 2455. (2003).
- [83] P. Cassagnau, F. Mélis, *Polymer*, 44, 6607. (2003).
- [84] M.W. Lee, X. Hu, C.Y. Yue, L. Li, K.C. Tam, K.J. Nakayama, *Appl. Polym. Sci.*, 86, 2070. (2002).
- [85] L.C. Wu, P. Chen, J. Zhang, J.S. He, *Polymer*, 47, 448. (2006).

-
- [86] Y. Zhao, D.A. Schiraldi, *Polymer* 46, 11640–11647. (2005).
- [87] S.C. Jana, S. Jain, *Polymer*, 42, 6897. (2001).
- [88] B. Chen, *Brit. Cer. Trans.*, 103, 6, 241-249(9). (2004).
- [89] S. Li, G.P. Simon, J.G. Matisons, *Polym. Eng. & Sci.*, 50(5), 991-999. (2010).
- [90] L.S. Schadler, *Nanocomposite Science and Technology; Wiley-VCH: Weinheim, Germany, Chapter 2*. (2003).
- [91] M.Q. Zhang, M. Z. Rong, K. Friedrich, *Handbook of Organic-Inorganic Hybrid Materials and Nanocomposites; Nalwa, H. S., Ed.; American Scientific Publishers: Stevenson Ranch, CA, Vol 2, pp 113-150*. (2003).
- [92] W. E. van Zyl, M. García, B.A.G. Schrauwen, B. J. Kooi, J. M. De Hosson, H. Verweij, *Macromol. Mater. Eng.*, 287, 106-110. (2002).
- [93] Zhang, Q.; Archer, L. A. *Langmuir*, 18, 10435. (b) Zhang,. (2002).
- [94] Y. Feng, Y. Jia, S. Guang, H. Xu, *J. App. Pol. Sci.*, 115(4):2212-2220. (2009).
- [95] M.E. Romero-Guzmán, A. Romo-Uribe, B. M. Zárate-Hernández, R. Cruz-Silva, *Rheol. Acta*, 48(6):641-652. (2012).
- [96] C. König, M. Van Duin, C. Pagnoulle and R. Jerome, *Prog. Polym. Sci.*, 23, 707–757. (1998).
- [97] G. H. Hu, Y. J. Sun and M. Lambla, *J. Appl. Polym. Sci.*, 61, 1039–1047. (1996).
- [98] A. Bhattacharya and B. N. Misra, *Prog. Polym. Sci.*, 29, 767–814. (2004).
- [99] G. Moad, *Prog. Polym. Sci.*, 24, 81–142. (1999).
- [100] C. Sanchez, G. J. Soler-Illia, F. Ribot, T. Lalot, C. R. Mayer and V. Cabuil, *Chem. Mater.*, 13, 3061–3083. (2001).
- [101] S. H. P. Bettini and J. A. M. Agnelli, *J. Appl. Polym. Sci.*, 74, 247–255. (1999).
- [102] E. Passaglia, S. Coiai, M. Aglietto, G. Ruggeri, M. Rubertà, F. Ciardelli, *Macromol. Symp.*, 198, 147–159. (2003).
- [103] H. Huang and N. C. Liu, *J. Appl. Polym. Sci.*, 67, 1957–1963. (1998).
- [104] Z. Zhou, L.M. Cui, Y. Zhang, Y. Zhang, N. Yin, *Eur. Polym. J.*, 44, 3057-3066. (2008).

-
- [105] Z. Zhou, L.M. Cui, Y. Zhang, N.Yin, *J. Polym. Sci. Part B, Polym. Phys.*, 46, 1762-1772. (2008).
- [106] S. Coiai, E. Passaglia, M. Aglietto and F. Ciardelli, *Macromolecules*, 37, 8414–8423. (2004).
- [107] G. H. Hu, H. Li, L. F. Feng and L. A. Pessan, *J. Appl. Polym. Sci.*, 88, 1799–1807. (2003).
- [108] H. Fischer, *Chem. Rev.*, 101, 3581–3610. (2001).
- [109] H. G. Börner and K. Matyjaszewski, *Macromol. Symp.*, 177, 1–15. (2002).
- [110] Z. Zhou, Y. Zhang, Y. Zhang and N. Yin, *J. Polym. Sci., Part B: Polym. Phys.*, 46, 526–533. (2008).
- [111] J. H. Choi, C. H. Jung, D. K. Kim and R. Ganesan, *Nucl. Instrum. Methods Phys. Res., Sect. B*, 266, 203–206. (2008).
- [112] J. H. Choi, C. H. Jung, D. K. Kim, D. H. Suh, Y. C. Nho, P. H. Kang, R. Ganesan, *Radiat. Phys. Chem.*, 78, 517–520. (2009).
- [113] Y.L. Liu, H.C. Lee, *J Polym Sci Part A: Polym.Chem*, 44, 4632. (2006).
- [114] N. Amir, A. Levina, M.S. Silverstein, *J Polym Sci Part A: Polym Chem*, 45, 4264. (2007).
- [115] W.Xu, C. Chung, Y. Kwon, *Polymer*, 48, 6286-6292. (2007).
- [116] C.M. Leu, Y.T. Chang; K.H. Wei, *Chem Mater*, 15, 3721-3727. (2003).
- [117] S.T. Iacono, S.M. Budy, J.M. Mabry, D.W. Smith, Jr. *Macromolecules*, 40, 9517-9522. (2007).
- [118] E. Thostenson, C. Li, T. Chou, T., *J. Comp. Sci. & Techn.*, 65, 491–516. . (2005).
- [119] K. Pielichowski, J. Njuguna, B. Janowski, J. Pielichowski, *J. Adv. Polym. Sci.* 201, 225–296. (2006).
- [120] J.K. Kim, K.H. Yoon, D.S. Bang. Y.B. Park, H.U. Kim, Y.H. Bang, *J. Appl. Pol. Sci.*, 107, 272–279. (2008).
- [121] O. Monticelli, E. Zunino, F. Carniato, E. Boccaleri, L. Marchese, A. Chincarini, *Polym. Adv. Technol.*, 21, 848–853. (2010).
- [122] I. Blanco, F. Agatino Bottino, *Polym. Compos.*, 34, 2, 225-232. (2013).

-
- [123] I. Blanco, L. Abate, M. L. Antonelli, F.A. Bottino¹, P. Bottino, *eXP. Pol. Let.*, 6, 12, 997–1006. (2012).
- [124] F. Wu, T. Xie, G. Yang, *J. Pol. Sci. Part B: Pol. Phys.*, 48, 16, 1853–1859. (2010).
- [125] K.J. Kim, S. Ramasundaram, J.S. Lee, *Polym. Comp.*, 29, 8, 894-901. (2008).
- [126] S. P. Ramasundaram, K. J. Kim, *Macromol. Symp.*, 249, 1, 295–302. (2007).
- [127] A. Ullah, J. Alongi, S. Russo, *Pol. Bulletin*, 67, 7, 1169-1183. (2011).
- [128] L. Zheng, R.J. Farris, E.B. Coughlin, *J. Polym. Sci.: Part A: Poly. Chem.*, 39, 2920–2928. (2001).
- [129] L. Zheng, R.J. Farris, E.B. Coughlin, *J. Polym. Sci.: Part A: Poly. Chem.*, 40, 885–891. (2002).
- [130] Y.L. Liu, M.C. Tseng, M.H. Fangchiang, *J. Polym. Sci.: Part A: Polym. Chem.*, 46, 5157–5166. (2008).
- [131] H. Zou, S. Wu, J. Shen, *Chem. Rev.*, 108, 3893-3957. (2008).
- [132] Y.G. Zhu, Z.Q. Li, D. Zhang, T.J. Tanimoto, *Polym. Sci., Part B: Polym. Phys.* 44, 1161. (2006).
- [133] P.D. Castrillo, D. Olmos, D.R. Amador, J.J. González-Benito, *Colloid Interface Sci.*, 308, 318. (2007).
- [134] L.S. Schadler, K.O. Laul, R.W. Smith, E.J. Petrovicova, *Therm. Spray Technol.*, 6, 475. (1997).
- [135] C.A. Wilkie, M.A. McKinney, '*Plastics Flammability Handbook*', Ed. Jürgen Troitzsch, Hanser, Munich, 58-76. (2004).
- [136] K. Pielichowski, J. Njuguna, '*Thermal degradation of polymeric materials*', 1st ed, Rapra Techn.Ltd, Shropshire, UK. (2005).
- [137] M. Demjanenko, K. Dusek, *Macromol.*, 13, 3, 571–579. (1980).
- [138] L.A. Pinheiroa, M.A. Chinelattob, S.V. Canevarolo, *Polym. Degr. & Stab.*, 86, 3, 445–453. (2004).
- [139] J.F. Rabek, *Comprehensive Chemical Kinetics*, 14, Elsevier, Amsterdam, p.425. (1975).

-
- [140] V. Kern, H. Cherdrón, *Makromol. Chem.*, 40, 101-117. (1960).
- [141] B. Fayolle, J. Verdu, M. Bastard, D. Piccoz, *J. Appl. Polym. Sci.*, 107, 1783–1792. (2008).
- [142] L.A. Dudina, L.V. Karmilova, E.N. Tyrapitsyna, N.S. Eenikolopyan, *Polymer Science*, 16, 2277. (1967).
- [143] G.E. Zaikov, Elsevier Applied Science Publishers, 82, 328-331. (1986).
- [144] S. Hasegawa, H. Takeshita, F. Yoshii, T. Sasaki, K. Makuuchi, S. Nishimoto, *Polymer*, 41, 111-120. . (2000).
- [145] V.M. Archodoulaki, S. Lüftl, S. Seidler, *Polym. Degr. & Stab.*, 86, 75-83. (2004).
- [146] *M. Orchin, R. S. Macomber, A. R. Pinhas, R. M. Wilson, The Vocabulary and Concepts of Organic Chemistry, New Jersey, John Willey & Sons.* (2005).
- [147] S. Korcek, J.B.H. Chenier, J. A. Howard, K.U. Ingold, *J. Can. Chem.*, 50, 2285-2297. (1950).
- [148] S. Lüftl, V.M. Archodoulaki, S. Seidler, *Polym. Degr. & Stab.*, 91, 464-471. (2006).
- [149] V. Guryanova, B. Kovarskaya, M. Neiman, L. Postnikov, V. Shlyapintokh, G. Kuznetsova, *Polym. Sci.* 7, 2385-2366. (1965).
- [150] V.A. Sukhov, L.A. Nikitina, A.A. Baturina, A.F. Lukonikov, N.S. Yanikolopyan, *Polym. Sci.*, 11, 909-918. (1969).
- [151] W. Kern, *Chemiker-Ztg/Chem Apparatur*, 91, 8, 255-262. (1967).
- [152] H. Nagahara, K. Kagawa, K. Hamanaka, K. Yoshida, T. Iwaisako, J. Masamoto, *Ind. Eng. Chem. Res.*, 39 (7), 2275–2280. (2000).
- [153] *J.A. Brydson, "Plastics Materials", 6th ed, Oxford.* (1995). Butterworth-Heinemann.
- [154] M. Mucha, *Coll. Polym. Sci.*, 262, 841-50. (1984).
- [155] Y. Duan, H. Li, L. Ye, X. Liu, *Appl. Polym. Sci.*, 99, 3085-3092. (2006).
- [156] N.L. Yang, V. Patel, *Abstr. Papers American Chem. Soc.*, 188, 149-154. (1984).
- [157] H. Hama, K. Tashiro, *Polymer*, 44, 6973-6988. (2003).
- [158] H. Cottin, M.C. Gazeau, J.F. Doussin, F. Raulin, *J. Photoch. & Photobio., A: Chem.*, 135, 53-64. (2000).

-
- [159] J.A. Howard, *Rubber Chem. Technol.*, 47, 976-981. (1974).
- [160] M. Suzuki, C.A. Wilkie, *Polymer Degradation and Stability*, 47, 2, 223-228 and 217-221. (1995).
- [161] M. Day, J.D. Cooney, C. Touchette-Barrette, S.E. Sheehan, *J. Anal. & Appl. Pyrol.*, 52, 2, 199-224. (1999).
- [162] H. Bair, *"Thermal Characterization of Polymeric Materials"*, 2nd Edn., Ed.E.A. Turi, Academic Press, San Diego, p.2276. (1997).
- [163] M.H. Yang, *Polymer Testing*, 19, 1, 105-110. (2000).
- [164] T.J. Xue, M.A. McKinney, C. Wilkie, *Polym. Degr. & Stab.*, 58, 1-2, 193-202. (1997).
- [165] B. D. Gesner, *J. Appl. Polym. Sci.*, 9, 3701. (1965).
- [166] A. Casale, O. Salvatore and G. Pizzigoni, *Polym. Eng. Sci.*, 15, 286. (1975).
- [167] N. Grassie, H.W. Melville, *Faraday Society Discussions*, 2, 378. (1947).
- [168] N.S. Allen, M. Edge, M. Rodriguez, C.M. Liauw, *Polym. Degr. & Stab.*, 71, 1-14. (2001).
- [169] D. Schulze, S. Trinkle, R. Mülhaupt, C. Friedrich, Springer Verlag, 42, 251-258. (2003).
- [170] S.R. Salman, N.D. Al-Shama'a, M.M.F. Al-Jarrah, *Polym. Plast. Technol. Eng.*, 31 (3-4), 213-219. (1992).
- [171] D.M. Kulich, S.K. Gaggar, *Polym. Durability*, 249 (31), 483-501. (1996).
- [172] J.K. Kim, C.K. Kang, *Polym. Plast. Technol. Eng.*, 34, 875-890. (1995).
- [173] B.E. Tiganis, L.S. Burn, P. Davis, A.J. Hill, *Polym. Degrad. Stab.*, 76, 425-434. (2002).
- [174] J.D. Peterson, S. Vyazovkin, C.A. Wight, *Macromol. Chem. Phys.*, 202, 6. (2002).
- [175] M.C. Bruns, J.H. Koo, O.A. Ezekoye, *Polym. Degr. & Stab.*, 94, 1013-1022. (2009).
- [176] F. Carrasco, J. Gámez-Pérez, O.O. Santana, M.Ll. MasPOCH, *Chem. Eng. J.*, 178, 451-460. (2011).
- [177] H.W. Milliman, M.S. Soto, A. Arostegui, D.A. Schiraldi, *Jour. Polym. Science*, 125, 2914-2919. (2012).
- [178] K. Magniez, B.L. Fox, M.G. Looney, *Polym. Eng. & Sci.*, 52, 7, 1402-1412. (2012).

-
- [179] J.W. Huang, W.C. Lu, M.Y. Yeh, C.H. Lin, I.s. Tsai, *Polym. Eng. & Sci.*, 48, 8, 1550-1995. (2008).
- [180] J.H. Chen, Y.D. Chiou, *J. Polym. Sci. Part B: Polym Phys*, 44, 2122–2134. (2006).
- [181] A.M.A.M. Altaweel, C. Ranganathaiah, B. Kothandaraman, *J. Adhes.*, 85, 200–215. (2009).
- [182] T.C. Cheam, S. Krimm, *Chem. Phys. Lett.*, 107, 613-613. (1984).
- [183] P.C. Painter, G. J. Pehlert, Y. Hu, M. Coleman, *Macromol.*, 32, 2055-2057. (1999).
- [184] B. Yang, J. Li, J. Wang, H. Xu, S. Guang, C. Li, *Jour. Appl. Polym. Sci.*, 111, 2963-2969. (2008).
- [185] H. Ma, Z. Xu, L. Tong, A. Gu, Z. Fang, *Polym. Degr. & Stability*, 91, 2951-2959. (2006).
- [186] T. Yuzawaa, C. Watanabea, N. Nemotob, H. Ohtanic, *Polym. Degr. & Stab.*, 98, 2, 671–676. (2013).
- [187] C. Watanabe et al.; *Polymer Degradation and Stability*, 94, 1467-1472. (2009).
- [188] T. Yuzawa; C. Watanabe; H. Ohtani, *Kobunshi Ronbunshu*, 69, 7, 334-345. (2012).
- [189] M.A. Rauf, I.C. McNeill, *Polym. Degr. & Stab.*, 40, 2, 263–266. (1993).
- [190] G. Adamusa, M. Kowalczuka, Z. Jedliński, A. Ballistrerib, T. Schererc, R.W. Lenz, *Polym. Degr. & Stab.*, 50, 3, 269–276. (1995).
- [191] I. C. McNeill, *J. Polym. Sci. Part A*, 4, 10, 2479–2485. (2003).
- [192] Xiaoyen. B. Huang, T. Dyakonov, Y. Cheng, L. Padron, T. Vickstrom, J. Kuhn, J. Hodkiewicz, W. Stevenson, T.K. William, *Appl. Spectr.*, 53, 11, 416A-450A and 1313-1482. (1999).
- [193] S.J. Jang, E.K. Yang, S.I. Jin, Y.D. Cho, E.K. Choe, C.R. Park, *Bull. Korean Chem. Soc.*, 33, 3, 833-838. (2012).
- [194] F. Samperi, C. Puglisi, R. Alicatk, G. Montaudo, *Polym. Degr. & Stab.*, 83, 3-10. (2004).
- [195] F. Samperi, C. Puglisi, R. Alicatk, G. Montaudo, *Polym. Degr. & Stab.*, 83, 11-17. (2004).
- [196] ISO 1133-1: *Plastics: Determination of the melt mass-flow rate (MFR) and the melt volume-flow rate (MVR) of thermoplastics.* (2011).

- [197] ASTM D1238 - 10: Standard Test Method for Melt Flow Rates of Thermoplastics by Extrusion Plastometer. (2010).
- [198] (1946). *D.W. Scott, J. Am. Chem. Soc., 68, 356.*
- [199] *M.G. Voronkov, V.I. Lavrent'yev, Top. Cun: Chem. 102, 199-236. 1982.*
- [200] J.L.Schwab, J.D. Lichtenhan, *Appl. Organometal. Chem., 12, 707-713. (1998).*
- [201] J. Kim, Ky. Lee, Ku. Lee, J. Bae, J. Yang, S. Hong, *Polym. Degr. & Stab., 79, 201–207. (2003).*
- [202] S. Wang, Y. Hu, L. Song, Z. Wang, Z. Chen, W. Fan, *Poly. Degr. & Stab., 77, 423–426. (2002).*
- [203] *Polyacetal (01/02S12), PERP Program – New Report Alert. (2002, October). Retrieved 05 16, 2013, from CHEMSYSTEMS:*
<http://www.chemsystems.com/reports/search/docs/abstracts/0102-S12-abs.pdf>
- [204] B. Forschler, C. Geiser, *Kunststoffe int., Carl Hanser Verlag, 10, 112-114. (2007).*
- [205] *J.D. Virosco, "Polyoxymethylene" PERP 2011S1, CHEMSYSTEMS, Nov.2011. PERP.*
- [206] M. E. Adams, R.E. Colborn, D.J. Buckley, M.E. Adams, D.J. Buckley, R.E. Colborn, "Acrylonitrile-butadiene-styrene Polymers", *Rapra techn., 6, 10. (1993).*
- [207] *"Acrylonitrile Butadiene Styrene (ABS) Market - Applications (Appliances, Electronics, Automotive, Consumer Goods & Construction), Global Industry Analysis, Size, Share, Growth And Forecast, 2012 - 2018", Transp.Mark.Resear. (2013). Retrieved 04 10, 2013, from*
<http://www.transparencymarketresearch.com/acrylonitrile-butadiene-styrene.html>
- [208] *PERP Program - ABS Resins. (2008). Retrieved 05 16, 2013, from CHEMSYSTEMS:*
http://www.chemsystems.com/about/cs/news/items/PERP%200607S8_ABS%20Resins.cfm
- [209] S. Ranganathan, W.E. Baker, K.E. Russell, R.A. Whitney, *J. Polyme. Sci.: Part A: Poly. Chem., 37, 3817–3825. (1999).*
- [210] R. Qi, J.L. Qian, C.X. Zhou, *J. Appl. Polym. Sci., 90, 1249-1254. (2003).*
- [211] L.A. Utracki, *Canad. J. Chem. Eng., 80, 6, 1008–1016. (2002).*
- [212] S.H. Choi, Y.C. Nho, *Radiat. Phys. Chem., 58, 157-168. (2000).*

-
- [213] E.S.A. Hegazy, H.A.A. El-Rehim, N.A. Khalifa, A.E.H. Ali, *Radiat. Phys. Chem.*, 55, 219-229. (1999).
- [214] W. Petasch, E. Raüchle, M. Walker, P. Elsner, *Surf. Coat. Technol.*, 74, 682-688. (1995).
- [215] E.A. Abdel-Razik, *J. Photochem. Photobiol. A*, 69, 121-130. (1992).
- [216] R. Qi, J.L. Qian, Z.F. Chen, X. Jin, C.X. Zhou, *J. Appl. Polym. Sci.*, 91, 2834-2839. (2004).
- [217] X.F. Zhang, Y.S. Chen, Y. Zhang, Z.L. Peng, Y.X. Zhang, W. Zhou, *J. Appl. Polym. Sci.*, 81, 831-836. (2001).
- [218] F. Elmaghor, L.Y. Zhang, R. Fan, H.Q. Li, *Polymer*, 45, 6719-6724. (2004).
- [219] S.C. Tjong, Y.Z. Meng, *Eur. Polym. J.*, 36, 123-129. (2000).
- [220] S. Balakrishnan, NR. Neelakantan, *Polym. Int.*, 45, 347-352. (1998).
- [221] S. Balakrishnan, NR. Neelakantan, D.N. Saheb, J.P. Jog, *Polymer.*, 39, 23, 5765-5771. (1998).
- [222] P. G. Harrison, *J. Organometall. Chem.*, 542, 2, 141-183. (1997).
- [223] POSS User's guide, v.2.06, <http://www.hybridplastics.com/docs/user-v2.06.pdf> (visited 25, March, 2013). (n.d.).
- [224] C.L. DeArmitt, *Polyhedral Oligomeric Silsesquioxance Handbook*, 1.0. (2010).
- [225] G. Lagaly, A. C. (1999).
- [226] J. Jancar, J. D.-3. (2010).
- [227] E.T. Kopesky, T.S. Haddad, R.E. Cohen, G.H. McKinley, *Macromol.*, 37, 8992-9004. (2004).
- [228] S. Iyer, D.A. Schiraldi, *Macromol.*, 40, 4942-4952. (S. Iyer, D.A. Schiraldi, *Macromol.*, 40, 4942, 2007).
- [229] N. Vila, M. Sanchez-Soto, S. Illescas, A. Gordillo, *Polym.-Plastics Techn. and Eng.*, 48, 470-477. (2009).
- [230] O. Monticelli, A. Fina, A. Ullah, P. Waghmare, *Macromol.*, 42, 6614-6623. (2009).
- [231] Y.J. Lee, JM. Huang, S.W. Kuo, J.S. Lu, F.C. Chang, *Polymer* 46, 173-181. (2005).
- [232] R. Silva, c. Salles, R. Mauler. R. Oliveira, *Polym Int*; 59, 1221-1225. (2010).

-
- [233] J. Ahmend, S.K. Varshney, R. Auras, S.W. Hwang, *Jour. Food Science*, 75-8, 97-108 . (2010).
- [234] S. Soong, R.E. Cohen, M.C. Boyce, *Polymer*, 48, 1410-1417. (2007).
- [235] I.-J Chin, S.-K. Lim, E.-P. Hong, Y.H. Song, H.J. Choi, *J. Mater. Sci.*, 45, 5984-5987. (2010).
- [236] H.W. Milliman, D. Boris, D.A. Schiraldi, *Macromol.*, 45, 1931-1936. (2012).
- [237] N.T. Dintcheva, E. Morici, R. Arrigo, F.P. La Mantia, V. Malatesta, J.J. Schwab, *eXpr. Polym. Lett.*, 6, 561-571. (2012).
- [238] D.W. van Krevelen, K. N. (2009). *Properties of Polymers: Their Correlation with Chemical Structure; their Numerical Estimation and Prediction from Additive Group Contributions*. Oxford: Elsevier.
- [239] Hansen, C. M. (1999). *Hansen Solubility Parameters: A User's Handbook*. Hoersholm: CRC Press.
- [240] Hildebrand, J. H. *The Solubility of Non-Electrolytes; New York: Reinhold (1936)*.
- [241] J. Hildebrand, R. L. Scott, *The Solubility of Nonelectrolytes, 3rd Ed., Reinhold, New York, 1950*.
- [242] J. Hildebrand, R.L. Scott, *Regular Solutions, Prentice-Hall Inc., Englewood Cliffs, NJ, 1962*.
- [243] Flory, P. (1953). *Principles of Polymer Chemistry*. Cornell University Press.
- [244] Hansen, C. M. *J Paint Technol*, 39, 511-514. (1967).
- [245] P.J. Hoftyzer, D. v. (1976). *Properties of Polymers, 2nd Ed, ch.7, 152-155* .
- [246] (1985). K.L. Hoy, *The Hoy tables of solubilty parameters, Union Carbide Corp.*
- [247] L. Liu, T. G.-6. (2007).
- [248] R. Misra, P. D. (2008). R. Misra, PhD Dissertation UMI No. 3346544, University of Southern Mississippi, Jackson, USA.
- [249] J.H. Flynn, "Thermal Analysis", *Encyclopedia of Polymer Science and Engineering, Suppl. Vol., John Wiley, 690-723*. (1989).

-
- [250] P.K. Roy, P. Sureka, C. Rajagopal, V. Choudhary, *Expr. Polym. Lett.*, 1, 4, 208-216. (2007).
- [251] H. Wang, J. Yang, S. Long, X. Wang, Z. Yang, G. Li, *Polym. Degr. & Stab.*, 83, 229-235. (2004).
- [252] J. Shi, B. Jing, X. Zou, H. Luo, W. Dai, *J. Mater. Sci.*, 44, 1251-1557. (2009).
- [253] R. Ebrahimi-Kahrizsangi, M.H. Abbasi, *Trans.Nonferrous Met.Soc.China*, 18, 217-221. (2007).
- [254] Y.Tonbul, K. Yurdakoç, *Turk J Chem*, 25, 333-339. (2001).
- [255] C. Komalan, K.E. George, K.T. Varughese, V.S. Mathew, S. Thomas, *Polym.Degr.&Stability*, 93, 2104-2112. (2008).
- [256] C.L. Chiang, F.Y. Wang, C.C.M. Ma, H.R. Chang, *Polym.Degr.&Stability*, 77, 273-278. (2002).
- [257] J. Wang, X.f. Cai, *J. Therm. Anal. Calorim.*, 107, 725–732. (2012).
- [258] S.S. Hajimirsadeghi, M.B. Teimouri, M. Rahimi-Nasrabadi, S. Dehghanpour, *J. Therm. Anal. Calorim.*, 98, 463–468. (2009).
- [259] H.E. Kissinger, *Anal. Chem.*, 29(11), 1702-1706. (1957).
- [260] G. Camino, S.M. Lomakin, M. Lazari, *Polymer*, 42, 2395-2402. (2000).
- [261] S. Chattopadhyay, G. Madras, *Polym. Degr. & Stab.*, 78, 519-524. (2002).
- [262] G. Sivalingam, G. Madras, *Poly. Degr. & Stab.*, 84, 393-398. (2004).
- [263] H. Chen, N. Liu, W. Fan, *Polym. Degr. & Stab.*, 91, 1726-1730. (2006).
- [264] F. Carrasco, *Thermochim. Acta*, 213, 114. (1993).
- [265] F. Carrasco, P. Pagès, *J. Appl. Polym. Sci.*, 61, 187-197. (1996).
- [266] J.E. House, *"Principles of Chemical Kinetics"*, Burlington, Academic Press (Elsevier), pg.275. (2007).
- [267] A.W. Coats, J.P. Redfern, *Nature*, 201(4914), 68-69. (1964).
- [268] J. Shi, B. Jing, X. Zou, H. Luo, W. Dai, *Jour.Mat.Sci.*, 44, 1251-1257. (2009).
- [269] N. Mehta, A. Kumar, *Journ.Optoelectr.Adv.Mat.*, 7(3), 1473-1478. (2005).

-
- [270] R.B. Fox, T.R. Price, *Adv. Chem. Ser.*, 96, 226-242. (1989).
- [271] S. Li, G. P. Simon, J. G. Matison, *Polym. Eng. Sci.*, 50, 991. (2010).
- [272] W. B. Xu, P. S. He, *J. Appl. Polym. Sci.*, 80, 304. (2001).
- [273] B.X. Fu, C. Yang, R.H. Somani, S.X. Zong, B.S. Hsiao, S. Phillips, R. Blanski, D. Ruth, *J Polym Sci Part B: Polym Phys*, 39, 2727–2739. (2001).
- [274] J.H. Chen, B.X. Yao, W.B. Su, Y.B. Yang, *Polymer*, 48, 1756–1769. (2007).
- [275] R. Erro, M. Gaztelumendi, J. Nazabal, *J. Polym. Sci. Part B: Polym. Phys.*, 34, 1055. (1996).
- [276] A. Fina, D. Tabuani, A. Frache, G. Camino, *Polymer*, 46, 7855. (2005).
- [277] M. Joshi, B.S. Butola, G. Simon, N. Kukaleva, *Macromol.*, 39, 1839-1849 . (2006).
- [278] M. Joshi, B. S. Butola, *Polymer*, 45, 4953-4968. (2004).
- [279] V. Pistor, D. Conto, F.G. Ornaghi, A.J. Zattera, *J. Nanomaterials*, 2012-283031. (2012).
- [280] B. Ranby, J. R. (1996). *Photodegradation, Photo-oxidation and Photostabilization of Polymers*. 236-238. New York: John Willey & Sons.
- [281] Y. Saito, S. Kobayashi, K. Nishida, *Jap. Soc. Calor. & Therm. Anal., Netsu Sokutei*, 25, 3, 56-66. (1998).
- [282] M. Rätzsch, G. Eckhardt, *Plaste und Kautschuk*, 20, 6, 424-432. (1973).
- [283] N. Grassie, R.S. Roche, *Makromol. Chem.*, 112, 2581, 16-33. (1968).
- [284] J.E. Pickett, *Polym. Degr. & Stab.*, 85, 681-687. (2004).
- [285] M. Gröning, *KTH Fibre and Polymer Technology*, 19. (2004).
- [286] Y. Feng, Y. Jia, S. Guang, H. Xu, *Jour. Appl. Polym. Sci.*, 115, 2212-2220. (2009).
- [287] J. Wu, T.S. Haddad, P.T. Mather, *Macromol.*, 42, 1142-1152. (2009).
- [288] D.M. Chang, *Polym. Eng. & Sci.*, 22, 6, 376-381. (1982).

RELATED BIBLIOGRAPHY

- [289] L. Zheng, S. Hong, G. Cardoen, E. Burgaz, S. P. Gido, E. B. Coughlin, *Macromolecules*, 37, 8606. (2004).
- [290] L.L. Bergesson_Nanotech.Law&Business_Winter 2007_473-483. (2007).
- [291] B.N. Manikantan, D.B. Frank, *Polymer Preprints*, 46(1), 367-368. (2005).
- [292] B. Fayolle, J. Verdu, D. Piccoz, A. Dahoun, J.M. Hiver, C. G'sell, *J. Appl. Polym. Sci.*, 111, 469–475. (2009).
- [293] V.V. Rajan, R. Wäber, J. Wieser, *J. Appl. Polym. Sci.*, 115, 2394–2401. (2010).
- [294] V.M. Archodoulaki, S. Lüftl, S. Seidler, *J. Appl. Polym. Sci.*, 105, 3679–3688. (2007).
- [295] R. Gächter, H. M. (1993). *Plastics Additives Handbook*, 134-145. Munich: Hanser .
- [296] R.S. Berns, *Principles of Colour Technology*, New York, Bilmeyer and Saltzman's, 67-72. (1991).
- [297] W. Greiner, L. N. (1995). *Thermodynamics and Statistical Mechanics*. p. 101. Springer-Verlag.
- [298] ISO ISO/TS 27687:2008; Nanotechnologies - Terminology and definitions for nano objects - nanoparticle, nanofibre and nanoplate; ICS: 07.030; 01.040.07. (2008).
- [299] ASTM E2456 - 06(2012) Standard Terminology Relating to Nanotechnology; DOI: 10.1520/E2456-06R12; ICS: 01.040.71; 71.100.01. (2012).
- [300] M. Lahelina, M. Annalaa, A. Nykänenb, J. Ruokolainenb, J. Seppälä, *Comp. Sci. & Tech.*, 71, 6, 900–907. (2011).
- [301] N. Heidarzadeh, M. Rafizadeh, F. Afshar Taromi, H. Bouhendi, *High Perf. Pol.*, 24, 7, 589-602. (2012).
- [302] X.L. Hu, Y.J. Li, Y.M. Dong, *Adv. Mat. Res.*, 266, 161-166. (2011).
- [303] EPA, *Science Policy Council, Nanotech. White Paper, December 2, 2005*.
- [304] D.J. Burgess, E. Duffy, F. Etzler, A.J. Hickey, *The AAPS Journal*, 6, 3, Article 20 . (2004).
- [305] C.S. Reddy, C.K. Das, *J. Appl. Polym. Sci.*, 102, 2117. (2007).
- [306] E. Markivic, K. Constantopolous, J.G. Matisons, *Adv. Silicon Sci*, vol.3, 1-46. (2011).

- [307] J. Hardy, 'Novel materials based on functionalised silsesquioxanes, PhD Thesis, The Open University, UK. (2001).
- [308] (2013, 3 27). Retrieved from http://www.pentron.com/index.php/products/product_detail/nano_bond_nano_particulate_reinforced_adhesive.
- [309] <http://www.hybridplastics.com/docs/conver1.htm>. (2013, 3 28).
- [310] <http://www.freepatentsonline.com/y2012/0128746.html>. (2013, 3 28).
- [311] J. Rouquerol, *Therm. Acta*, 144, 2, 209–224. (1989).
- [312] A.C. Naranjo, T.A. Osswald, J. Sierra, '*PLASTICS testing and characterization: industrial applications*', Hanser, Munich. (2008).
- [313] P. Mariani, G. Carianni, A. Monteverdi, 'New Rheological Method to Evaluate Thermo-Oxidative Degradation of a Coating Grade Polyethylene', European PLC Conference Proceedings. (2001).
- [314] H. Pasch, W. Schrepp, '*Maldi-Tof Mass Spectrometry of Synthetic Polymers*', Springer Verlag, Heidelberg. (2003).
- [315] J. Scheirs, '*Compositional and Failure Analysis of Polymers: A Practical Approach*', John Wiley & Sons, Chichester. (2000).
- [316] (1997). M. P. Sepe, *Thermal Analysis of Polymers, Rapra Rev. Rep.*, 8, 11.
- [317] G. Höhne, W.F. Hemminger, H.J. Flammersheim, '*Differential Scanning Calorimetry*', 2nd Ed., Springer-Verlag, Berlin . (2003).
- [318] (2010). SCENIHR: *Scientific Basis for the Definition of the Term "nanomaterial"*; ISBN 978-92-79-12757-1; DOI:10.2772/39703.
- [319] (2008). "*Maleic Anhydride: A global strategic business report*", Glob. Busin. Analy Inc., MCP-2095, San Jose (USA).
- [320] Huntsman. (n.d.). Retrieved 04 17, 2013, from http://www.huntsman.com/performance_products/a/Products/Maleic%20anhydride

-
- [321] S.N. Magonov, *Atomic Force Microscopy in Analysis of Polymers, Encyclopedia of Analytical Chemistry, John Wiley and Sons.* (2006).
- [322] H.G.M. Edwards, A.F. Johnson, I.R. Lewis, *J. Raman Spectrosc.*, 24, 475–483. (1993).
- [323] V. Selvakumar, K. Palanikumar, K. Palanivelu, *J. Miner. & Mat. Charact. & Eng.*, 9, 8, 671-681. (2010).
- [324] M.I.B. Tavares, R.F. Nogueira, R.A.S. San Gil, N.M. Silva, *A. Magn. Reson.* 3, 1/2, 42-44. (2004).
- [325] Z. Penga, L.X. Konga, S.D. Lib, *Synth. Metals*, 152, 1–3, 25–28. (2005).
- [326] *Global ABS Industry - Growth Reliant on Chinese End Use Sectors.* (2011, October). Retrieved 05 16, 2013, from RESEARCHANDMARKETS:
http://www.chemsystems.com/about/cs/news/items/PERP%200607S8_ABS%20Resins.cfm
- [327] H. Wang, X. Tao, E. Newton, *Polym. Int.*, 53, 20-26. (2004).
- [328] J.G. Calbert et al., *"Formaldehyde and Other Aldehydes"*, National Academy Press, Washington D.C., p.107. (1981).
- [329] (1997). E.G. Shockey, A.G. Bolf, P.F. Jones, J.J. Schwab, K.P. Chaffee, *Air Force Research Laboratory (AFMC).*
- [330] J. Yanga, J. Gaoa, Y. Dua, X. Liua, *Polym.-Plas. Techn.&Eng.*, 52, 8. 2013.
- [331] J. Gao, Y. Du, C. Dong, *Polym. Comp.*, 31, 10, 1822–1827. 2010.
- [332] (2013). Y. Du¹, J. Gao, J. Yang, X. Liu, *J. Appl. Polym. Sci.*, 129, 1, 174–180.
- [333] (2006). S.Y. Soong, R. E. Cohen, M.C. Boyce, A.D. Mulliken, *Macromol.*, 39, 8, 2900–2908.

CHAPTER 8

ANNEX: PUBLISHED ARTICLES

8. ANNEX: PUBLISHED PAPERS

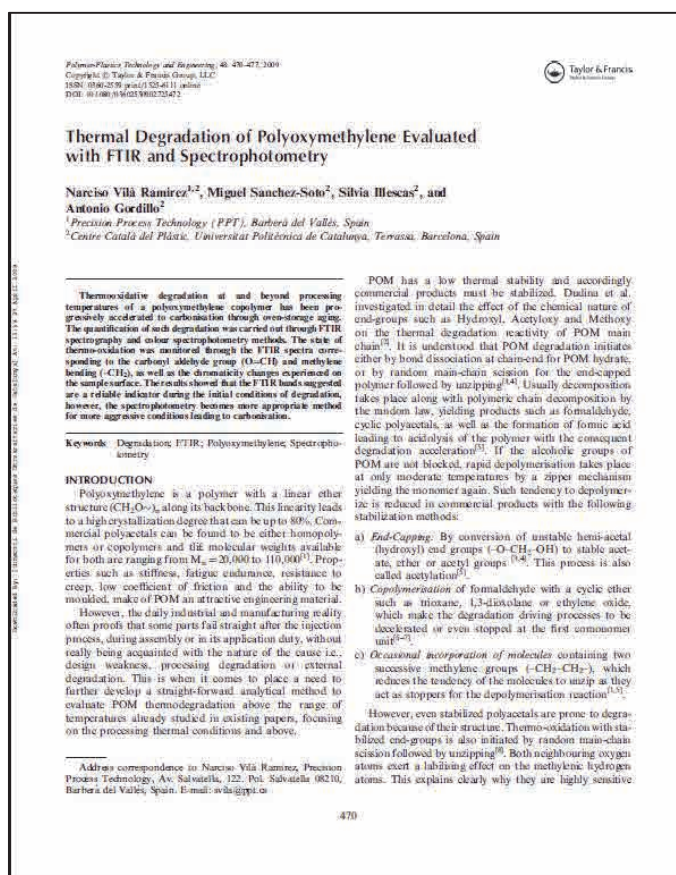
8.1. THERMAL DEGRADATION OF POLYOXYMEHTYLENE EVALUATED WITH FTIR AND SPECTROPHOTOMETRY



Taylor & Francis
Taylor & Francis Group

POLYMER-PLASTICS
TECHNOLOGY
AND
ENGINEERING

- PUBLICATION (indexed article):
 - Journal: Polymer-Plastics Technology and Engineering
 - Volume: 48
 - Pages: 470–477
 - Date: 1st April 2009
 - DOI: 10.1080/03602550902725472
- PUBLISHER: Taylor & Francis
- MAIN AUTHOR: Narciso Vila Ramirez
- CO-AUTHORS: Miguel Sanchez-Soto, Silvia Illescas and Antonio Gordillo
- LINK: <http://www.tandfonline.com/doi/abs/10.1080/03602550902725472>



8.2. ENHANCEMENT OF POM THERMOOXIDATION RESISTANCE THROUGH POSS NANOPARTICLES



- PUBLICATION (indexed article):
 - Journal: POLYMER COMPOSITES
 - Volume: 32, Issue 10
 - Pages: 1584–1592
 - Date: 12th September 2011
 - DOI: DOI 10.1002/pc.21191
- PUBLISHER: Society of Plastics Engineers
- MAIN AUTHOR: Narciso Vila Ramirez
- CO-AUTHORS: Miguel Sanchez-Soto, Silvia Illescas
- LINK: <http://onlinelibrary.wiley.com/doi/10.1002/pc.21191/abstract>

Enhancement of POM Thermooxidation Resistance Through POSS Nanoparticles

Narciso Vila Ramirez,^{1,2} Miguel Sanchez-Soto,² Silvia Illescas²
¹Precision Process Technology (PPT), Av. Salvatella, 122, Pol.Salvatella, 08210 Barberà del Vallès, Spain

²Centre Català del Plàstic, Universitat Politècnica de Catalunya, C/Colom 114, 08222 Terrassa, Barcelona, Spain

Thermooxidative degradation at and beyond processing temperatures has been carried out on polyoxymethylene (POM) enhanced with four different types of POSS, being Glycidyl, Glycidylethoxybutyl, Aminopropylisobutyl, and Poly(ethylene glycol). The quantification of such degradation was carried out through FTIR spectroscopy, color spectrophotometry, and thermogravimetric analysis methods. The results showed that the presence of POSS in the blend improves dramatically the thermal stability of the POM matrix. The best performance was found with Aminopropylisobutyl, whereby the onset of degradation temperature increased by more than 50°C. Said improvement is referred to the conditions where the nanocomposite developed only 2% of carbonyl yield and 8% of yellowing of the 100% deterioration suffered by the standard POM copolymer. POLYM. COMPOS., 0000-000, 2011. © 2011 Society of Plastics Engineers

INTRODUCTION

Polymetric nanocomposites are increasingly gaining interest in the materials engineering community due to their enhanced performance. A nanocomposite may be defined as a polymer that incorporates nanosized particles (that at least one of whose dimensions is in the nanometer range). These nanofillers have been found to improve the mechanical, chemical, electrical, and thermal properties of base polymer significantly at very low filler concentration compared with conventional macrocomposites. This has opened up possibilities for producing high-performance

lightweight composites without compromising other properties such as optical behavior or weight [1–3].

Particularly, Polyhedral Oligosiloxanes (POSS) are nanosized cage structures that are generally represented by $(RSiO)_n$ and can be easily incorporated into thermoplastics, or thermosetting polymers [3, 4]. These nanostructured skeletons use silicon atoms with covalent bonds to link to a broad range of organic groups providing different functionality, solubility, polarity, and reactivity depending on the group chosen. The bottom line is that the addition of POSS can provide notable improvements in thermal stability, oxidation resistance, viscosity, and lower flammability [5].

The bulk matrix analyzed in this article is Polyoxymethylene (POM), being a copolymer with a linear ether structure with oxyethylene units in the main chain.

Although POM is an attractive engineering material due to its properties of high stiffness, fatigue endurance, resistance to creep, and low friction coefficient, it has a low thermal resistance even in stabilized copolymers, which leads to quick degradation through random chain scission induced by hydroperoxides (POOH), as well as depolymerization from POOH decomposition [6–10].

With the above, hybrid POM/POSS nanocomposites become an encouraging match to overcome the described instability that POM has on its own.

Whereas there is plenty of literature on thermal degradation and oxidation of polyoxymethylene up to the melting temperature [6–8, 11–16], and a fair deal of attention is being paid currently on POSS nanocomposites [1–5], the degradation characterization of POM/POSS in particular demands thorough analysis and reporting. This article is focused on evaluating and quantifying the degradation development of polyoxymethylene enhanced with four different POSS matrix mixtures, being Glycidyl, Glycidylethoxybutyl, Aminopropylisobutyl, and Poly(ethylene glycol). The evaluation methods are FTIR Spectroscopy, Color Spectrophotometry and Thermogravimetric Analysis (TGA), which already proved to be effective in the


Correspondence to: N. Vila Ramirez, e-mail: nvila@pvt.com
 Contract grant sponsor: "Ministerio de Educación y Ciencia" of the Spanish Government (Financiado de la Delegación Técnica de Polímeros, contrato grant number: ENE-2009194), contrato grant sponsor: ENE-C program of the Universitat Politècnica de Catalunya
 DOI: 10.1002/pc.21191
 Published online in Wiley InterScience (www.interscience.wiley.com).
 © 2011 Society of Plastics Engineers

POLYMER COMPOSITES—2011

8.3. PLASTIC NANOCOMPOSITES FOR BETTER THERMAL RESISTANCE



- PUBLICATION (online article):
 - Journal: PLASTICS RESEARCH ONLINE
 - Pages: 1-3
 - Date: 2nd December 2011
 - DOI: DOI 10.1002/spepro.003966
- PUBLISHER: Society of Plastics Engineers
- MAIN AUTHOR: Narciso (Sin) Vilà Ramirez
- CO-AUTHORS: Miguel Sanchez-Soto and Silvia Illescas.
- LINK: <http://www.4spepro.org/view.php?source=003966-2011-12-1>



10.1002/spepro.003966

Plastic nanocomposites for better thermal resistance

See Vilà, Miguel Sanchez-Soto, and Silvia Illescas

Combining nanofiller with a polymeric matrix raises the degradation temperature by up to 51°C and it reduces yellowing by 50%.

Polymeric nanotechnology is gaining interest in the materials engineering community because it can enhance plastics' performance. Polyoxymethylene (POM) is a plastic that is widely used in technical applications requiring dimensional stability and a very low coefficient of friction. However, its thermal stability is low, compared to other engineering polymers, and this can be a disadvantage.

Polyhedral oligomeric silsesquioxane (POSS) nanofillers have become very popular fillers in polymer nanotechnology for the notable improvements they provide to thermal stability, oxidation resistance, viscosity, and lower flammability.¹ They are often used as an inexpensive incorporation method into both thermoplastic and thermosetting polymers.²⁻⁴ The key attributes defining POSS molecules are nanosized cage structures based on a silica core and the ability to tailor a variety of molecular 3D symmetries, orientations, and functional groups. We worked to enhance POM's thermal stability by creating new nanocomposites (formulas using POSS).⁵ We monitored their degradation using conventional chemical and physical methods and also by measuring their color to see how much they yellow.

We incorporated four different POSS nanofillers into the POM matrix. These were glycidyl, glycidyl(isobutyl), amino(propyl)isobutyl, and poly(ethylene glycol), and we named the composites G1POSS, G2POSS, AminoPOSS, and PEGPOSS, respectively. We prepared the composites by conventional melt blending with a twin-screw co-rotating extruder mixer. To degrade them, we subjected the four POM nanocomposites and the standard POM to thermal oxidation at different temperatures from 200^o to 304^oC in steps of 20^oC and periods of time from 0 to 75 min in steps of 15 min.

We tracked the degradation of the POM composites with attenuated total reflectance Fourier transform IR spectroscopy (ATR-FTIR), watching changes in the absorbance of carbonyl and methylene groups (see Figure 1). This showed the formation of end groups generated during the thermo-oxidative process by bond dissociation and β -scission of $-(\text{O}-\text{C})-$ in the main chain of the polymer.⁶

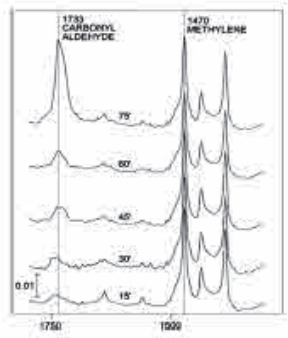


Figure 1. ATR-FTIR spectra of a progressively degrading POM at 240°C (from 15 min to 75 min (75) with carbonyl group development).

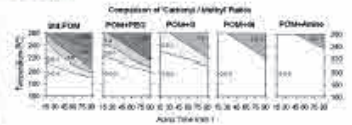


Figure 2. ATR-FTIR spectra of carbonyl/methylene ratio versus degradation conditions at terms of glycol bands. Std. POM: standard polyoxymethylene; PEG: Poly(ethylene glycol); G: Glycidyl; GI: Glycidyl(isobutyl); Amino: Amino(propyl)isobutyl.

The analysis of the carbonyl/methylene ratio (glycol bands in Figure 2) shows that all of the nanocomposites exhibited an important

Continued on next page

8.4. EFFECTS OF POSS NANOPARTICLES ON ABS-G-MA THERMOXIDATION RESISTANCE



Polymer COMPOSITES

- PUBLICATION (indexed article):
 - Journal: POLYMER COMPOSITES
 - Volume: 33, Issue 10
 - Pages: 1707–1718
 - Date: 9th September 2012
 - DOI: DOI 10.1002/pc.22304
- PUBLISHER: Society of Plastics Engineers
- MAIN AUTHOR: Narciso Vila Ramirez
- CO-AUTHORS: Miguel Sanchez-Soto
- LINK: <http://onlinelibrary.wiley.com/doi/10.1002/pc.22304/abstract>




8.5. THERMAL STABILIZATION ABILITY OF POLYHEDRAL OLIGOMERIC SILSESQUIOXANE NANOFILLERS

NANOFILLERS



- PUBLICATION (online article):
 - Journal: PLASTICS RESEARCH ONLINE
 - Pages: 1-3
 - Date: 17th December 2012
 - DOI: DOI 10.2417/spepro.004523
- PUBLISHER: Society of Plastics Engineers
- MAIN AUTHOR: Narciso (Sin) Vilà Ramirez
- CO-AUTHORS: Miguel Sanchez-Soto.
- LINK: www.4spepro.org/view.php?source=004523-2012-11-27



Society of Plastics Engineers

PLASTICS RESEARCH ONLINE

10.2417/spepro.004523

Thermal stabilization ability of polyhedral oligomeric silsesquioxane nanofillers

Sin Vilà and Miguel Sanchez-Soto

The polyhedral oligomeric silsesquioxane nanofillers examined in this study provided little or no improvement to the thermal properties of melt-blended acrylonitrile butadiene styrene polymer composites.

The recent developments in thermoplastic nanotechnology using nanofillers have opened up the possibilities of enhancing the mechanical, chemical, and thermal properties of polymers.¹⁻⁷ Within the broad range of nanoparticles available, polyhedral oligomeric silsesquioxane (POSS) have become popular because of their organic/inorganic nature and easy incorporation into the polymer matrix.^{2,3} Compared with copolymerization methods, the use of melt-blending techniques to produce thermoplastic nanocomposites is an attractive approach because it is high yielding, simple, and inexpensive. The enhancement of properties with melt-blending is, however, not always effective owing to poor interactions between the POSS and matrix.^{4, 8}

In this work,⁹ we focused on creating new melt-blended nanocomposites with acrylonitrile butadiene styrene (ABS) grafted with maleic anhydride (ABS-g-Ma), with the attempt to enhance its thermal stability. We assessed the resulting nanocomposites with different analytical methods to investigate the key factors playing a role in the overall effectiveness of the POSS incorporation.

We modified ABS-g-Ma with three different POSS nanofillers incorporated into its matrix, namely aminopropyltriethoxy siloxane, and triethoxy, resulting in three nanocomposites: APOSS, GPOSS, and TPOSS, respectively. These composites were prepared using melt blending with a twin-screw compounding, and the degradation conditions consisted of submitting the nanocomposites and the standard ABS-g-Ma to cross-linking at different temperatures from 200–320°C in steps of 40°C and 0–75-min periods of time in steps of 15 min. We assessed the degree of dispersion of POSS molecules into the matrix prior to degradation by scanning electron microscopy (see Figure 1), and observed no obvious differences between samples. The nanocomposites showed no POSS aggregation or interfacial delamination as in conventional good dispersion and miscibility between the nanofillers and matrix was achieved.

The small differential scanning calorimetry to identify the glass transition temperature (T_g) of each composite, and the possible effect of the transition on the matrix prior to degradation. The heatflow plot depicted in Figure 2 shows that all nanocomposites have a small decay

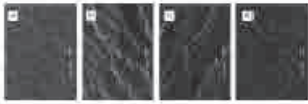


Figure 1. Scanning electron micrograph at 10000x magnification of (a) acrylonitrile butadiene styrene (ABS) grafted with maleic anhydride (ABS-g-Ma), and ABS-g-Ma composites with polyhedral oligomeric silsesquioxane (POSS): (b) ABS-g-Ma/Aminopropyltriethoxy (APOSS), (c) ABS-g-Ma/Glycidyltrimethoxy (GPOSS) and (d) ABS-g-Ma/Triethoxy (TPOSS).

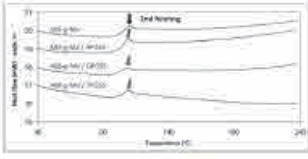


Figure 2. Differential scanning calorimetry heatflow plot during the thermal heating of ABS-g-Ma and its nanocomposites: ABS-g-Ma/APOSS, ABS-g-Ma/GPOSS and ABS-g-Ma/TPOSS.

Continued on next page



END OF THESIS